NASA TECHNICAL NOTE

NASA TN D-8043

NASA TN D-8043

SUPERSONIC DYNAMIC STABILITY CHARACTERISTICS OF A SPACE SHUTTLE ORBITER

Delma C. Freeman, Jr., Richmond P. Boyden, and E. E. Davenport

Langley Research Center
Hampton, Va. 23665

NATIONAL AERONAUTICS AND SPACE ADMINISTRATION • WASHINGTON, D. C. • JANUARY 1976

1. Report No.	2. Government Accession No.
NASA TN D-8043	

4. Title and Subtitle
SUPERSONIC DYNAMIC STABILITY CHARACTERISTICS OF A SPACE SHUTTLE ORBITER

5. Report Date
January 1976

6. Performing Organization Code

7. Author(s)
Delma C. Freeman, Jr., Richmond P. Boyden, and E. E. Davenport

8. Performing Organization Report No.
L-10063

9. Performing Organization Name and Address
NASA Langley Research Center
Hampton, Va. 23665

10. Work Unit No.
506-26-30-01

11. Contract or Grant No.

12. Sponsoring Agency Name and Address
National Aeronautics and Space Administration
Washington, D.C. 20546

13. Type of Report and Period Covered
Technical Note

14. Sponsoring Agency Code

15. Supplementary Notes

16. Abstract

Supersonic forced-oscillation tests of a 0.0165-scale model of a modified 089B Rockwell International shuttle orbiter were conducted in the Langley Unitary Plan wind tunnel for several configurations over a Mach range from 1.6 to 4.63. The tests covered angles of attack up to 30°. The period and damping of the basic unaugmented vehicle were calculated along the entry trajectory using the measured damping results. Some parameter analysis was made with the measured dynamic derivatives.

17. Key Words (Suggested by Author(s))	18. Distribution Statement
Dynamic stability Shuttle orbiter Forced oscillations Aerodynamics	Unclassified – Unlimited Subject Category 02

19. Security Classif. (of this report)	20. Security Classif. (of this page)	21. No. of Pages	22. Price*
Unclassified	Unclassified	164	$6.25

*For sale by the National Technical Information Service, Springfield, Virginia 22161

SUPERSONIC DYNAMIC STABILITY CHARACTERISTICS OF A SPACE SHUTTLE ORBITER

Delma C. Freeman, Jr., Richmond P. Boyden,
and E. E. Davenport
Langley Research Center

SUMMARY

Supersonic forced-oscillation tests of a 0.0165-scale model of a modified 089B shuttle orbiter model have been made in the Langley Unitary Plan wind tunnel. These tests, which have provided the only measured orbiter-damping data for the shuttle program, were made for several configurations over a Mach number range from 1.6 to 4.63, measuring the pitch, roll, and yaw damping. The tests also measured the normal force due to pitch rate and the cross derivatives, yawing moment due to roll rate and rolling moment due to yaw rate. The tests covered an angle-of-attack range from 0° to 30°. Static tests have been made for the same configurations and test conditions, and these data are presented to verify the dynamic test results. The measured dynamic data and three-degree-of-freedom longitudinal and lateral motion equations were used to compute the period and damping of the basic unaugmented vehicle along the entry trajectory.

The results of this investigation demonstrated that the model exhibits positive damping in pitch throughout the test angle-of-attack range for Mach numbers from 1.6 to 2.86. For a Mach number of 3.96 the model exhibited a region of pitch undamping at angles of attack near 16°. The model had positive damping in yaw throughout the test angle-of-attack and Mach number range. The rolling oscillation-test results show that the model exhibited positive roll damping for the entire angle-of-attack range for all Mach numbers except 2.36 where there was undamping at angles of attack above 26°.

INTRODUCTION

As part of the space shuttle development effort, a program has been initiated at the National Aeronautics and Space Administration (NASA) Langley Research Center to measure experimentally the dynamic stability derivatives of the shuttle orbiter through the entry to the landing phases of flight. The measured derivatives were then used to predict the vehicle dynamics for the orbiter with an unaugmented control system. Since neither

theoretical estimates nor experimental data exist over a wide Mach number and angle-of-attack range, the program was designed to provide experimentally measured damping data from subsonic to hypersonic speeds at angles of attack up to 30^{o}.

As part of this study, supersonic forced-oscillation tests of a 0.0165-scale model of a modified 089B shuttle orbiter model were conducted in the Langley Unitary Plan wind tunnel. These tests were conducted for several configurations over a Mach number range from 1.6 to 4.63, measuring the pitch, roll, and yaw damping. The tests also measured the normal force due to pitch rate and the cross derivatives, yawing moment due to roll rate and rolling moment due to yaw rate. Static tests were also run for the same configurations and test conditions. These data are presented to verify the dynamic test results. The period and damping of the basic configuration and its sensitivity to variations of the primary and cross-damping derivatives were computed using three-degree-of-freedom longitudinal and lateral motion equations to assess the importance of the damping parameters in predicting vehicle flight characteristics. The results for the corresponding study of the shuttle orbiter for Mach numbers of 0.3 and 1.2 are contained in reference 1, and the hypersonic results are shown in reference 2.

SYMBOLS

The static longitudinal data are referred to the stability-axis system and all other data are referred to the body-axis system. (See fig. 1.) The origin of the axes was located to correspond to the center-of-gravity (c.g.) positions shown in figure 2. A dot over a quantity indicates a first derivative with respect to time.

b reference span, meters

C_D drag coefficient

$C_{D_{\delta e}}$ $= \dfrac{\partial C_D}{\partial \delta_e}$, per degree

C_L lift coefficient

$C_{L_{\delta e}}$ $= \dfrac{\partial C_L}{\partial \delta_e}$, per degree

C_l rolling-moment coefficient, $\dfrac{\text{Rolling moment}}{q_\infty Sb}$

C_{l_p} $= \dfrac{\partial C_l}{\partial\left(\dfrac{pb}{2V}\right)}$, per radian

$C_{l_{\dot{p}}} = \dfrac{\partial C_l}{\partial\left(\dfrac{\dot{p}b^2}{4V^2}\right)}$, per radian

$C_{l_p} + C_{l_{\dot{\beta}}} \sin \alpha$ damping-in-roll parameter, per radian

$C_{l_r} = \dfrac{\partial C_l}{\partial\left(\dfrac{rb}{2V}\right)}$, per radian

$C_{l_{\dot{r}}} = \dfrac{\partial C_l}{\partial\left(\dfrac{\dot{r}b^2}{4V^2}\right)}$, per radian

$C_{l_r} - C_{l_{\dot{\beta}}} \cos \alpha$ rolling moment due to yaw rate parameter, per radian

$C_{l_\beta} = \dfrac{\partial C_l}{\partial \beta}$, per radian or per degree

$C_{l_{\dot{\beta}}} = \dfrac{\partial C_l}{\partial\left(\dfrac{\dot{\beta}b}{2V}\right)}$, per radian

$C_{l_\beta} \cos \alpha + k^2 C_{l_{\dot{r}}}$ effective dihedral parameter, per radian

$C_{l_\beta} \sin \alpha - k^2 C_{l_{\dot{p}}}$ rolling moment due to roll displacement parameter, per radian

C_m pitching-moment coefficient, $\dfrac{\text{Pitching moment}}{q_\infty S\bar{c}}$

$C_{m_q} = \dfrac{\partial C_m}{\partial\left(\dfrac{q\bar{c}}{2V}\right)}$, per radian

$C_{m_{\dot{q}}} = \dfrac{\partial C_m}{\partial\left(\dfrac{\dot{q}\bar{c}^2}{4V^2}\right)}$, per radian

$C_{m_q} + C_{m_{\dot{\alpha}}}$ damping-in-pitch parameter, per radian

$C_{m_\alpha} = \dfrac{\partial C_m}{\partial \alpha}$, per radian

$C_{m_{\dot{\alpha}}} = \dfrac{\partial C_m}{\partial\left(\dfrac{\dot{\alpha}\bar{c}}{2V}\right)}$, per radian

$C_{m_\alpha} - k^2 C_{m_{\dot{q}}}$ oscillatory longitudinal-stability parameter, per radian

$C_{m_{\delta e}} = \frac{\partial C_m}{\partial \delta_e}$, per degree

C_N normal-force coefficient, $\frac{\text{Normal force}}{q_\infty S}$

$C_{N_q} = \frac{\partial C_N}{\partial\left(\frac{q\bar{c}}{2V}\right)}$, per radian

$C_{N_{\dot{q}}} = \frac{\partial C_N}{\partial\left(\frac{\dot{q}\bar{c}^2}{4V^2}\right)}$, per radian

$C_{N_q} + C_{N_{\dot{\alpha}}}$ normal force due to pitch rate parameter, per radian

$C_{N_\alpha} = \frac{\partial C_N}{\partial \alpha}$, per radian

$C_{N_{\dot{\alpha}}} = \frac{\partial C_N}{\partial\left(\frac{\dot{\alpha}\bar{c}}{2V}\right)}$, per radian

$C_{N_\alpha} - k^2 C_{N_{\dot{q}}}$ normal force due to pitch displacement parameter, per radian

C_n yawing-moment coefficient, $\frac{\text{Yawing moment}}{q_\infty Sb}$

$C_{n_p} = \frac{\partial C_n}{\partial\left(\frac{pb}{2V}\right)}$, per radian

$C_{n_{\dot{p}}} = \frac{\partial C_n}{\partial\left(\frac{\dot{p}b^2}{4V^2}\right)}$, per radian

$C_{n_p} + C_{n_{\dot{\beta}}} \sin \alpha$ yawing moment due to roll rate parameter, per radian

$C_{n_r} = \frac{\partial C_n}{\partial\left(\frac{rb}{2V}\right)}$, per radian

$C_{n_{\dot{r}}} = \frac{\partial C_n}{\partial\left(\frac{\dot{r}b^2}{4V^2}\right)}$, per radian

$C_{n_r} - C_{n_{\dot{\beta}}} \cos \alpha$ damping-in-yaw parameter, per radian

C_{n_β} $= \frac{\partial C_n}{\partial \beta}$, per radian or per degree

$C_{n_{\dot{\beta}}}$ $= \frac{\partial C_n}{\partial\left(\frac{\dot{\beta} b}{2V}\right)}$, per radian

$C_{n_\beta} \cos \alpha + k^2 C_{n_{\dot{r}}}$ oscillatory directional-stability parameter, per radian

$C_{n_\beta} \sin \alpha - k^2 C_{n_{\dot{p}}}$ yawing moment due to roll displacement parameter, per radian

C_Y side-force coefficient, $\frac{\text{Side force}}{q_\infty S}$

C_{Y_β} $= \frac{\partial C_Y}{\partial \beta}$, per radian or per degree

$\bar{c}$ reference chord, meters

F_D drag force, newtons

F_L lift force, newtons

f frequency of oscillation, hertz

I_X, I_Y, I_Z moments of inertia about X, Y, and Z body axes, $kg\text{-}m^2$

I_{XZ} product of inertia, $kg\text{-}m^2$

k reduced-frequency parameter ($\omega\bar{c}/2V$ in pitch, $\omega b/2V$ in roll and yaw), radians

l model body length (nose to flap hinge line), meters

M free-stream Mach number

M_X rolling moment, newton-meter

M_Y pitching moment, newton-meter

M_Z yawing moment, newton-meter

P period, seconds

p	angular velocity of model about X-axis, radians/second
q	angular velocity of model about Y-axis, radians/second
q_∞	free-stream dynamic pressure, pascals
R	Reynolds number based on body length
r	angular velocity of model about Z-axis, radians/second
S	reference area, meters^2
t	time, seconds
$t_{1/2}$	time to damp to half-amplitude, seconds
V	free-stream velocity, meters/second
X,Y,Z	body reference axes
X_S,Y_S,Z_S	stability reference axes
x	distance along X-axis, cm
z_{cg}	distance along the Z-axis to center of gravity, cm
α	angle of attack, degrees or radians
β	angle of sideslip, radians
δ_{BF}	body flap deflection, positive when trailing edge is down, degrees
δ_e	elevon deflection, positive when trailing edge is down, degrees
ϕ	angle of roll, radians
ω	angular velocity, $2\pi f$, radians/second

APPARATUS AND MODEL

A drawing of the 0.0165-scale model used in the investigation is presented in figure 2. The model had a double-delta planform wing with an 81° sweep on the fillet and a 45° leading-edge sweep on the main wing. The model had a vertical tail with a rudder that could be deflected for yaw control and flared to provide a speed brake. (See fig. 3.) Wing trailing-edge control surfaces were used to provide both pitch and roll control, and a body flap was used to produce longitudinal trim. An orbital maneuvering system (OMS pods), located as shown in figure 2, was removed for a portion of the tests.

The supersonic static and dynamic force tests were conducted in the Langley Unitary Plan wind tunnel. Photographs of the model mounted in the tunnel for forced-oscillation tests are presented in figure 4.

Forced-Oscillation Balance Mechanisms

Pitch and yaw.- A photograph of the small-amplitude forced-oscillation balance used for the pitch and the yaw tests is shown in figure 5(a). An offset crank which fits into the balance crosshead mechanism is driven in a rotary motion by a variable-frequency electric motor. The offset crank serves to oscillate the movable portion of the balance (and thereby the model) about the pivot axis in an essentially sinusoidal motion. The amplitude of the motion is dependent on the throw of the particular crank used. The allowable range is from 0.5° to 2°. An amplitude of about 1° was used for both the pitch and the yaw tests of this study.

The instrumented beams which measure the torque required to oscillate the model are located between the pivot axis and the model mounting surface. This torque-bridge location eliminates the pivot-friction characteristics from the model system and thereby removes the need to correct the data for varying pivot friction associated with changing aerodynamic load. Although this bridge is physically forward of the pivot axis, all torques are measured with respect to the pivot axis.

A mechanical spring, which is an integral part of the fixed-balance support, is connected to the oscillation balance forward of the torque beams by means of a flexure plate. The plate is electron-beam welded to both the front of the spring and the forward portion of the oscillation balance. Welding the spring in this manner minimizes the mechanical friction which the use of mechanical fasteners would create. A strain-gage bridge mounted on the mechanical spring provides a signal proportional to the model-angular displacement with respect to the sting. Although the forced-oscillation balance may be oscillated through a frequency range from about 1 Hz to 30 Hz, the most accurate measurement of the damping coefficient is obtained at the frequency-of-velocity resonance as shown in reference 3.

Strain-gage bridges also are located on the oscillation balance torque beams to measure normal force and rolling moment in the pitching and yawing modes, respectively.

Roll.- The small-amplitude oscillatory-roll balance used for the rolling tests is shown in figure 5(b). The basic principles of operation of the oscillatory roll mechanism are the same as those for the pitch-yaw mechanism previously discussed. An electric motor with eccentric drive oscillates the forward movable portion of the balance and model in an essentially sinusoidal motion. The model is rigidly forced in a fixed 2.5° amplitude oscillation about the sting axis at a variable frequency. A mechanical torsion-spring internal to the balance is attached to the front of the strain-gage balance section to permit the model to be oscillated at the frequency for velocity resonance. In this way, the mechanical torsion spring, in addition to any aerodynamic spring term $C_{l_\beta} \sin \alpha$, balances out the model inertia. The only torque then required to oscillate the model at that particular frequency is equal to the torque caused by the aerodynamic damping. (See ref. 3.) The strain gages are located forward of all the bearings and other friction-producing components. In addition to rolling moment, the torque beams are instrumented with strain-gage bridges to measure yawing moment due to rolling. A strain-gage bridge is mounted on the mechanical torsion spring to provide a signal proportional to the model angular displacement in roll.

TESTS

The forced-oscillation tests were conducted to determine the pitch damping $\left(C_{m_q} + C_{m_{\dot{\alpha}}}\right)$, yaw damping $\left(C_{n_r} - C_{n_{\dot{\beta}}} \cos \alpha\right)$, and roll damping $\left(C_{l_p} + C_{l_{\dot{\beta}}} \sin \alpha\right)$; the change in normal force due to pitch rate parameter $\left(C_{N_q} + C_{N_{\dot{\alpha}}}\right)$; and the cross derivatives: yawing moment due to rolling velocity $\left(C_{n_p} + C_{n_{\dot{\beta}}} \sin \alpha\right)$ and rolling moment due to yawing velocity $\left(C_{l_r} - C_{l_{\dot{\beta}}} \cos \alpha\right)$. The dynamic longitudinal-stability derivatives were measured for a pitch amplitude of 1° for the natural frequencies of the model-balance combination corresponding to values of the reduced-frequency parameter k of 0.004 to 0.0087. The dynamic lateral-stability derivatives measured during the yaw oscillation tests were for a yaw amplitude of 1° for frequencies corresponding to values of the reduced-frequency parameter k of 0.0062 to 0.0137. The dynamic derivatives measured during the roll oscillation tests were measured for an amplitude of 2.5° for frequencies corresponding to values of k from 0.0150 to 0.0257. Pitch and yaw dynamic tests were conducted with two representative center-of-gravity (c.g.) locations (fig. 2) and results are presented for both positions. A description of the data reduction procedure is presented in the appendix.

The static tests were conducted to determine the static longitudinal-stability and lateral-stability characteristics of the model to aid in the interpretation of the dynamic test results. Both the static and dynamic force tests were conducted over an angle-of-attack

range from approximately -1° to 30°. The static lateral-stability characteristics were determined from incremental differences in C_n, C_l, and C_Y measured over the angle-of-attack range at fixed angles of sideslip of 0° and 2°. The test conditions were as follows:

Mach number	q_∞, Pa	R
1.60	23 030	3.55×10^6
1.90	22 890	3.55
2.36	26 860	4.43
2.86	23 700	4.43
3.96	17 620	4.43
4.63	13 930	4.43

For the Mach numbers of 1.60 and 1.90, the model was tested with transition fixed by the application of No. 60 grit, 3.05 cm aft on the nose and 1.02 cm streamwise on the wing and vertical tail. For the higher Mach numbers (M = 2.36 to M = 4.63), No. 45 grit was used in the same locations. The static force data presented have been corrected for sting bending, and all drag data presented are total drag in that the base drag has not been subtracted out.

CALCULATIONS

Linearized three-degree-of-freedom equations of motion, as presented in reference 4, were used to calculate the period and damping of the phugoid, short-period, and other oscillations; the damping of the longitudinal aperiodic modes; the period and damping of the Dutch-roll oscillations; and the damping of the lateral aperiodic modes for the basic unaugmented vehicle. All the stability calculations and motion studies were made with the use of the measured stability derivatives combined with the static longitudinal and lateral data and the mass properties presented in tables I and II, respectively. These data were obtained from the shuttle data base. Calculations were made for the discrete flight conditions listed in table III. These calculations were obtained from the nominal entry trajectory presented in figure 6.

RESULTS AND DISCUSSION

To verify and interpret the results of the forced-oscillation tests, a series of static force tests were made using the same model and test conditions that were used for the dynamic tests. Both the static and dynamic tests were conducted with the body flap on and

off in order to establish possible sting effects induced by the close proximity of the flap to the sting. These results show no apparent sting effects on the measured vehicle damping characteristics.

A brief description of the figures is as follows:

Static Longitudinal Characteristics

The static longitudinal characteristics of the model with and without the body flap $\left(\delta_{BF} = 0^{o}\right)$ are presented in figure 7. Removing the body flap resulted in a small destabilizing effect which increased with angle of attack and decreased with Mach number.

Static Lateral Characteristics

The static lateral stability data for the model are presented in figures 8 and 9. These data show the effect of vertical tail and body flap, respectively. The results show the expected trends in directional stability C_{n_β} and dihedral effect $-C_{l_\beta}$ for the removal of the vertical tail and also show the loss of effectiveness with increasing angle of attack until the vertical tail becomes ineffective at an angle of attack above 14^{o} to 16^{o}. This loss of effectiveness has been observed in tests of similar configurations (ref. 5). Installation of the body flap had no effect on the static lateral characteristics of the model. (See fig. 9.)

Pitching Oscillation Tests

The oscillatory stability parameters measured in the pitching oscillation tests at Mach numbers of 1.6, 1.9, 2.36, 2.86, 3.96, and 4.63 are presented in figures 10 to 17. The results of damping tests conducted with the most forward (0.65ℓ) and most aft (0.67ℓ) center-of-gravity locations are compared in figure 10. These results show that the effect of center-of-gravity (c.g.) position on pitch damping was small and produced an increment

in $C_{m_\alpha} - k^2 C_{m_{\dot{q}}}$ compatible with the magnitude of the center-of-gravity shift. Figure 10 also contains comparisons of the oscillatory longitudinal-stability parameters with C_{m_α} determined from the results of the static tests. There is good agreement at all test Mach numbers.

In general, the model exhibited positive damping $\left(\text{negative values of } C_{m_q} + C_{m_{\dot{\alpha}}}\right)$ throughout the test angle-of-attack range for Mach numbers of 1.6 and 2.86; however, rather abrupt nonlinearities occurred for all Mach numbers from 2.36 to 4.63, and at Mach numbers of 3.96 and 4.63 (figs. 10(e) and 10(f)) regions of pitch undamping occurred. At Mach 3.96 the region of dynamic instability encompassed the nominal entry angle-of-attack range for that Mach number. These nonlinearities in pitch damping are also reflected in the normal-force coefficients. (See figs. 14(e) and 14(f).) Figure 11 shows that removing the body flap tended to reduce the magnitude of the nonlinearities in pitch damping as did removal of the OMS pods (fig. 13). These influences of the body flap and OMS on the pitch damping indicate that some induced effects cause a change in the loading over the wing and aft portion of the body.

Figure 12 shows the effects on pitch-damping characteristics of deflecting the body flap and elevons downward for longitudinal trim of the orbiter with the aft center-of-gravity location (0.67ℓ). The data show essentially the same trends in $C_{m_q} + C_{m_{\dot{\alpha}}}$ as was discussed previously; however, deflection of the elevons and body flap tended to reduce the magnitude of the dynamic instability near the entry trim angle of attack (16° to 18°) at Mach 3.96 (fig. 12(d)).

Presented in figures 14 through 17 are the changes in normal force due to pitching velocity $\left(C_{N_q} + C_{N_{\dot{\alpha}}}\right)$. Figure 14 shows a comparison of the in-phase $C_{N_\alpha} - k^2 C_{N_{\dot{q}}}$ with C_{N_α} determined from the static test results. There is good agreement between the static and dynamic results. The normal force due to pitching velocity exhibits the nonlinearities that were pointed out in the discussion of the pitch damping.

Yawing Oscillation Test Results

The oscillatory stability parameters measured in the yawing oscillation tests are presented in figures 18 to 23. The in-phase $\left(C_{n_\beta} \cos\alpha + k^2 C_{n_{\dot{r}}}\right)$ and out-of-phase $\left(C_{n_r} - C_{n_{\dot{\beta}}} \cos\alpha\right)$ parameters are given in figures 18 through 20. Data showing the effect of varied centers of gravity (c.g.) on the yaw-damping parameter $\left(C_{n_r} - C_{n_{\dot{\beta}}} \cos\alpha\right)$ are presented in figure 18. A comparison of the in-phase parameter $\left(C_{n_\beta} \cos\alpha + k^2 C_{n_{\dot{r}}}\right)$ and the $C_{n_\beta} \cos\alpha$ computed from the static tests for the forward center of gravity is also included. There is good agreement between the static and dynamic results throughout the test angle-of-attack and Mach number range. The model exhibited positive yaw damping $\left(\text{negative } C_{n_r} - C_{n_{\dot{\beta}}} \cos\alpha\right)$ throughout the test angle-of-attack and Mach number range except at the highest angle of attack at a Mach number of 2.86 (fig. 18(c)).

The effect of the vertical tail on the yaw damping is presented in figure 19. Over the entire range of supersonic Mach numbers the damping increment of the vertical tail is small and poorly defined; however, the in-phase derivative does show a definite tail contribution to static stability. The reason for this lack of contribution of the vertical tail to the yaw damping is not understood. Hypersonic tests of this same configuration at Mach 8.0 (ref. 2) show a similar result. Even though the vertical tail contributes to yaw damping at 0° angle of attack, at α's above 2° this increment disappears indicating that there are some effects of the complex shock patterns on the aft portion of the body on the flow in the region of the vertical tail. This lack of contribution of the vertical tail to yaw damping has been seen in the results of previous tests reported in references 6 and 7, respectively.

Data showing the effect of the OMS pods on the yaw damping are presented in figure 20. These data show that the OMS has essentially no effect on yaw damping. These contrast with results of the pitch test where there were significant nonlinearities introduced in the pitch damping by the OMS pods (fig. 13).

The rolling moment due to yawing-velocity parameter $\left(C_{l_r} - C_{l_{\dot{\beta}}} \cos \alpha\right)$ is presented in figures 21 to 23. A comparison of the in-phase $C_{l_\beta} \cos \alpha + k^2 C_{l_{\dot{r}}}$ with $C_{l_\beta} \cos \alpha$ computed from the static data is presented in figure 21. These data show that $C_{l_r} - C_{l_{\dot{\beta}}} \cos \alpha$ is slightly positive at a 0° angle of attack and increases with increased α for all Mach numbers except 2.36 and 2.86. At these Mach numbers $C_{l_r} - C_{l_{\dot{\beta}}} \cos \alpha$ is negative at angles of attack above 26°. The OMS and vertical tail appear to have very little effect on this parameter (figs. 22 and 23).

Rolling Oscillation Test Results

The oscillatory-stability parameters measured in the rolling oscillation tests are shown in figures 24 to 27. Data showing the effect of the vertical tail on the roll damping $\left(C_{l_p} + C_{l_{\dot{\beta}}} \sin \alpha\right)$ are presented in figure 24, together with a comparison of the in-phase parameter $\left(C_{l_\beta} \sin \alpha - k^2 C_{l_{\dot{p}}}\right)$. The $C_{l_\beta} \sin \alpha$ is computed from the static test results. The model exhibited positive damping (negative values of $C_{l_p} + C_{l_{\dot{\beta}}} \sin \alpha$) for the entire angle-of-attack range for all Mach numbers except at 2.36 where there was some undamping at angles of attack above 26°. The roll damping was, in general, fairly linear with angle of attack for the test Mach number range. There is a small definable increment in $C_{l_p} + C_{l_{\dot{\beta}}} \sin \alpha$ due to the vertical tail at angles of attack below 20° at all Mach numbers. This increment then decreases at Mach numbers of 3.96 and 4.63. Data presented in figure 25 show that removing the OMS pods had very little effect on the roll damping.

The yawing moment due to rolling velocity $\left(C_{n_p} + C_{n_{\dot{\beta}}} \sin \alpha\right)$ measured in the roll tests is presented in figures 26 and 27. A comparison of the in-phase $C_{n_\beta} \sin \alpha - k^2 C_{n_{\dot{p}}}$ with the static $C_{n_\beta} \sin \alpha$ is also presented in figure 26. The results show that for the

complete configuration at Mach numbers of 1.6 and 1.9, the parameter $C_{n_p} + C_{n_{\dot{\beta}}} \sin \alpha$ was nonlinear and positive over the test angle-of-attack range. At Mach numbers of 2.36 and higher, $C_{n_p} + C_{n_{\dot{\beta}}} \sin \alpha$ was negative at angles of attack above 12°. The data of figure 26 also show a definable vertical-tail contribution to $C_{n_p} + C_{n_{\dot{\beta}}} \sin \alpha$ over most of the angle-of-attack range. Figures 27(c), 27(d), and 27(e) indicate that the OMS pods significantly reduced the magnitude of $C_{n_p} + C_{n_{\dot{\beta}}} \sin \alpha$ at Mach numbers above 2.36, but the exact cause of this reduction could not be determined.

MOTION STUDY ANALYSIS

In order to assess the impact of the results measured in the forced-oscillation tests, three-degree-of-freedom longitudinal and lateral motion equations have been used to calculate the vehicle longitudinal and lateral period and damping. These analyses were based on (1) the measured dynamic derivatives with the $\dot{\alpha}$ and $\dot{\beta}$ terms assumed zero, (2) static data presented in table I, and (3) vehicle mass properties as given in table II. The calculations were made for the basic airframe in that no stability augmentation was input. Although the vehicle was designed to fly in the active control mode, an analysis of the unaugmented vehicle characteristics indicates the existence of significant anomalies that must be taken into consideration in the vehicle flight-control system design.

Longitudinal Analysis

Because of the requirements for a large center-of-gravity travel for the shuttle orbiter (65 to 67.5 percent or 6.8 percent $\bar{c}$), the effect of static margin on the vehicle longitudinal oscillatory and aperiodic modes was computed. These results are presented in figure 28. For these analyses the damping was assumed to vary linearly between the center-of-gravity (c.g.) positions tested. The calculations have been made for Mach numbers along the vehicle entry trajectory (fig. 6) of 2.0, 3.0, 4.0, and 5.0. At Mach numbers of 2.0 and 3.0 (fig. 28(a)) for the forward center of gravity (65-percent l) where the vehicle has static stability, the results show the characteristic short period and phugoid oscillation. As the center of gravity moves aft and the vehicle becomes statically unstable, the short period and phugoid oscillation breaks down, and the roots of the stability quartic combine to form a third oscillation and two aperiodic modes, one of which is unstable. For the high supersonic Mach numbers ($M = 4.0$ and $M = 5.0$), the model was neutrally statically stable at the forward center of gravity, and the divergent aperiodic mode for the aft center of gravity ($0.675l$) had a value of $1/t_{1/2}$ of -0.75. This value corresponds to a time to double amplitude of 1.33 seconds. These results show the unstable aperiodic mode to be the main concern and the unstable aperiodic mode is associated directly with the vehicle static stability at the aft center of gravity. The feasibility of flying this level of instability would depend directly on the ability to determine the vehicle

attitude accurately enough to prevent the divergence from building to a level of pitch acceleration which the aerodynamic control could not overcome. Flight with an unaugmented control system with this level of instability would be difficult.

In order to determine the importance of the pitch-damping derivative C_{m_q} on the vehicle dynamics, calculations have been made to determine the effects of varying this parameter plus or minus an order of magnitude, and portions of these results are presented in figure 29. The results from the calculations at the supersonic Mach numbers show that the damping of the short period oscillation is proportional to the pitch damping. Increases in Mach number decreased the effect of the damping on the vehicle characteristics.

Lateral Analysis

The effects of center-of-gravity (c.g.) position and variation of the derivatives C_{n_r}, C_{n_p}, C_{l_p}, and C_{l_r} on the calculated period and damping of the vehicle lateral oscillatory and aperiodic modes are presented in figures 30 to 34. The solution of the lateral stability quartic show that for the measured values of damping the vehicle exhibited the characteristic Dutch-roll oscillation throughout the Mach number range with a roll-spiral oscillation at Mach numbers of 2.0 and 3.0; these analyses also showed the uncombined roll and spiral modes at the higher Mach numbers. The effects of center-of-gravity position on the lateral period and damping are presented in figure 30. The only significant result in these data is that at a Mach number of 4.0, as the center of gravity moved aft, the roll mode and the spiral mode combined to form the roll-spiral oscillation. References 8 and 9 indicate that the formation of the oscillation can have some marked effects on the vehicle flyability making it difficult to maintain a given heading.

Yaw derivatives.- Increasing or decreasing the yaw damping (fig. 31) from the value obtained from the tests caused the roll-spiral oscillation to break down into two aperiodic modes. The roll mode was very sensitive to the variation of C_{n_r} and was directly proportional to values of C_{n_r}, becoming increasingly stable with increased damping and increasingly unstable with negative damping. Changes in C_{n_r} had essentially no effect on the Dutch-roll oscillation.

The effect of C_{n_p} on the vehicle lateral period and damping is presented in figure 32. These results show that increasing negative values of C_{n_p} result in the breakdown of the roll-spiral oscillation with a slightly unstable spiral mode. Increasing C_{n_p} caused the roll-spiral oscillation to become slightly unstable at the higher positive values of C_{n_p}. Changes in C_{n_p} also affected the Dutch-roll oscillation with positive increases in C_{n_p} resulting in a more damped oscillation.

Roll derivatives.- The effect of roll damping C_{l_p} on the calculated vehicle period and damping is presented in figure 33. The Dutch-roll oscillation was extremely sensitive

to the value of C_{l_p} with decreased damping resulting in a highly unstable oscillation. Increases in Mach number did decrease the effect of C_{l_p} on the Dutch roll, but even at a Mach number of 5, the effect was significant. Changes in C_{l_p} to undamped values also resulted in the breakdown of the roll-spiral oscillation into the roll and spiral modes for the Mach range investigated.

The effect of rolling moment due to yawing velocity C_{l_r} on calculated vehicle damping is presented in figure 34. Changing C_{l_r} has small effects on the Dutch-roll oscillation, but large changes, either positive or negative, cause the roll-spiral oscillation to break down and form the aperiodic roll and spiral modes.

SUMMARY OF RESULTS

This investigation was conducted to determine the supersonic dynamic stability characteristics of a 0.0165-scale model of a space shuttle orbiter. These tests were made over a range of Mach numbers of 1.6 to 4.63 at angles of attack up to 30°. By using the measured damping data and static data from the shuttle data base, three-degree-of-freedom longitudinal and lateral motion analyses have been made. A summary of the results follows:

1. For both the longitudinal and lateral data there was good agreement between the in-phase parameters computed from the static test results and those measured in the forced-oscillation tests.

2. The model exhibited positive damping in pitch throughout the test angle-of-attack range for Mach numbers from 1.6 to 2.86. For a Mach number of 3.96 the model exhibited a region of undamping at angles of attack near 16°.

3. The model exhibited positive damping in yaw throughout the test angle-of-attack and Mach number range except at the highest angle of attack at a Mach number of 2.86.

4. The rolling-oscillation tests results show that the model exhibited positive roll damping for the test angle-of-attack range for all Mach numbers except 2.36. At this Mach number some undamping was indicated at angles of attack above 26°.

5. The results from the longitudinal analysis showed that the damping of the short period oscillation was proportional to pitch damping. Increases in Mach number decreased the effect of the pitch damping on the vehicle characteristics.

6. At Mach numbers of 4.0 and 5.0 the vehicle with an aft center of gravity had an unstable aperiodic mode in pitch with a time to double amplitude of 1.33 seconds. It would be difficult to fly this level of instability with an unaugmented control system.

7. The lateral analysis indicated that the roll-spiral oscillation was very sensitive to variations in yaw damping whereas the oscillatory Dutch roll was not affected by the

value of yaw damping. The roll mode and the roll-spiral oscillation were sensitive to changes in yaw damping.

8. The lateral analysis also showed that at the lower Mach numbers (M = 2.0 and M = 3.0) the Dutch-roll oscillation was extremely sensitive to the roll damping. The influence of roll damping on the Dutch roll was decreased at the higher Mach numbers but even at a Mach number of 5 the effect was significant.

Langley Research Center
National Aeronautics and Space Administration
Hampton, Va. 23665
October 6, 1975

APPENDIX

MEASUREMENTS AND REDUCTION OF DYNAMIC STABILITY DATA

Basic Principles

Strain-gage bridges are used to measure the torque required to oscillate the model and the angular displacement of the model with respect to the fixed portion of the sting. Additional bridges are provided on the pitch-yaw balance to provide signals proportional to normal force and rolling moment and on the roll balance to provide signals proportional to yawing moment. The constant components of the bridge outputs are removed by using conventional bridge-balance circuits. The nonconstant components are amplified and passed through mechanically coupled, but electrically independent, sine-cosine resolvers. These resolvers rotate with constant angular velocity at the frequency of model oscillation and resolve each signal into orthogonal components. The components are rectified by phase-sensitive demodulators and are read on damped, digital voltmeters to provide direct-current voltages proportional to the amplitudes of the orthogonal components. The individual resolvers are electrically alined so that the phase angle between the torque required to oscillate the model and the angular displacement and between the secondary signal (rolling moment, yawing moment, or normal force) and angular displacement may also be determined from the orthogonal components.

The resolver-damped voltmeter system acts as an extremely narrow band-pass filter with the center frequency always being the frequency of oscillation of the model. In this way, as explained in reference 1, the effects of random signal inputs because of tunnel turbulence or other causes are eliminated. Thus, only those components of the desired torques, forces, and angular displacement which occur at the frequency of oscillation are used in computing the dynamic stability characteristics of the model.

The frequency of oscillation is measured by an electronic counter which counts for 1 second the pulses generated by a photocell device. This device had a slotted disk attached to the shaft of the motor turning the resolvers.

The computation of the various parameters presented below is an extension of the material in reference 6.

Computation of Pitching Parameters

For the pitching tests, measurements were made of the amplitude of the torque required to oscillate the model in pitch T_Y, the amplitude of the angular displacement in pitch of the model with respect to the sting Θ, the phase angle η between T_Y and Θ, and the angular velocity of the forced oscillation ω. The viscous-damping moment coefficient in pitch (in-phase with pitching velocity) for this single-degree-of-freedom system was computed as

$$C_Y = \frac{T_Y \sin \eta}{\omega \Theta} \tag{1}$$

and the spring-inertia parameter in pitch (in-phase with displacement) was computed as

$$K_Y - I_Y \omega^2 = \frac{T_Y \cos \eta}{\Theta} \tag{2}$$

where K_Y is the torsional-spring coefficient of the system and I_Y is the moment of inertia of the system about the body Y-axis. In sketch (a), the relationship between displacement and torque is shown.

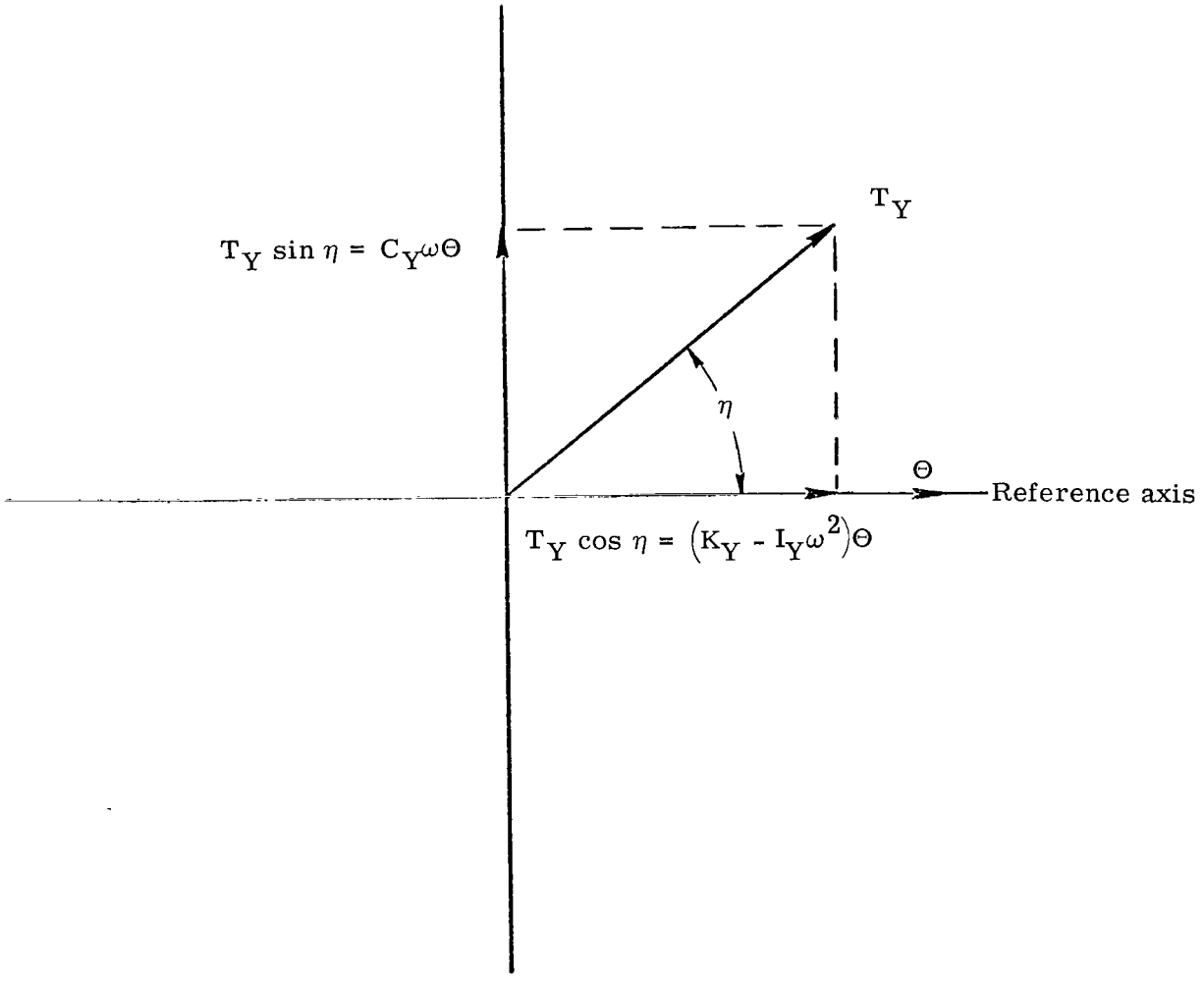

Sketch (a) Vector diagram of torque and displacement for dynamic stability pitch tests.

APPENDIX

For these tests, the damping-in-pitch parameter was computed as

$$C_{m_q} + C_{m_{\dot{\alpha}}} = -\frac{2V}{q_\infty S\bar{c}^2}\left[\left(C_Y\right)_{\text{wind on}} - \left(C_Y\right)_{\text{wind off}}\right] \tag{3}$$

and the oscillatory longitudinal-stability parameter was computed as

$$C_{m_\alpha} - k^2 C_{m_{\dot{q}}} = -\frac{1}{q_\infty S\bar{c}}\left[\left(K_Y - I_Y\omega^2\right)_{\text{wind on}} - \left(K_Y - I_Y\omega^2\right)_{\text{wind off}}\right] \tag{4}$$

The wind-off value of C_Y is determined at the frequency of wind-off velocity resonance since the value of C_Y is independent of frequency and can be determined most accurately at the frequency of velocity resonance. (See ref. 3.) The wind-on and wind-off values of $K_Y - I_Y\omega^2$ are determined at the same frequency since $K_Y - I_Y\omega^2$ is a function of frequency.

During the pitch oscillation tests, measurements were also made of the normal force N induced by the pitching oscillation and of the phase angle ζ between N and the pitching displacement. The normal-force coefficient in-phase with pitching velocity for this system was computed as

$$C_{N,Z} = \frac{N \sin \zeta}{\omega\Theta} \tag{5}$$

and the force acceleration parameter (in-phase with pitching displacement) in pitch was computed as

$$\frac{K_Y}{l} - mx\omega^2 = \frac{N \cos \zeta}{\Theta} \tag{6}$$

where K_Y is the torsional-spring coefficient of the system, l is its effective length with respect to the balance pivot, m is the model mass, and x is the distance from the balance pivot to the center of the model mass (positive forward).

The normal force due to pitch rate parameter was computed as

$$C_{N_q} + C_{N_{\dot{\alpha}}} = -\frac{2V}{q_\infty S\bar{c}}\left[\left(C_{N,Z}\right)_{\text{wind on}} - \left(C_{N,Z}\right)_{\text{wind off}}\right] \tag{7}$$

and the normal force due to pitch displacement parameter was computed as

$$C_{N_\alpha} - k^2 C_{N_{\dot{q}}} = -\frac{1}{q_\infty S}\left[\left(\frac{K_Y}{l} - mx\omega^2\right)_{\text{wind on}} - \left(\frac{K_Y}{l} - mx\omega^2\right)_{\text{wind off}}\right] \tag{8}$$

The wind-off and wind-on values of $\frac{K_Y}{l} - mx\omega^2$ are determined at the same frequency. The normal-force data for wind-on conditions are taken simultaneously with the pitch data at the frequency for velocity resonance in pitch of the system.

Computation of Yawing Parameters

For the yawing tests, measurements were made of the torque required to oscillate the model in yaw T_Z, the amplitude of the angular displacement in yaw of the model with respect to the sting ψ, the phase angle λ between T_Z and ψ, and the angular velocity of the forced oscillation ω. The viscous-damping moment coefficient in yaw C_Z for this single-degree-of-freedom system was computed in a manner similar to the pitch case as

$$C_Z = \frac{T_Z \sin \lambda}{\omega \psi} \tag{9}$$

and the spring-inertia parameter in yaw was computed as

$$K_Z - I_Z \omega^2 = \frac{T_Z \cos \lambda}{\psi} \tag{10}$$

where K_Z is the torsional spring coefficient of the system and I_Z is the moment of inertia of the system about the body Z-axis.

For these tests, the damping-in-yaw parameter was computed as

$$C_{n_r} - C_{n_{\dot{\beta}}} \cos \alpha = -\frac{2V}{q_\infty S b^2}\left[(C_Z)_{\text{wind on}} - (C_Z)_{\text{wind off}}\right] \tag{11}$$

and the oscillatory directional-stability parameter as

$$C_{n_\beta} \cos \alpha + k^2 C_{n_{\dot{r}}} = \frac{1}{q_\infty S b}\left[\left(K_Z - I_Z \omega^2\right)_{\text{wind on}} - \left(K_Z - I_Z \omega^2\right)_{\text{wind off}}\right] \tag{12}$$

APPENDIX

The wind-off value of C_Z is determined at the frequency of wind-off velocity resonance, and the wind-off and wind-on values of $K_Z - I_Z\omega^2$ are determined at the same frequency.

As part of the yawing oscillation tests, measurements were made of the amplitude of the rolling torque T'_X induced by the yawing oscillation and the phase angle γ between T'_X and the yawing displacement ψ. The rolling-moment coefficient in-phase with yawing velocity for this system was

$$C_{l,Z} = \frac{T'_X \sin \gamma}{\omega\psi} \tag{13}$$

and the rolling-moment parameter in-phase with yawing displacement was

$$A + I_{XZ}\omega^2 = \frac{T'_X \cos \gamma}{\psi} \tag{14}$$

where A is the torsional spring coefficient in roll induced by a yawing displacement and I_{XZ} is the product of inertia of the system.

For these tests the rolling moment due to yaw rate parameter was computed as

$$C_{l_r} - C_{l_{\dot\beta}} \cos \alpha = -\frac{2V}{q_\infty Sb^2}\left[\left(C_{l,Z}\right)_{\text{wind on}} - \left(C_{l,Z}\right)_{\text{wind off}}\right] \tag{15}$$

and the effective dihedral parameter was computed as

$$C_{l_\beta} \cos \alpha + k^2 C_{l_{\dot r}} = \frac{1}{q_\infty Sb}\left[\left(A + I_{XZ}\omega^2\right)_{\text{wind on}} - \left(A + I_{XZ}\omega^2\right)_{\text{wind off}}\right] \tag{16}$$

The wind-off and wind-on values of $A + I_{XZ}\omega^2$ are determined at the same frequency since $A + I_{XZ}\omega^2$ is a function of frequency.

Computation of Rolling Parameters

For the rolling tests, measurements were made of the amplitude of the torque required to oscillate the model in roll T_X, the amplitude of the angular displacement in roll of the model with respect to the fixed portion of the sting Φ, the phase angle σ between T_X and Φ, and the angular velocity of the forced oscillation ω. The viscous-damping coefficient in roll C_X for this single-degree-of-freedom system was computed in a manner similar to the pitch and yaw cases as

$$C_X = \frac{T_X \sin \sigma}{\omega\Phi} \tag{17}$$

and the spring-inertia parameter in roll was computed as

$$K_X - I_X\omega^2 = \frac{T_X \cos \sigma}{\Phi} \tag{18}$$

where K_X is the torsional spring coefficient of the system and I_X is the moment of inertia of the system about the body X-axis.

For these tests, the damping-in-roll parameter was computed as

$$C_{l_p} + C_{l_{\dot\beta}} \sin \alpha = -\frac{2V}{q_\infty Sb^2}\left[(C_X)_{\text{wind on}} - (C_X)_{\text{wind off}}\right] \tag{19}$$

and the rolling moment due to roll-displacement parameter as

$$C_{l_\beta} \sin \alpha - k^2 C_{l_{\dot p}} = -\frac{1}{q_\infty Sb}\left[\left(K_X - I_X\omega^2\right)_{\text{wind on}} - \left(K_X - I_X\omega^2\right)_{\text{wind off}}\right] \tag{20}$$

As in the pitch and yaw cases, the wind-off value of C_X is determined at the frequency of wind-off velocity resonance since the value of C_X is independent of frequency and can be determined most accurately at the frequency of velocity resonance. The wind-on and wind-off values of $K_X - I_X\omega^2$ are determined at the same frequency since $K_X - I_X\omega^2$ is a function of frequency.

As part of the rolling oscillation tests, measurements were made of the amplitude of the yawing torque T'_Z induced by the rolling oscillation and the phase angle ϵ between T'_Z and the rolling displacement Φ. The yawing-moment coefficient in-phase with rolling velocity for this system was

$$C_{n,X} = \frac{T'_Z \sin \epsilon}{\omega \Phi} \tag{21}$$

and the yawing-moment parameter in-phase with rolling displacement was

$$B + I_{XZ}\omega^2 = \frac{T'_Z \cos \epsilon}{\Phi} \tag{22}$$

where B is the torsional spring coefficient in yaw induced by a roll displacement and I_{XZ} is the product of inertia of the system.

APPENDIX

For these tests, the yawing moment due to roll rate parameter was computed as

$$C_{n_p} + C_{n_{\dot{\beta}}} \sin \alpha = -\frac{2V}{q_\infty Sb^2}\left[(C_{n,X})_{\text{wind on}} - (C_{n,X})_{\text{wind off}}\right] \tag{23}$$

and the yawing-moment due to roll-displacement parameter was computed as

$$C_{n_\beta} \sin \alpha - k^2 C_{n_{\dot{p}}} = -\frac{1}{q_\infty Sb}\left[\left(B + I_{XZ}\omega^2\right)_{\text{wind on}} - \left(B + I_{XZ}\omega^2\right)_{\text{wind off}}\right] \tag{24}$$

The wind-off and the wind-on values of $B + I_{XZ}\omega^2$ are determined at the same frequency since $B + I_{XZ}\omega^2$ is a function of frequency.

It should be emphasized that the measurement of the primary damping parameters $\left(C_{m_q} + C_{m_{\dot{\alpha}}},\ C_{n_r} - C_{n_{\dot{\beta}}} \cos \alpha, \text{ and } C_{l_p} + C_{l_{\dot{\beta}}} \sin \alpha\right)$ is inherently more accurate than the measurements of the secondary damping parameters $\left(C_{N_q} + C_{N_{\dot{\alpha}}},\ C_{l_r} - C_{l_{\dot{\beta}}} \cos \alpha,\right.$ and $\left. C_{n_p} + C_{n_{\dot{\beta}}} \sin \alpha\right)$ where the small damping parameters are measured in the presence of large forces and moments in-phase with the displacements.

REFERENCES

1. Boyden, Richmond P.; and Freeman, Delma C., Jr.: Subsonic and Transonic Dynamic Stability Characteristics of a Space Shuttle Orbiter. NASA TN D-8042, 1975.

2. Uselton, Bob L.; and Jenke, Leroy M.: Pitch-, Yaw-, and Roll-Damping Characteristics of a Shuttle Orbiter at $M_\infty = 8$. AEDC-TR-74-129, U.S. Air Force, May 1975. (Available from DDC as AD A 011 648.)

3. Braslow, Albert L.; Wiley, Harleth G.; and Lee, Cullen Q.: A Rigidly Forced Oscillation System for Measuring Dynamic-Stability Parameters in Transonic and Supersonic Wind Tunnels. NASA TN D-1231, 1962. (Supersedes NACA RM L58A28.)

4. Etkin, Bernard: Dynamics of Flight. John Wiley & Sons, Inc., c.1959.

5. Ware, George M.; Spencer, Bernard, Jr.; and Fournier, Roger H.: Supersonic Aerodynamic Characteristics of the North American Rockwell ATP Shuttle Orbiter. NASA TM X-2804, 1973.

6. Kilgore, Robert A.; and Adcock, Jerry B.: Supersonic Aerodynamic Damping and Oscillatory Stability in Pitch and Yaw for a Model of a Variable-Sweep Fighter Airplane With Twin Vertical Tails. NASA TM X-2555, 1972.

7. Kilgore, Robert A.: Some Transonic and Supersonic Dynamic Stability Characteristics of a Variable-Sweep-Wing Tactical Fighter Model. NASA TM X-2163, 1971.

8. Grantham, William D.; Moore, Frederick L.; Deal, Perry L.; and Patton, James M., Jr.: Simulator Study of Coupled Roll-Spiral Mode Effects on Lateral-Directional Handling Qualities. NASA TN D-5466, 1970.

9. Chambers, Joseph R.; and Grafton, Sue B.: Investigation of Lateral-Directional Dynamic Stability of a Tilt-Wing V/STOL Transport. NASA TN D-5637, 1970.

TABLE I.- ORBITER STATIC AERODYNAMICS USED IN ANALYSIS

α, deg	Untrimmed lift coefficient derived from shuttle data base for –			
	M = 2.0	M = 3.0	M = 4.0	M = 5.0
0	-0.047	-0.050	-0.05	-0.05
5	.126	.081	.053	.044
7.5	.220	.146	.112	.099
10	.309	.221	.176	.156
12.5	.405	.299	.247	.220
15	.501	.375	.321	.284
20	.685	.528	.467	.426
25	.861	.676	.608	.569
30	1.024	.823	.749	.714
35	-----	.955	.885	.850
40	-----	1.066	.999	.962
45	-----	1.144	1.088	1.049

α, deg	Untrimmed drag coefficient derived from shuttle data base for –			
	M = 2.0	M = 3.0	M = 4.0	M = 5.0
0	0.142	0.105	0.090	0.082
5	.148	.104	.085	.075
7.5	.160	.112	.093	.082
10	.184	.128	.106	.093
12.5	.213	.157	.124	.110
15	.255	.185	.156	.139
20	.365	.274	.239	.217
25	.506	.396	.353	.329
30	.693	.554	.502	.477
35	----	.746	.689	.660
40	----	.970	.909	.876
45	----	1.218	1.161	1.122

TABLE I.- Continued

α, deg	Untrimmed pitching-moment coefficient (forward c.g.) derived from shuttle data base for –			
	M = 2.0	M = 3.0	M = 4.0	M = 5.0
0	0.016	-0.010	-0.018	-0.022
5	-.009	-.010	-.015	-.018
7.5	-.019	-.010	-.014	-.016
10	-.028	-.011	-.014	-.015
12.5	-.032	-.013	-.014	-.014
15	-.036	-.015	-.015	-.014
20	-.046	-.020	-.018	-.016
25	-.058	-.028	-.022	-.019
30	-.064	-.037	-.038	-.025
35	----	-.048	-.037	-.036
40	----	-.062	-.050	-.050
45	----	-.079	-.070	-.067

α, deg	$C_{L_{\delta e}}$ per degree derived from shuttle data base for –			
	M = 2.0	M = 3.0	M = 4.0	M = 5.0
0	0.003	0.0015	0.0010	0.0005
5	.003	.0015	.0010	.0005
7.5	.003	.0015	.0010	.0005
10	.003	.0015	.0010	.0005
12.5	.003	.0015	.0010	.0005
15	.003	.0015	.0010	.0005
20	.003	.0015	.0010	.0005
25	.003	.0015	.0010	.0030
30	.0035	.0015	.0025	.0030
35	-----	.0020	.0025	.0035
40	-----	.0020	.0035	.0035
45	-----	.0030	.0035	.0035

TABLE I.- Continued

α, deg	$C_{D_{\delta e}}$ per degree derived from shuttle data base for –			
	M = 2.0	M = 3.0	M = 4.0	M = 5.0
0	0.003	-0.0005	-0.0005	-0.0004
5	0	-.00025	-.00025	.0006
7.5	0	-.0001	-.0001	.0007
10	.0002	0	0	0
12.5	.0003	.0002	.0002	.0002
15	.0005	.0004	.0004	.0004
20	.0005	.0008	.0008	.0008
25	.001	.0013	.0013	.0013
30	.0018	.0018	.0018	.0018
35	-----	.0025	.0025	.0023
40	-----	.0032	.0032	.0027
45	-----	-----	-----	.0040

α, deg	$C_{m_{\delta e}}$ (forward c.g.) per degree derived from shuttle data base for –			
	M = 2.0	M = 3.0	M = 4.0	M = 5.0
0	-0.003	-0.0015	-0.0015	-0.0005
5	-.003	-.0015	-.0015	-.0005
7.5	-.003	-.0015	-.0015	-.0005
10	-.003	-.0015	-.0015	-.0015
12.5	-.003	-.0015	-.0015	-.0015
15	-.003	-.0015	-.0015	-.0015
20	-.003	-.004	-.004	-.0025
25	-.003	-.004	-.004	-.0025
30	-.003	-.004	-.004	-.0045
35	-----	-.006	-.006	-.0045
40	-----	-.006	-.006	-.006
45	-----	-.008	-.008	-.006

TABLE I.- Continued

α, deg	C_{n_β} (forward c.g.) per degree derived from shuttle data base for –			
	M = 2.0	M = 3.0	M = 4.0	M = 5.0
0	0.00140	0.00110	0.0080	0.00060
5	.00090	.00070	.00050	.00040
7.5	.00060	.00045	.00035	.00025
10	.00025	.0002	.00010	0.
12.5	-.00020	-.00015	-.00025	-.00032
15	-.00100	-.0005	-.00055	-.00060
20	-.00235	-.00140	-.00110	-.00090
25	-.00285	-.00180	-.00150	-.00125
30	-.00325	-.00220	-.00210	-.00145
35	-------	-.00240	-.00200	-.00165
40	-------	-.00260	-.00220	-.00185
45	-------	-.00270	-.00240	-.00200

α, deg	C_{l_β} per degree derived from shuttle data base for –			
	M = 2.0	M = 3.0	M = 4.0	M = 5.0
0	-0.00018	-0.00020	-0.00004	0.00002
5	-.00040	-.00043	-.00039	-.00031
7.5	-.00051	-.00055	-.00048	-.00042
10	-.00064	-.00068	-.00071	-.00065
12.5	-.00077	-.00086	-.00089	-.00086
15	-.00084	-.00107	-.00106	-.00099
20	-.00100	-.00136	-.00134	-.00132
25	-.00115	-.00144	-.00145	-.00143
30	-.00123	-.00152	-.00152	-.00156
35	------	-.00152	-.00162	-.00167
40	------	-.00150	-.00166	-.00178
45	------	-.00148	-.00163	-.00178

TABLE I.- Concluded

α, deg	C_{Y_β} per degree derived from shuttle data base for –			
	M = 2.0	M = 3.0	M = 4.0	M = 5.0
0	-0.021	-0.0185	-0.0170	-0.0155
5	-.0185	-.0175	-.0150	-.0145
7.5	-.0180	-.0165	-.0155	-.0140
10	-.0170	-.0155	-.0145	-.0130
12.5	-.0160	-.0145	-.0135	-.0125
15	-.0150	-.0140	-.0127	-.0115
20	-.0110	-.0115	-.0103	-.009
25	-.0110	-.0115	-.0112	-.010
30	-.008	-.0105	-.0103	-.009
35	-----	-.0105	-.0090	-.0080
40	-----	-.0110	-.0090	-.0080
45	-----	-.0120	-.0100	-.0080

TABLE II.- ORBITER MASS PROPERTIES

[Derived from shuttle data base]

Mass	84 096 kg
I_Y	7 710 435 kg-m^2
I_X	1 014 138 kg-m^2
I_Z	7 870 419 kg-m^2
I_{XZ}	199 300 kg-m^2

TABLE III.- FLIGHT CONDITIONS FOR ANALYSES

[Derived from shuttle data base]

Mach number	α, deg	Altitude, m	Velocity, m/sec	Dynamic pressure, Pa
2.04	12.2	23 737.8	593.1	9 011
3.03	14.6	28 235.7	910.7	10 026
4.04	17.8	32 574.3	1227.7	9 332
5.02	21.10	35 780.8	1563.6	7 881

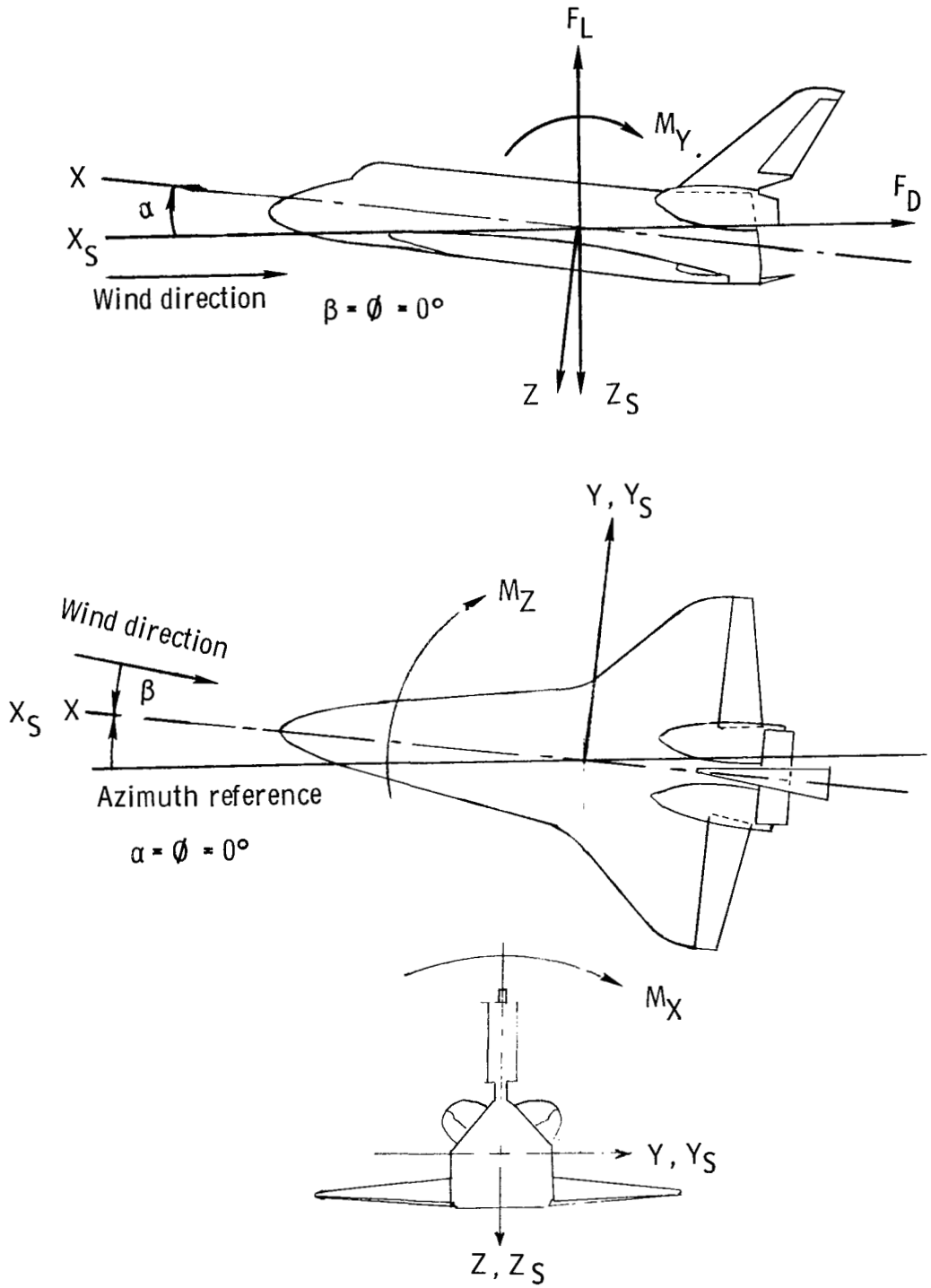

Figure 1.- System of axes used in investigation. Arrows indicate positive direction of moments, forces, and angles.

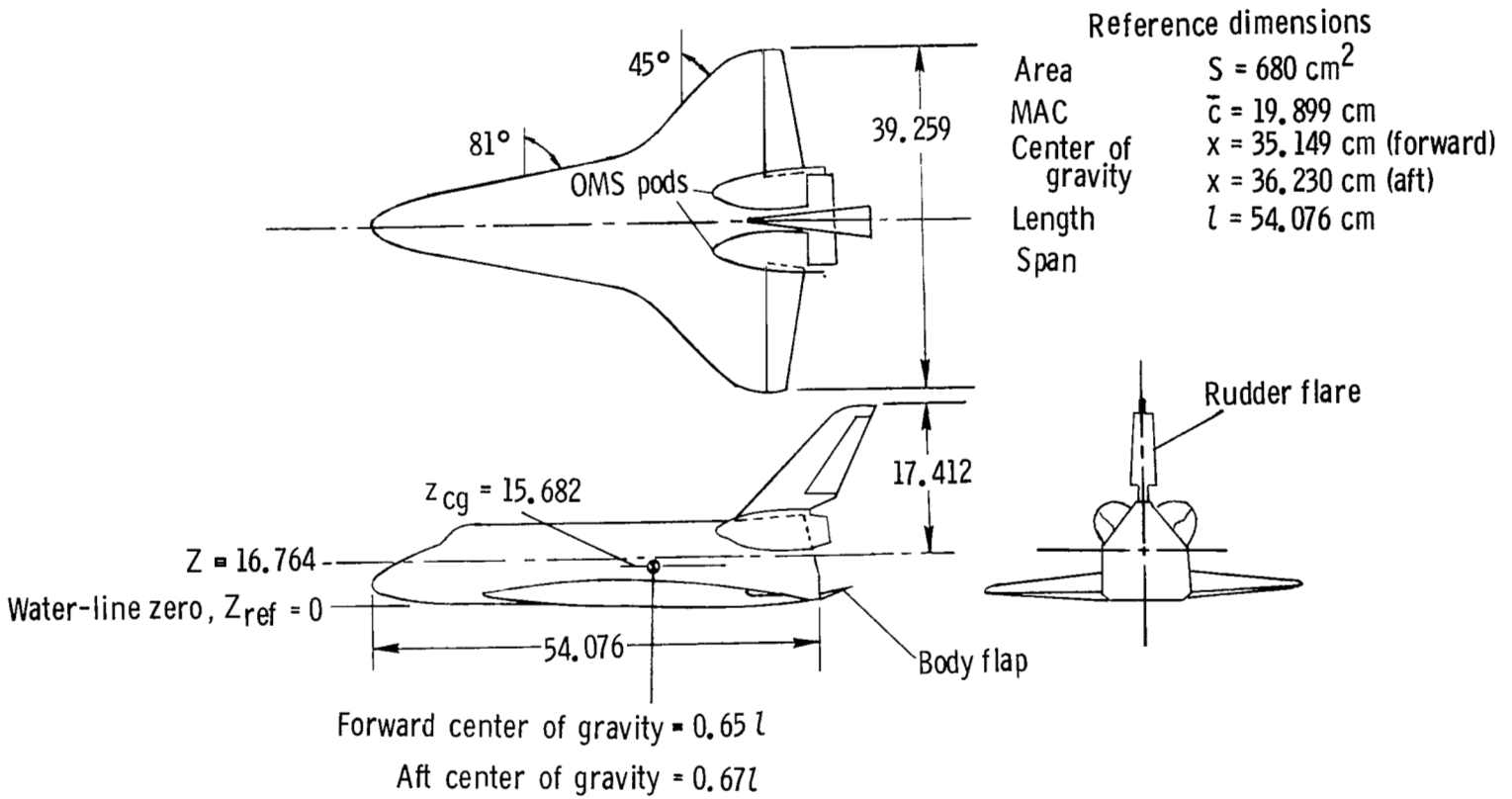

Figure 2.- Sketch of configuration tested. All dimensions given in centimeters.

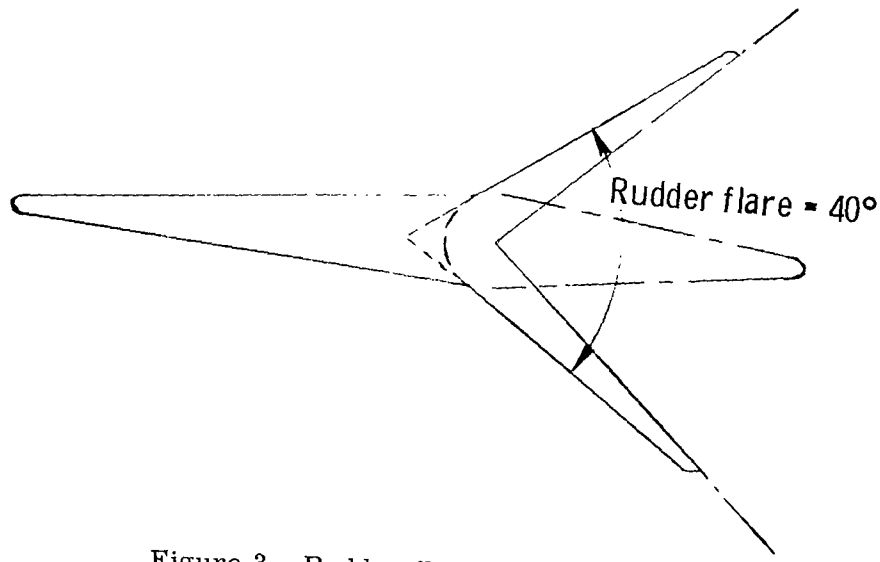

Figure 3.- Rudder flare angle definition.

L-73-5603

(a) Side view.

Figure 4.- Photographs of the model mounted for forced-oscillation tests in the Langley Unitary Plan wind tunnel.

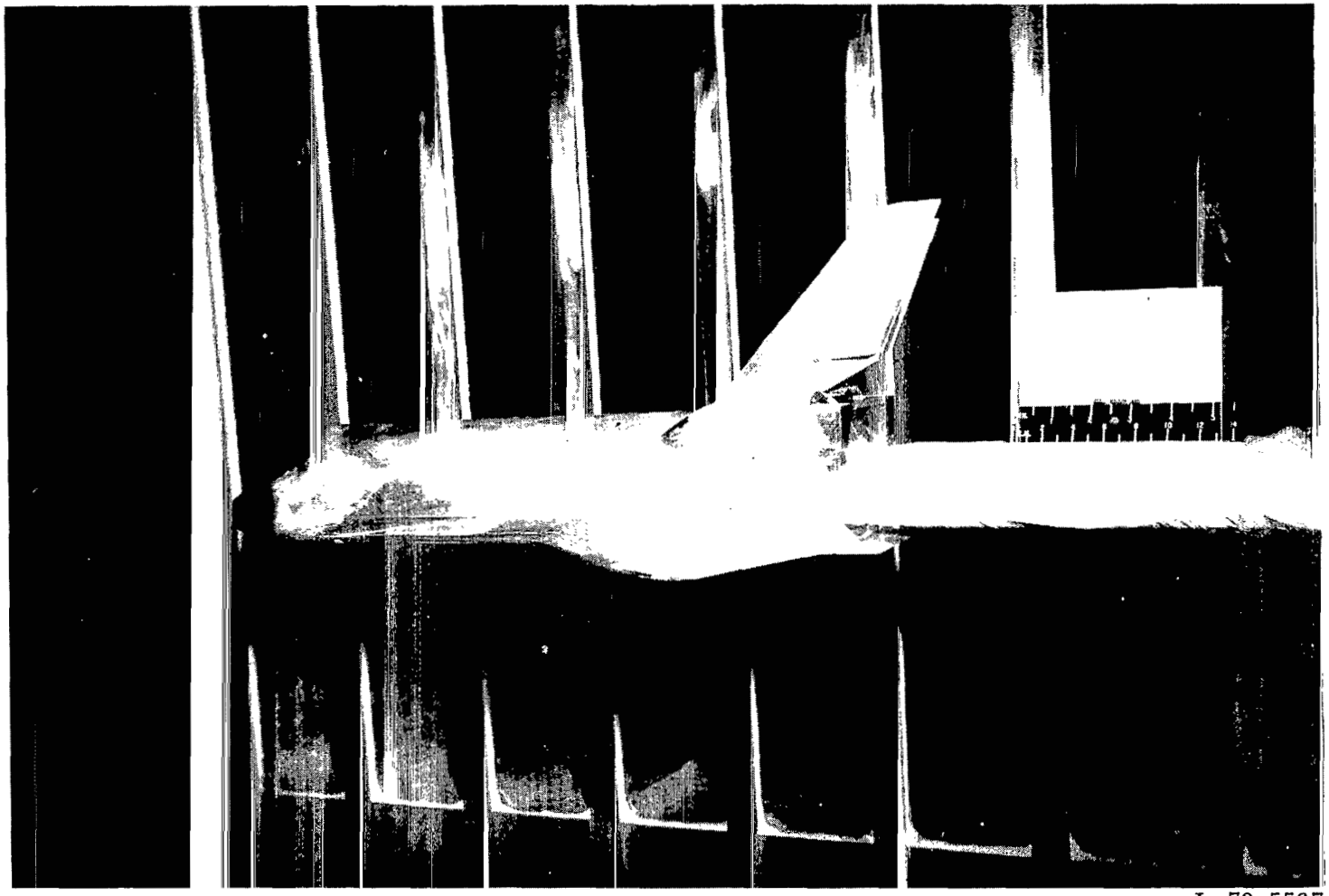

L-73-5567

(b) Base view.

Figure 4.- Concluded.

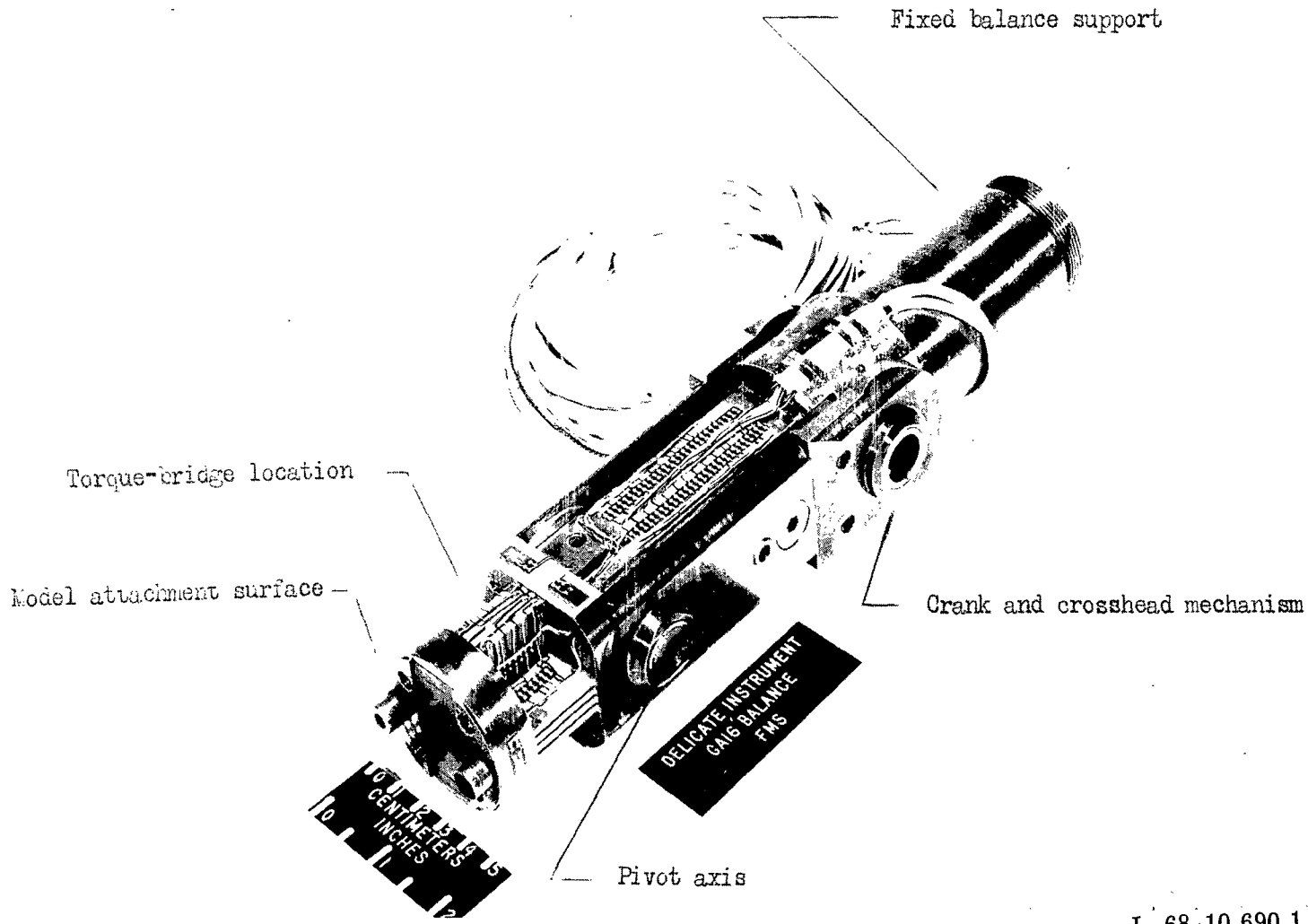

(a) Pitch-yaw balance.

Figure 5.- Photographs of small-amplitude forced-oscillation balances.

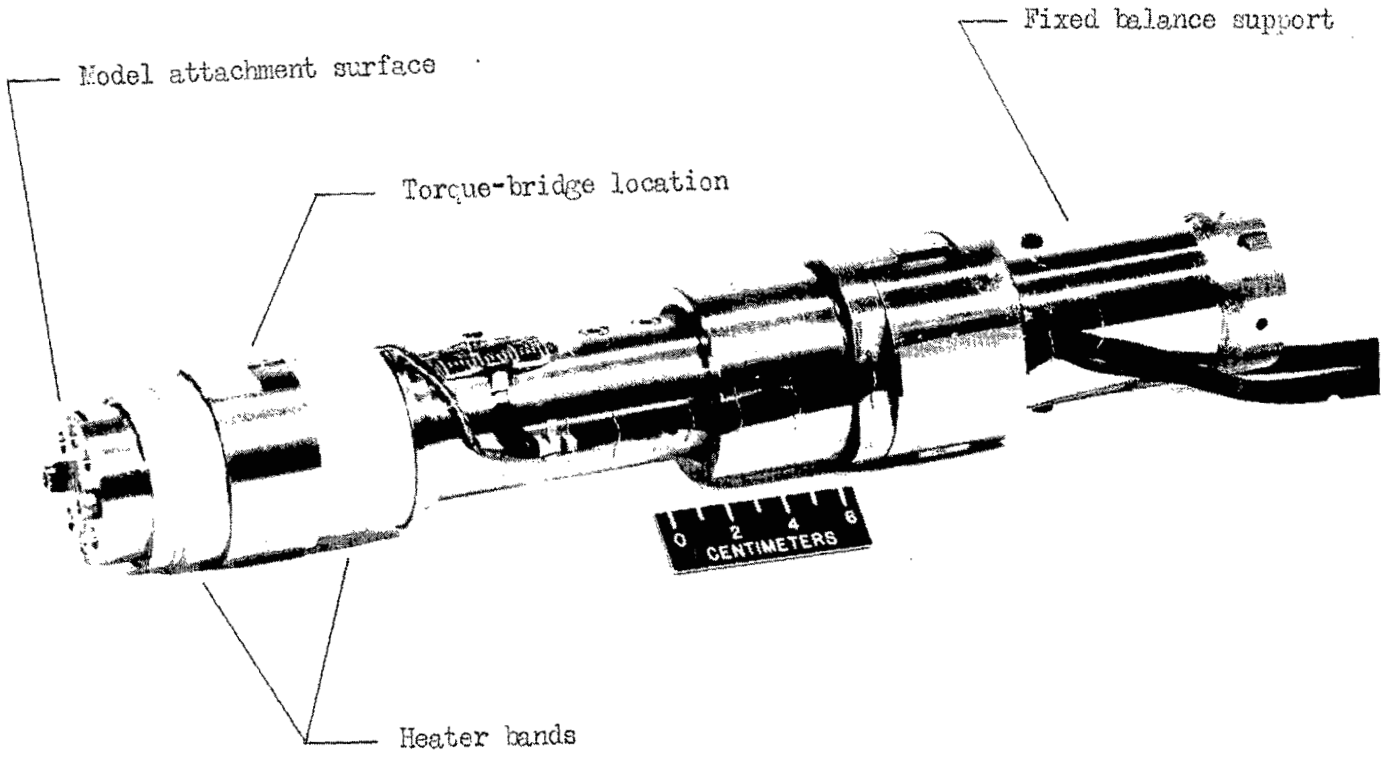

(b) Roll balance.

Figure 5.- Concluded.

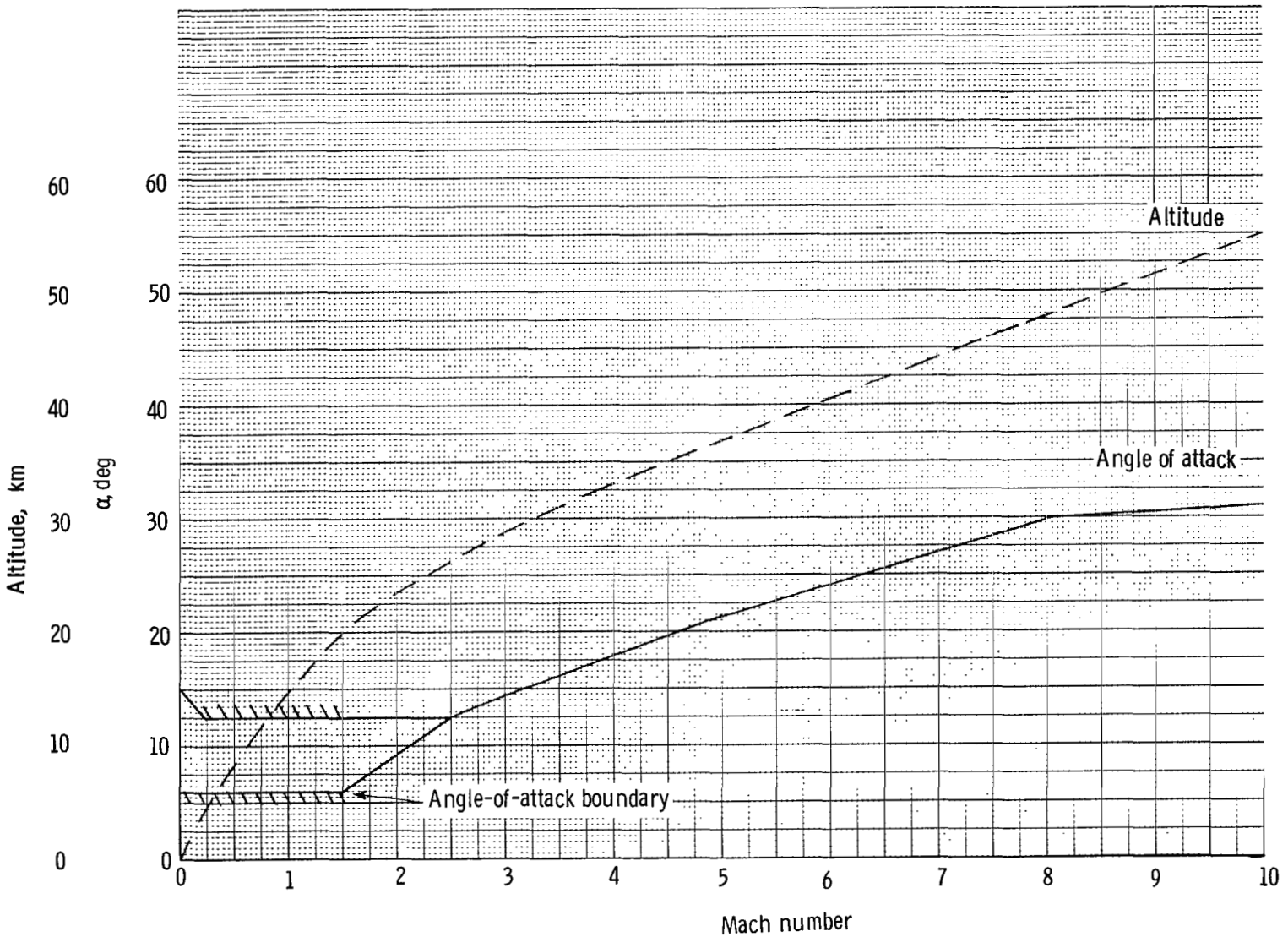

Figure 6.- Shuttle entry flight profile (forward c.g.).

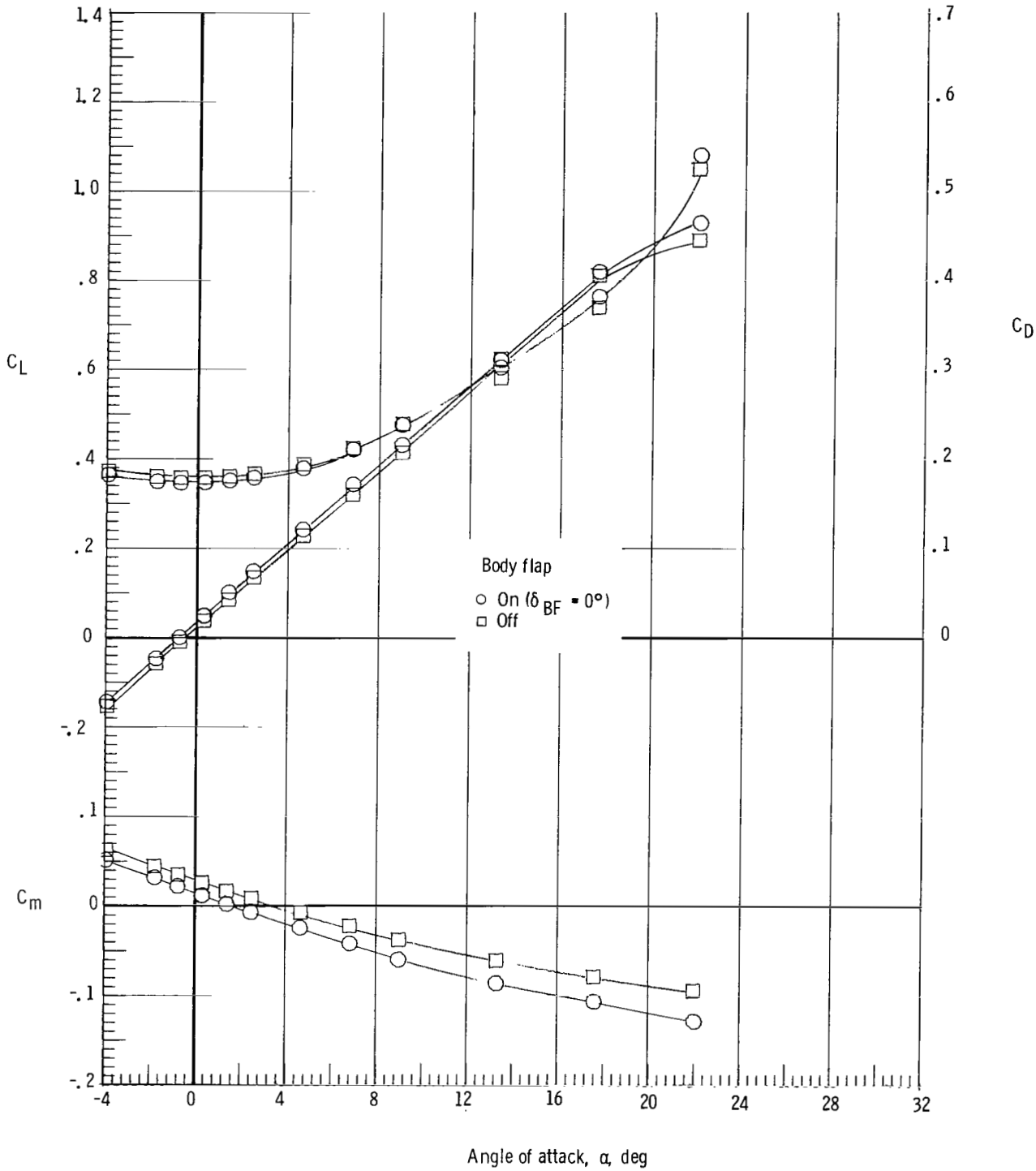

(a) M = 1.60.

Figure 7.- Effect of body flap on the static longitudinal characteristics of the model. Forward c.g.; $\delta_e = 0^o$; rudder flare, 40^o; and $\delta_{BF} = 0^o$.

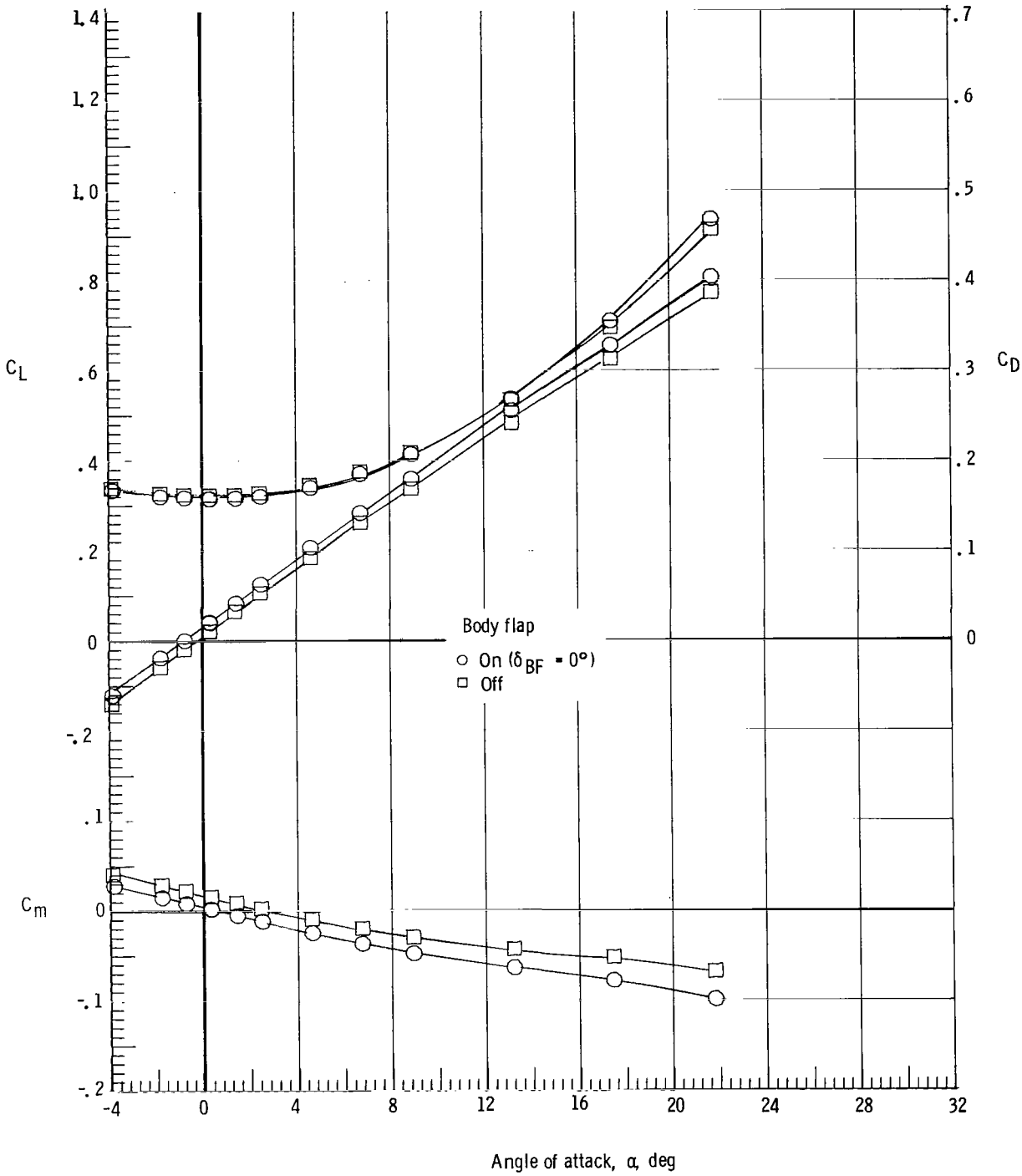

(b) M = 1.90.

Figure 7.- Continued.

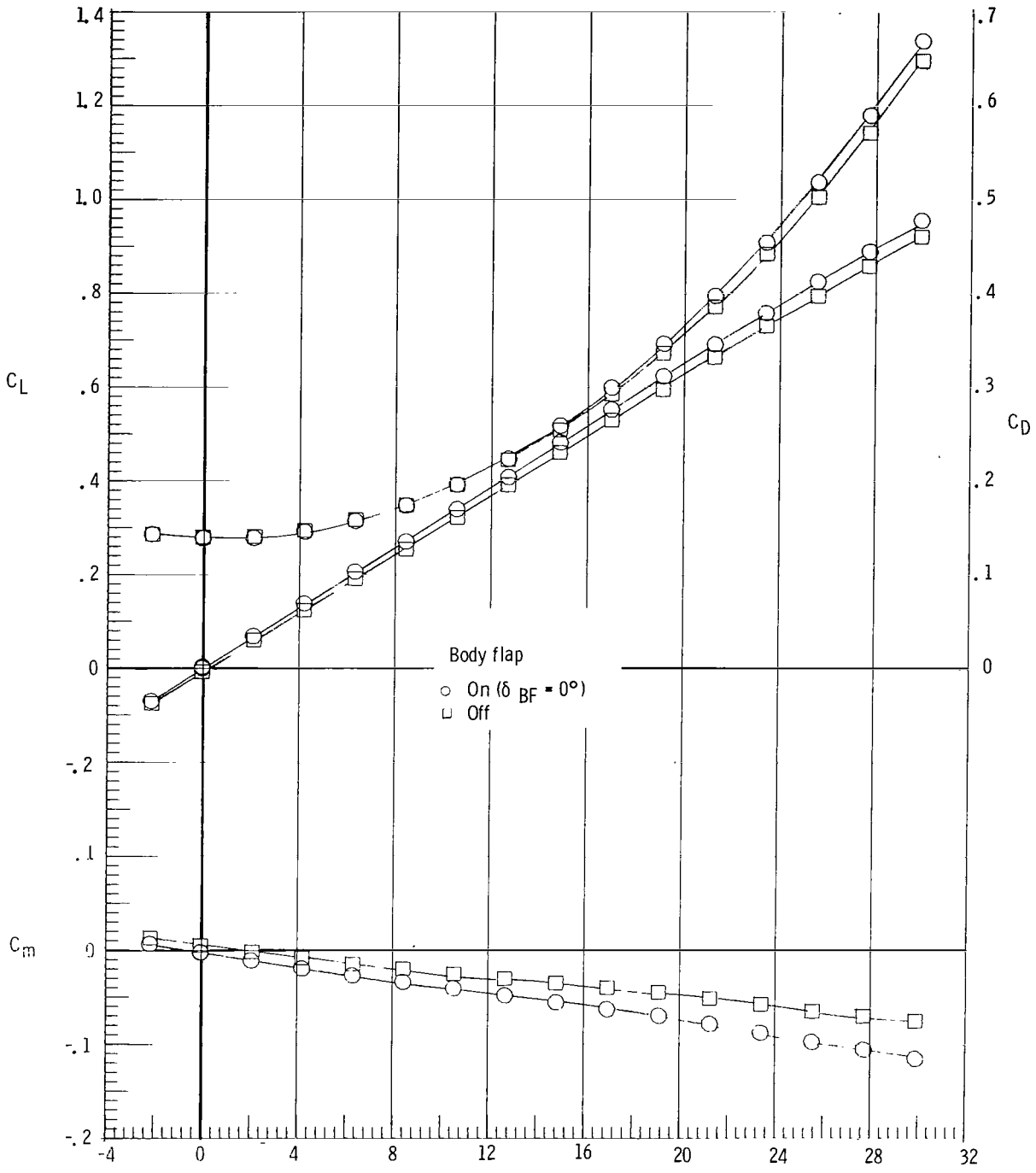

(c) M = 2.36.

Figure 7.- Continued.

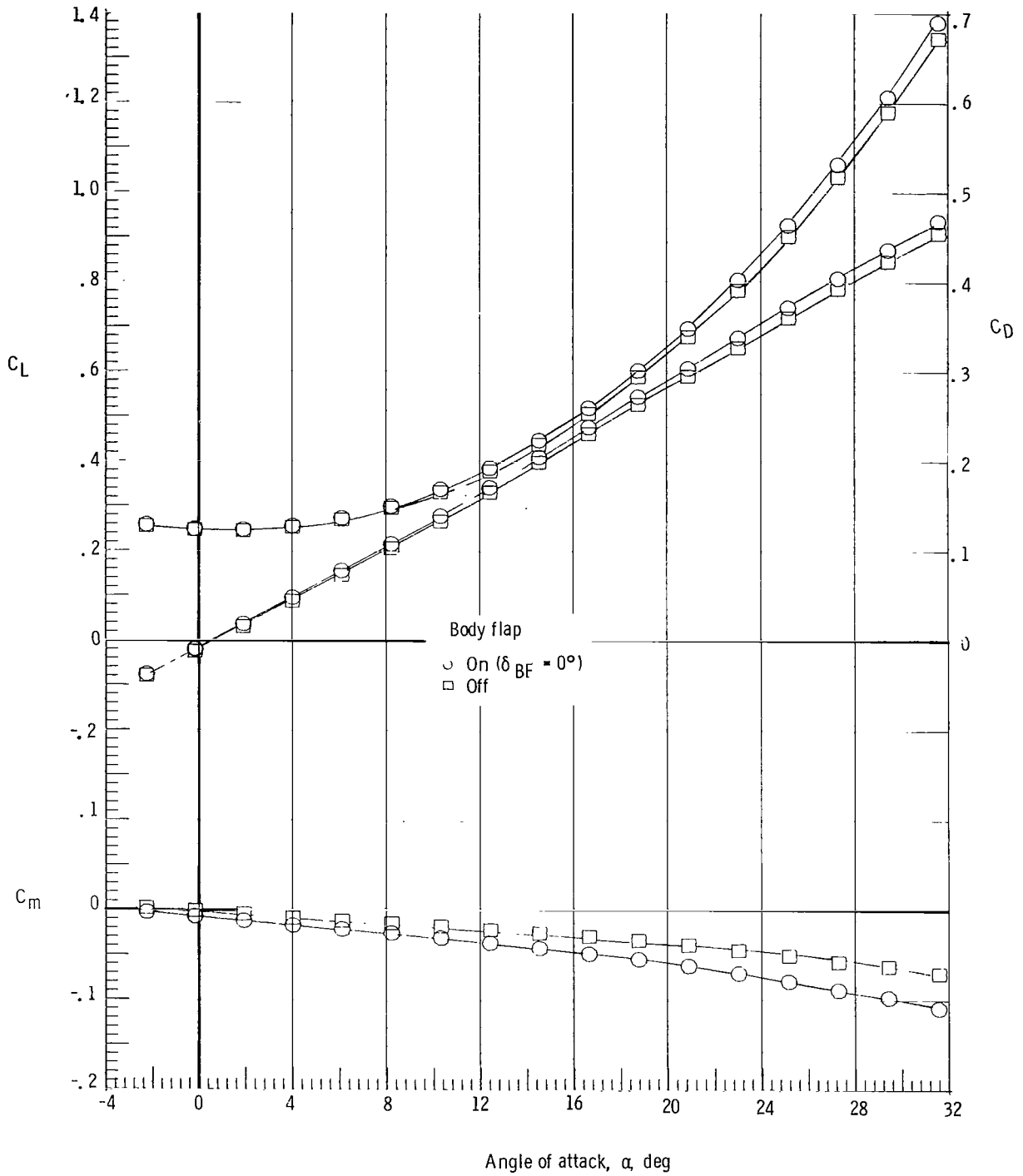

(d) M = 2.86.

Figure 7.- Continued.

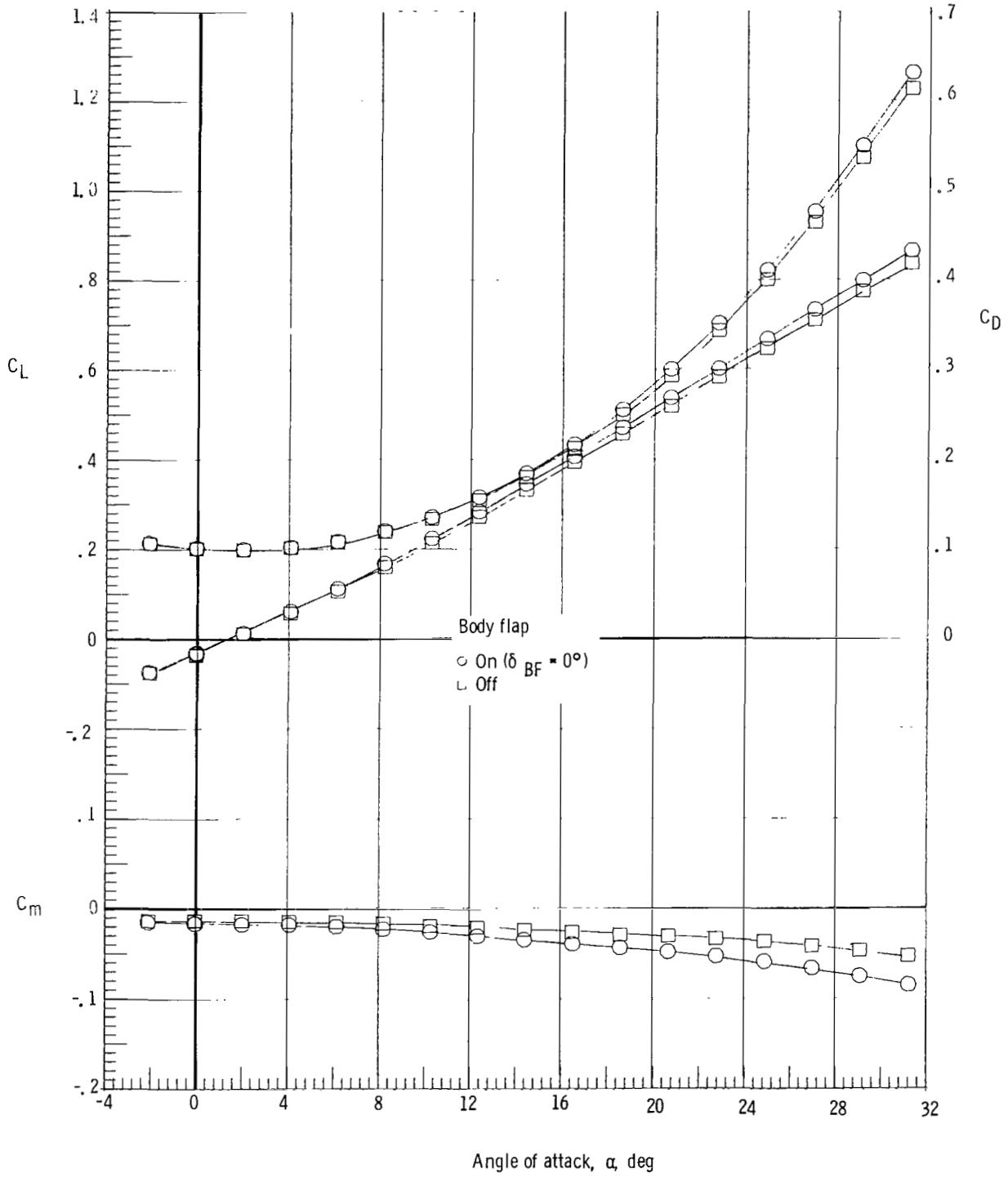

(e) M = 3.96.

Figure 7.- Continued.

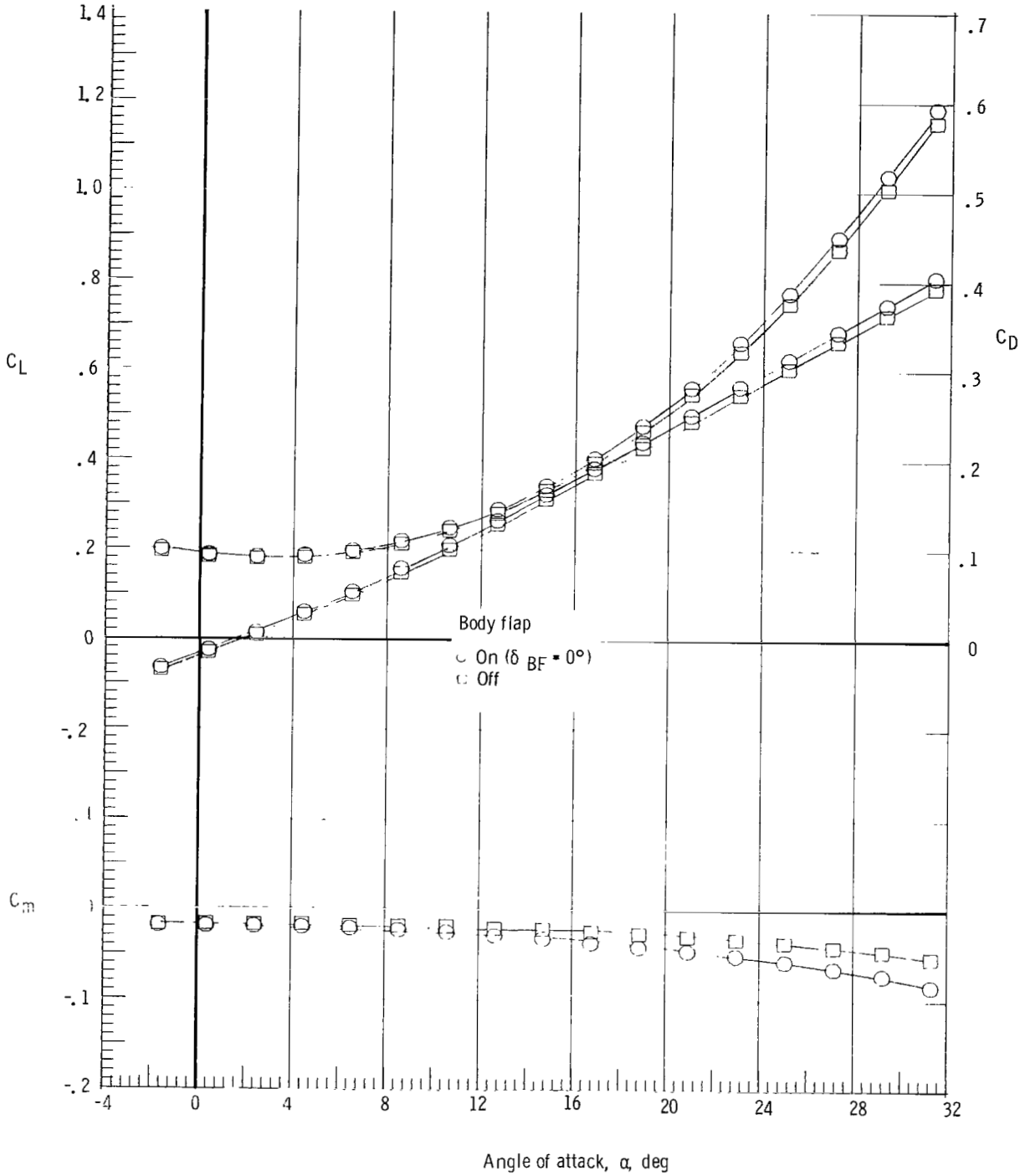

(f) M = 4.63.

Figure 7.- Concluded.

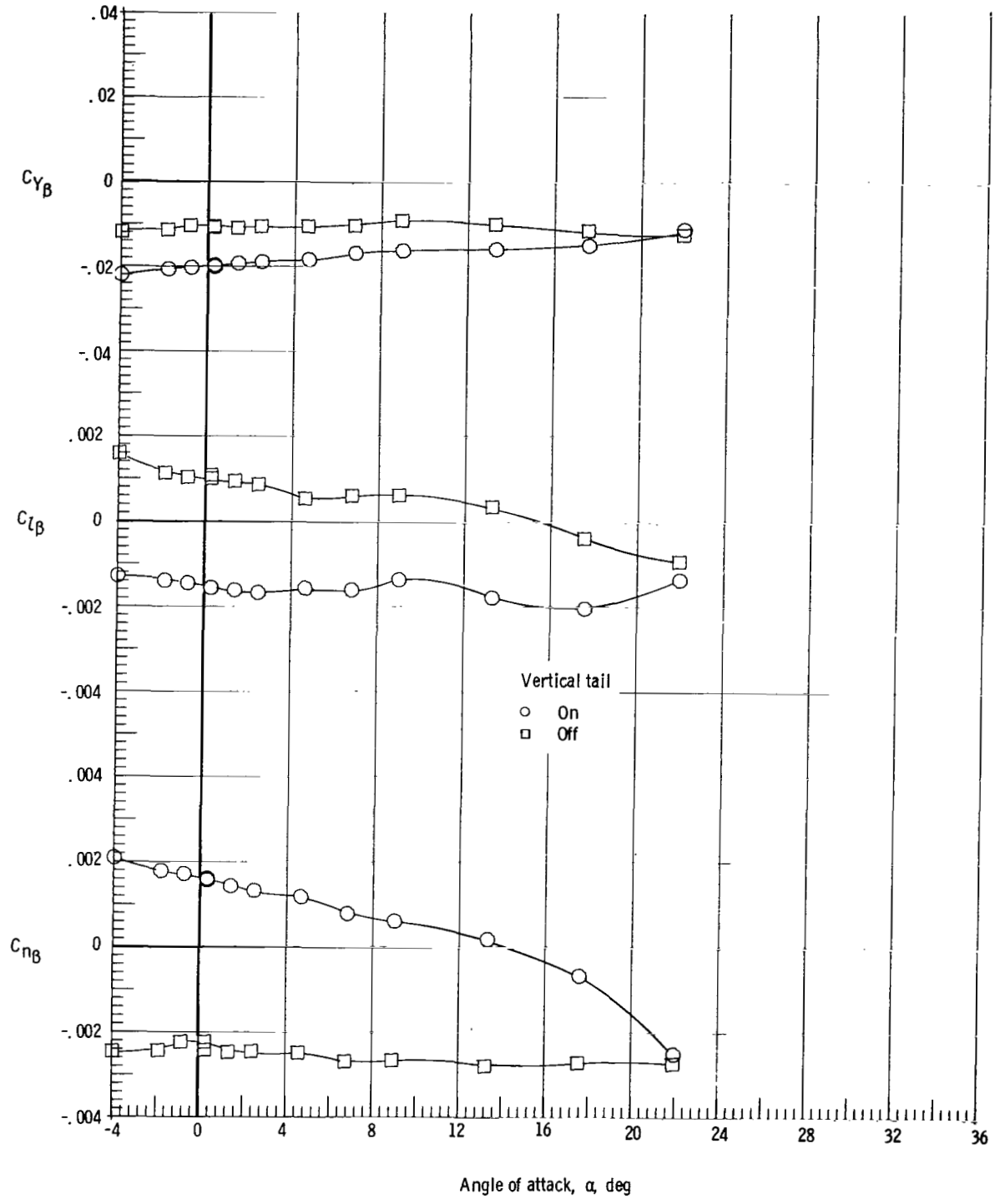

(a) M = 1.60.

Figure 8.- Effect of vertical tail on the static lateral characteristics of the model. Forward c.g.; $\delta_e = 0^o$; rudder flare, 40^o; and $\delta_{BF} = 0^o$.

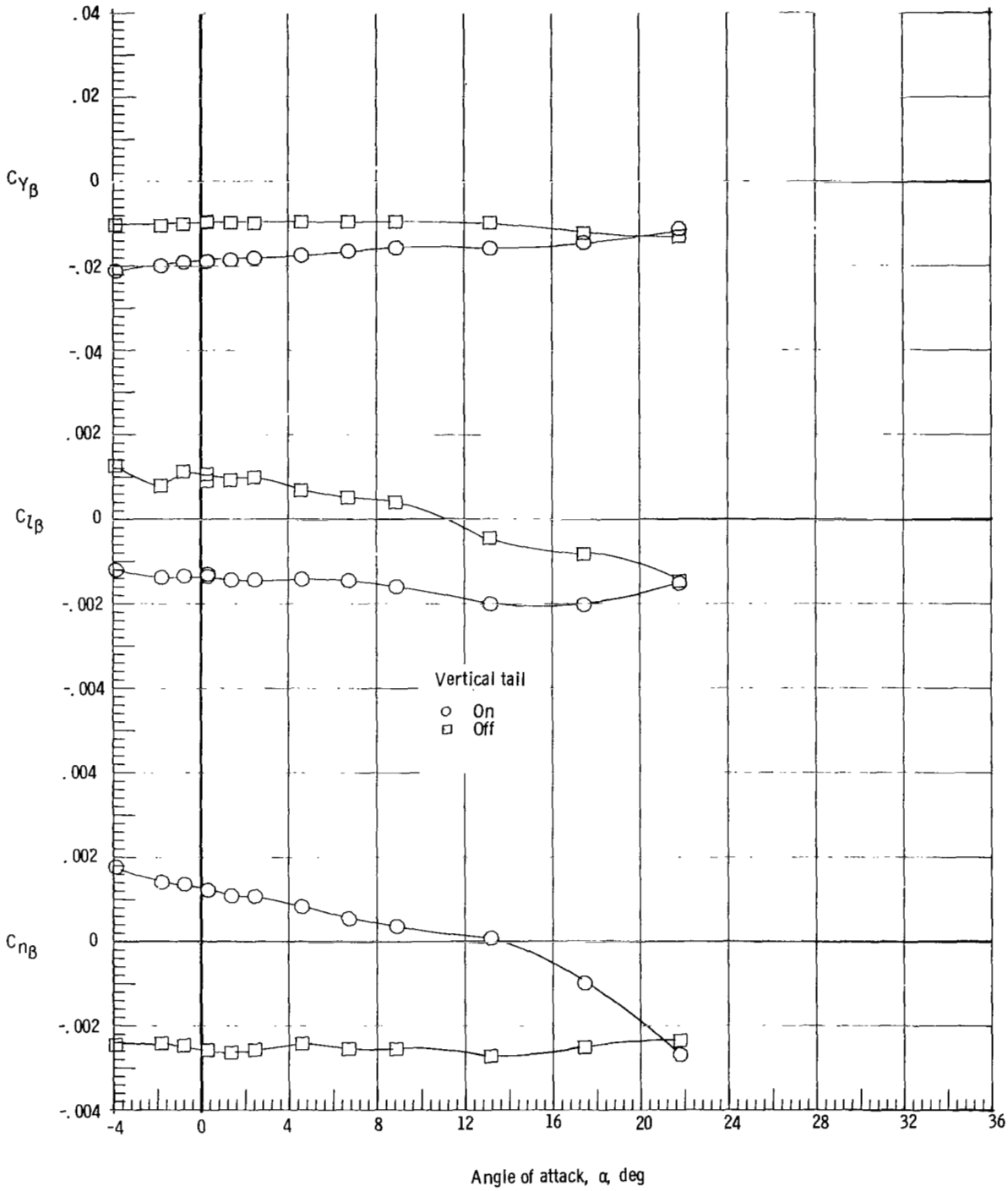

(b) M = 1.90.

Figure 8.- Continued.

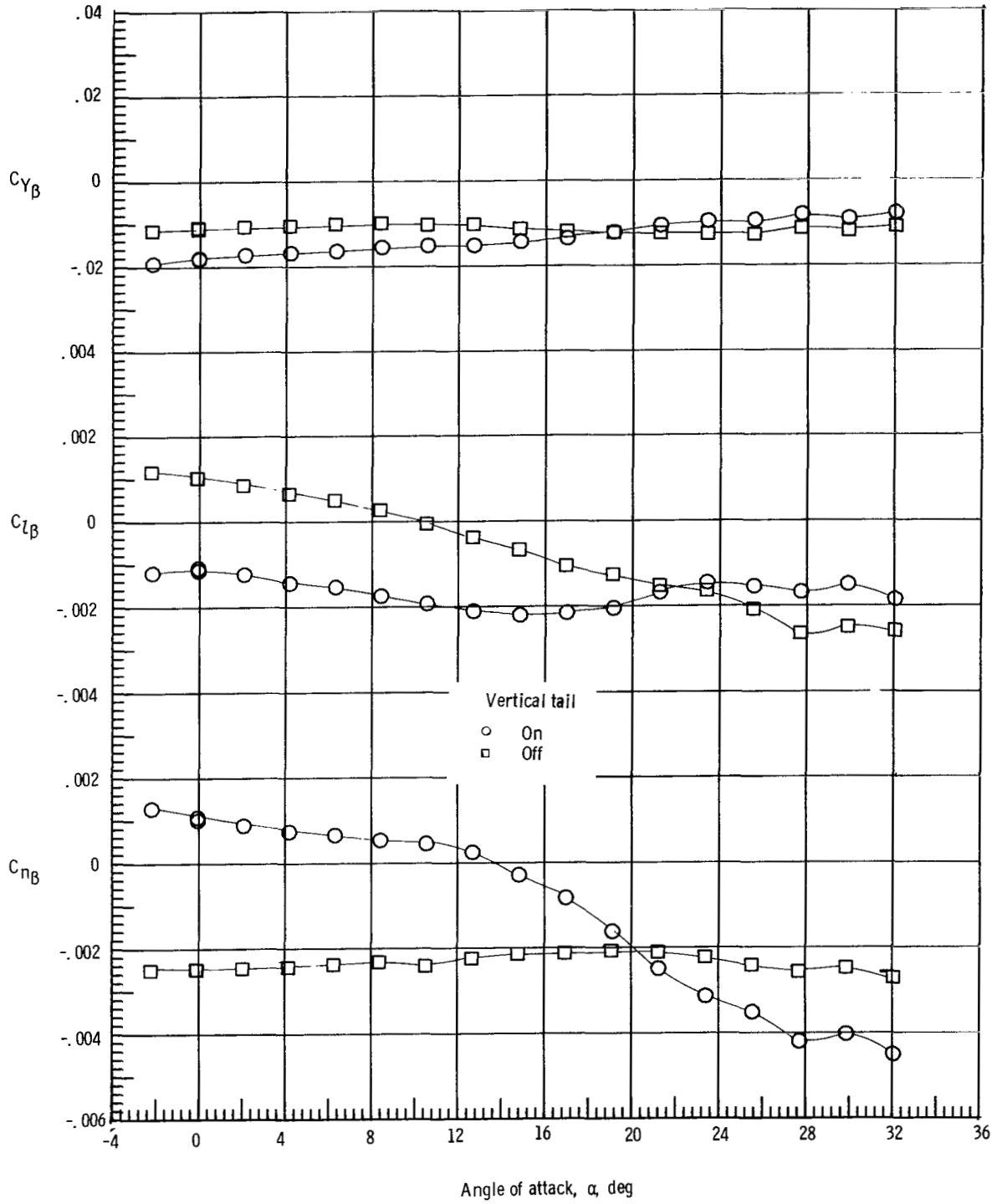

(c) M = 2.36.

Figure 8.- Continued.

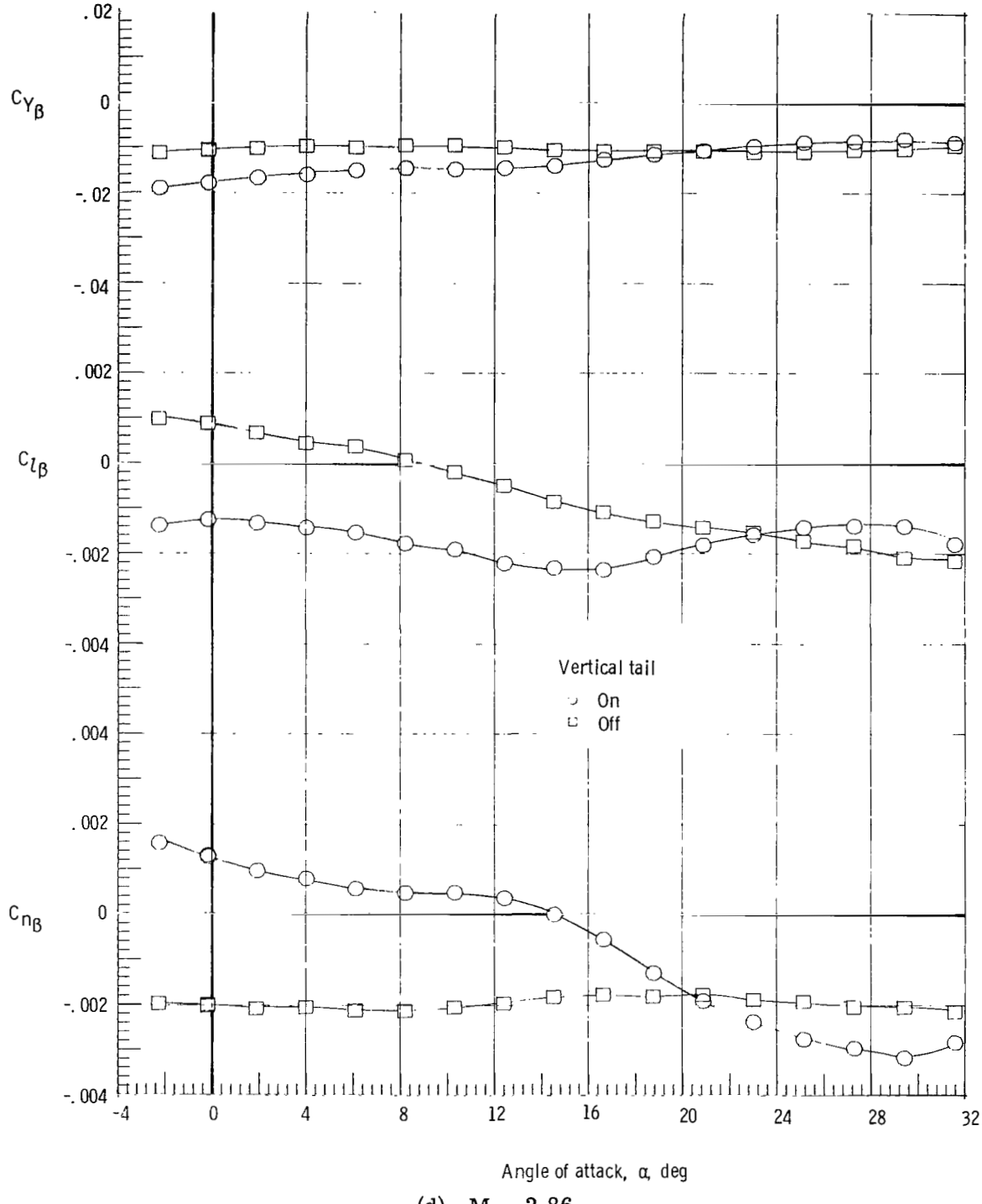

(d) M = 2.86.

Figure 8.- Continued.

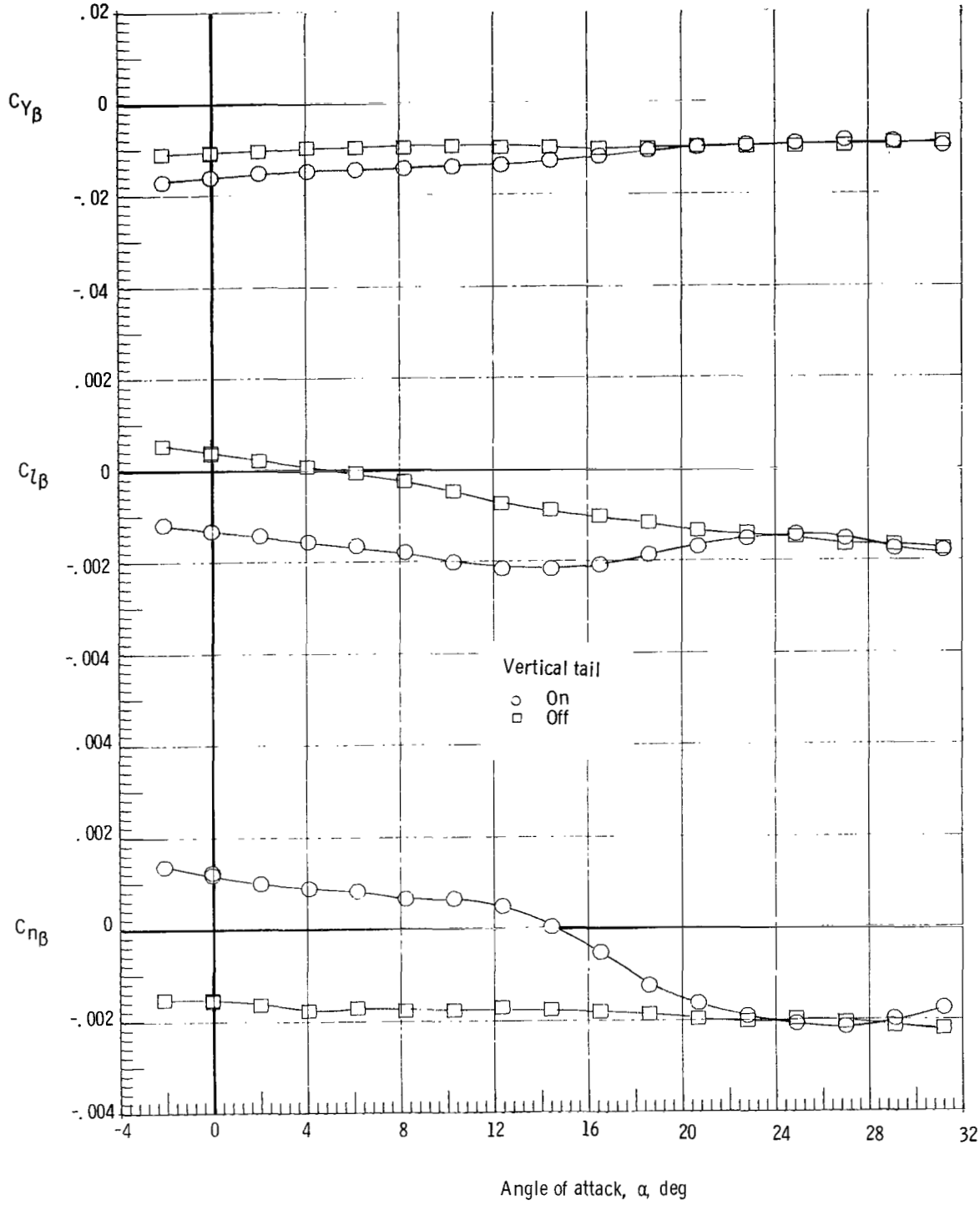

(e) M = 3.96.

Figure 8.- Continued.

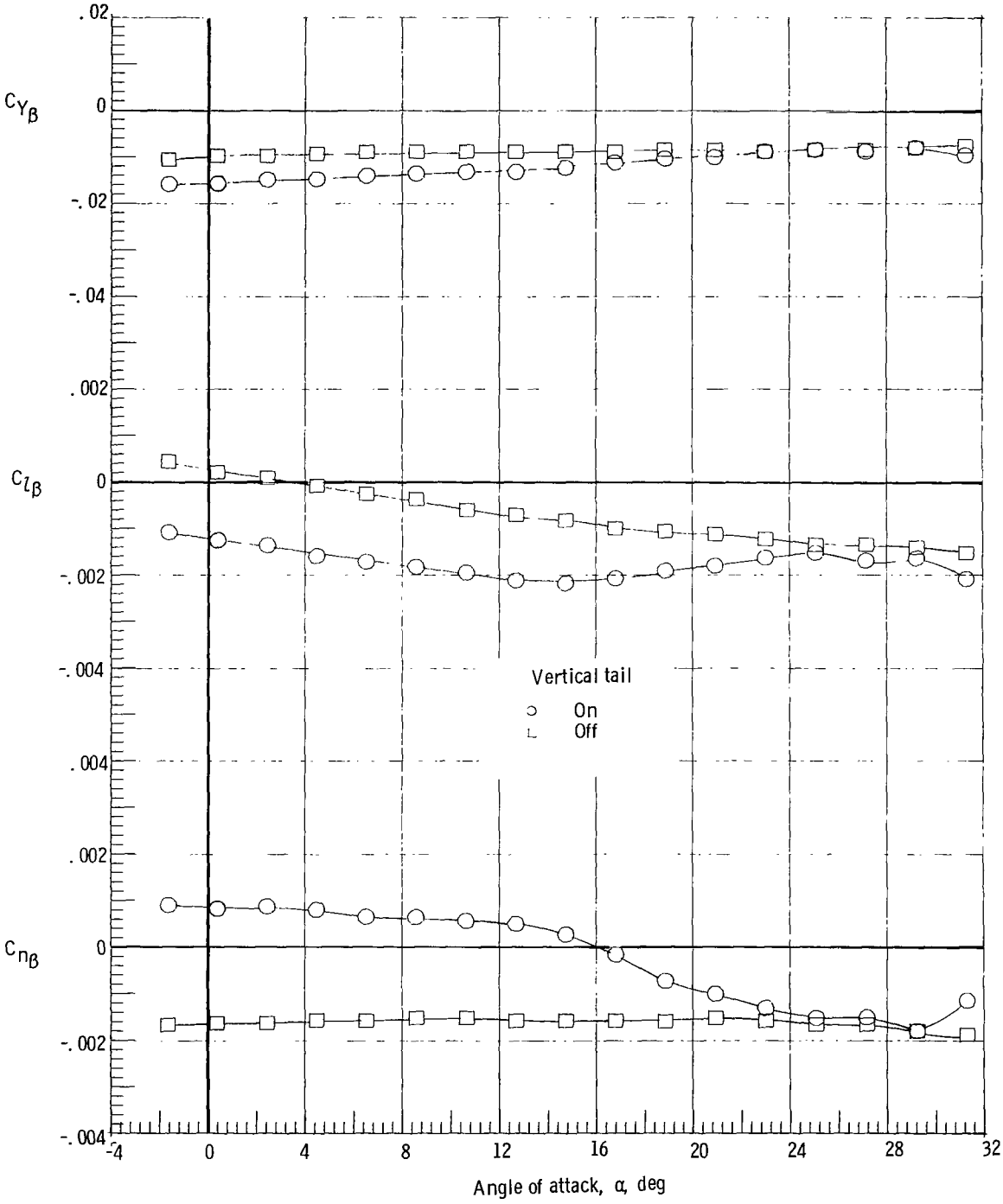

(f) M = 4.63.

Figure 8.- Concluded.

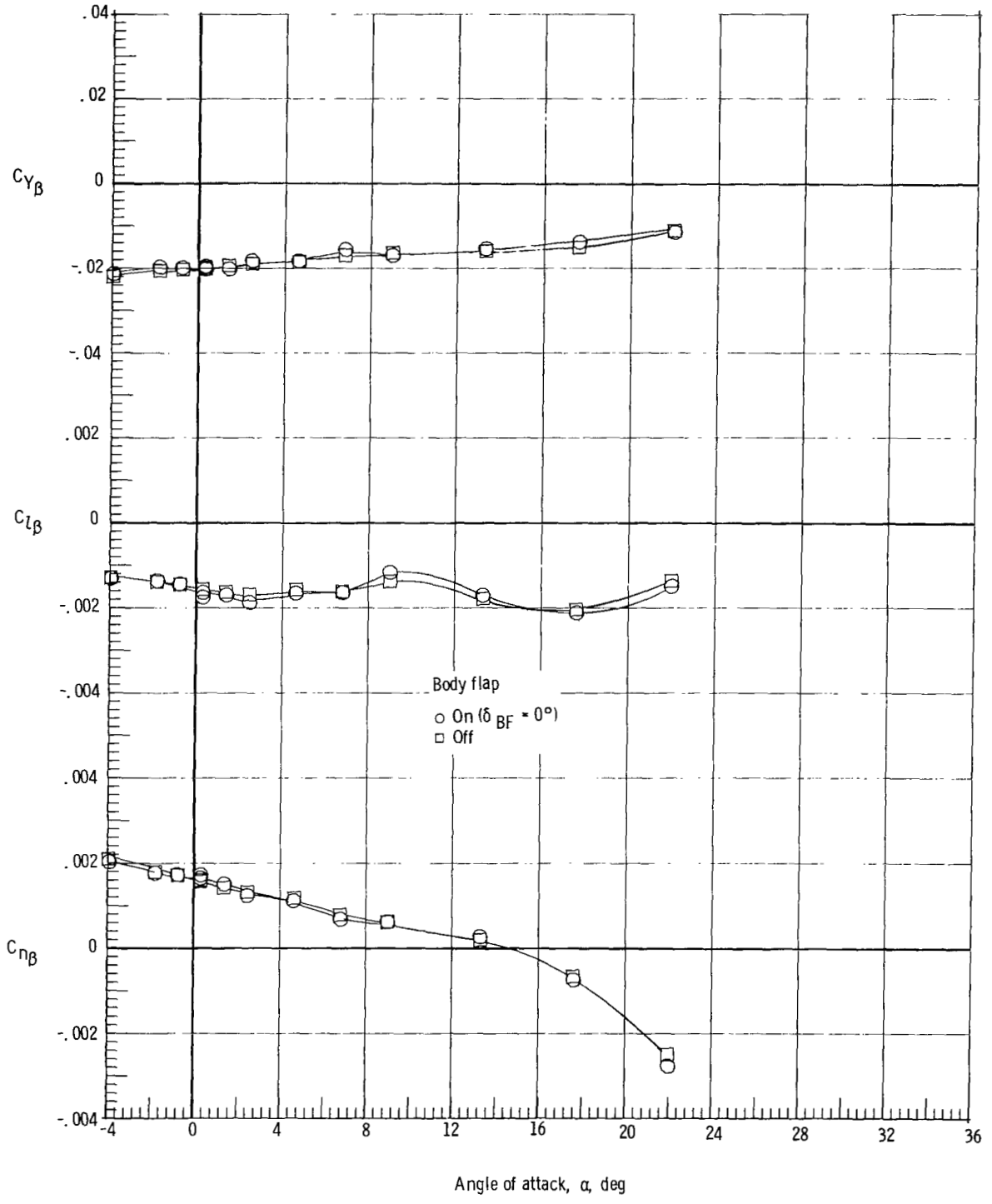

(a) M = 1.60.

Figure 9.- Effect of body flap on the static lateral characteristics of the model. Forward c.g.; $\delta_e = 0^o$; rudder flare, 40^o; and $\delta_{BF} = 0^o$.

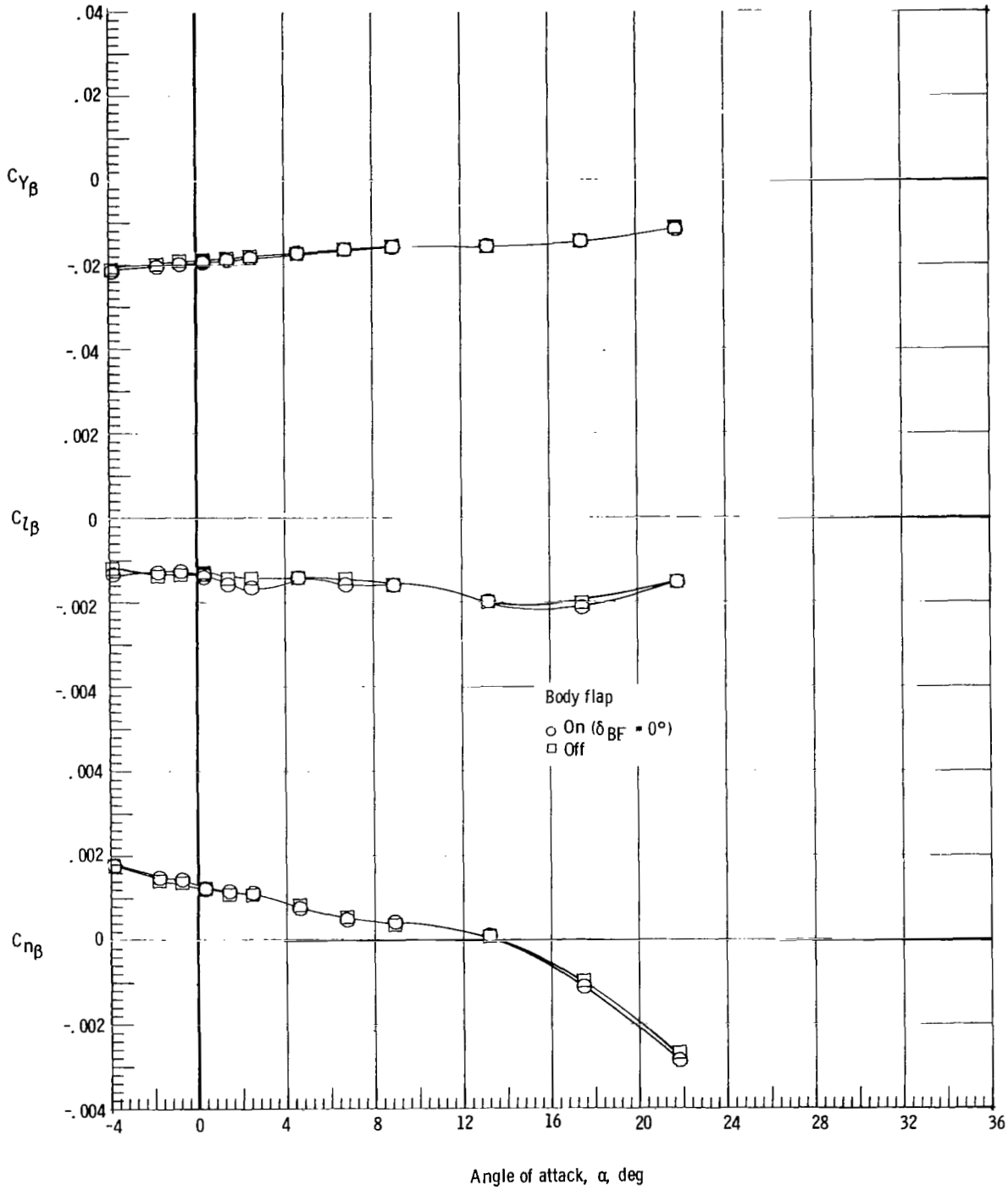

(b) M = 1.90.

Figure 9.- Continued.

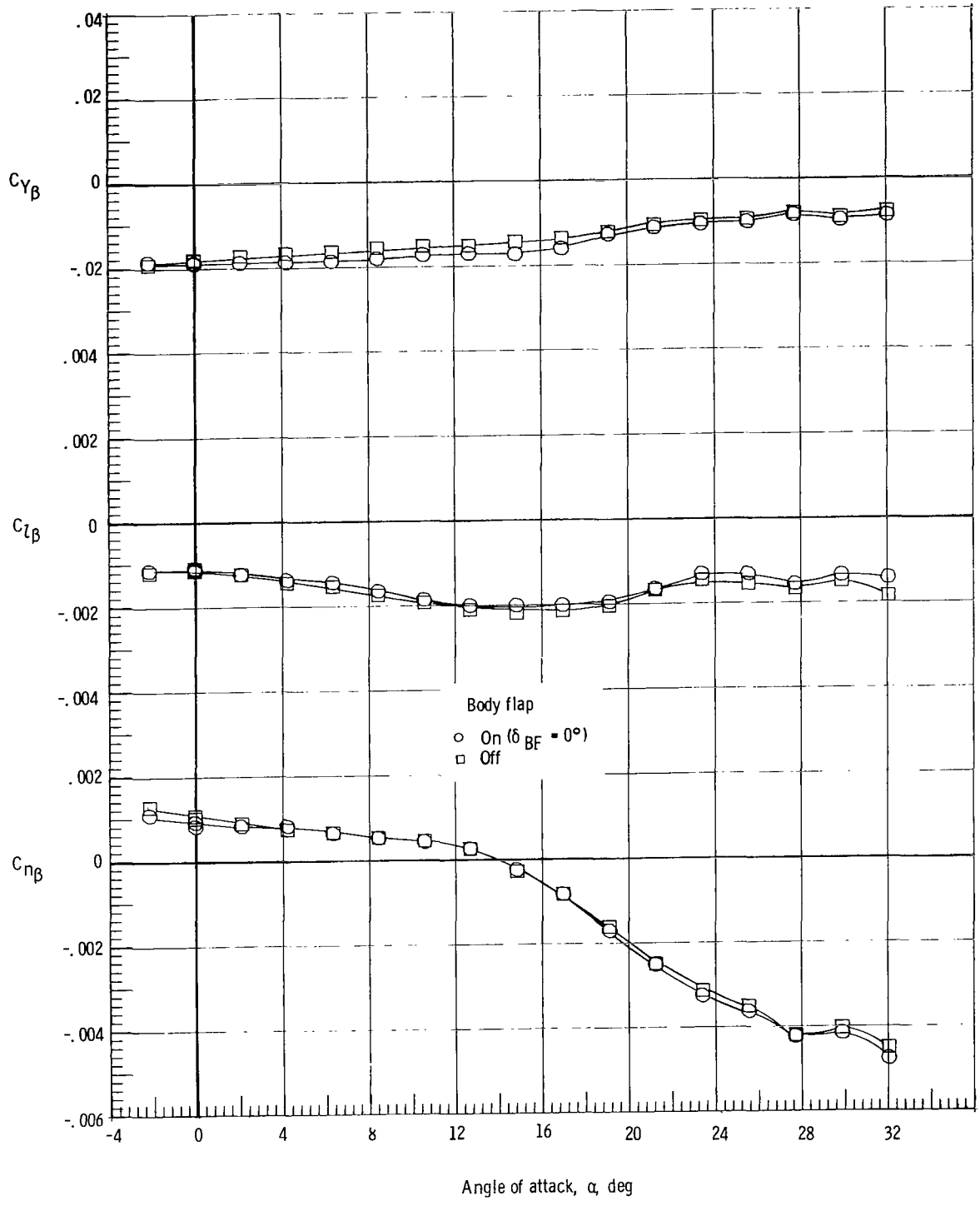

(c) M = 2.36.

Figure 9.- Continued.

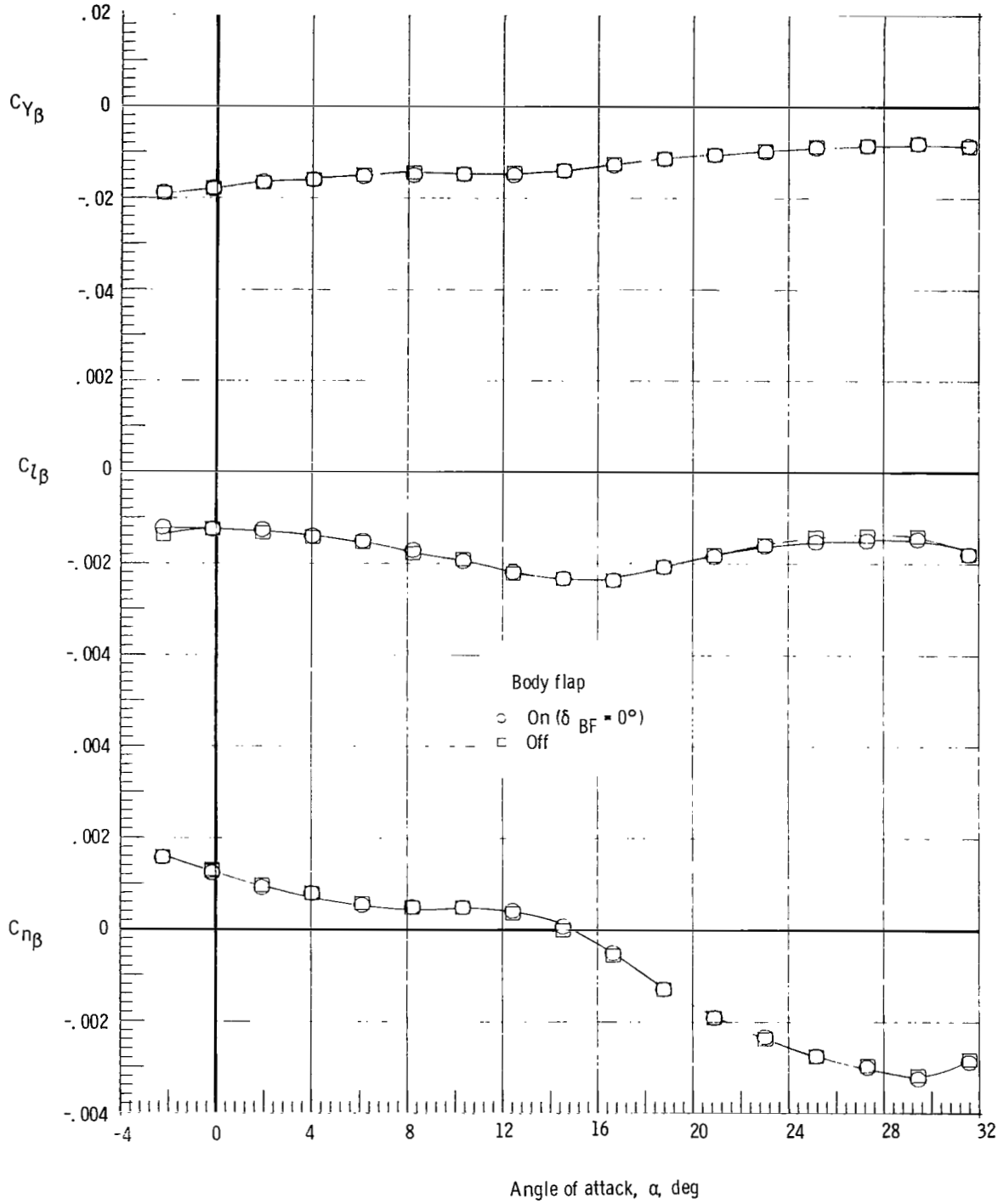

(d) M = 2.86.

Figure 9.- Continued.

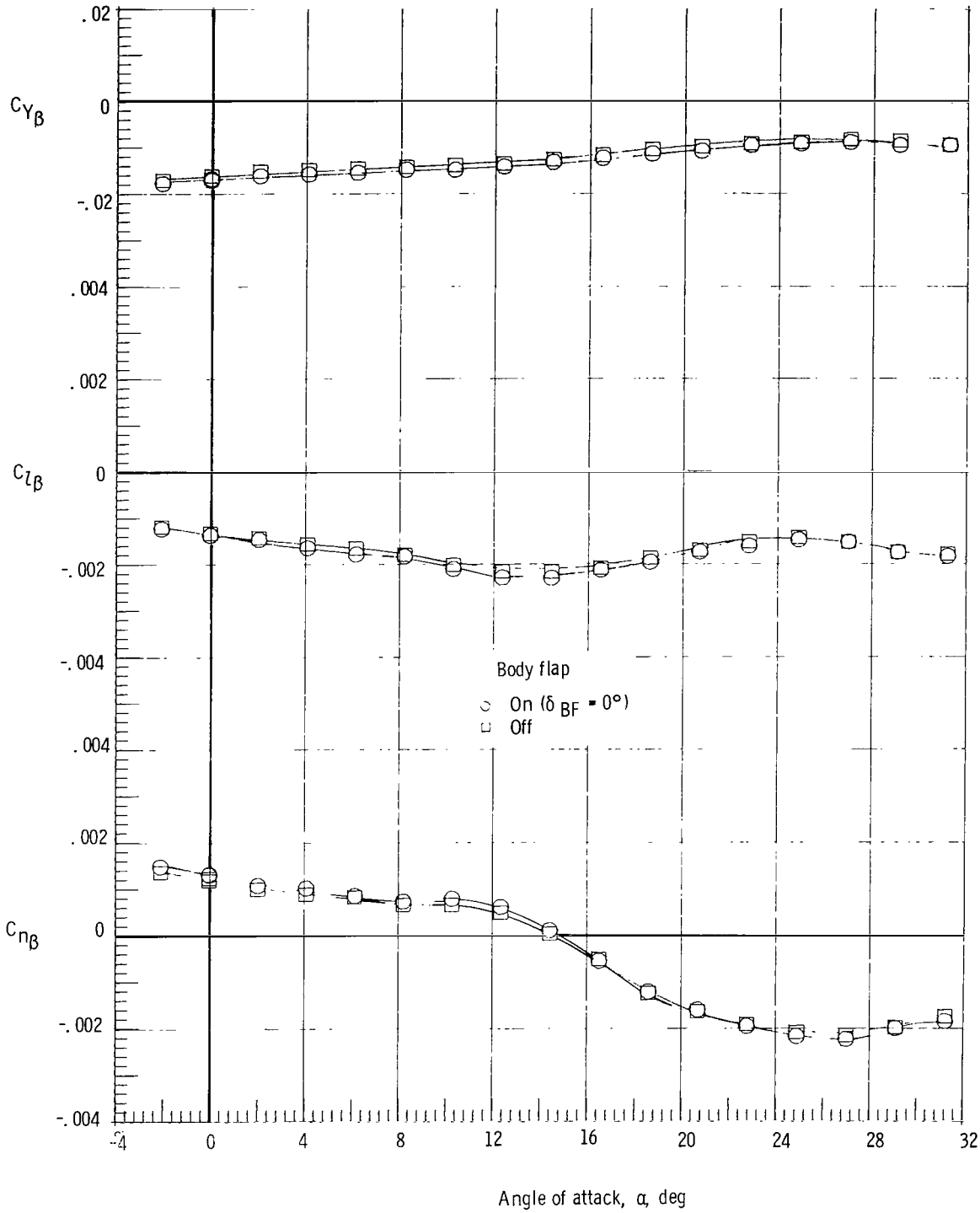

(e) M = 3.96.

Figure 9.- Continued.

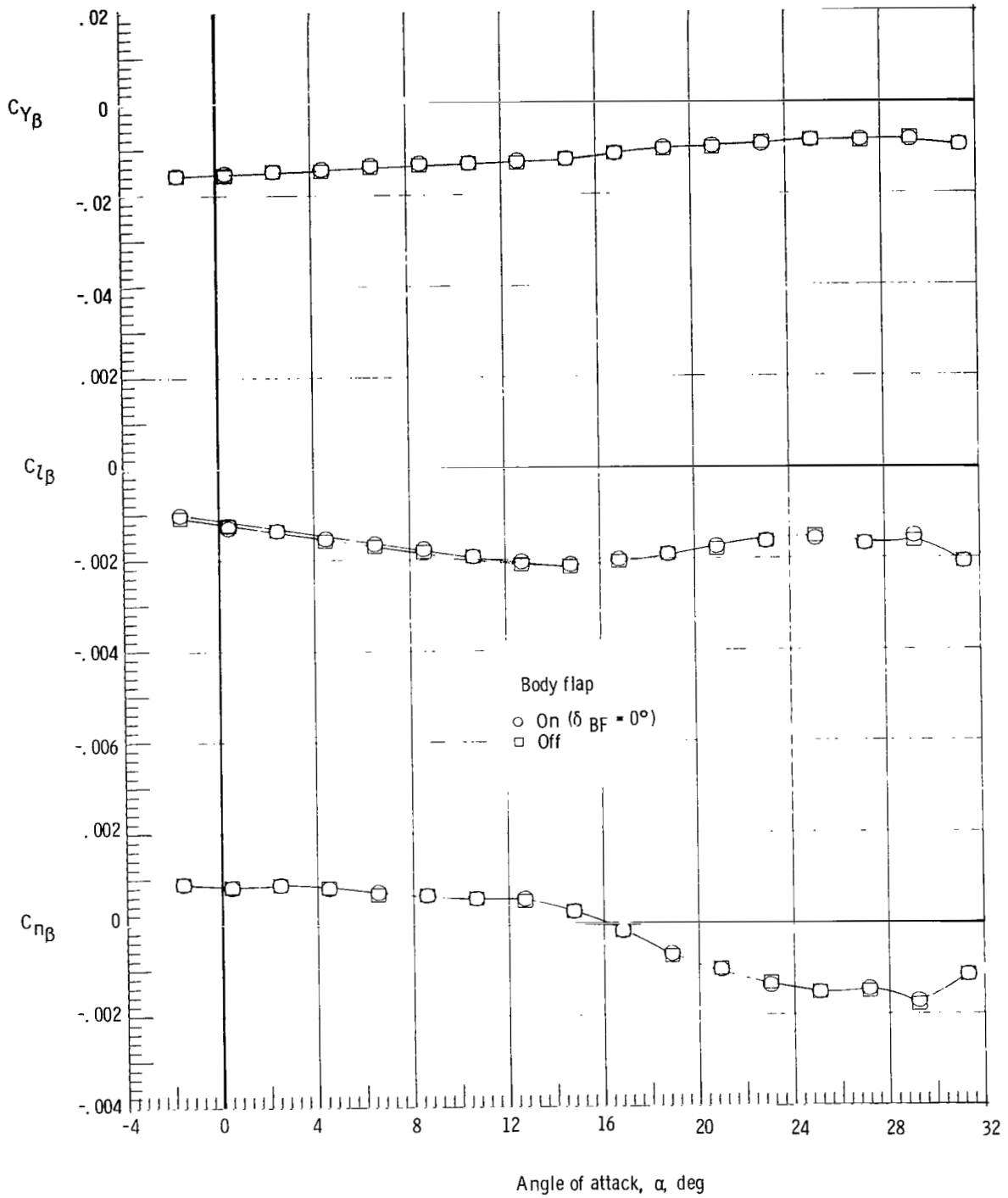

(f) M = 4.63.

Figure 9.- Concluded.

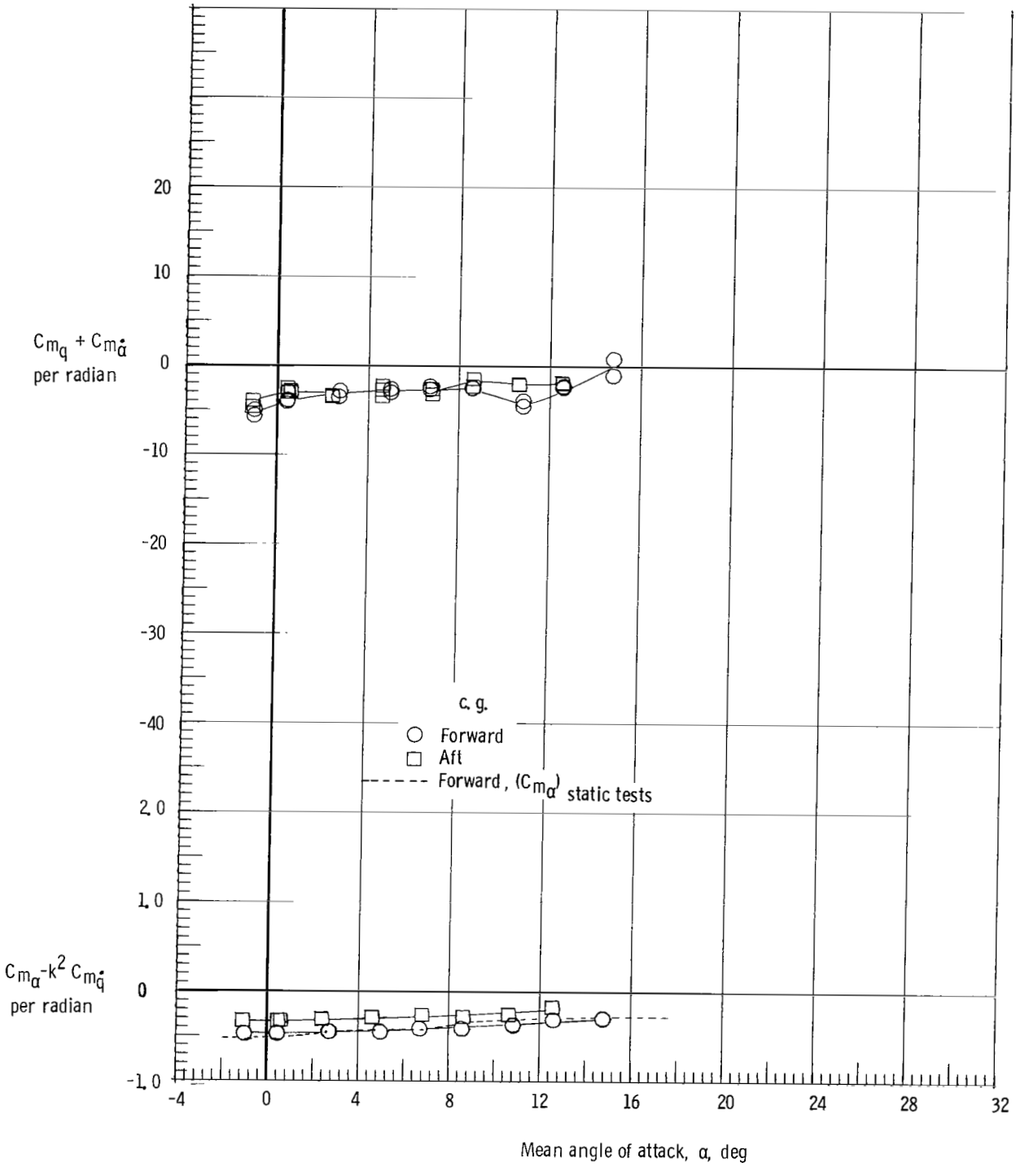

(a) M = 1.60.

Figure 10.- Effect of center-of-gravity (c.g.) position on damping-in-pitch parameter and on oscillatory stability-in-pitch parameter. $\delta_e = 0^o$; rudder flare, 40^o; and $\delta_{BF} = 0^o$.

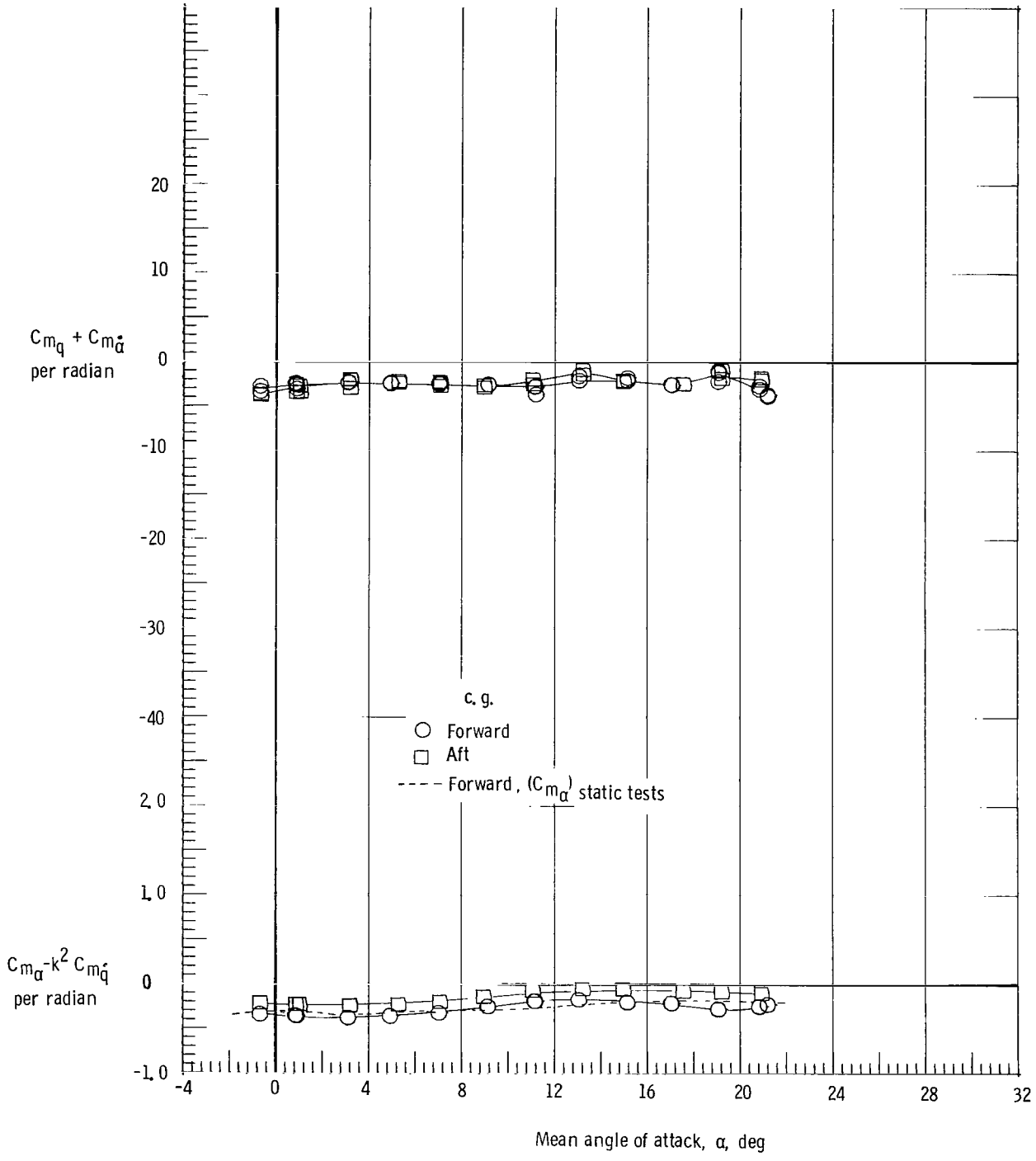

(b) M = 1.90.

Figure 10.- Continued.

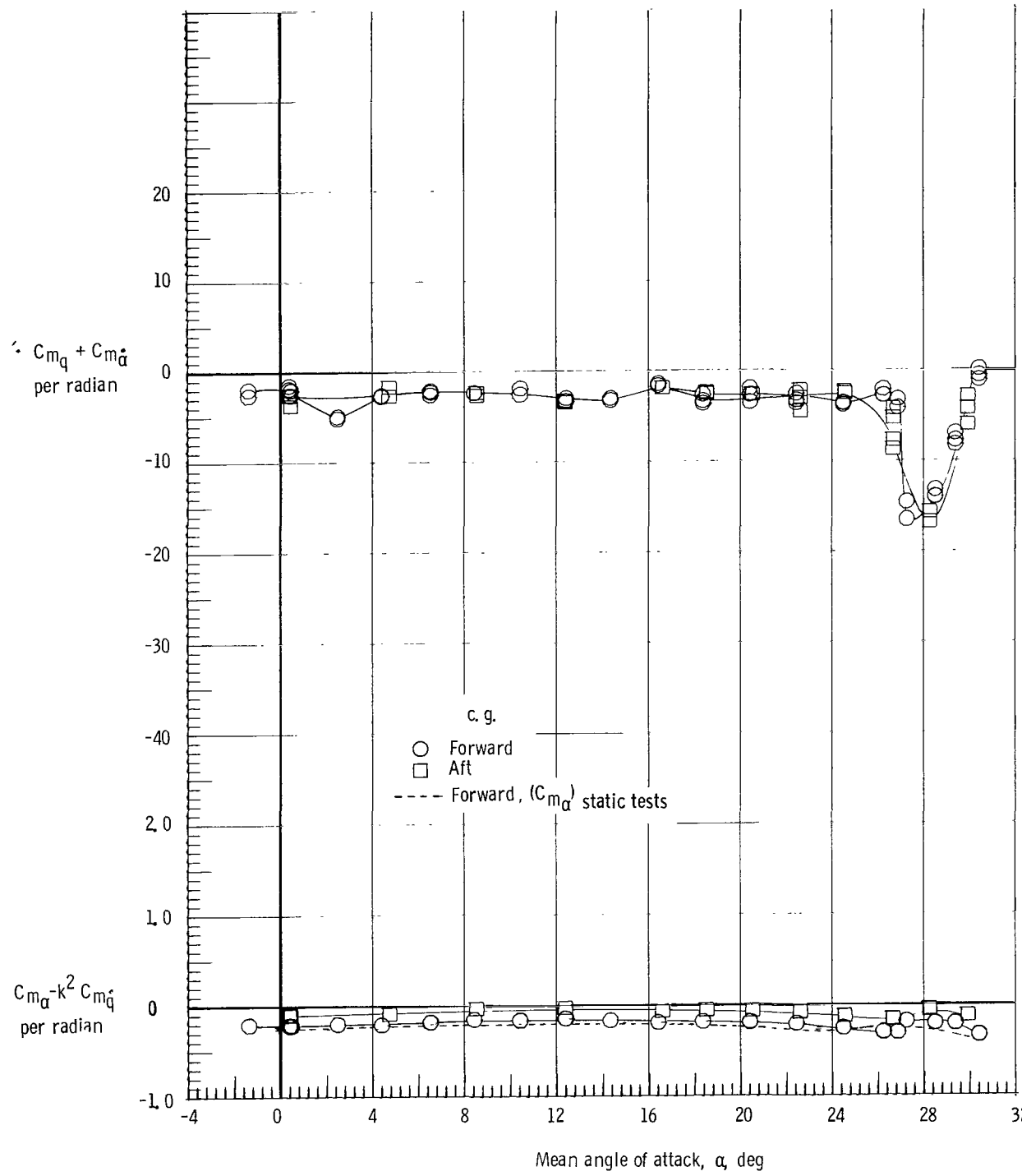

(c) M = 2.36.

Figure 10.- Continued.

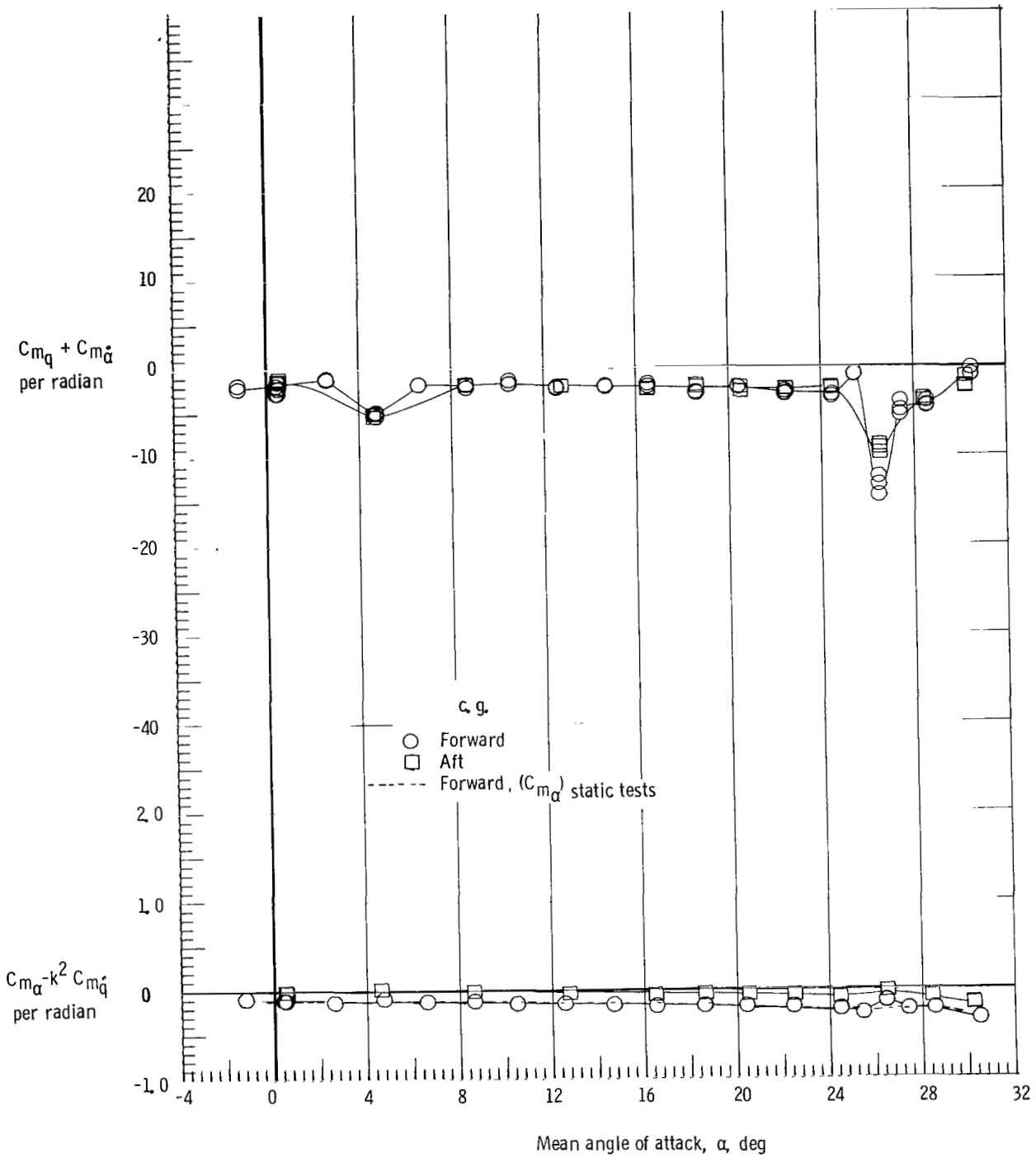

(d) M = 2.86.

Figure 10.- Continued.

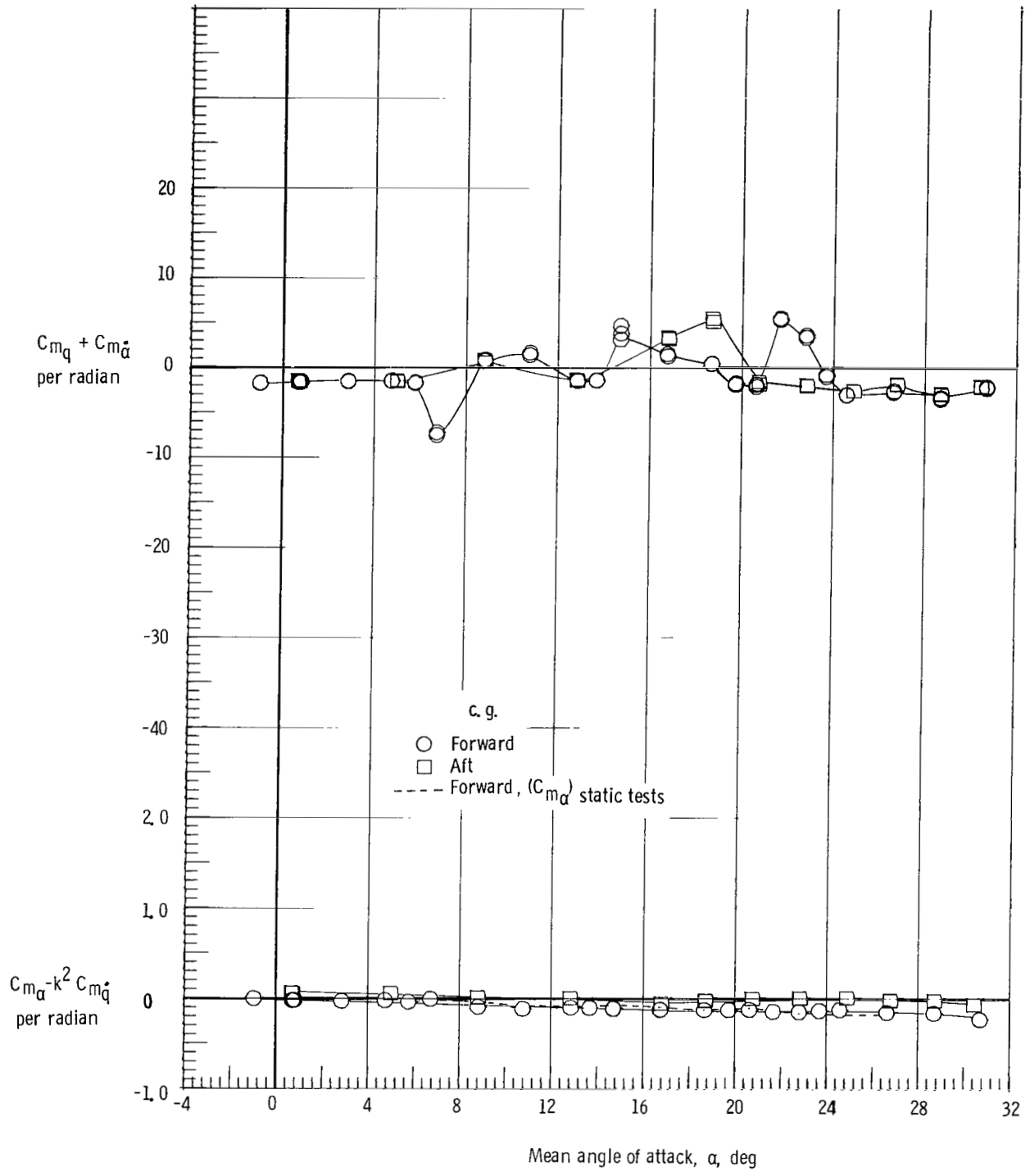

(e) M = 3.96.

Figure 10.- Continued.

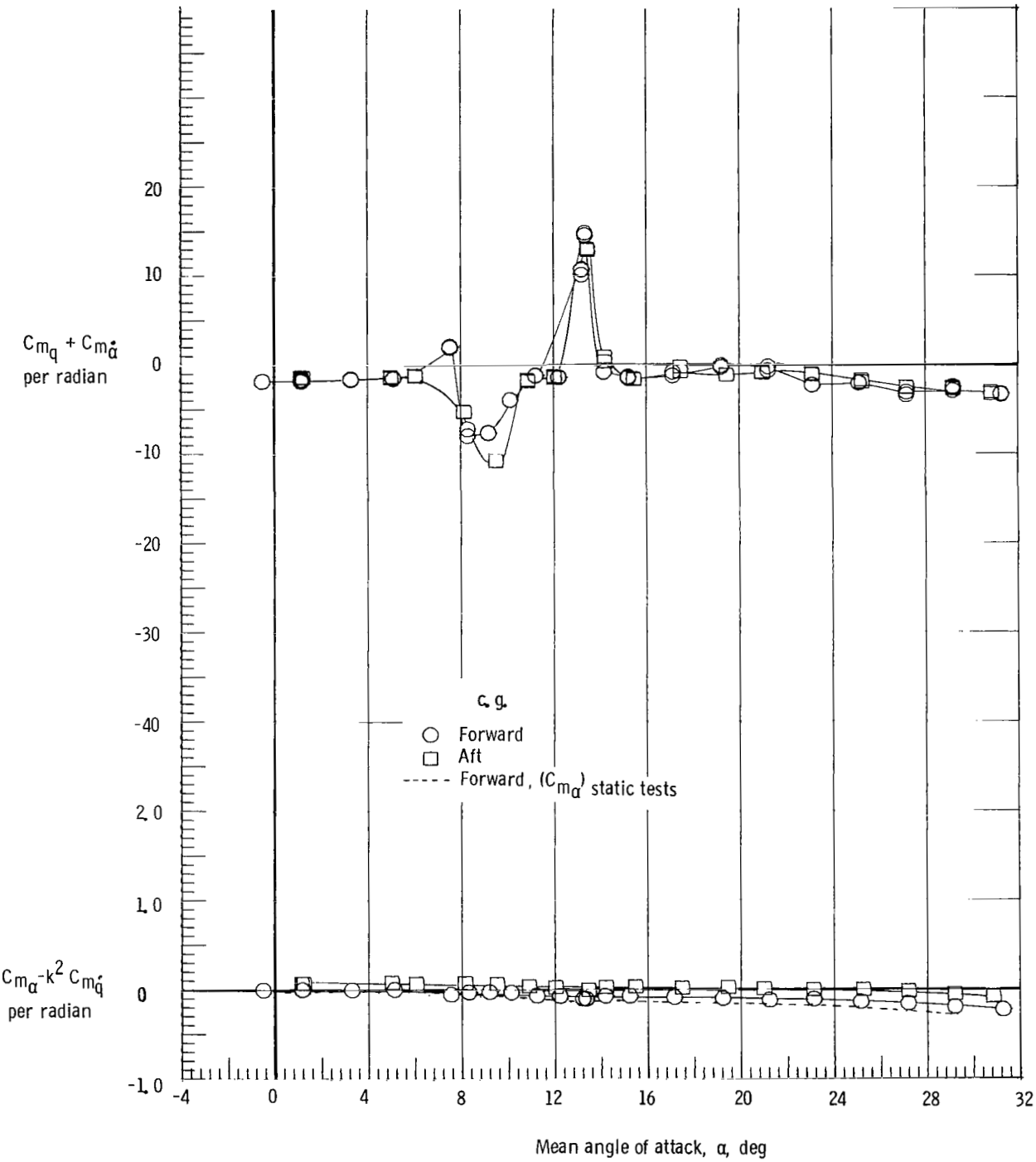

(f) M = 4.63.

Figure 10.- Concluded.

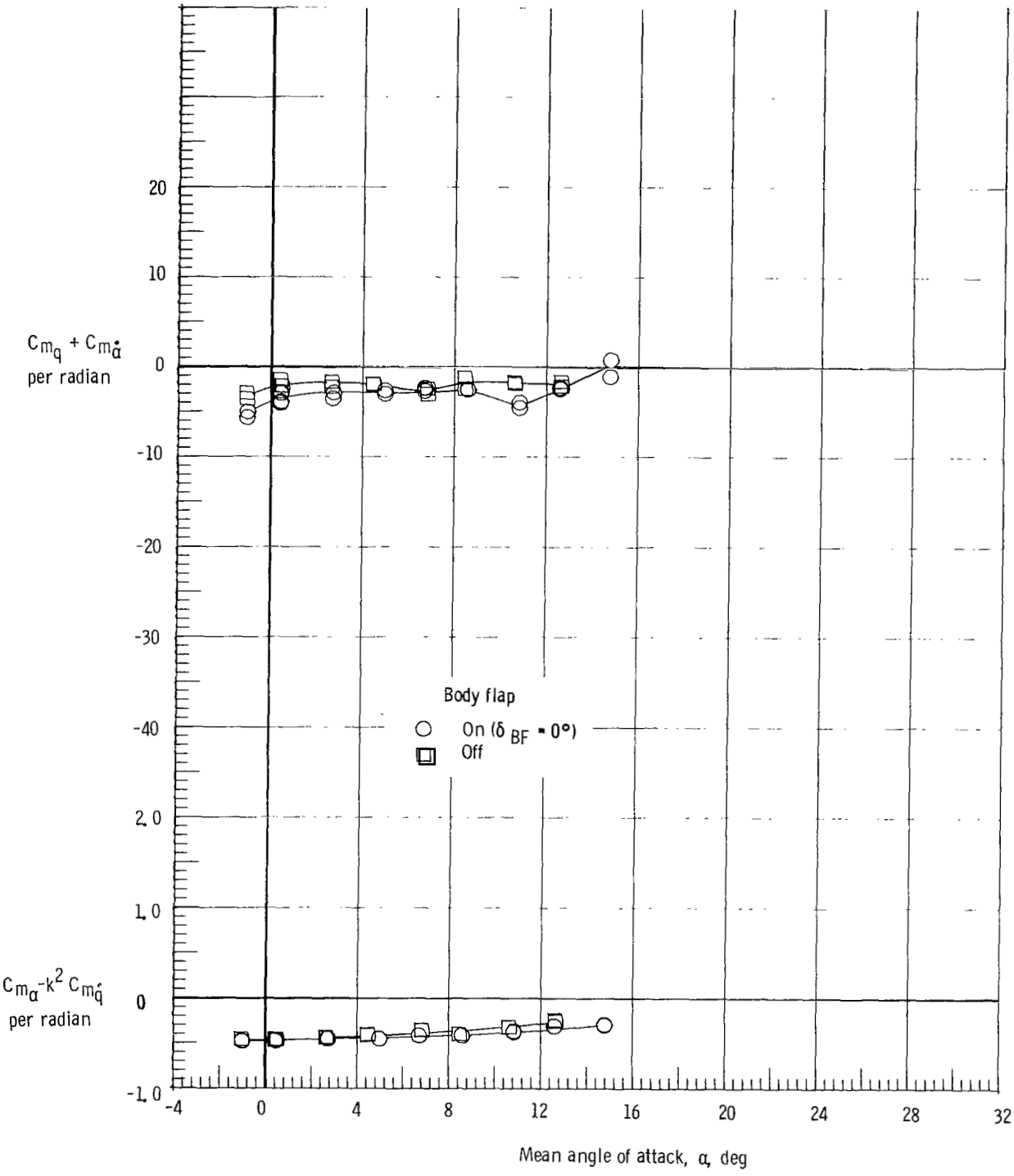

(a) M = 1.60.

Figure 11.- Effect of body flap on damping-in-pitch parameter and on oscillatory stability-in-pitch parameter. Forward c.g.; $\delta_e = 0^o$; and rudder flare, 40^o.

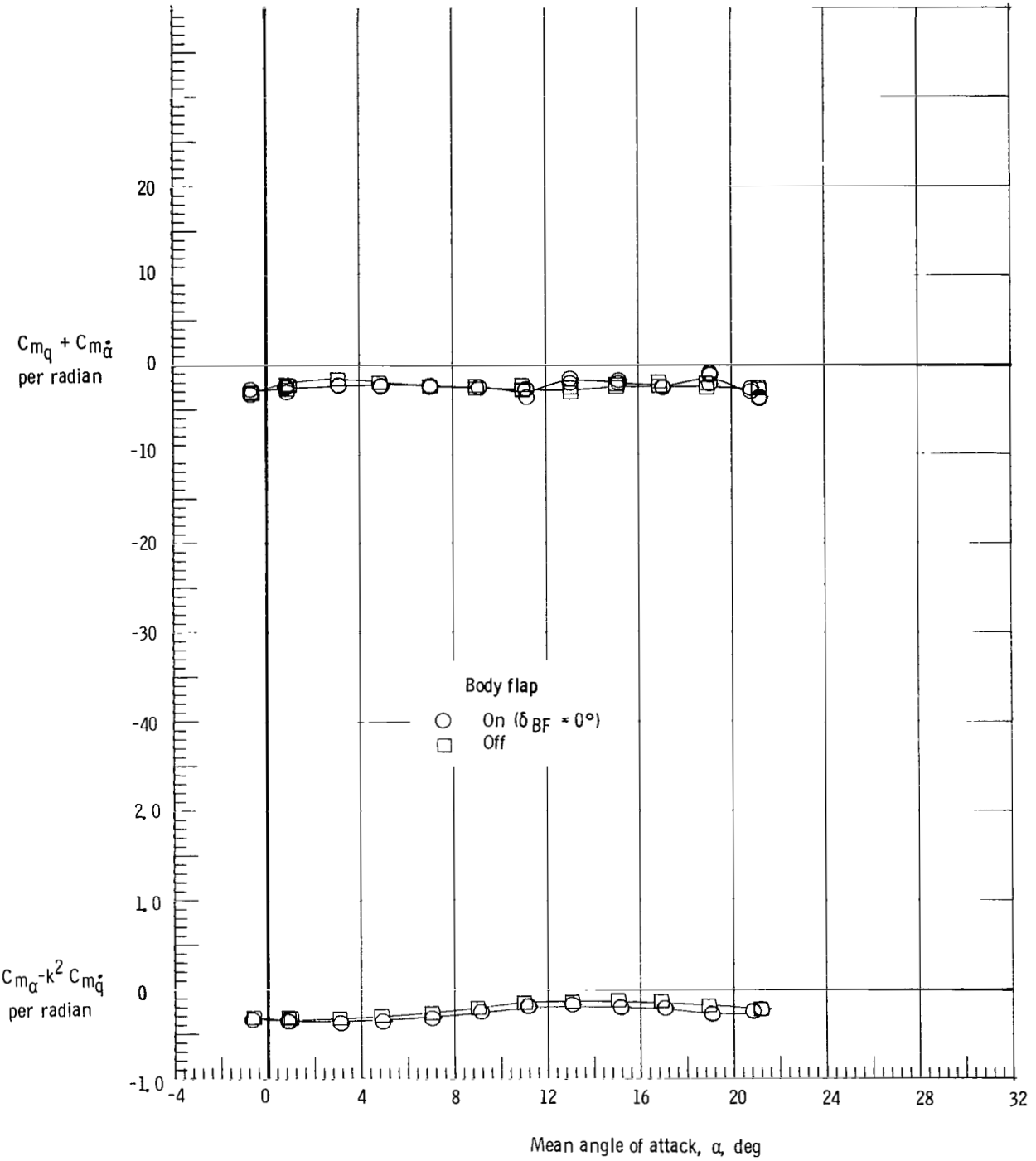

(b) M = 1.90.

Figure 11.- Continued.

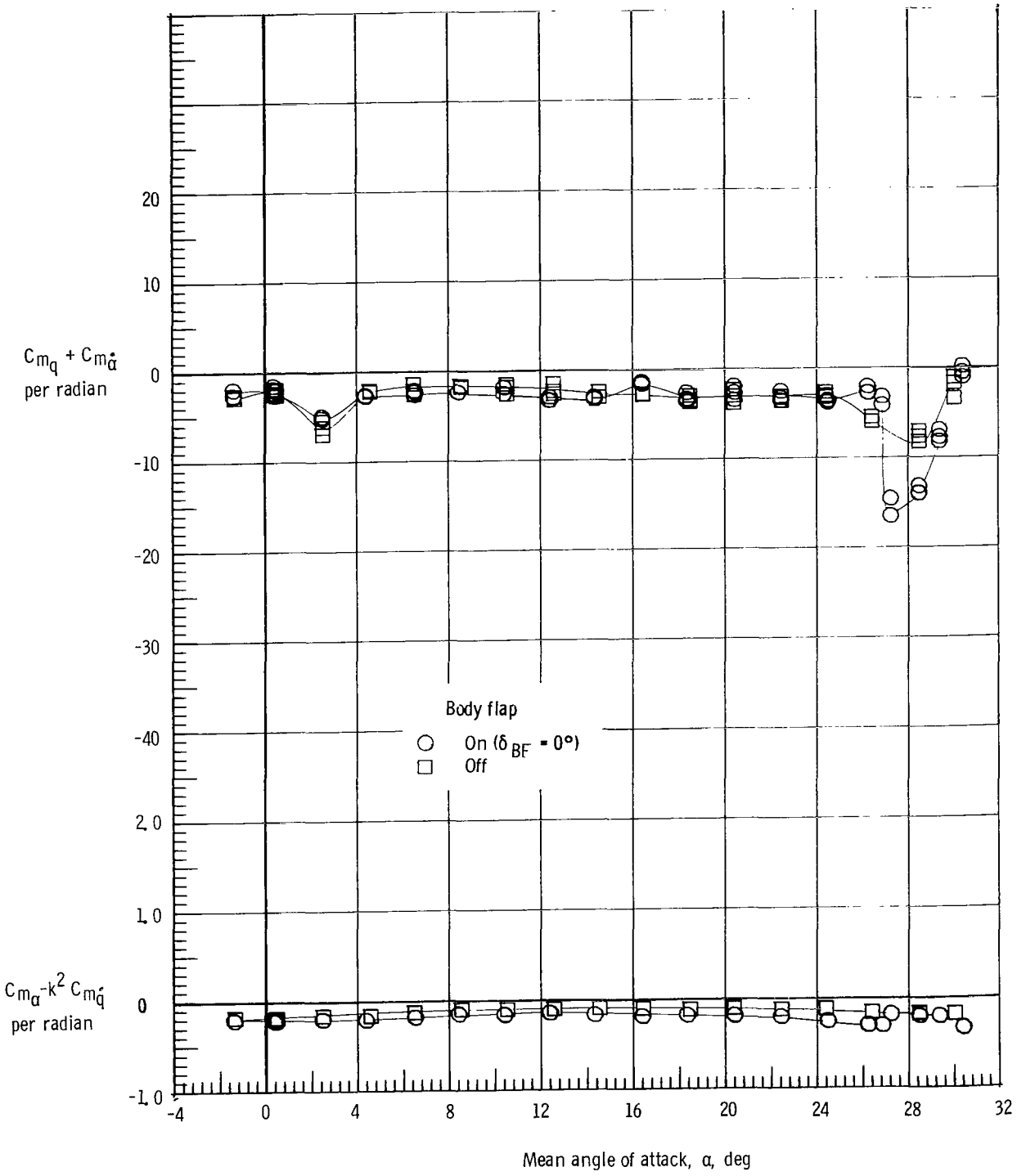

(c) M = 2.36.

Figure 11.- Continued.

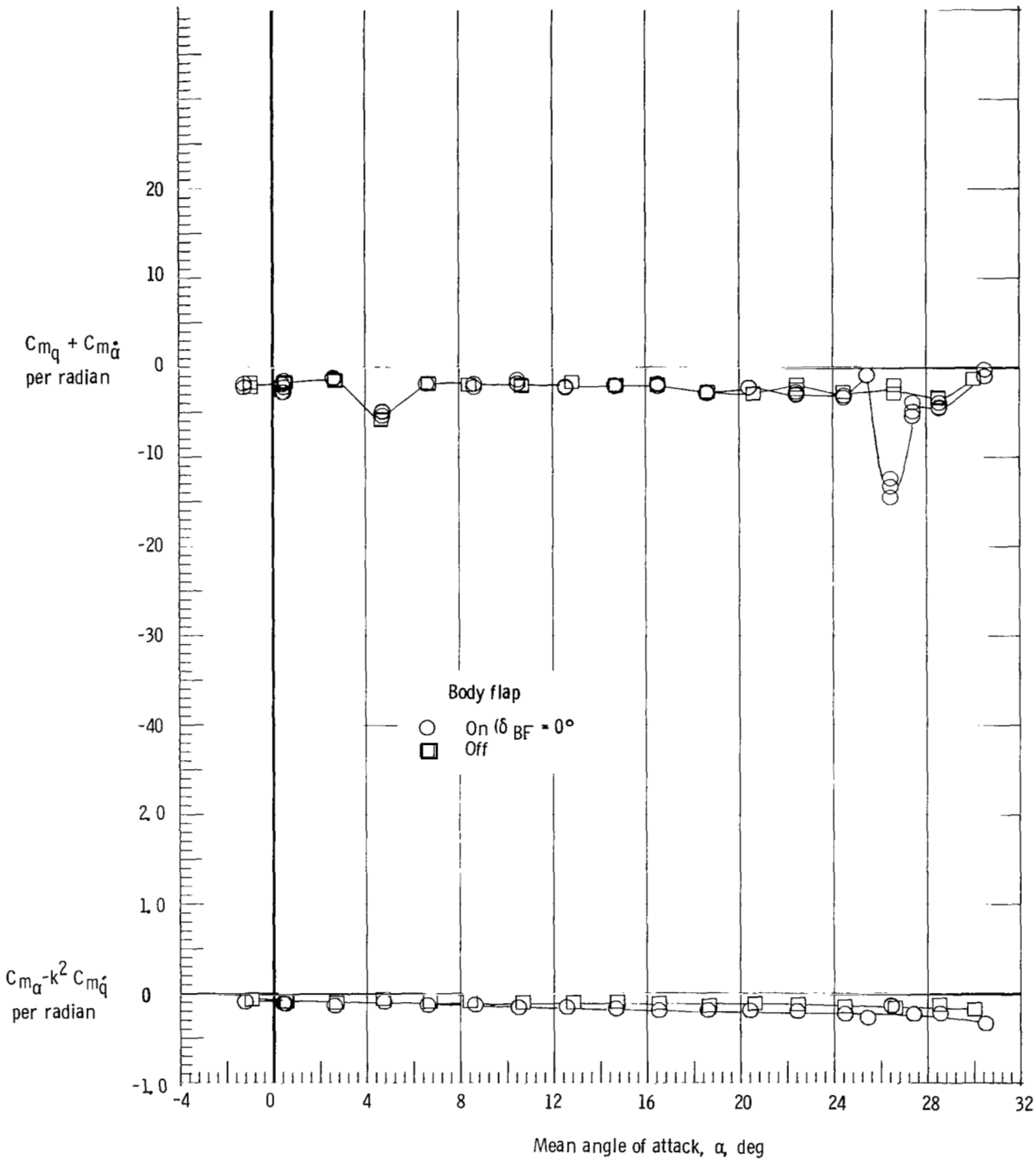

(d) M = 2.86.

Figure 11.- Continued.

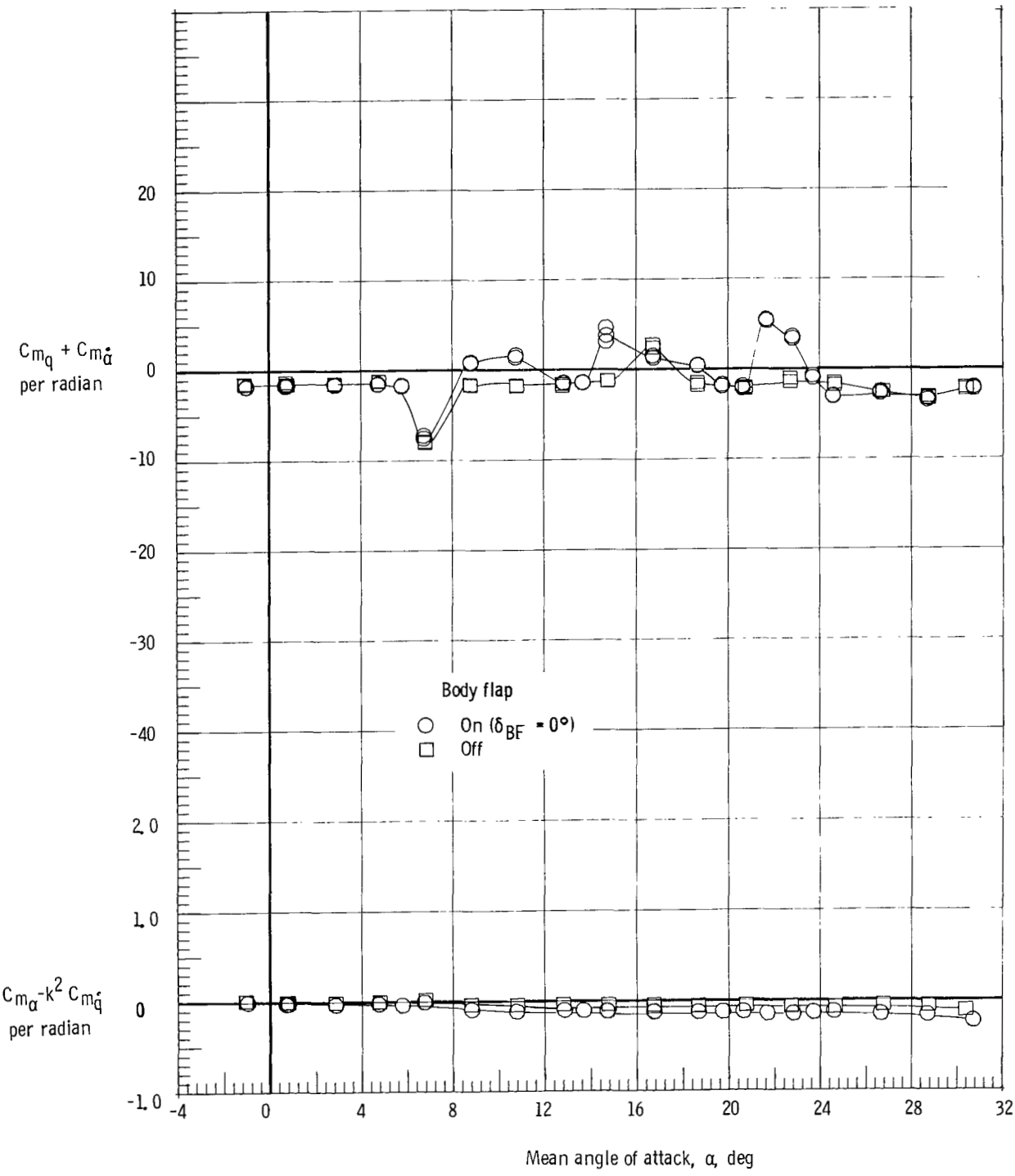

(e) M = 3.96.

Figure 11.- Continued.

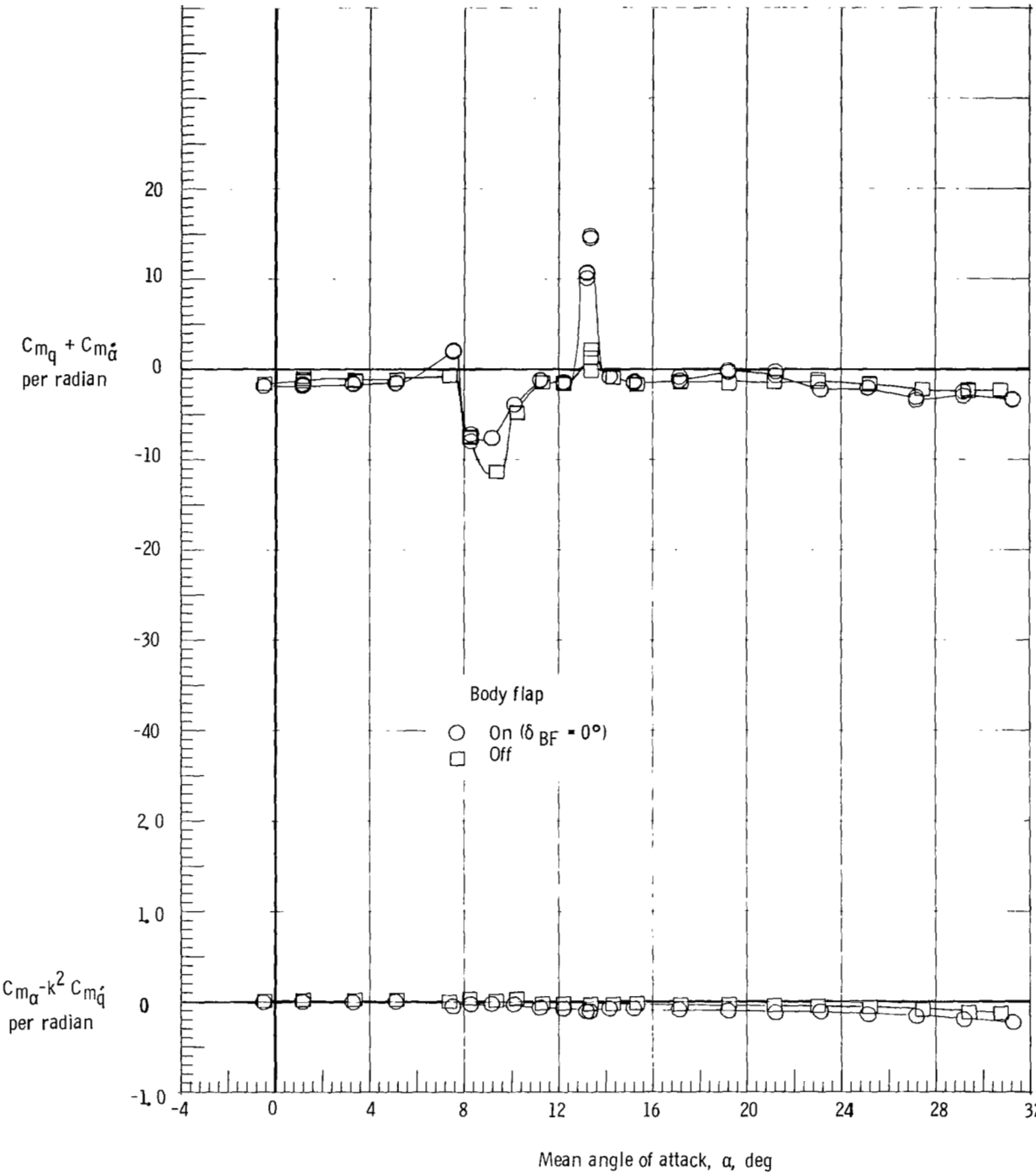

(f) M = 4.63.

Figure 11.- Concluded.

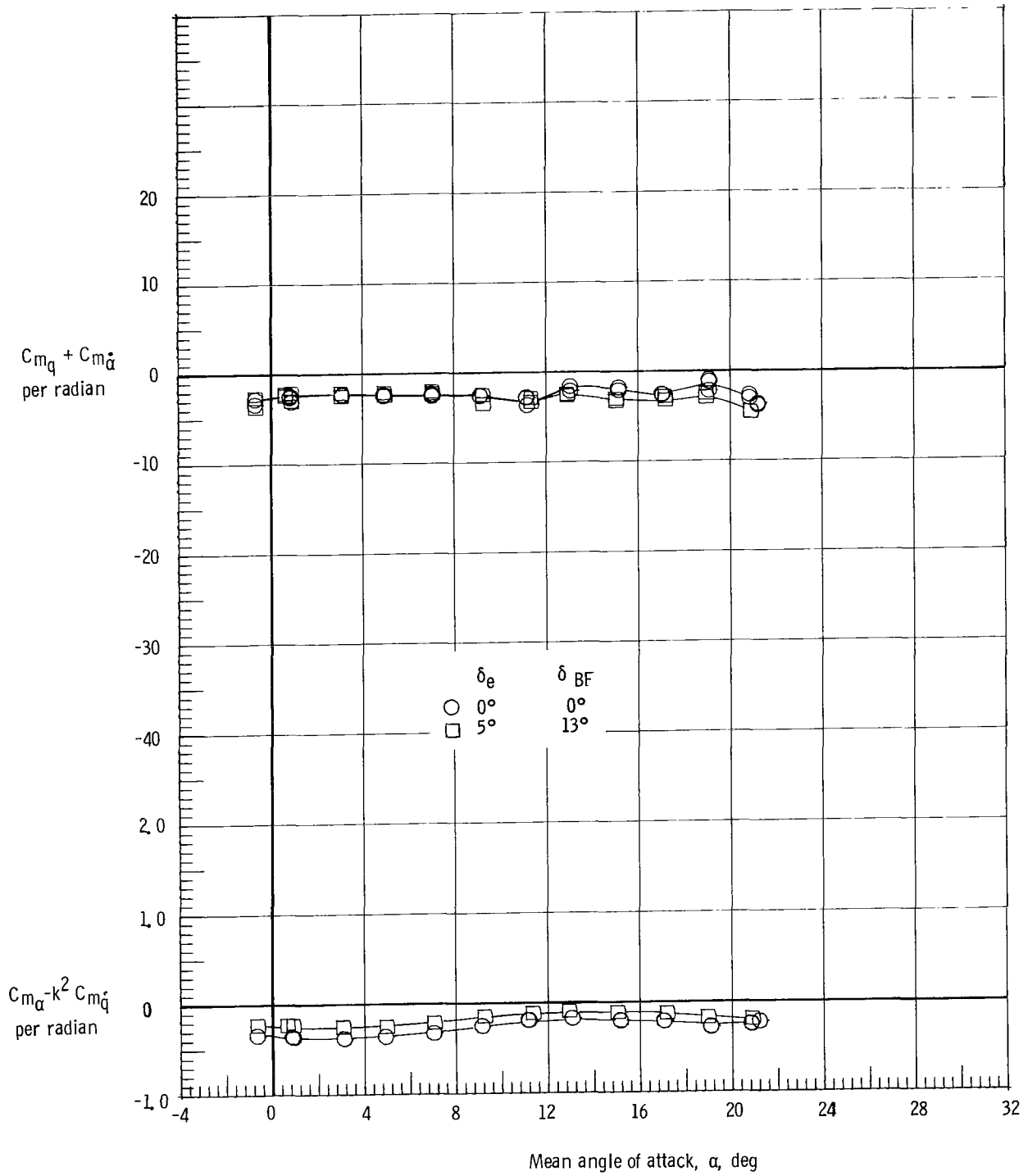

(a) M = 1.90.

Figure 12.- Effect of elevon and body flap deflection on damping-in-pitch parameter and on the oscillatory stability-in-pitch parameter. Aft c.g.; and rudder flare, 40°.

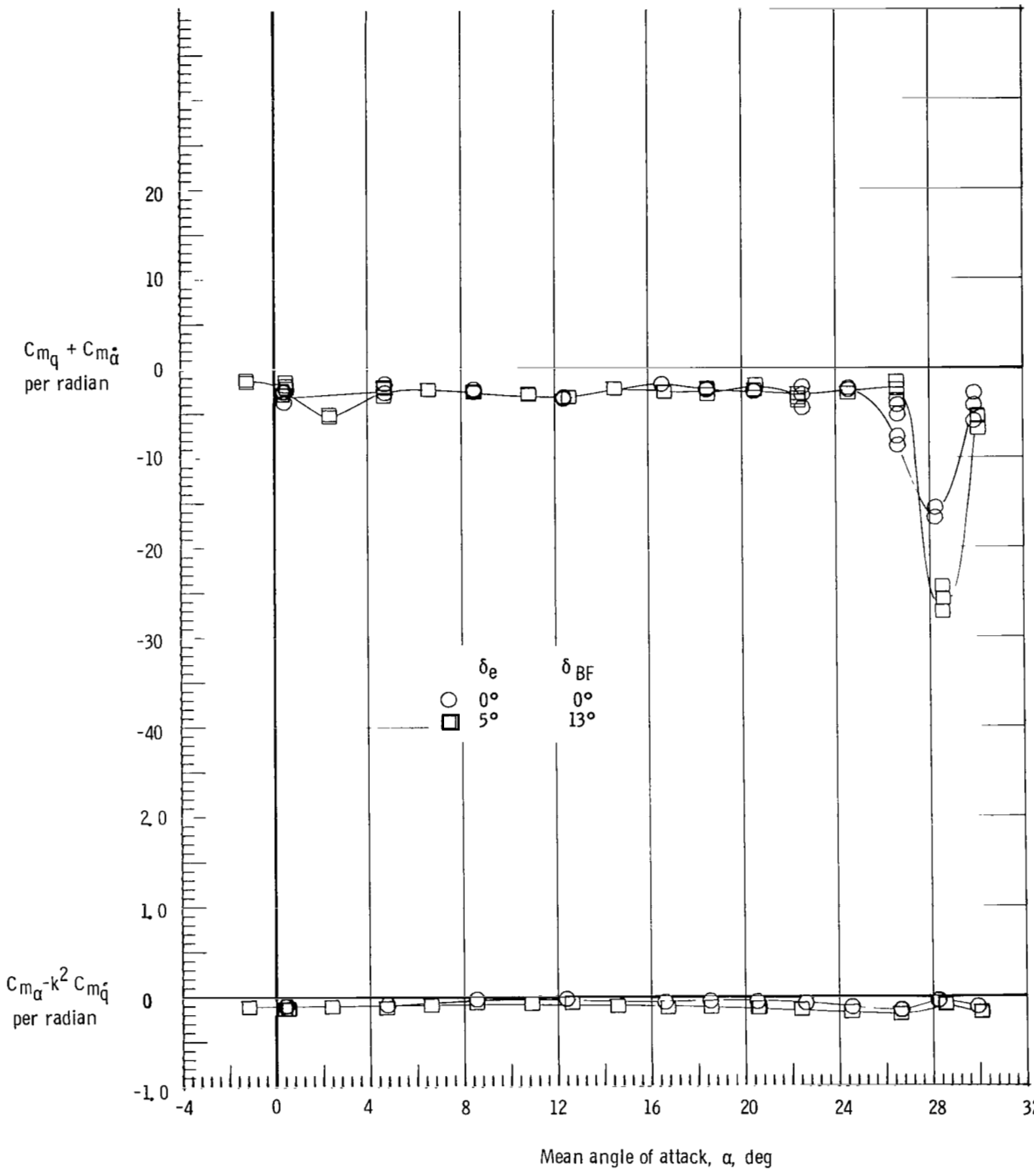

(b) M = 2.36.

Figure 12.- Continued.

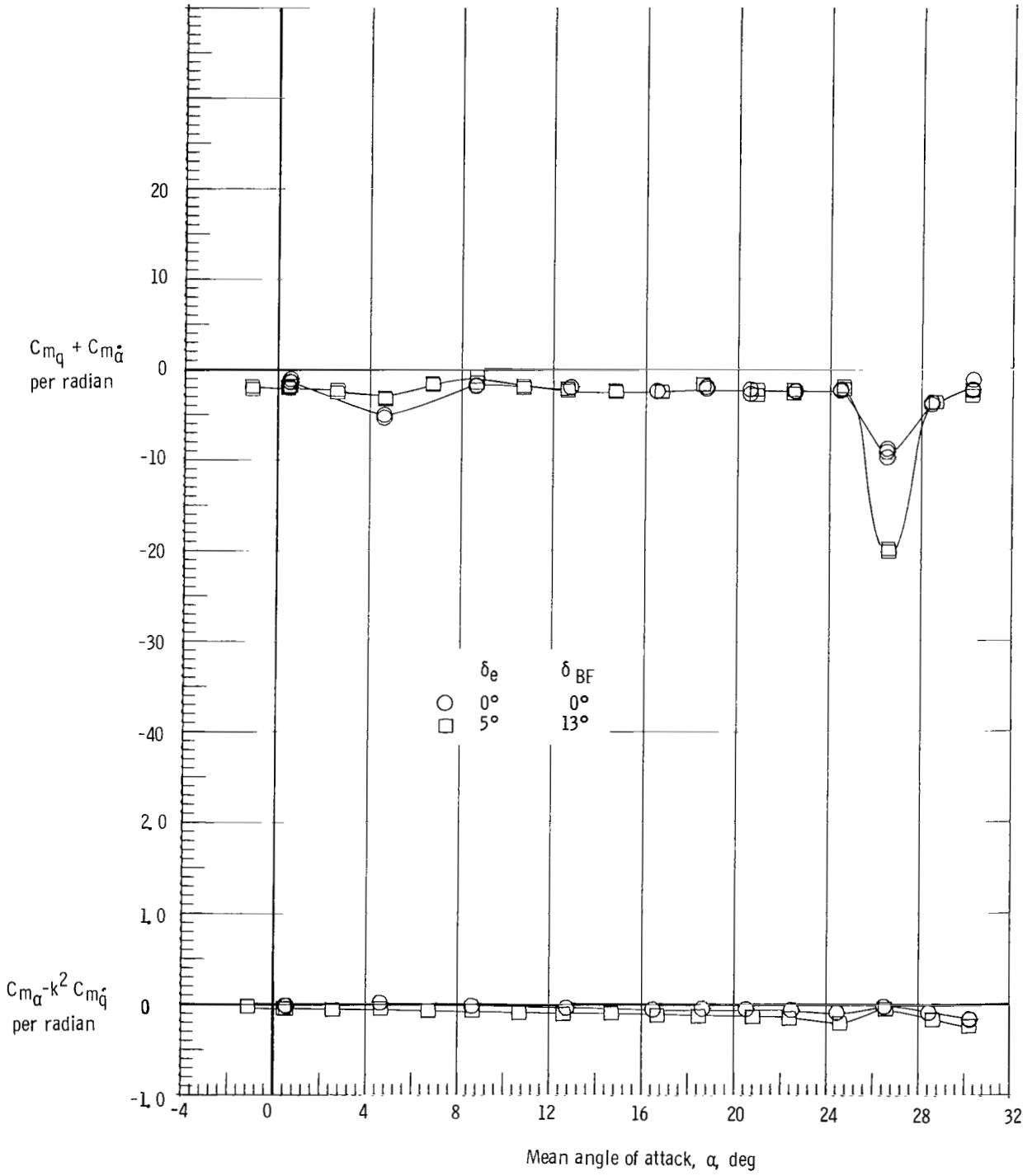

(c) M = 2.86.

Figure 12.- Continued.

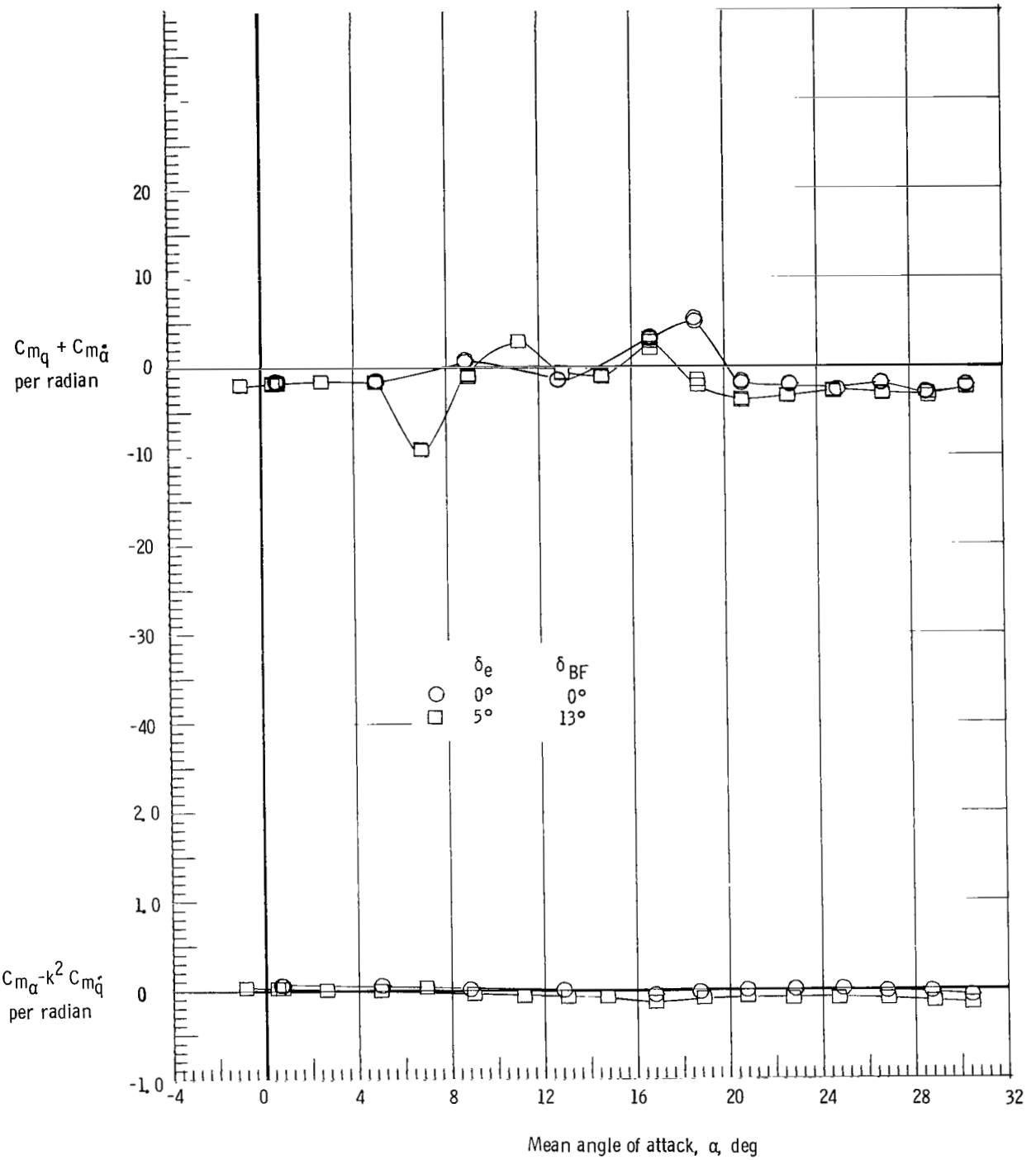

(d) M = 3.96.

Figure 12.- Continued.

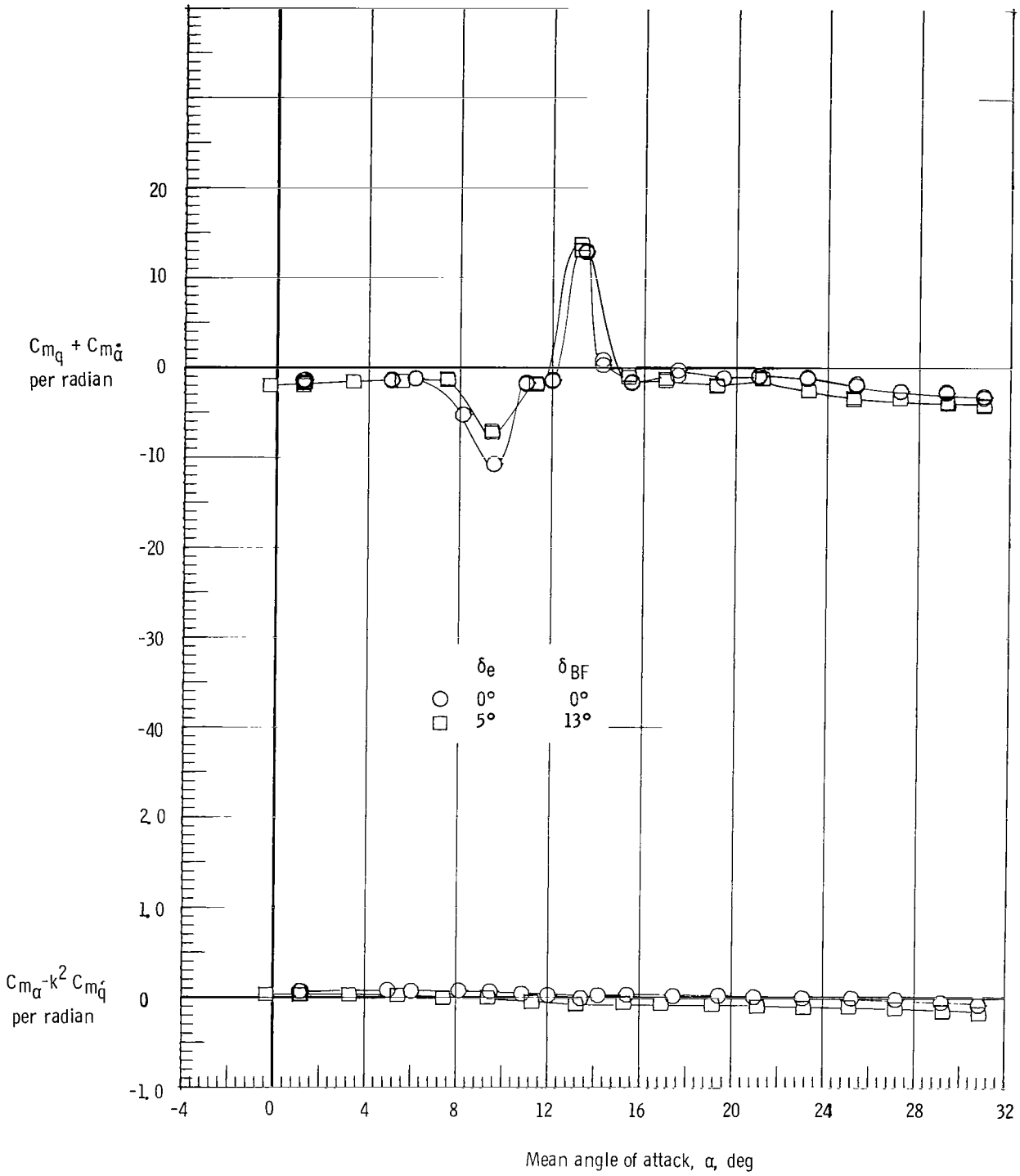

(e) M = 4.63.

Figure 12.- Concluded.

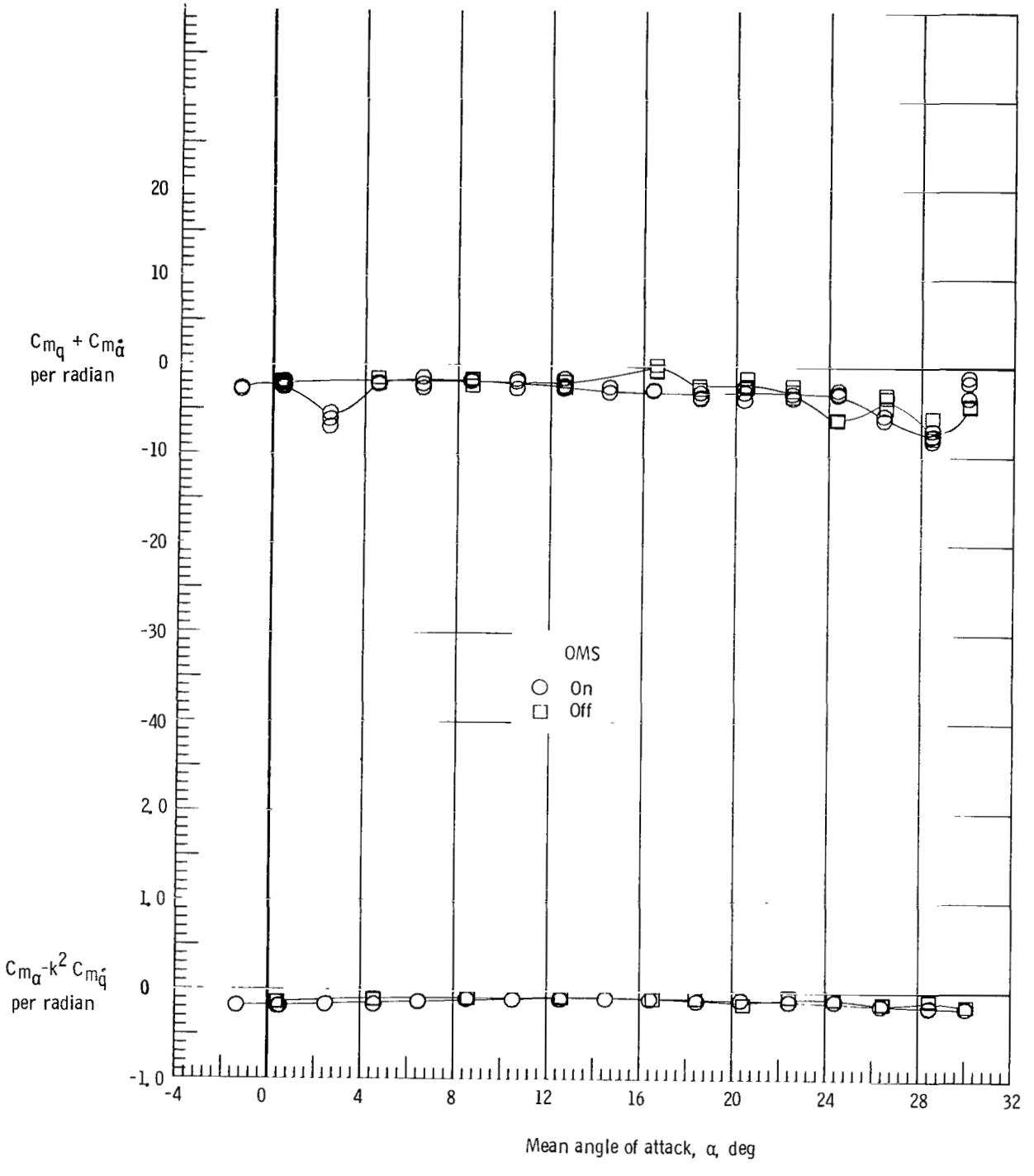

(a) M = 2.36.

Figure 13.- Effect of OMS installation on damping-in-pitch parameter and on oscillatory stability-in-pitch parameter. Forward c.g.; $\delta_e = 0^o$; body flap removed; and rudder flare, 40^o.

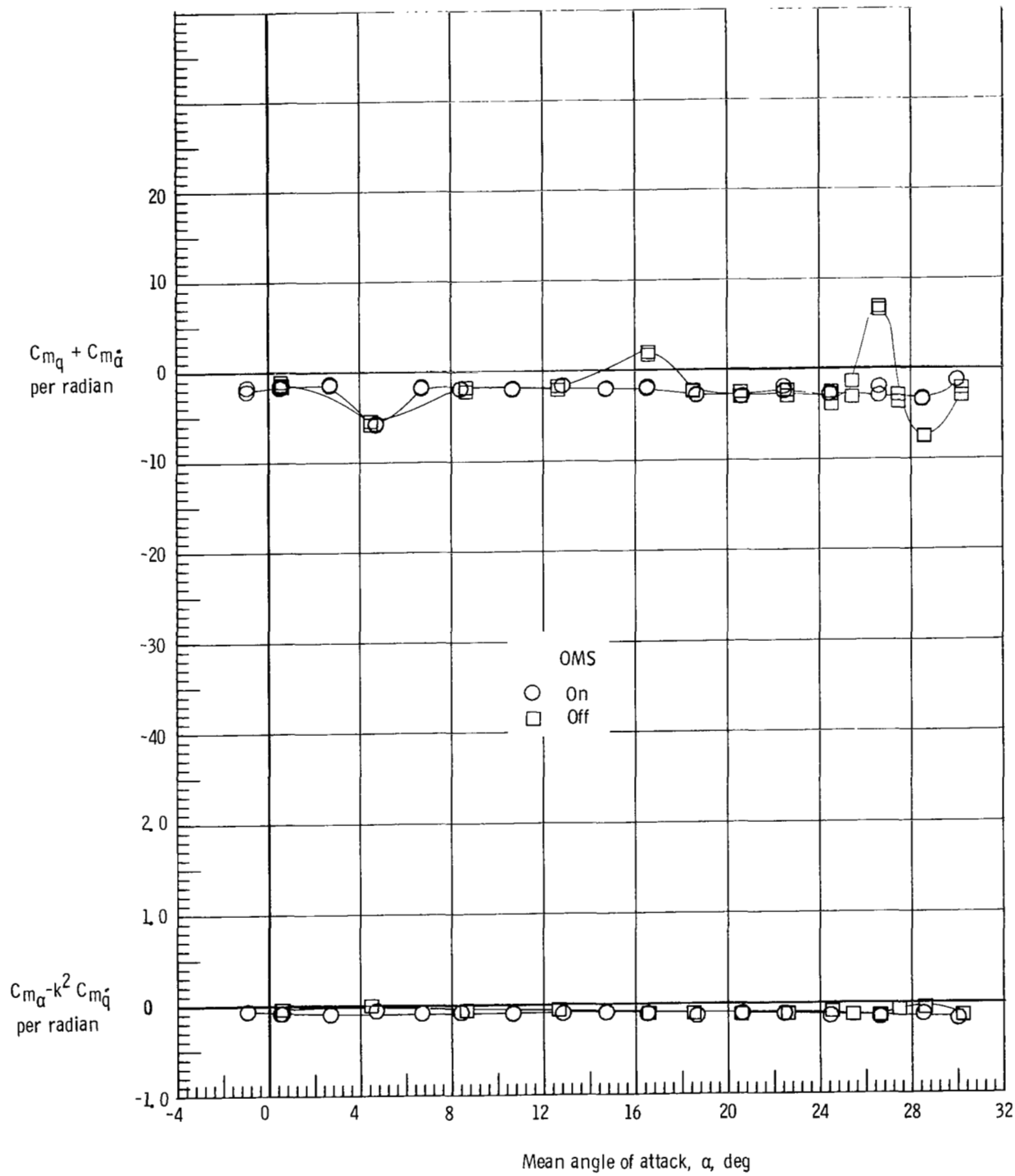

(b) M = 2.86.

Figure 13.- Continued.

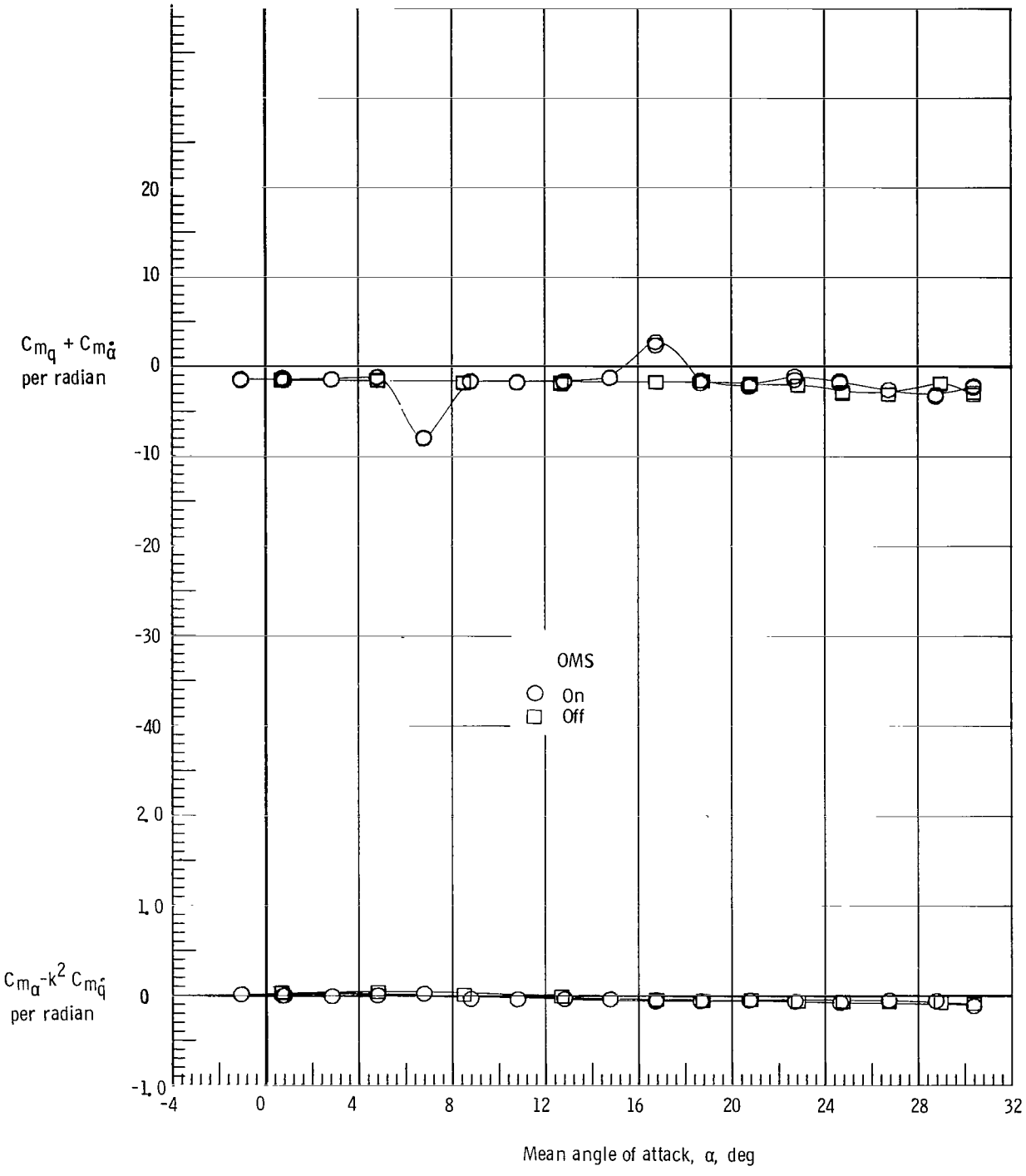

(c) M = 3.96.

Figure 13.- Continued.

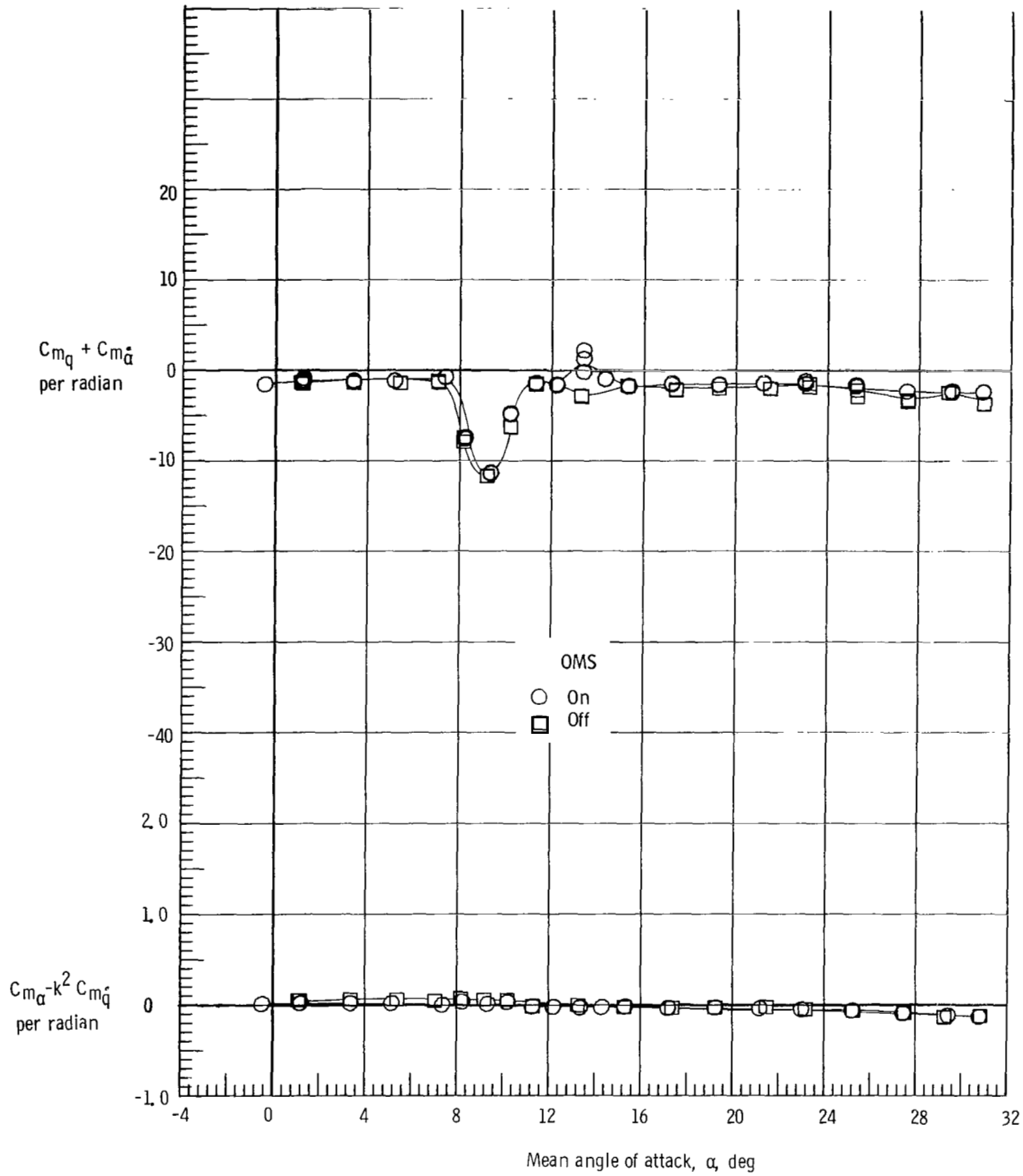

(d) M = 4.63.

Figure 13.- Concluded.

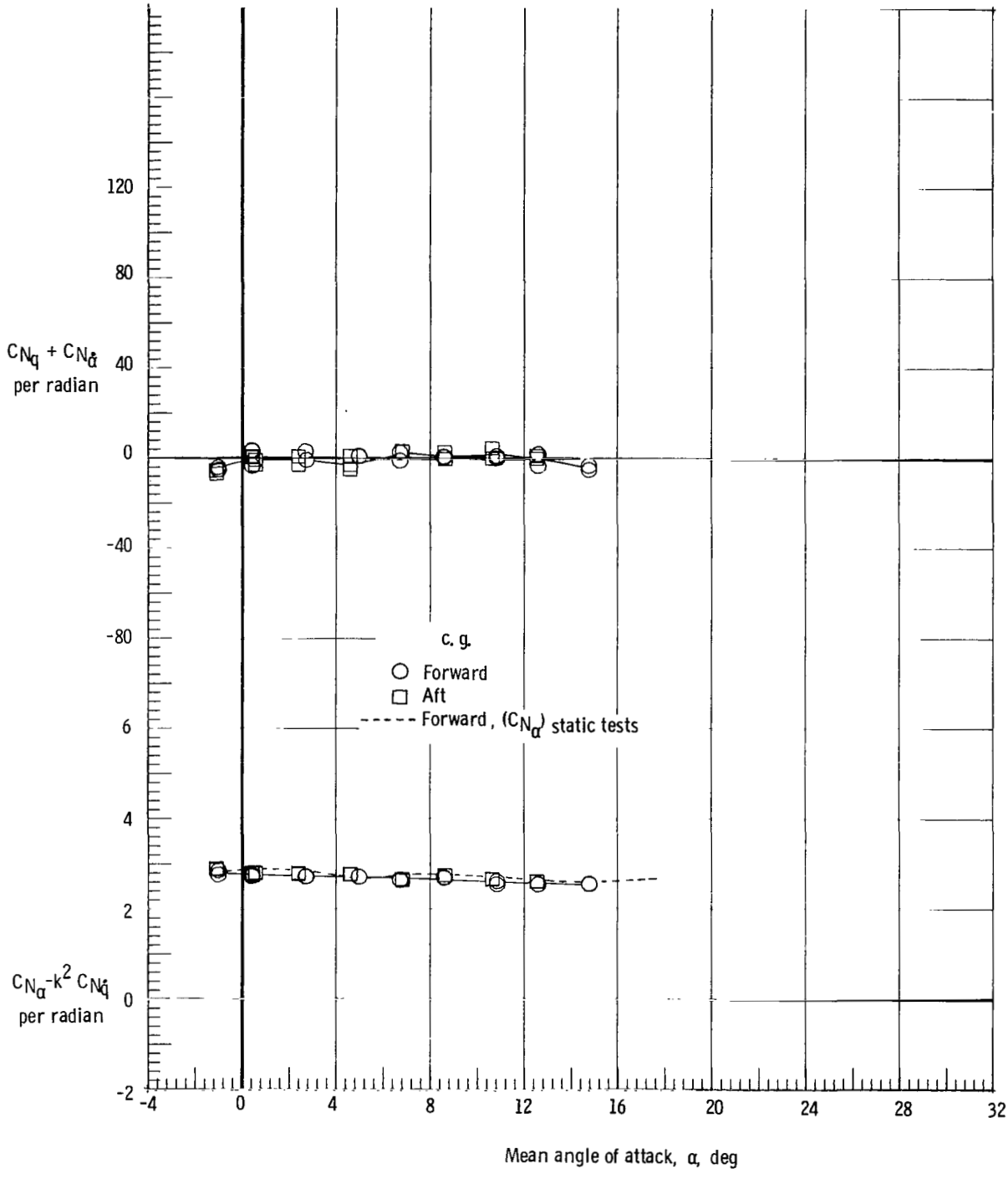

(a) M = 1.60.

Figure 14.- Effect of center-of-gravity (c.g.) position on normal force due to pitch rate parameter and normal force due to pitch displacement parameter. $\delta_e = 0^o$; $\delta_{BF} = 0^o$; and rudder flare, 40^o.

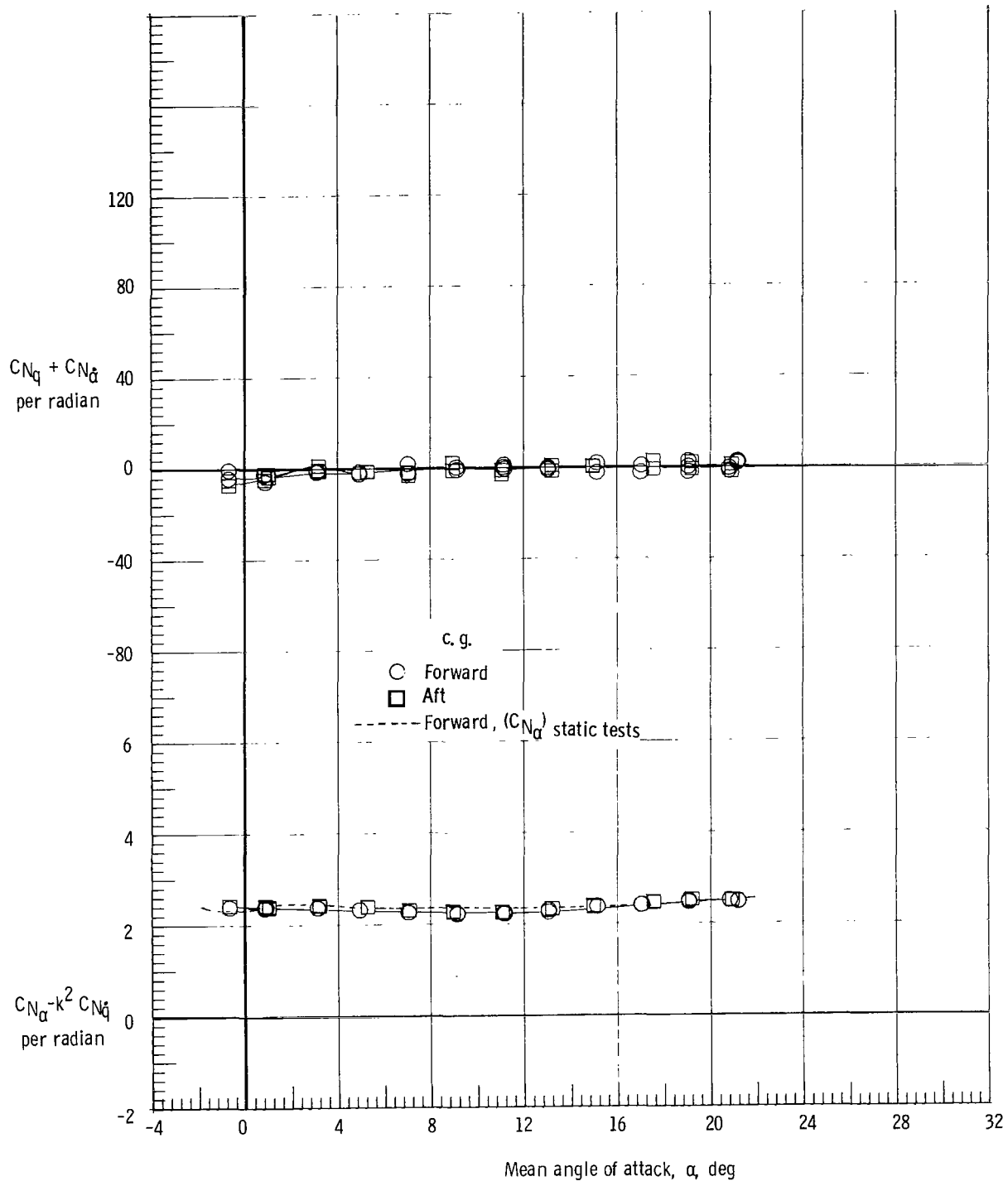

(b) M = 1.90.

Figure 14.- Continued.

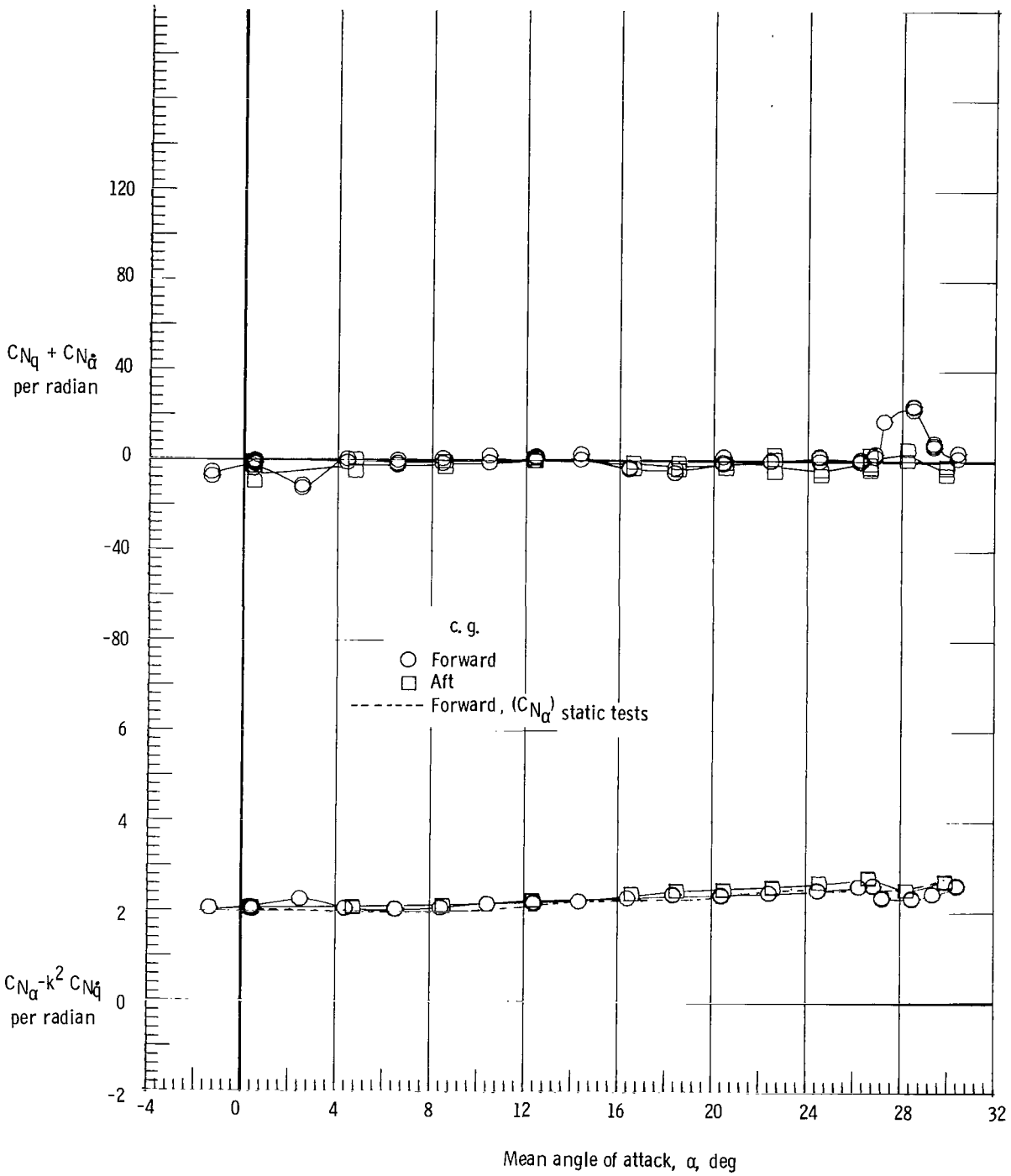

(c) M = 2.36.

Figure 14.- Continued.

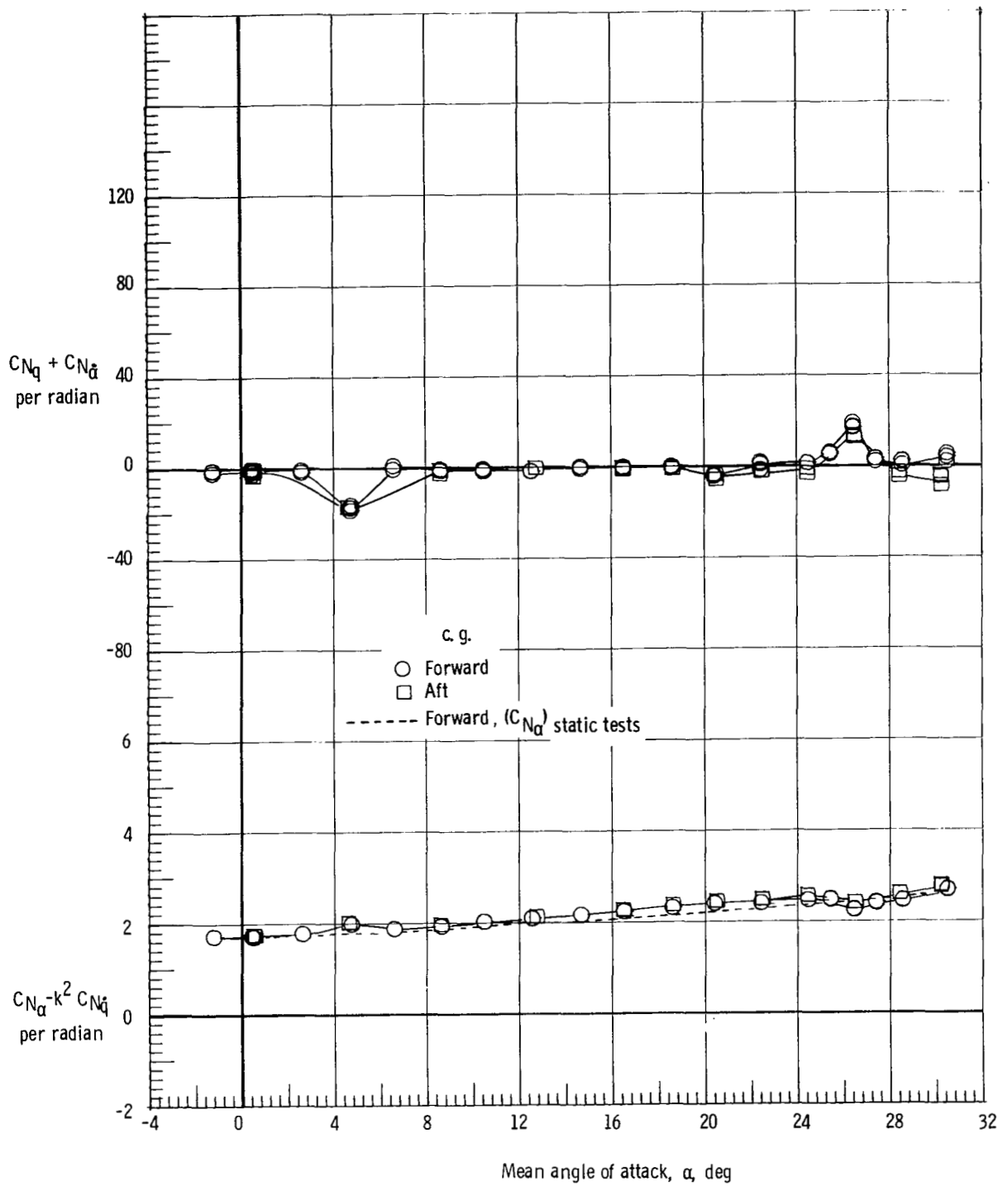

(d) M = 2.86.

Figure 14.- Continued.

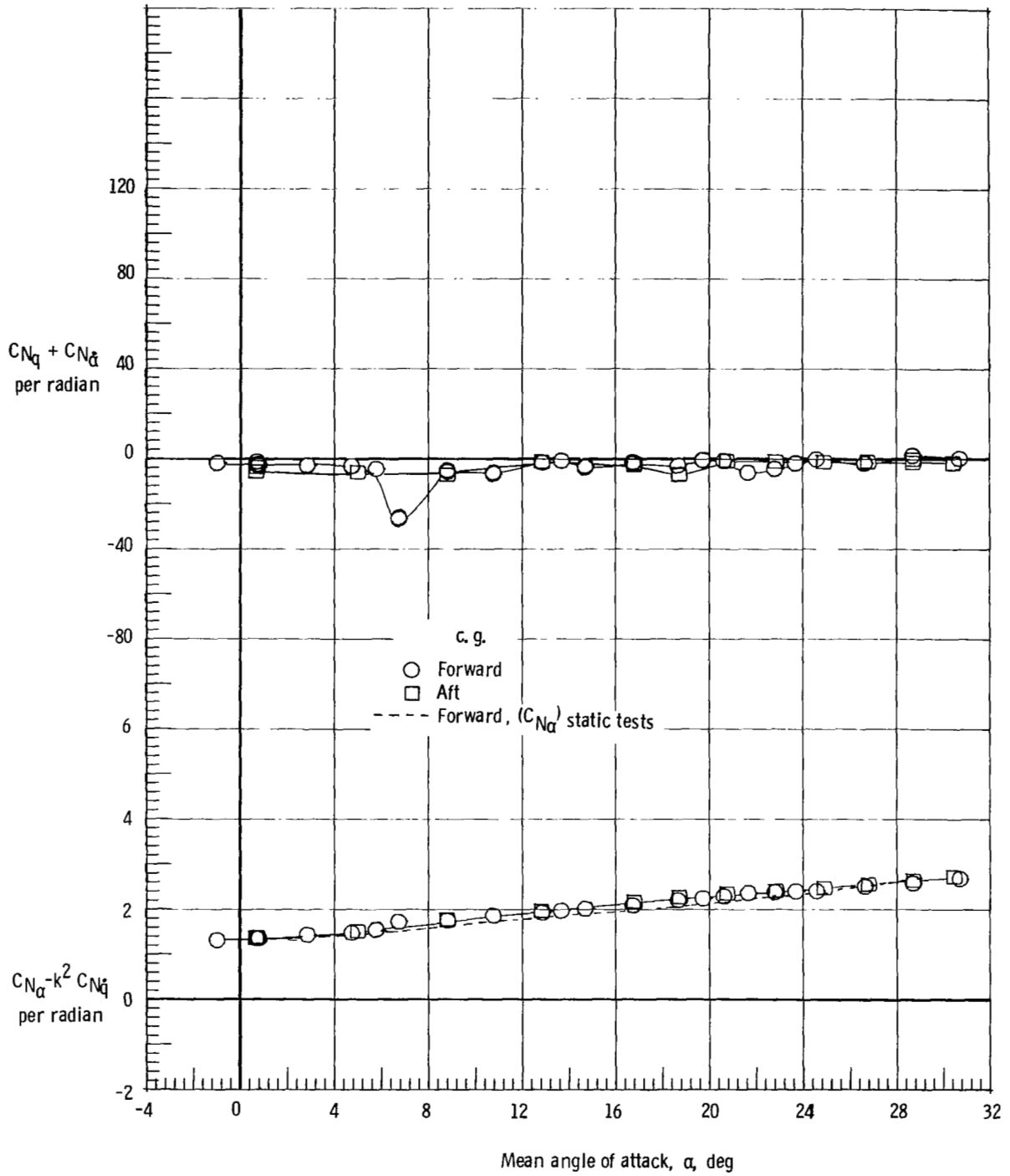

(e) M = 3.96.

Figure 14.- Continued.

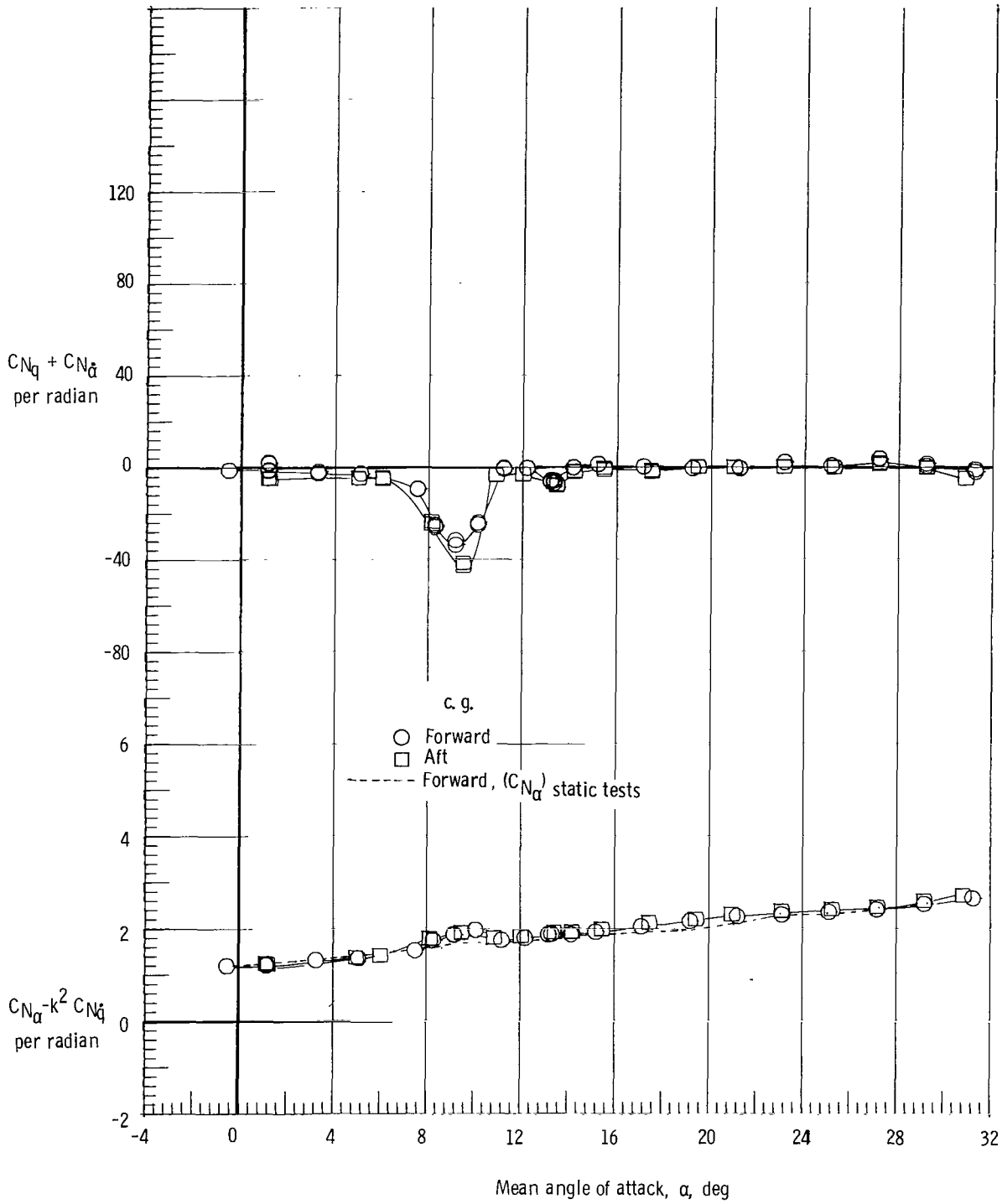

(f) M = 4.63.

Figure 14.- Concluded.

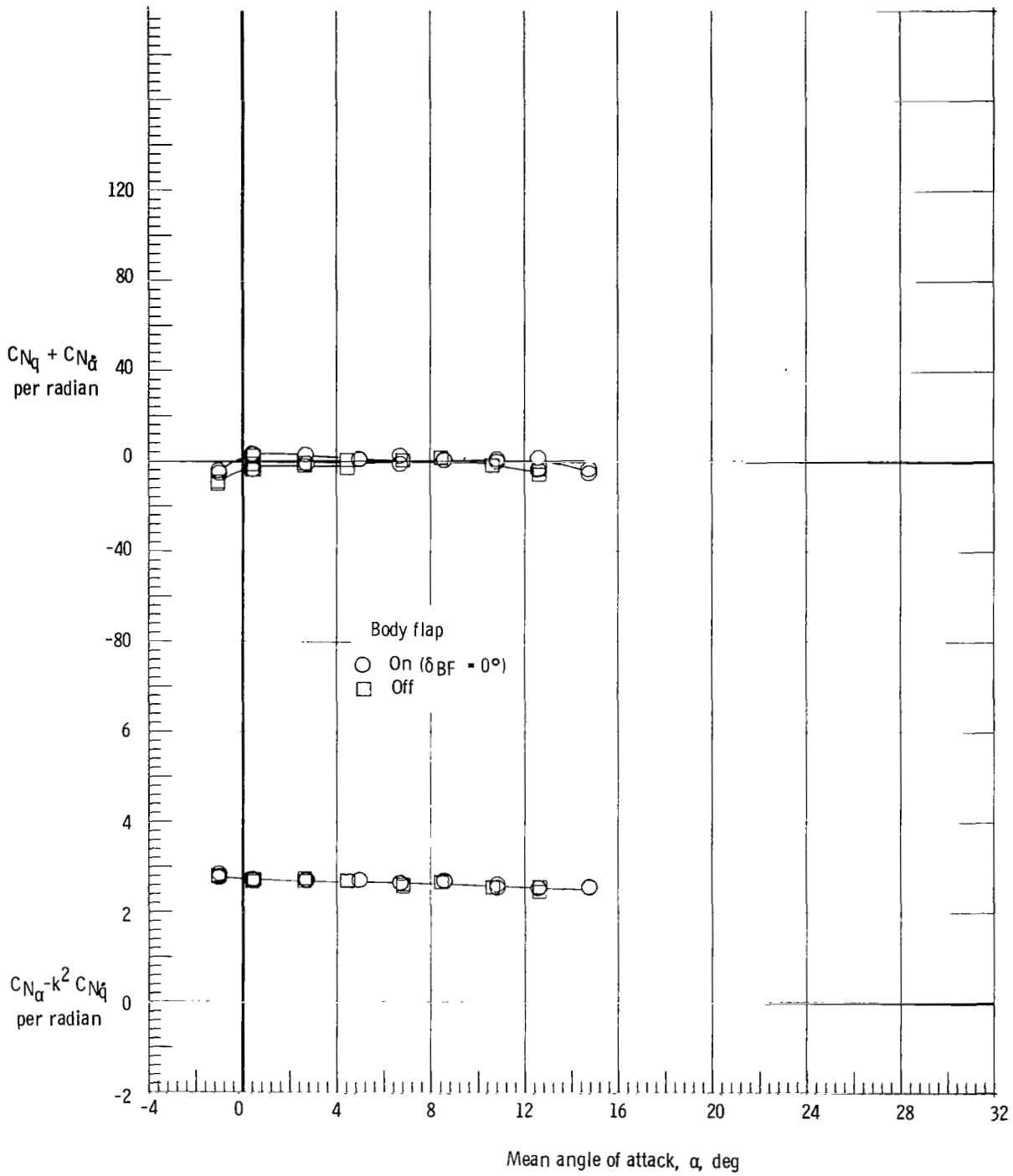

(a) M = 1.60.

Figure 15.- Effect of body flap on normal force due to pitch rate parameter and normal force due to pitch displacement parameter. Forward c.g.; $\delta_e = 0^o$; and rudder flare, 40^o.

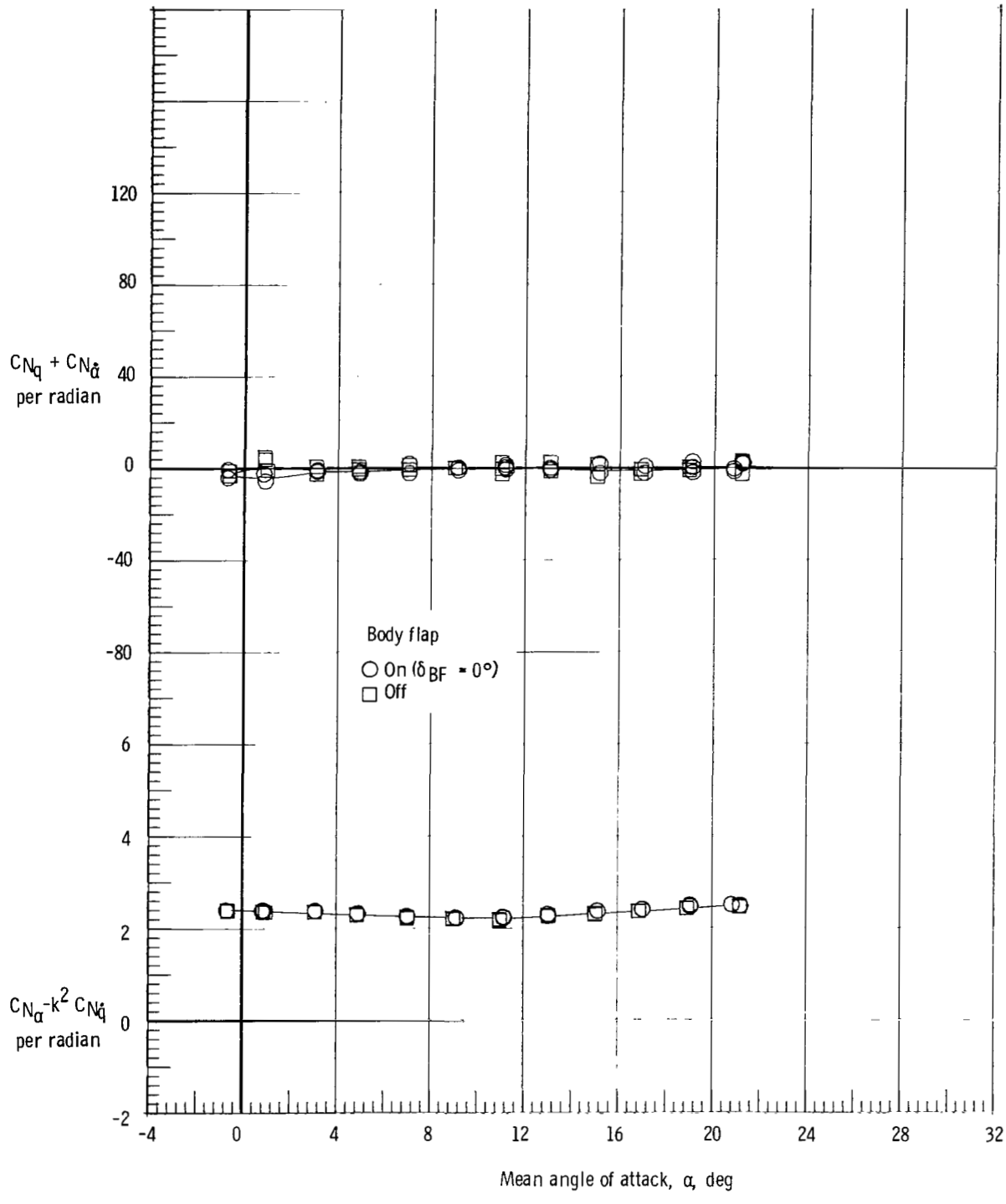

(b) M = 1.90.

Figure 15.- Continued.

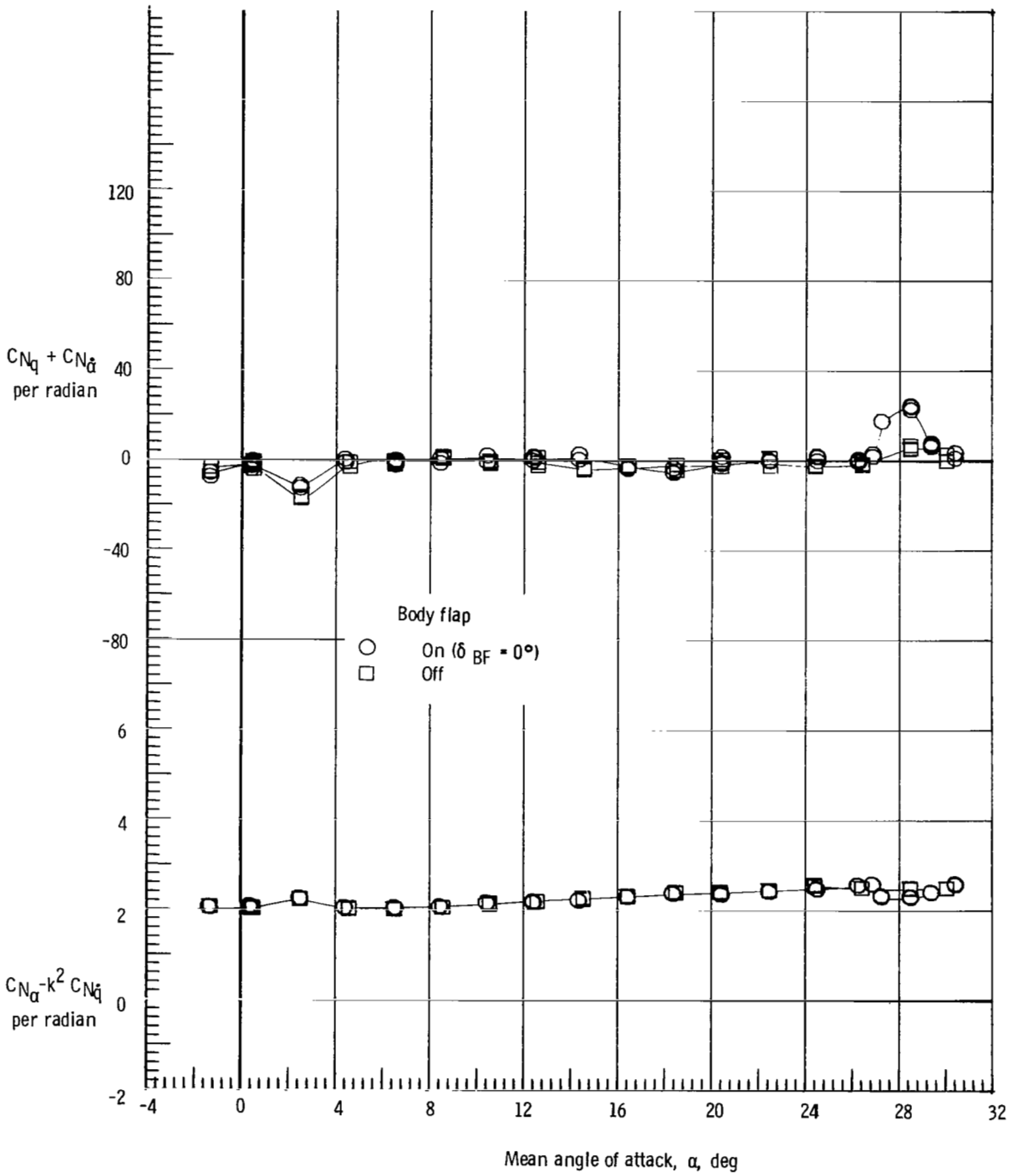

(c) M = 2.36.

Figure 15.- Continued.

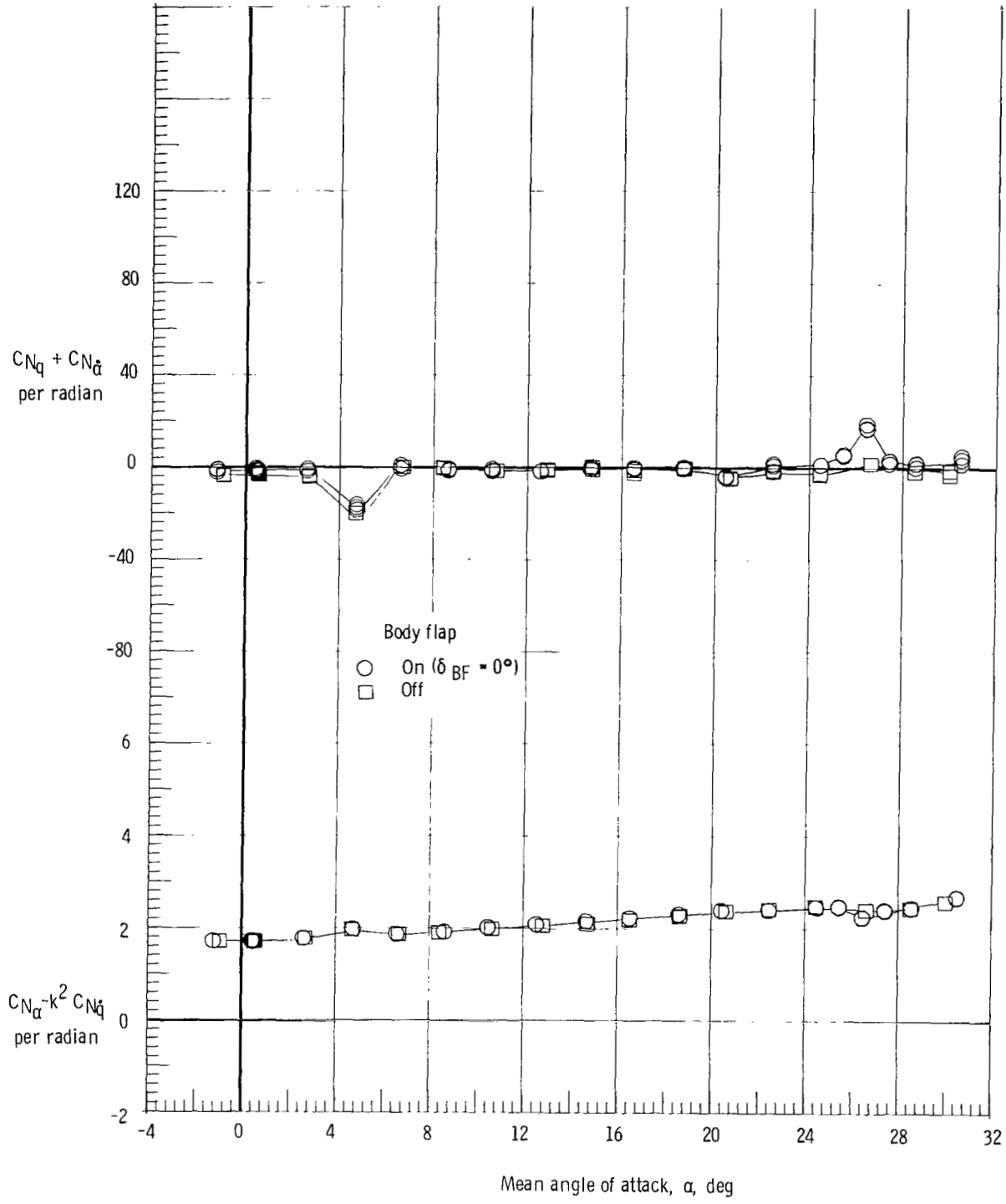

(d) M = 2.86.

Figure 15.- Continued.

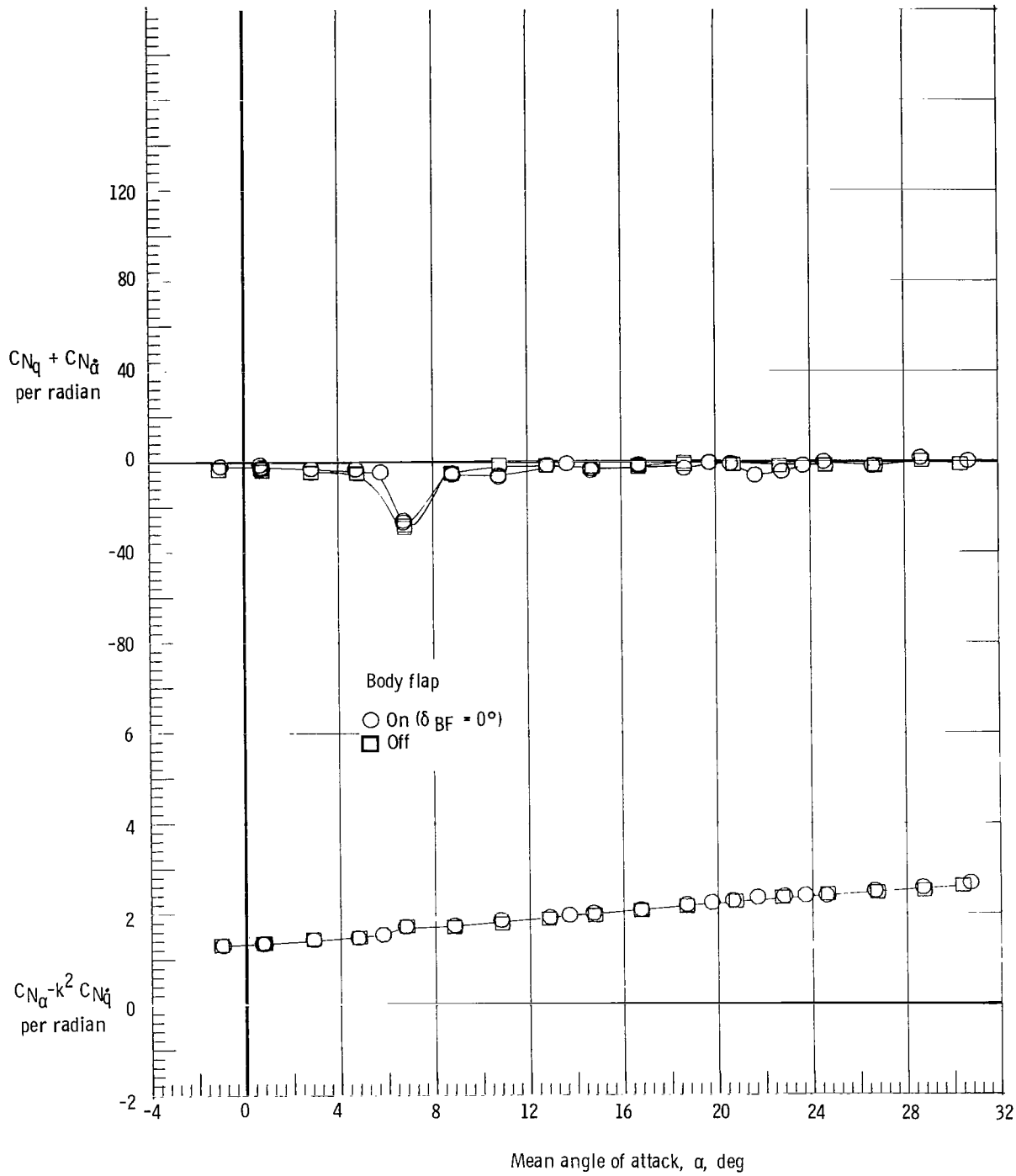

(e) M = 3.96.

Figure 15.- Continued.

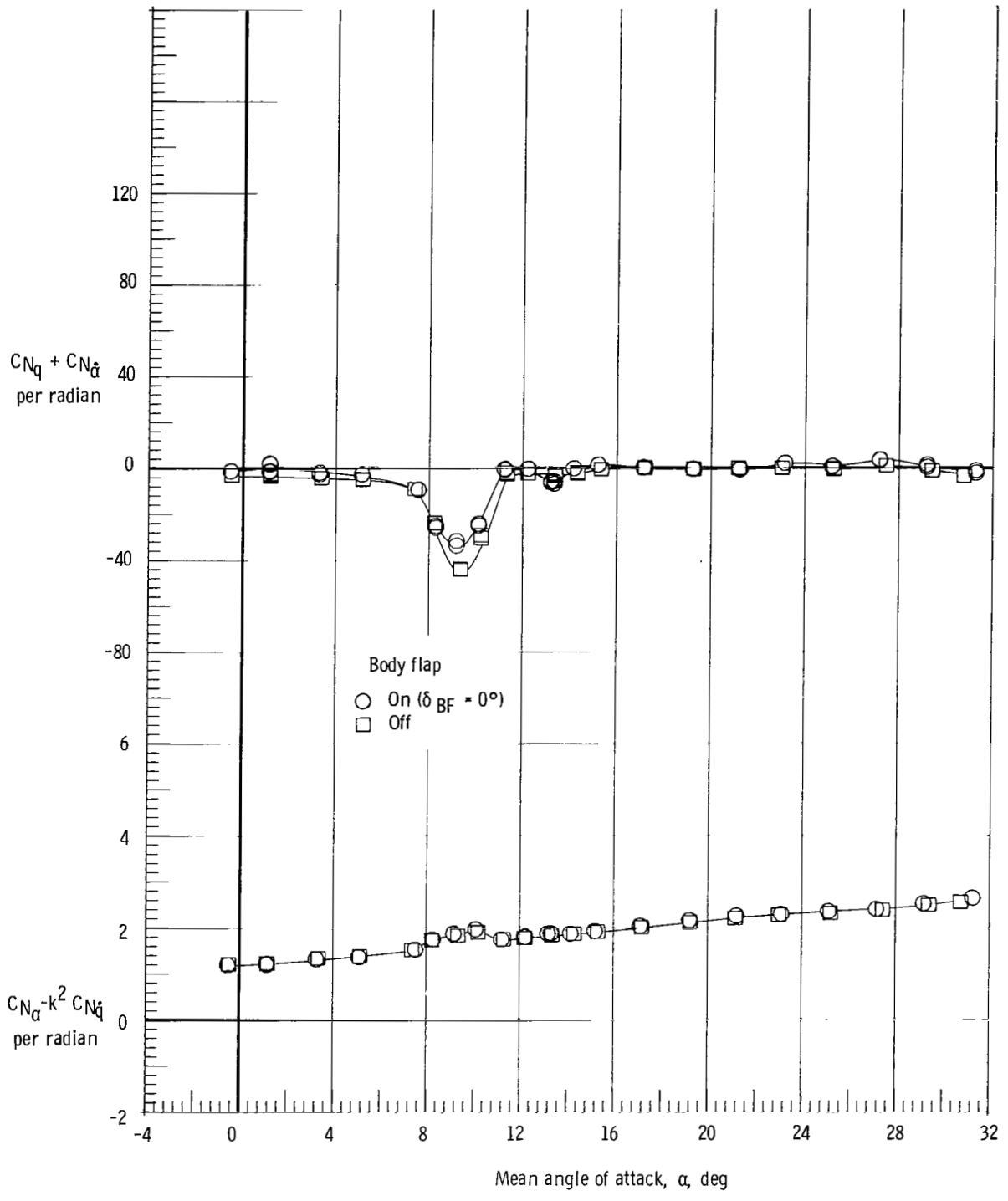

(f) M = 4.63.

Figure 15.- Concluded.

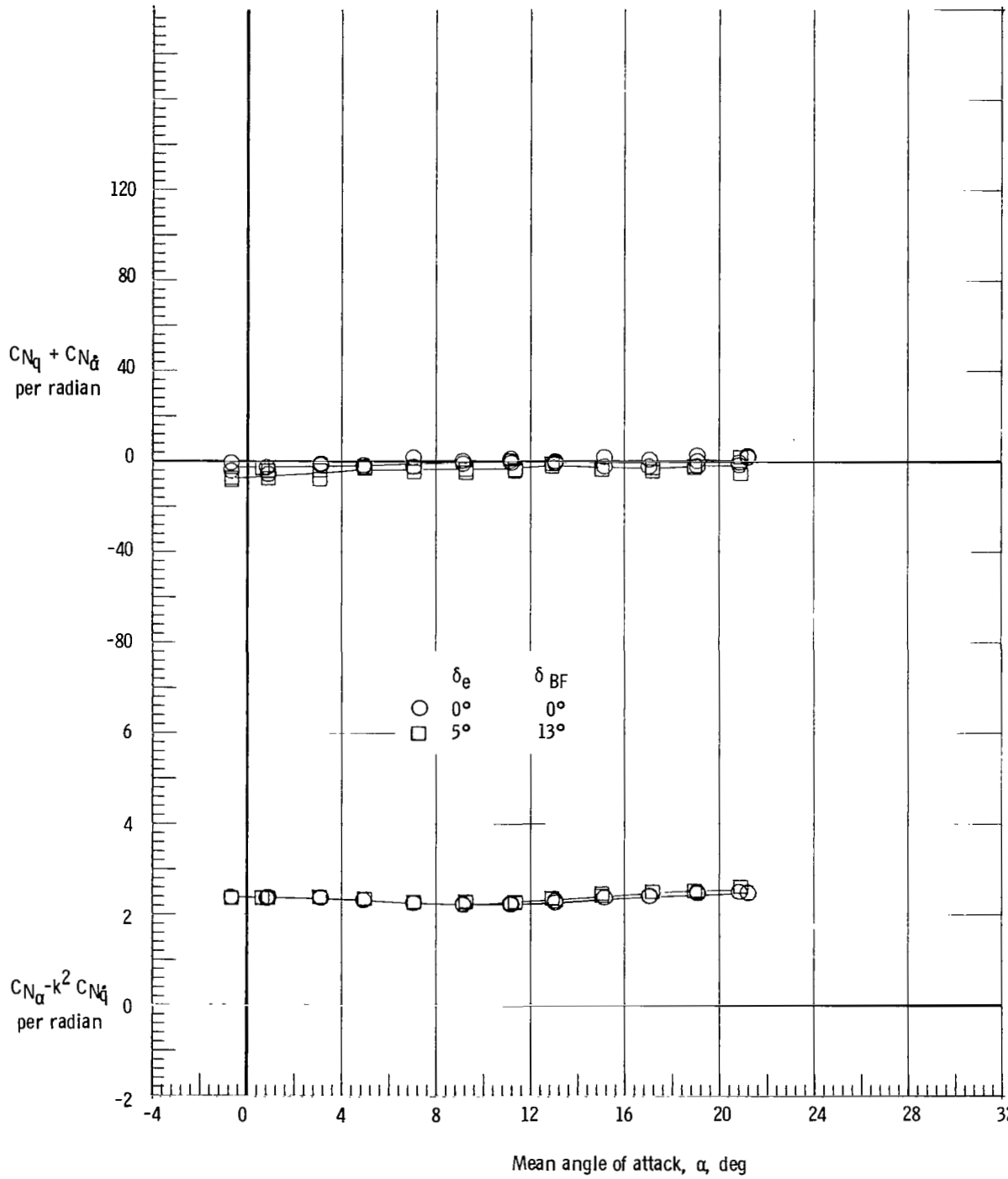

(a) M = 1.90.

Figure 16.- Effect of elevon and body flap deflection on normal force due to pitch rate parameter and on normal force due to pitch displacement parameter. Aft c.g.; and rudder flare, 40°.

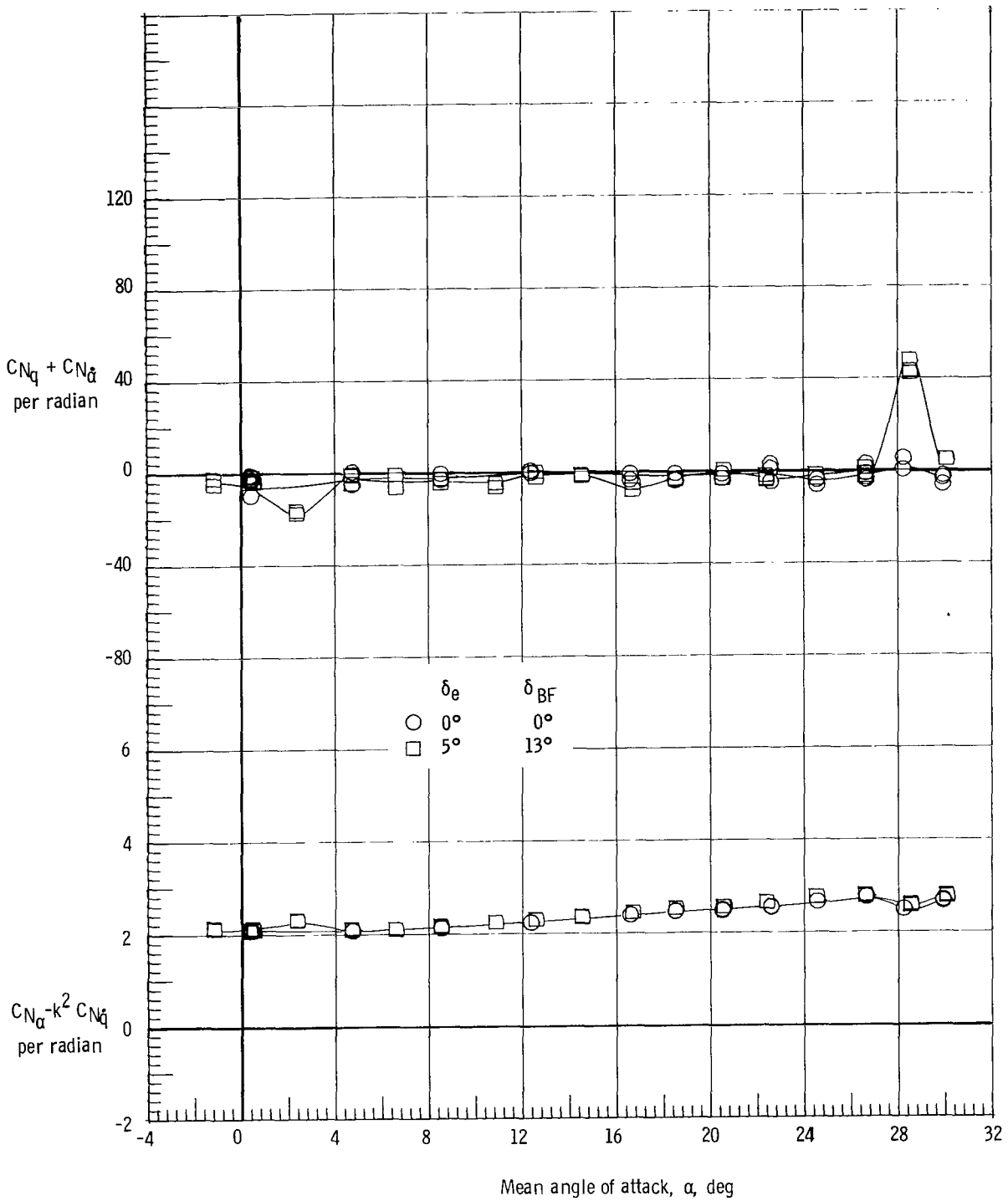

(b) M = 2.36.

Figure 16.- Continued.

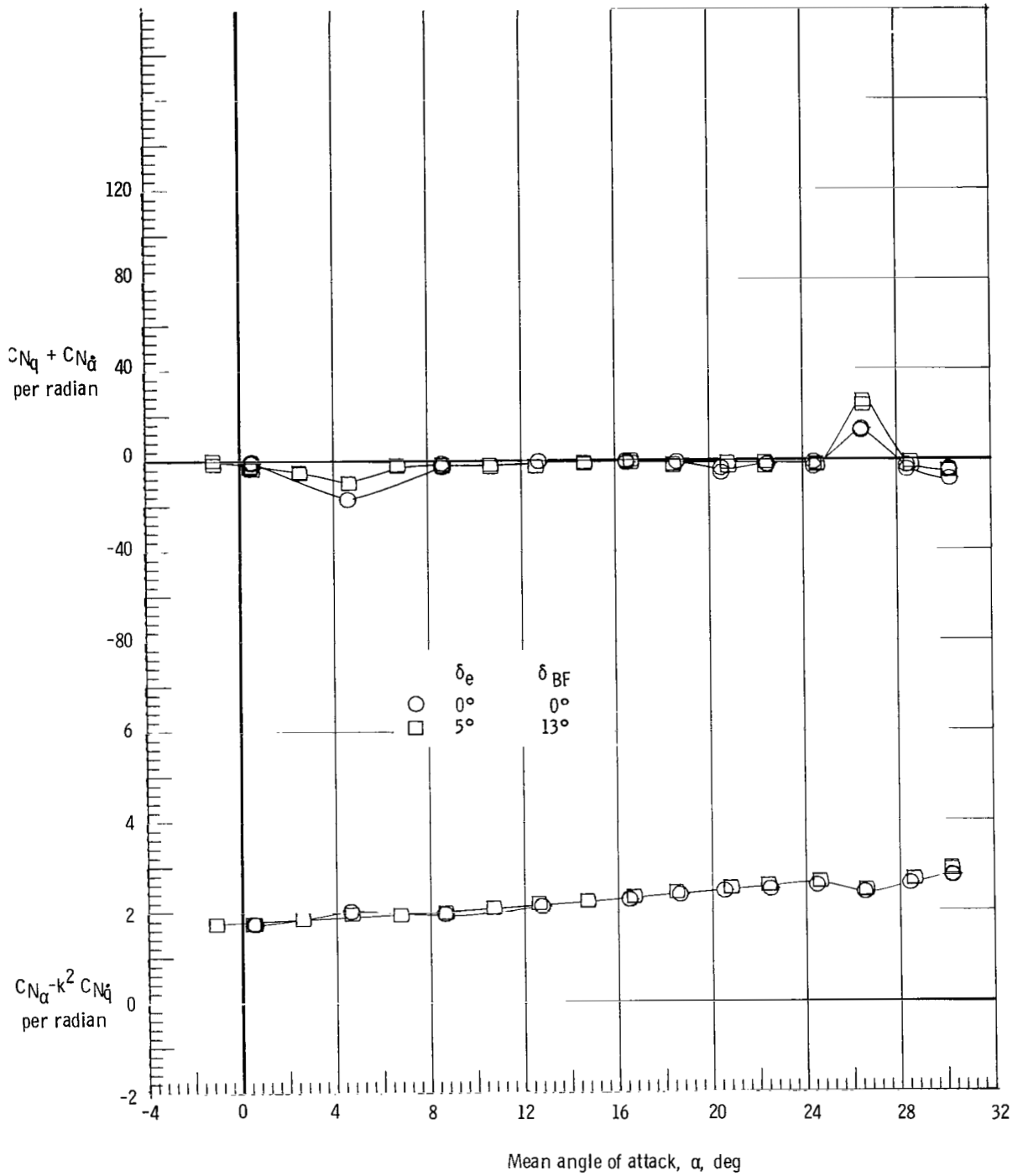

(c) M = 2.86.

Figure 16.- Continued.

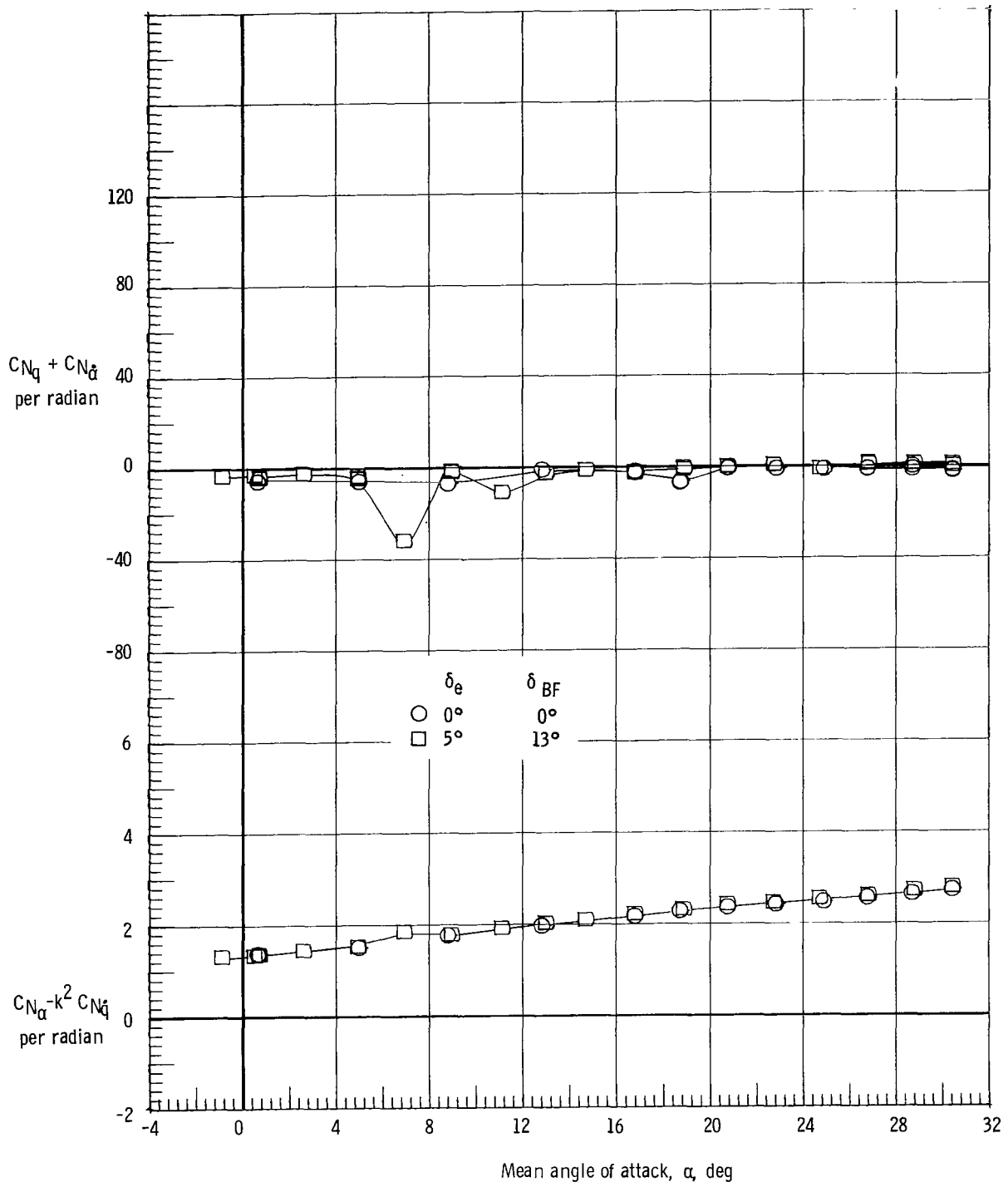

(d) M = 3.96.

Figure 16.- Continued.

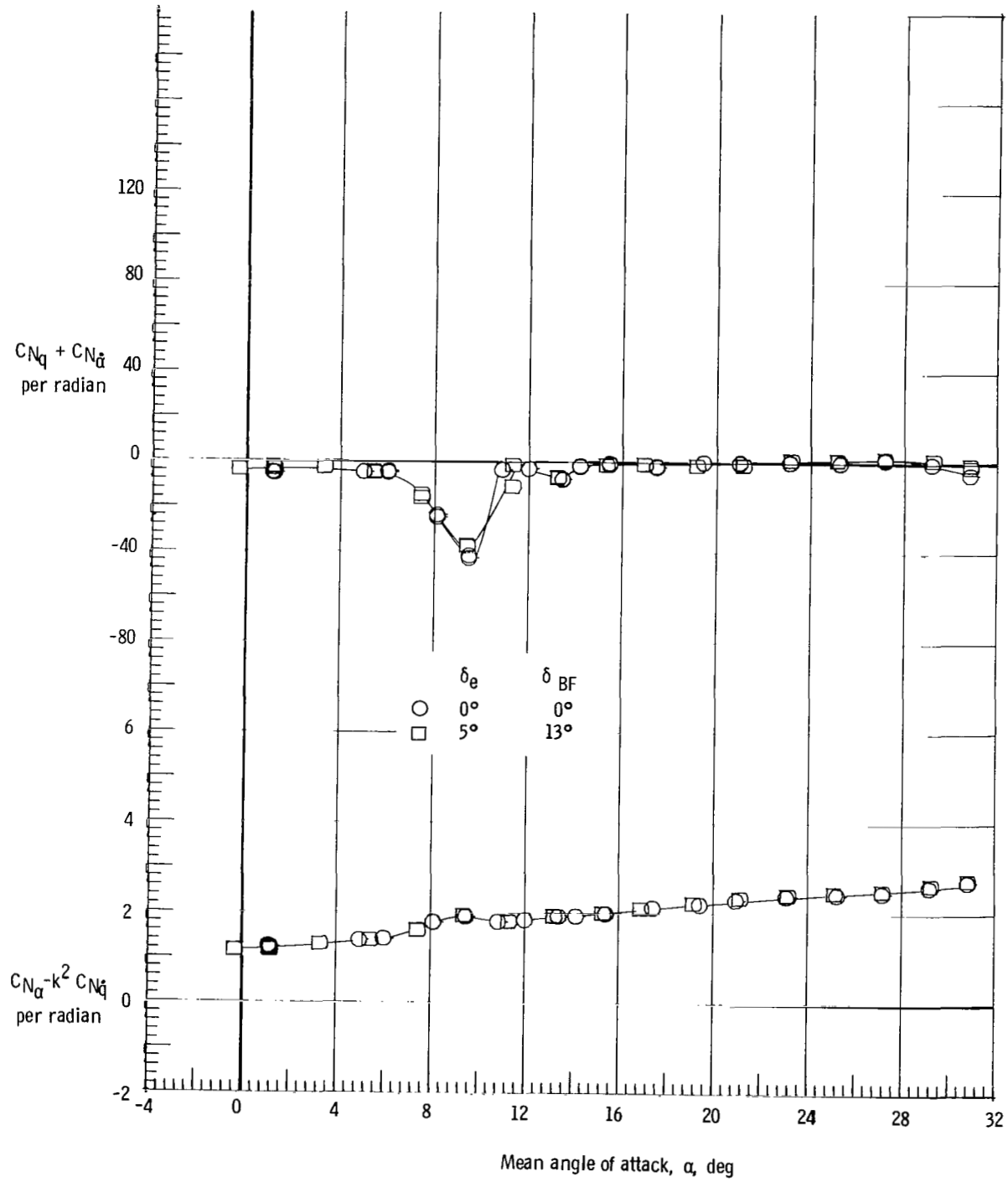

(e) M = 4.63.

Figure 16.- Concluded.

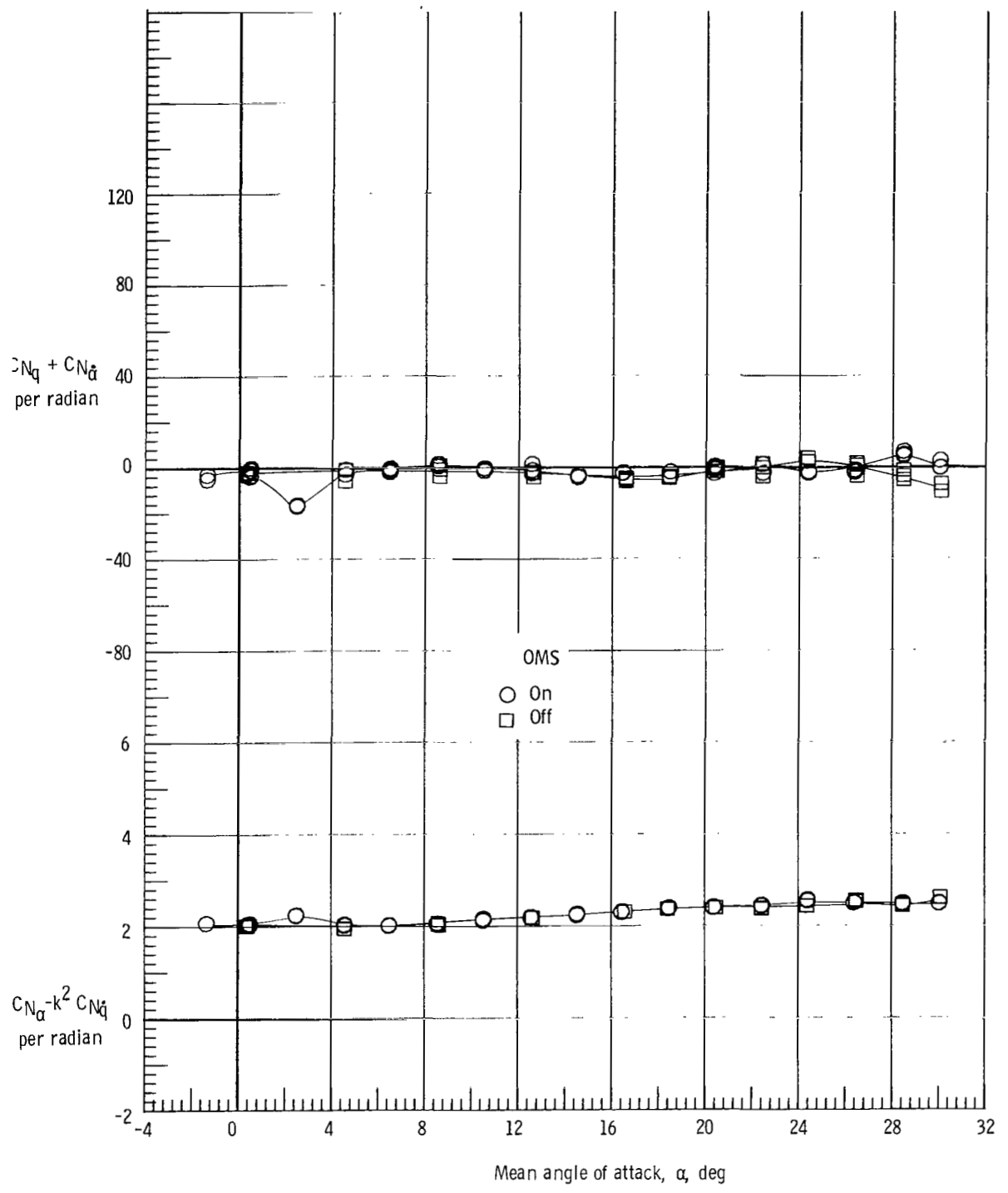

(a) M = 2.36.

Figure 17.- Effect of OMS on normal force due to pitch rate parameter and normal force due to pitch displacement parameter. Forward c.g.; $\delta_e = 0^o$; body flap removed; and rudder flare, 40^o.

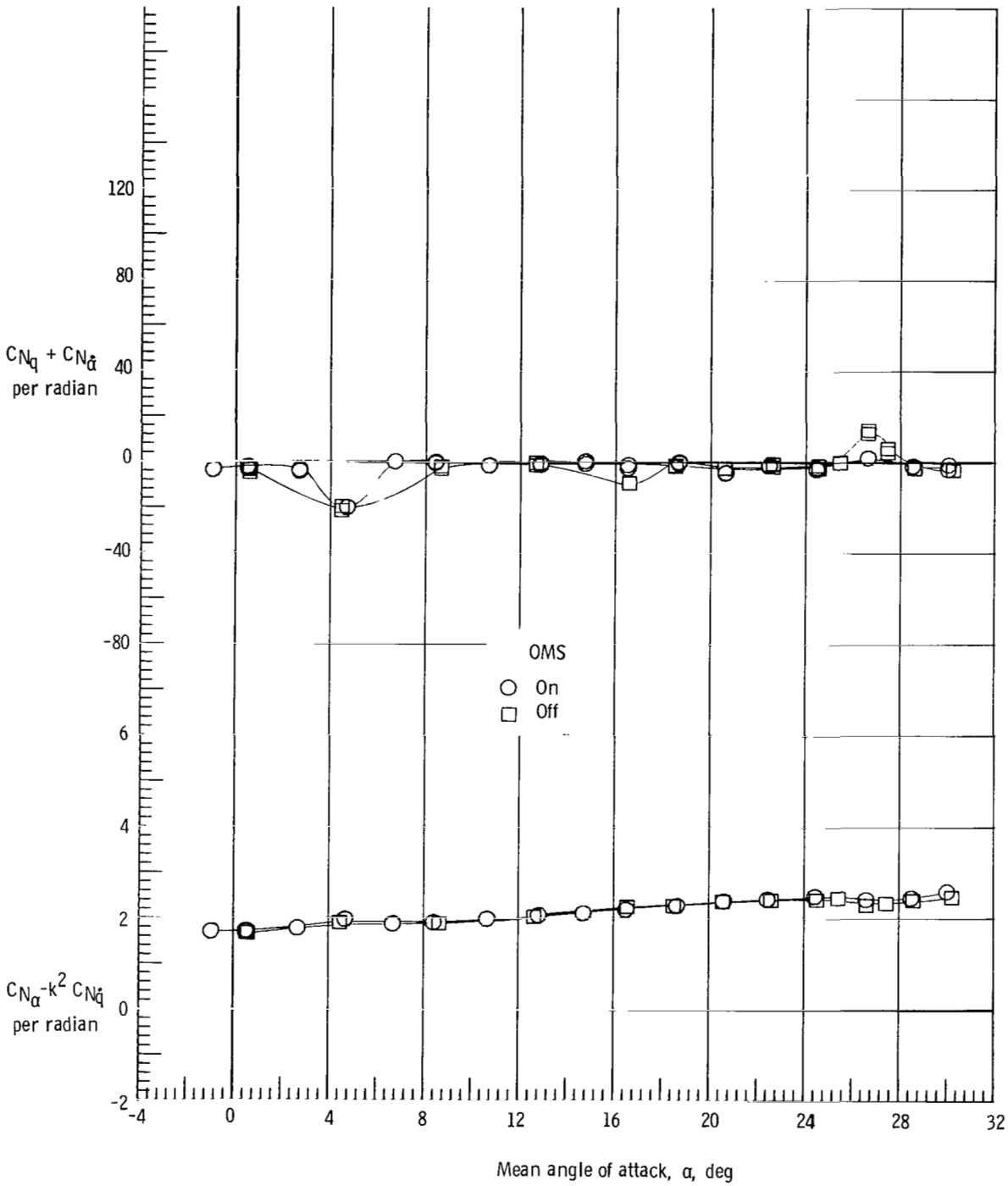

(b) M = 2.86.

Figure 17.- Continued.

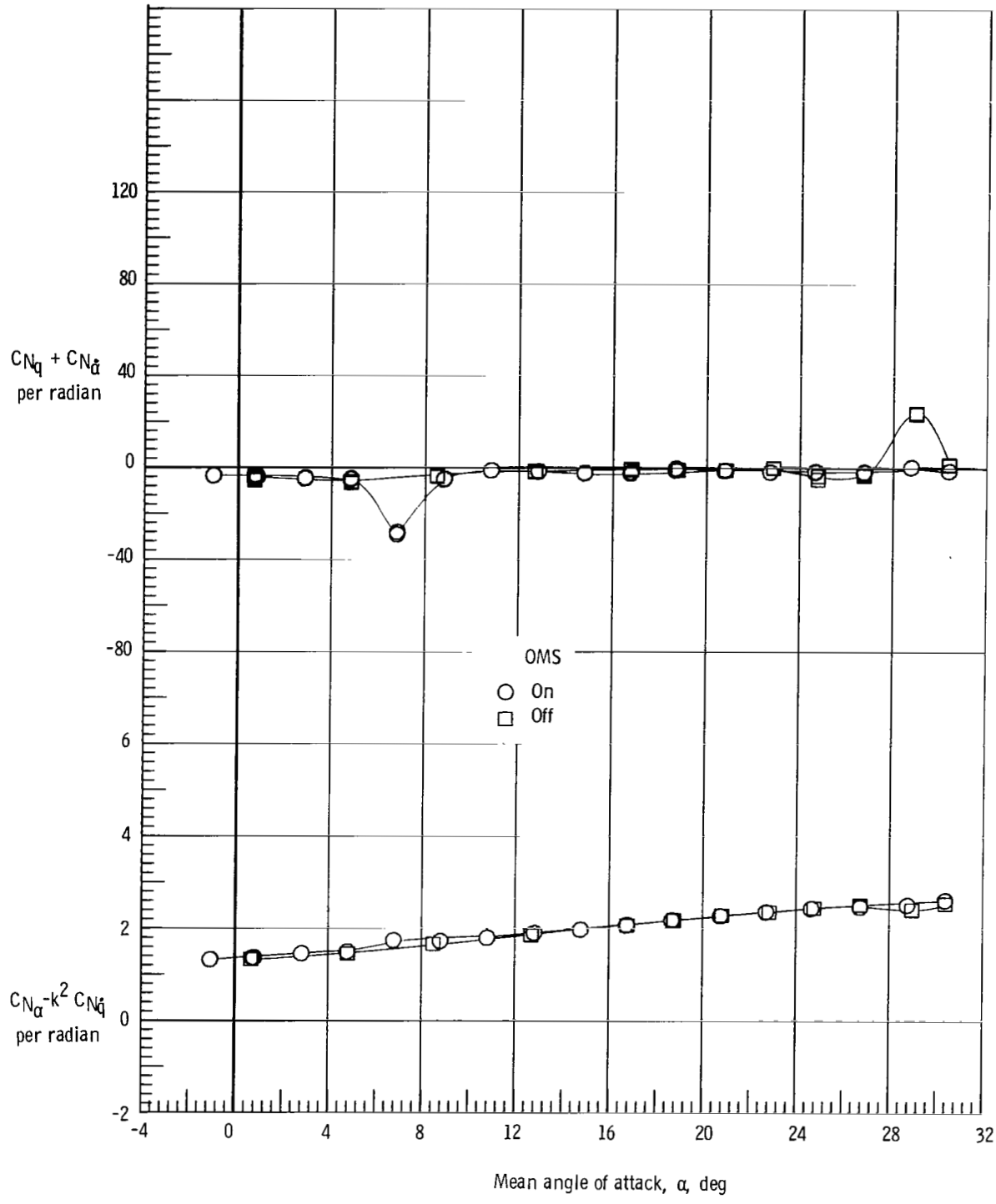

(c) M = 3.96.

Figure 17.- Continued.

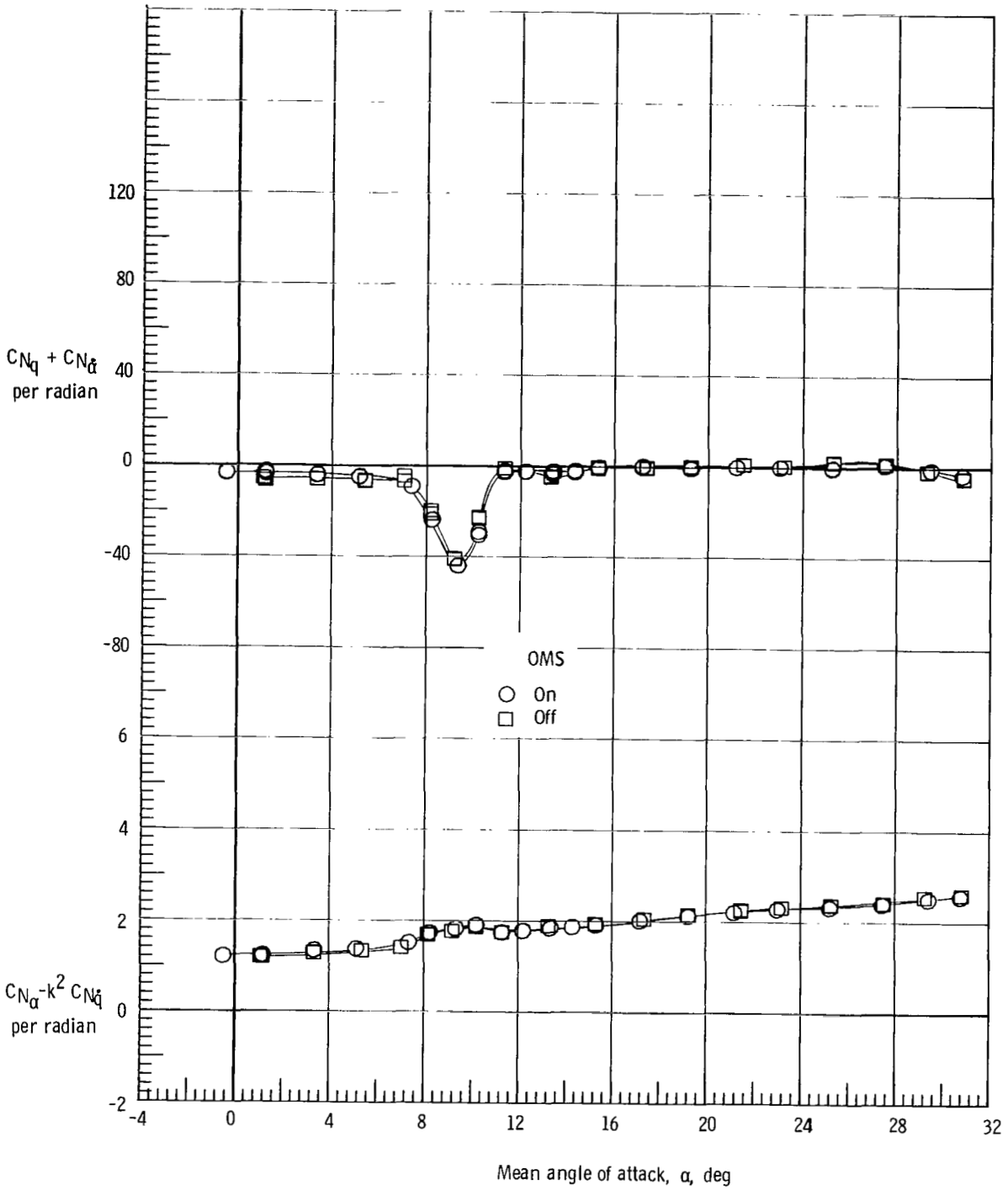

(d) M = 4.63.

Figure 17.- Concluded.

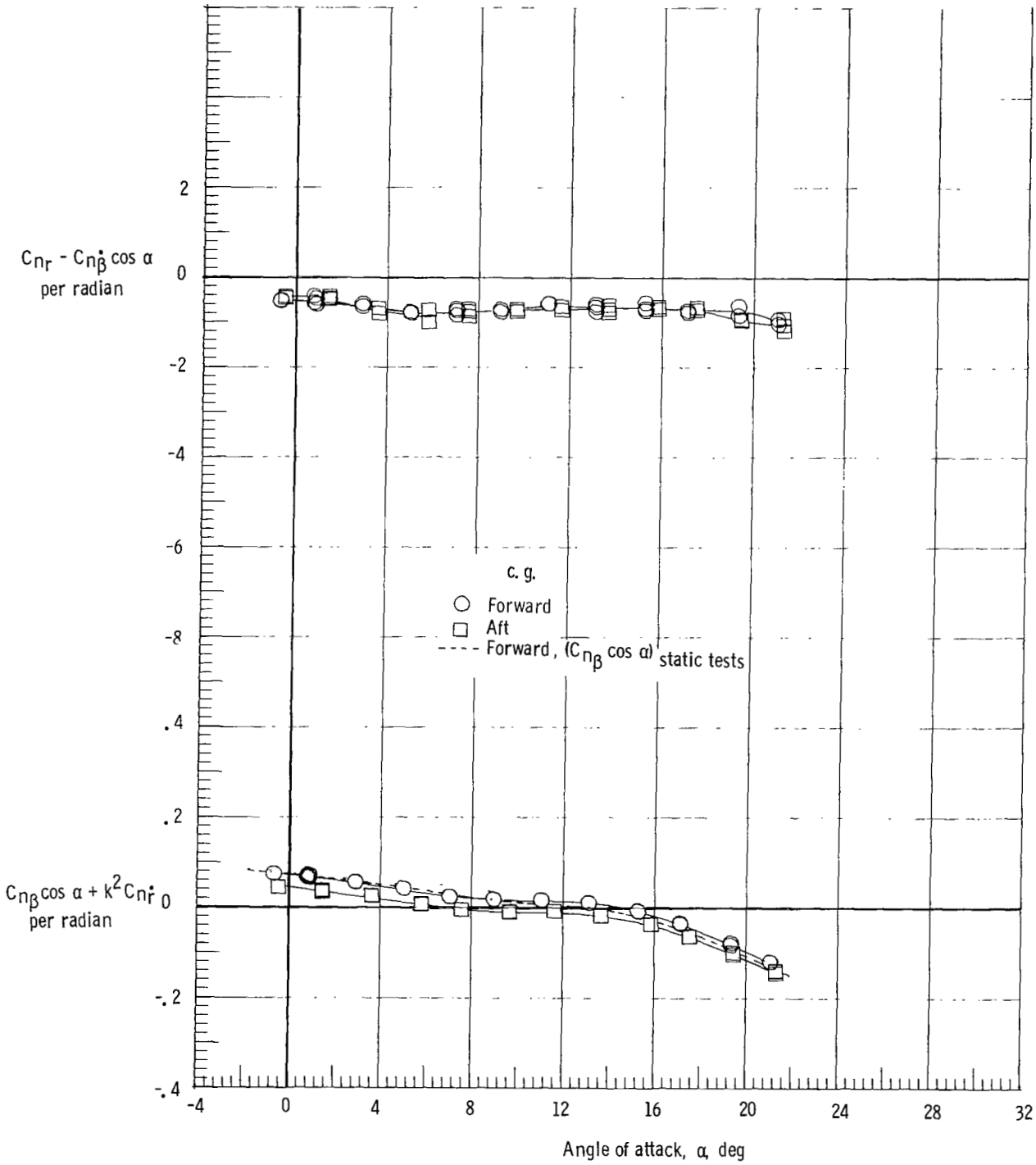

(a) M = 1.90.

Figure 18.- Effect of center-of-gravity (c.g.) position on damping-in-yaw parameter and on oscillatory directional-stability parameter. $\delta_e = 0^o$; body flap removed; and rudder flare, 40^o.

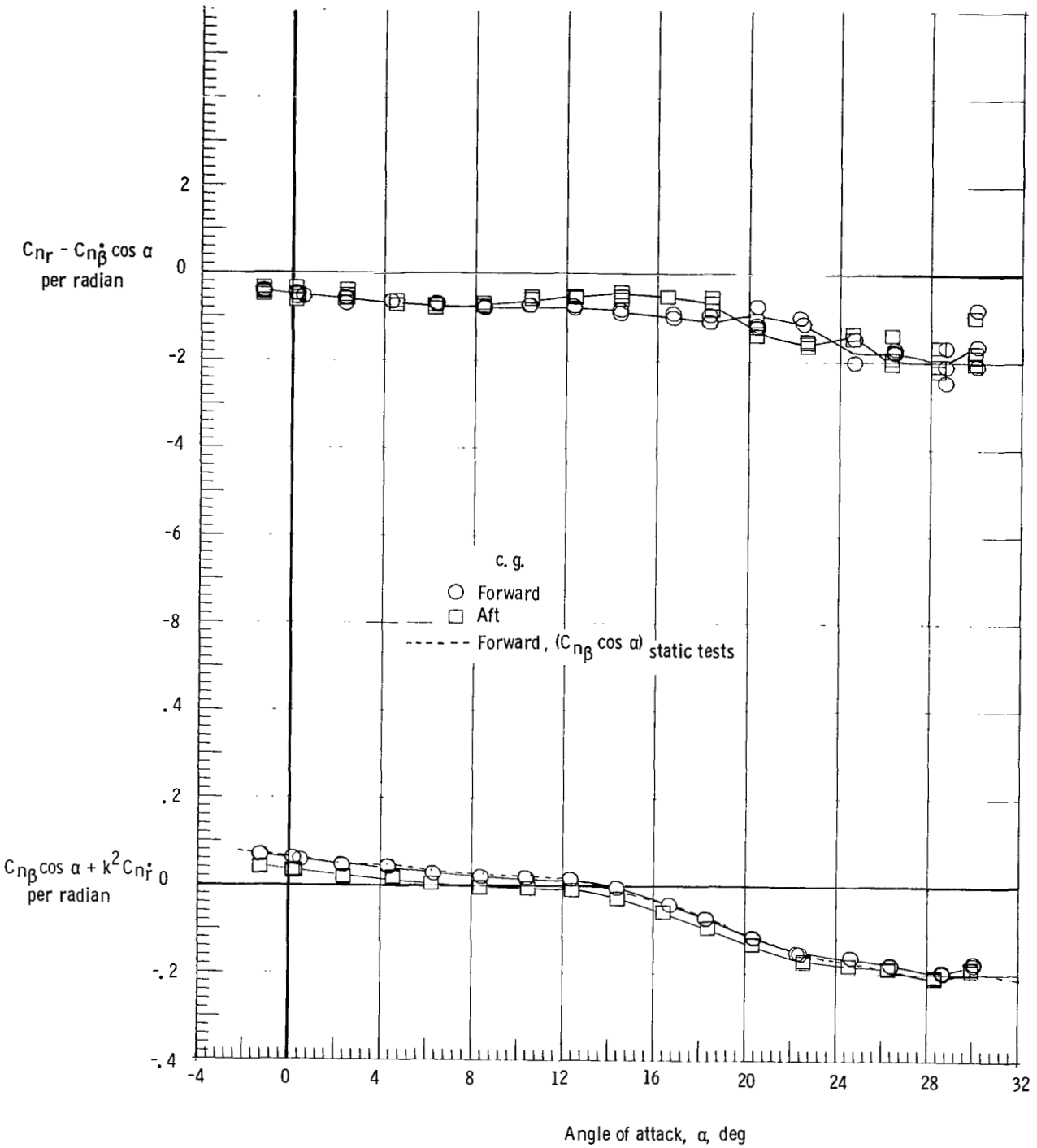

(b) M = 2.36.

Figure 18.- Continued.

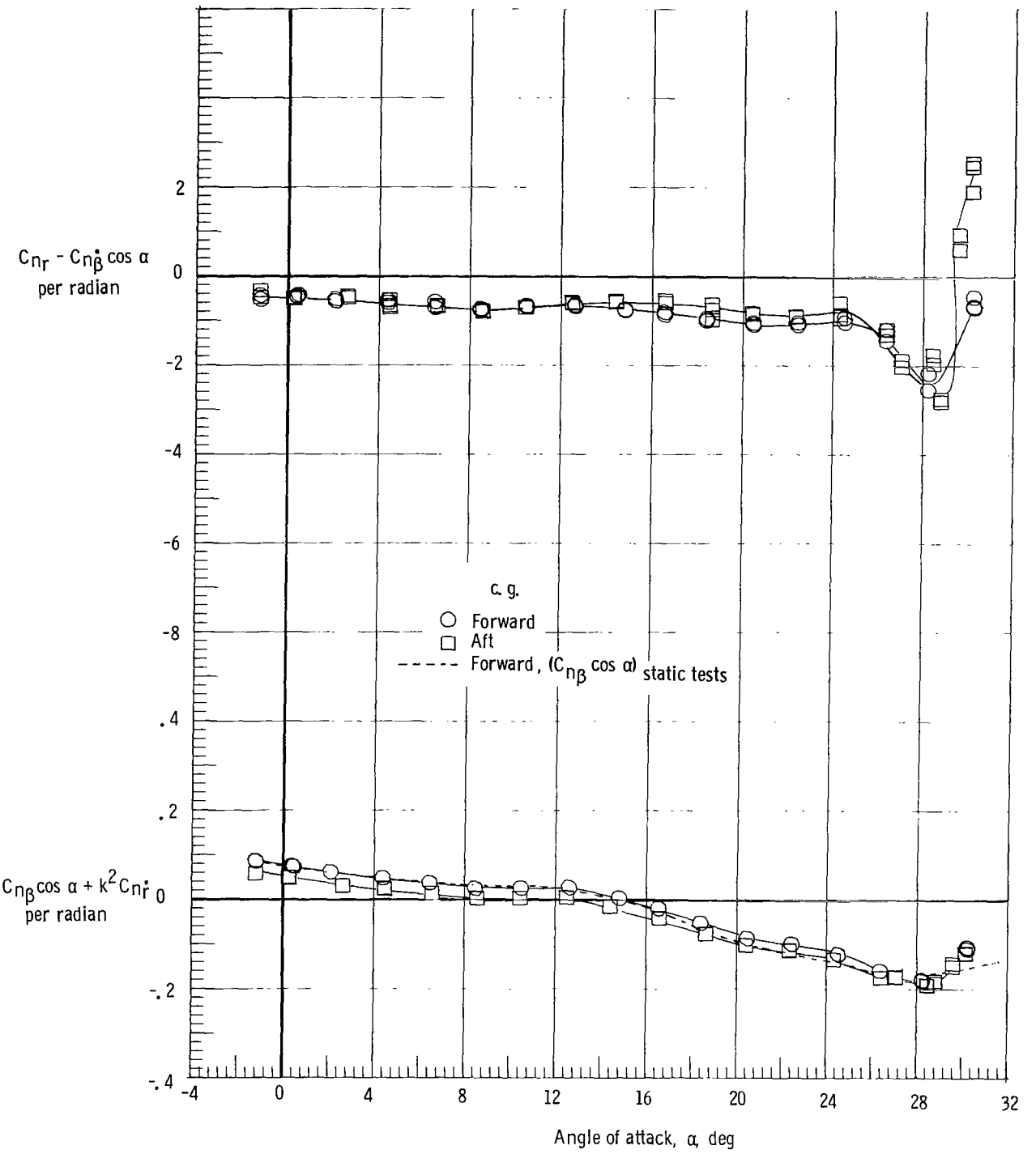

(c) M = 2.86.

Figure 18.- Continued.

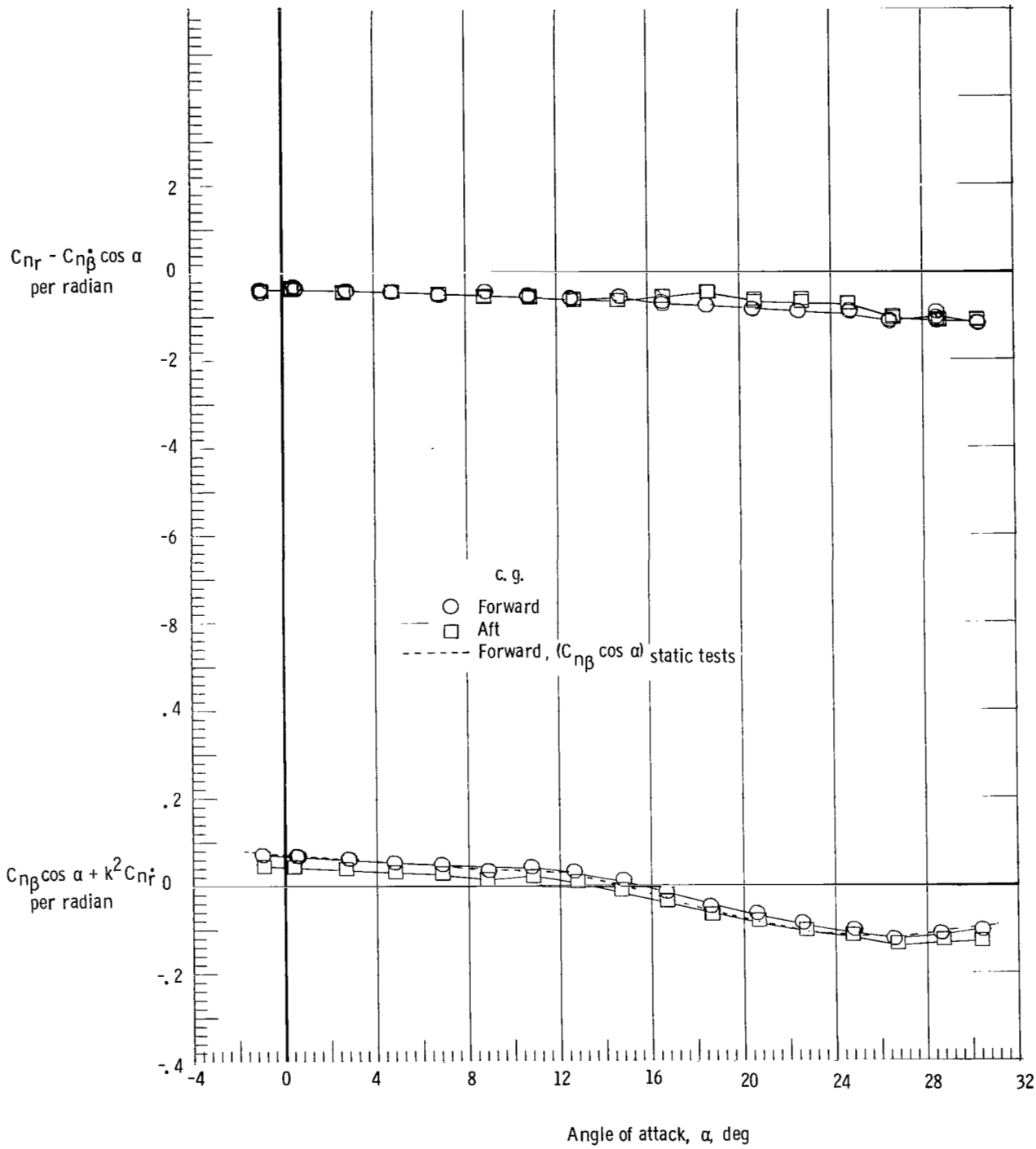

(d) M = 3.96.

Figure 18.- Continued.

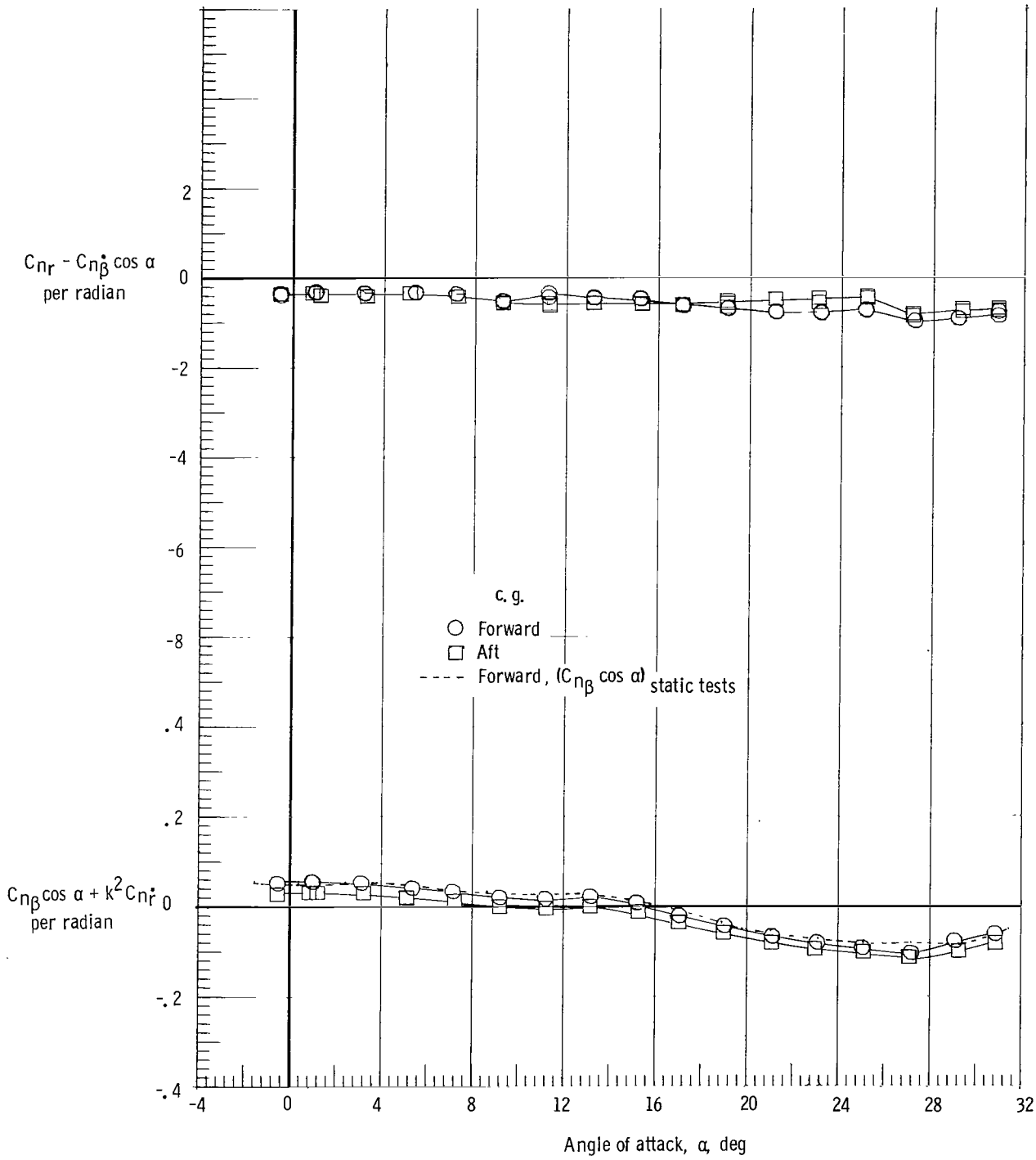

(e) M = 4.63.

Figure 18.- Concluded.

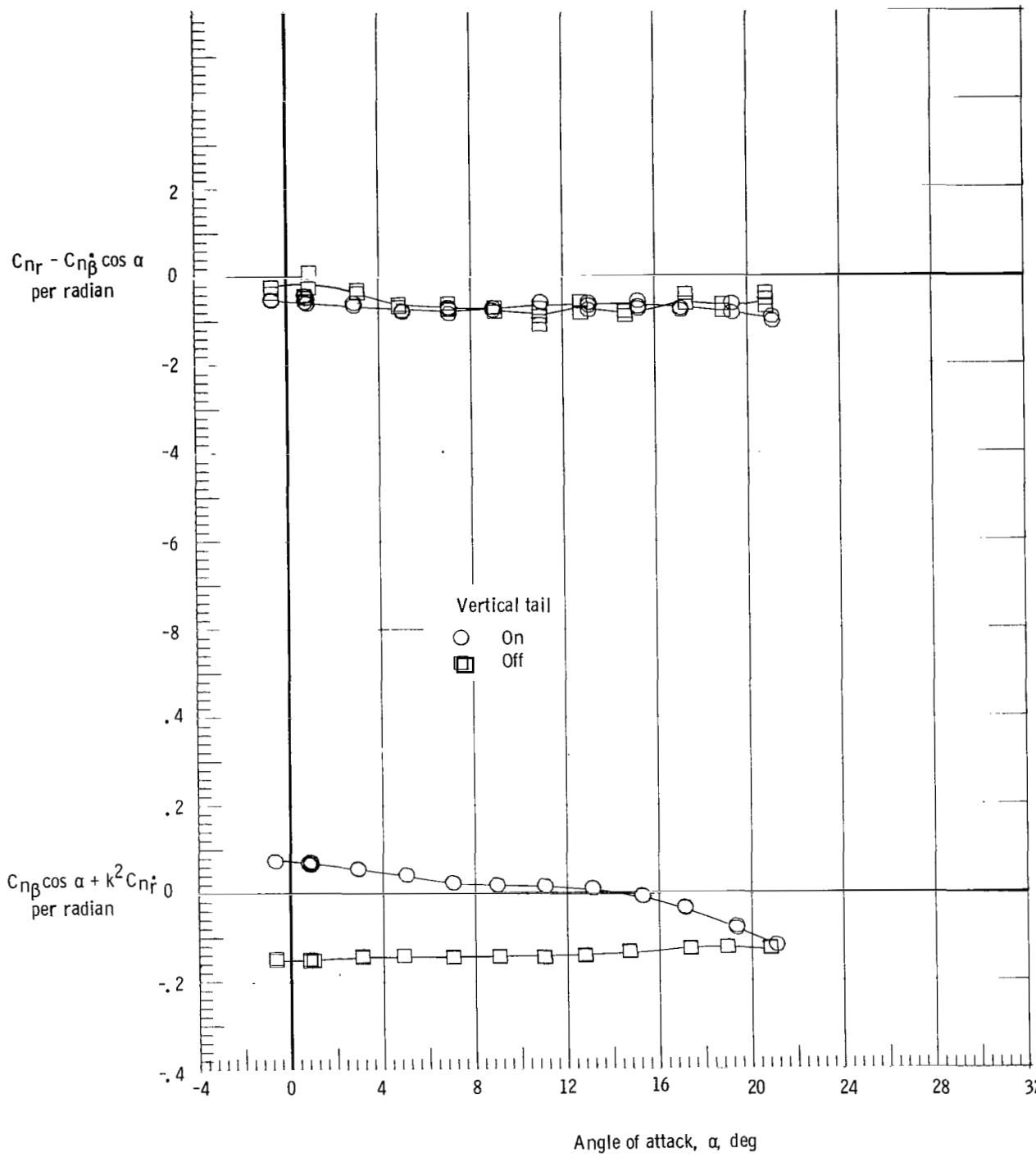

(a) M = 1.90.

Figure 19.- Effect of vertical tail on damping-in-yaw parameter and on oscillatory directional-stability parameter. Forward c.g.; $\delta_e = 0^o$; body flap removed; and rudder flare, 40^o.

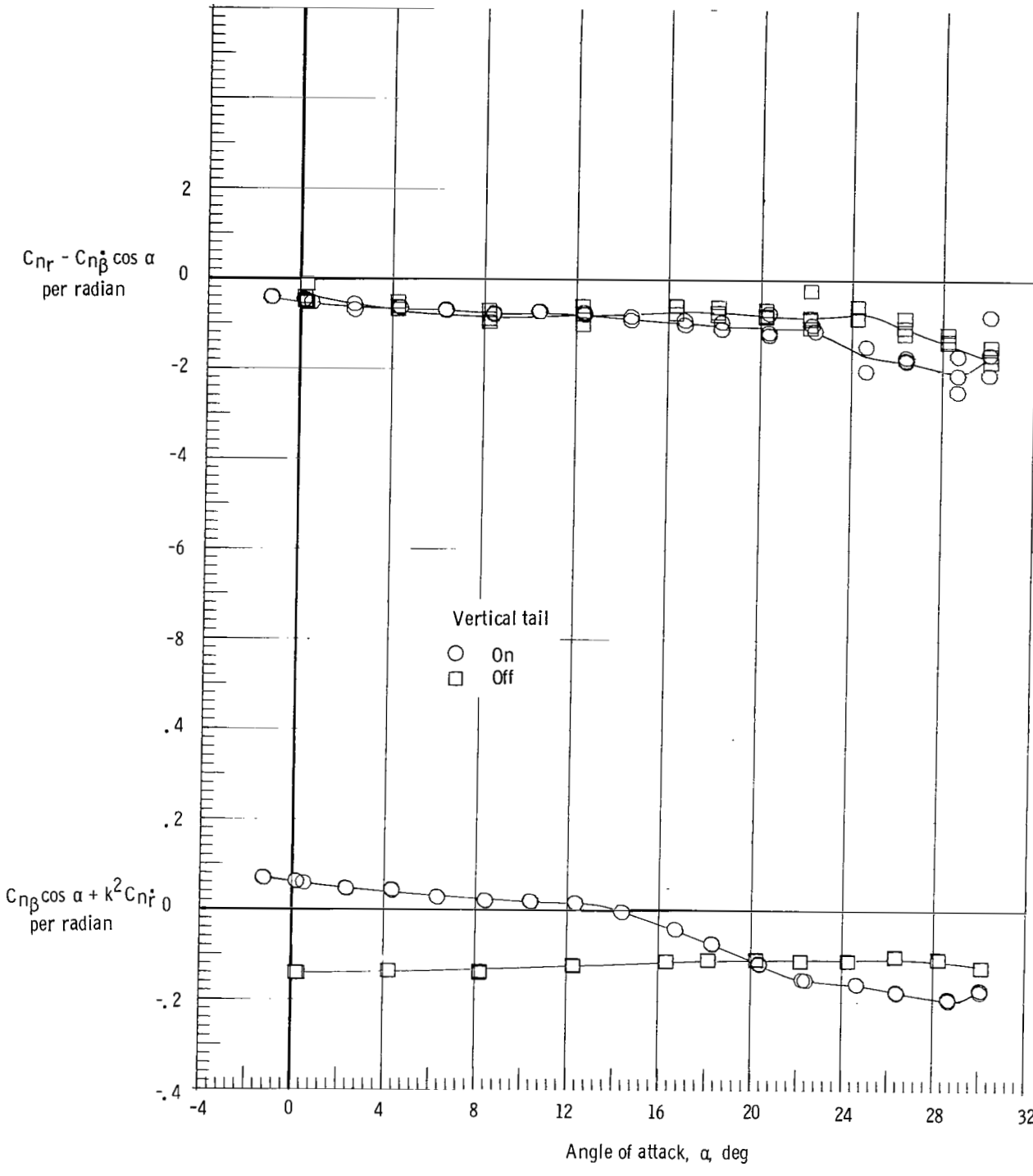

(b) M = 2.36.

Figure 19.- Continued.

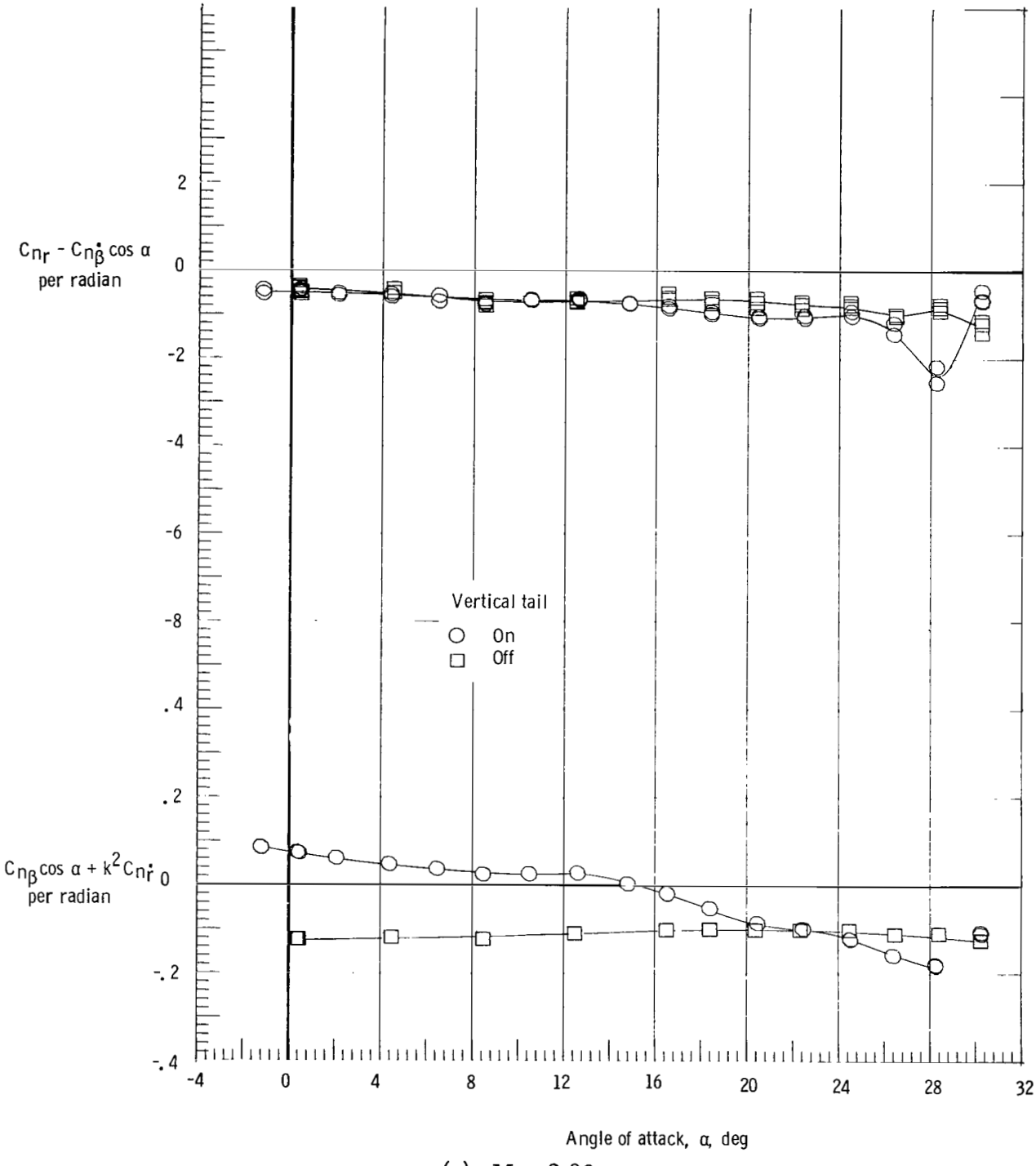

(c) M = 2.86.

Figure 19.- Continued.

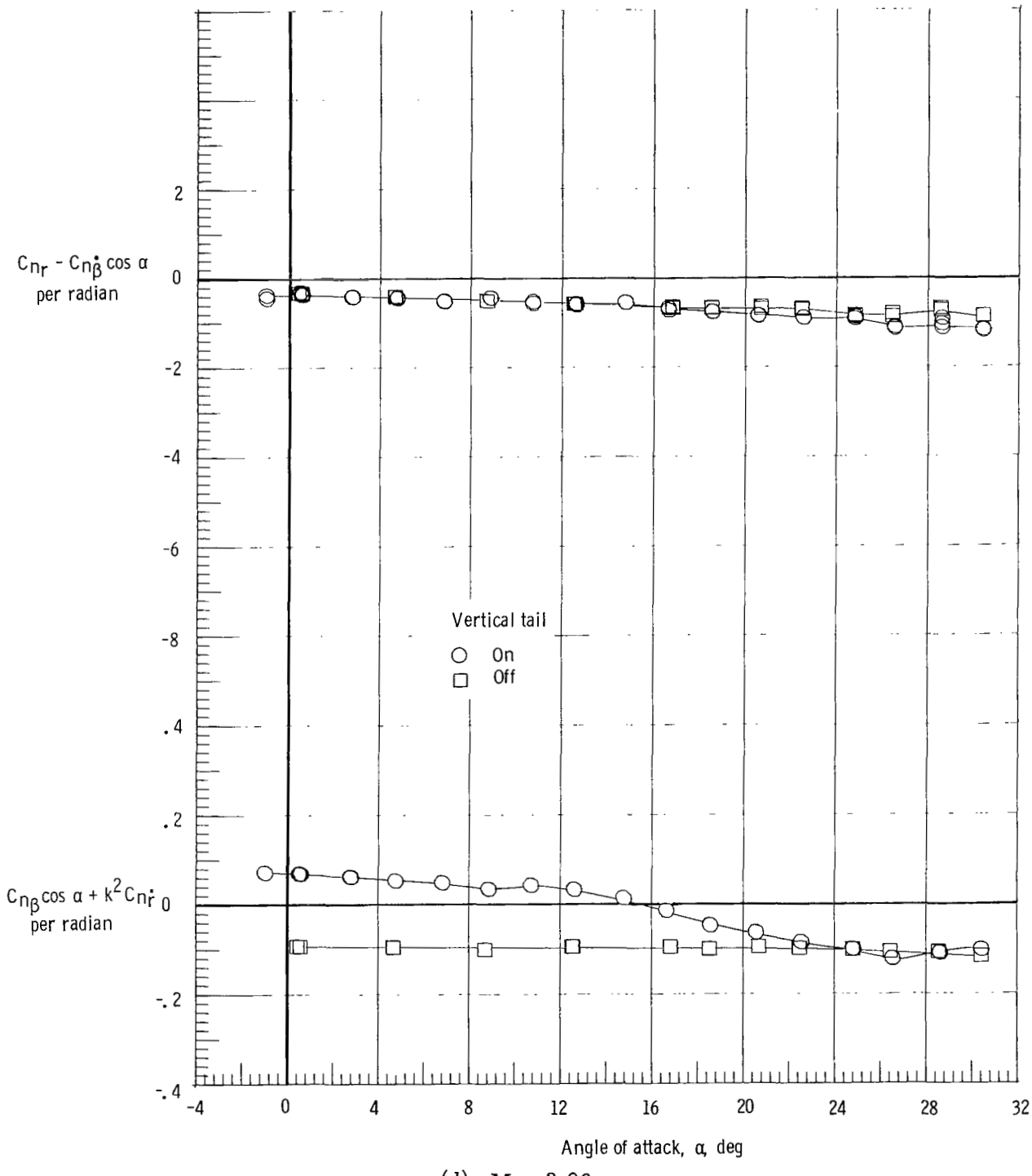

(d) M = 3.96.

Figure 19.- Continued.

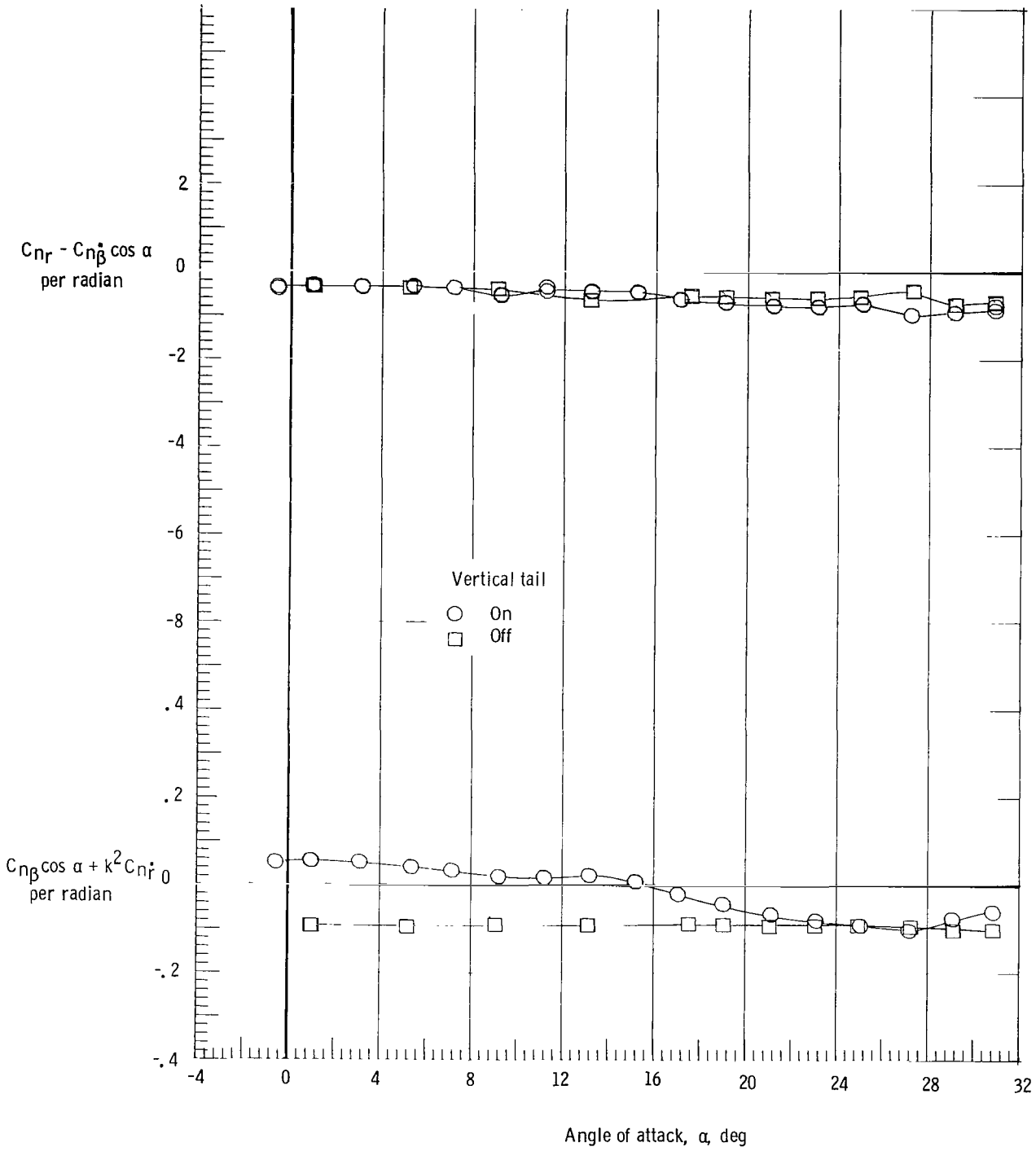

(e) M = 4.63.

Figure 19.- Concluded.

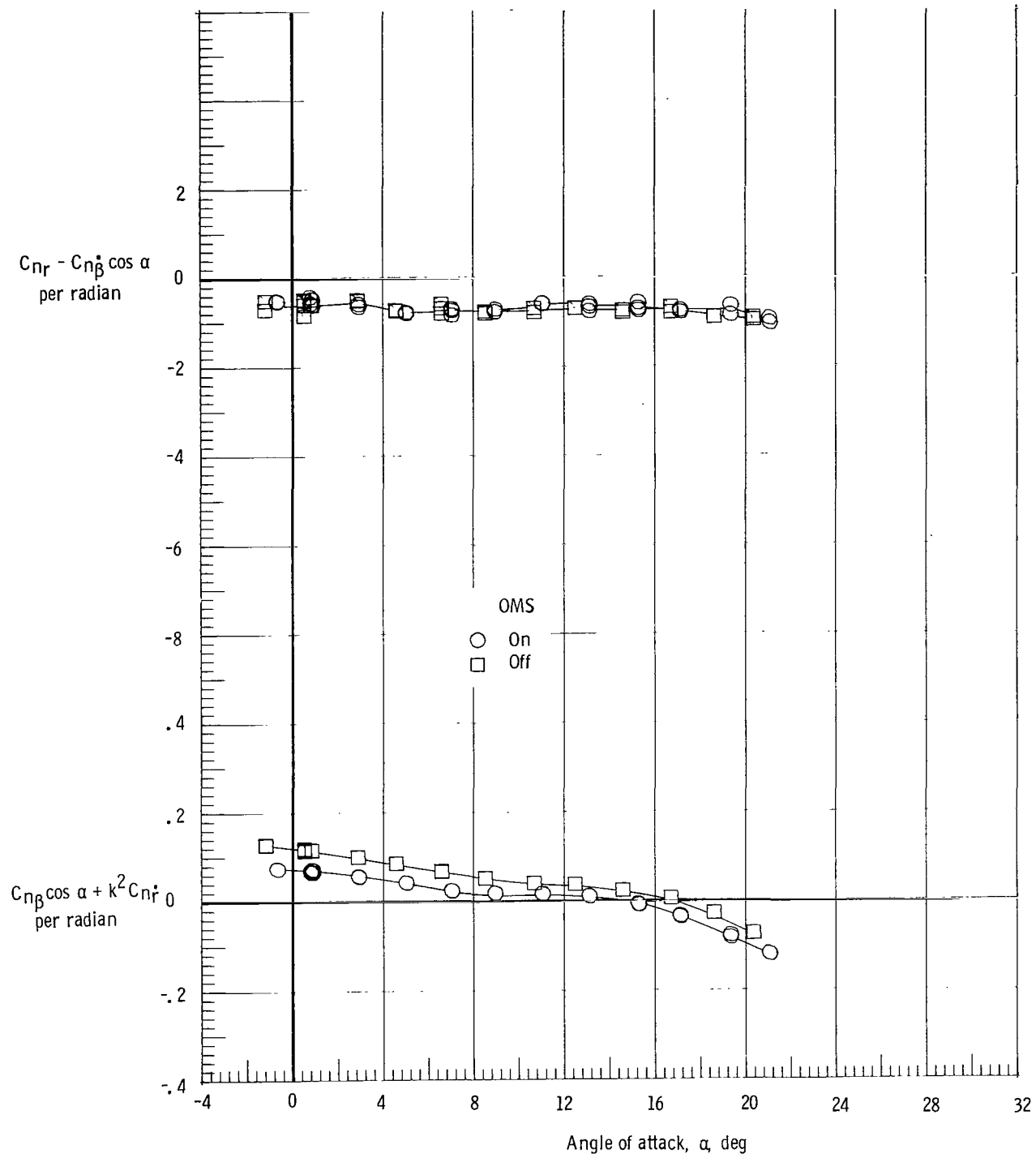

(a) M = 1.90.

Figure 20.- Effect of OMS installation on damping-in-yaw parameter and on oscillatory directional-stability parameter. Forward c.g.; $\delta_e = 0^o$; body flap removed; and rudder flare, 40^o.

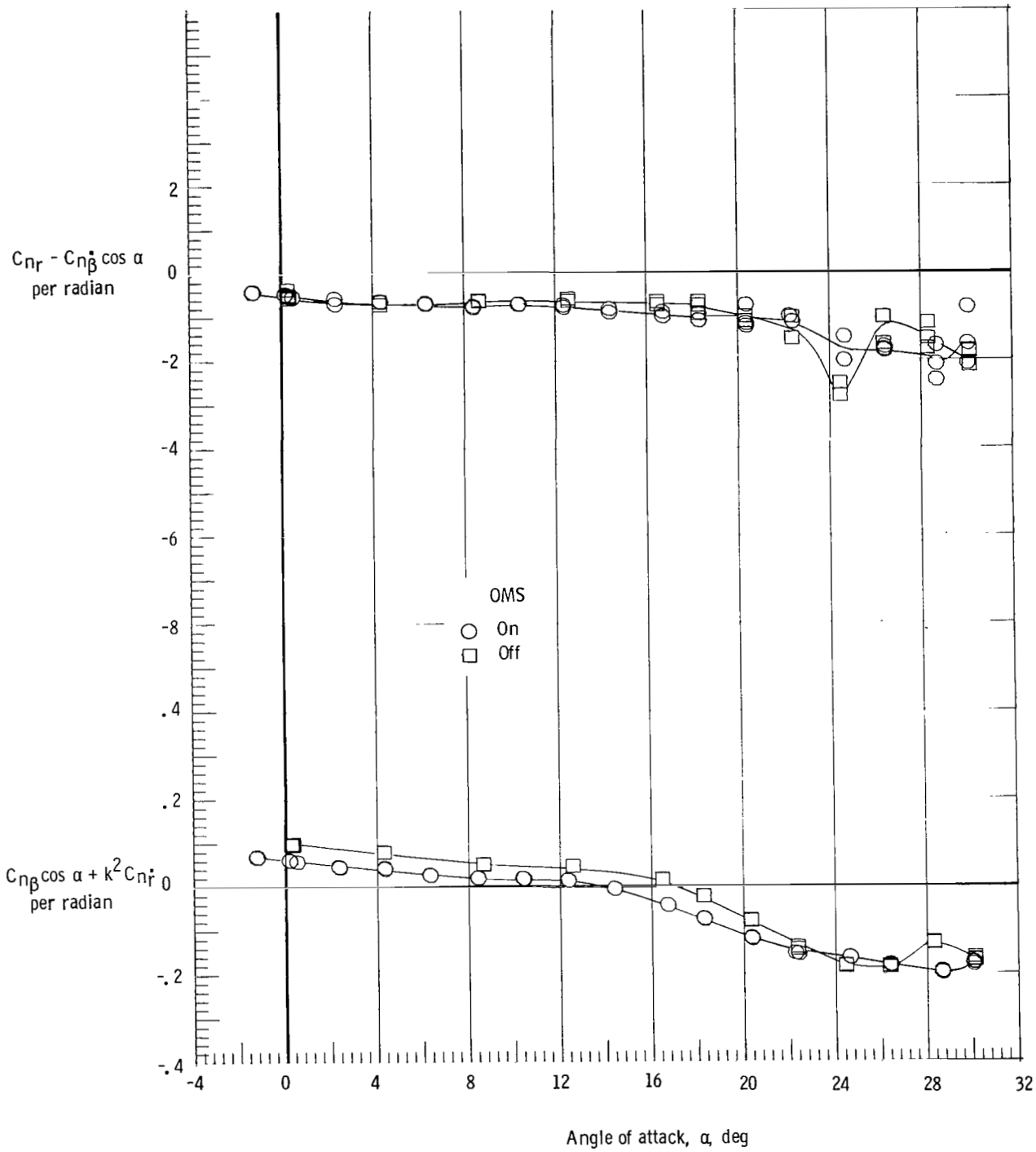

(b) M = 2.36.

Figure 20.- Continued.

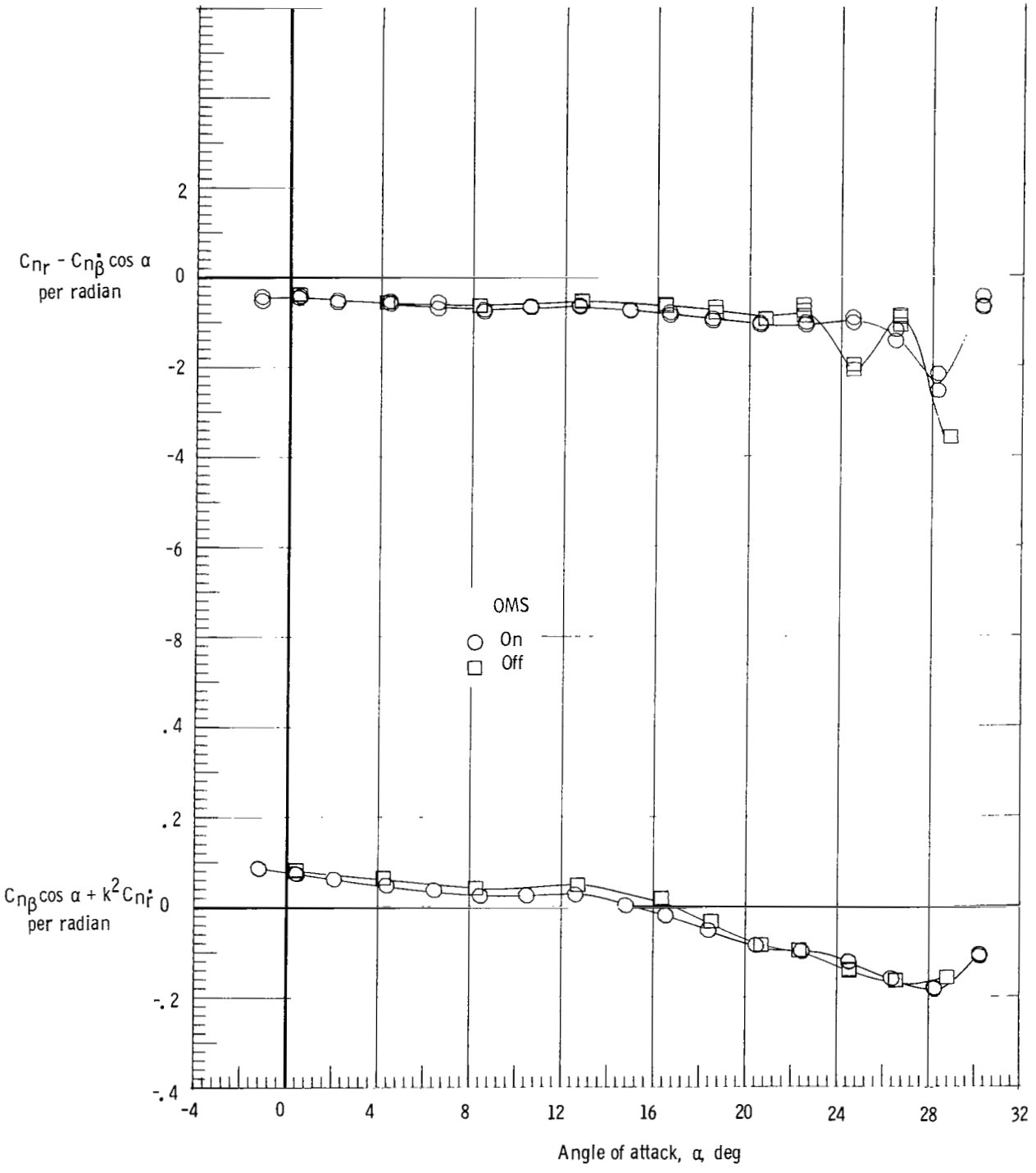

(c) M = 2.86.

Figure 20.- Continued.

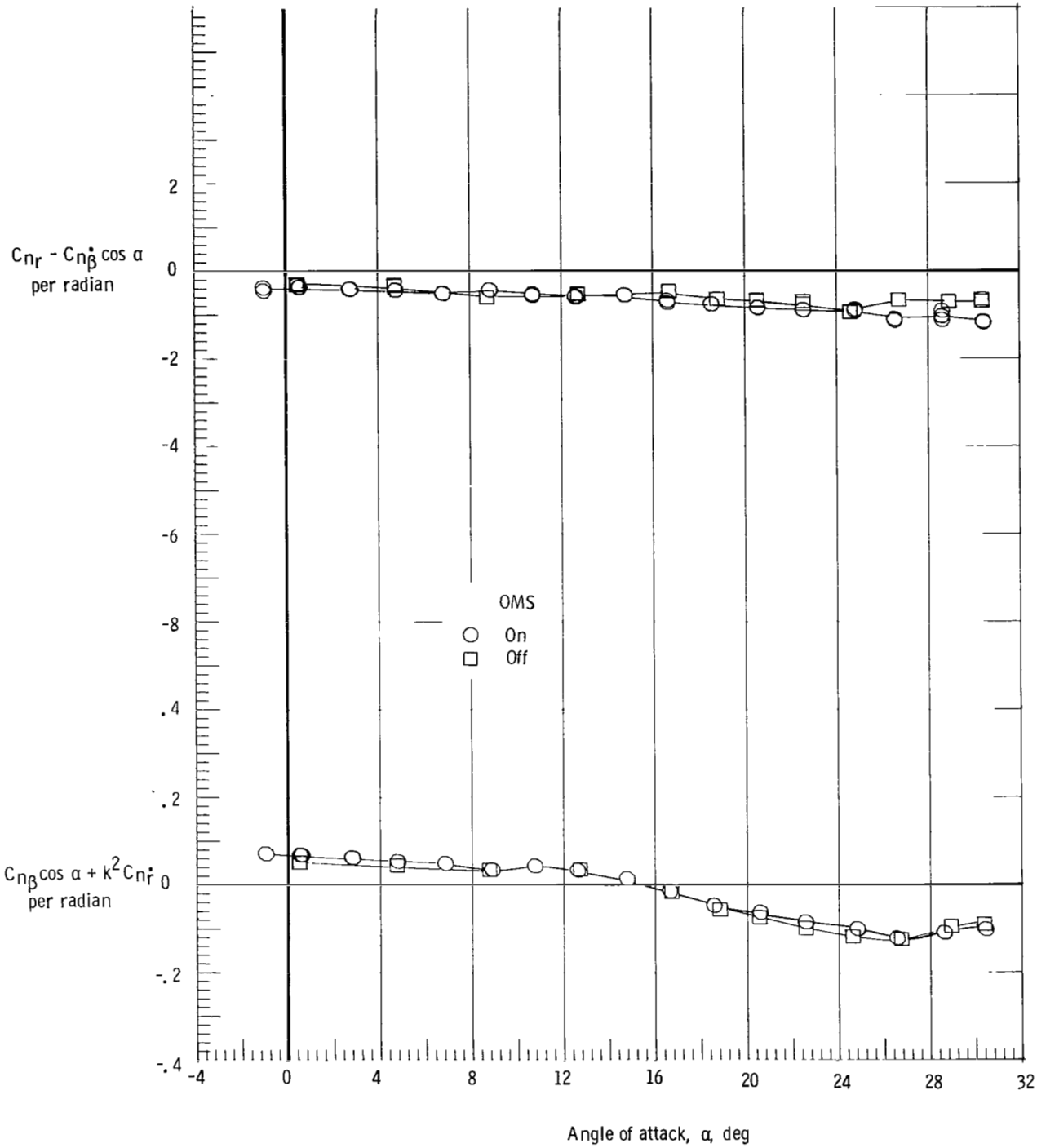

(d) M = 3.96.

Figure 20.- Continued.

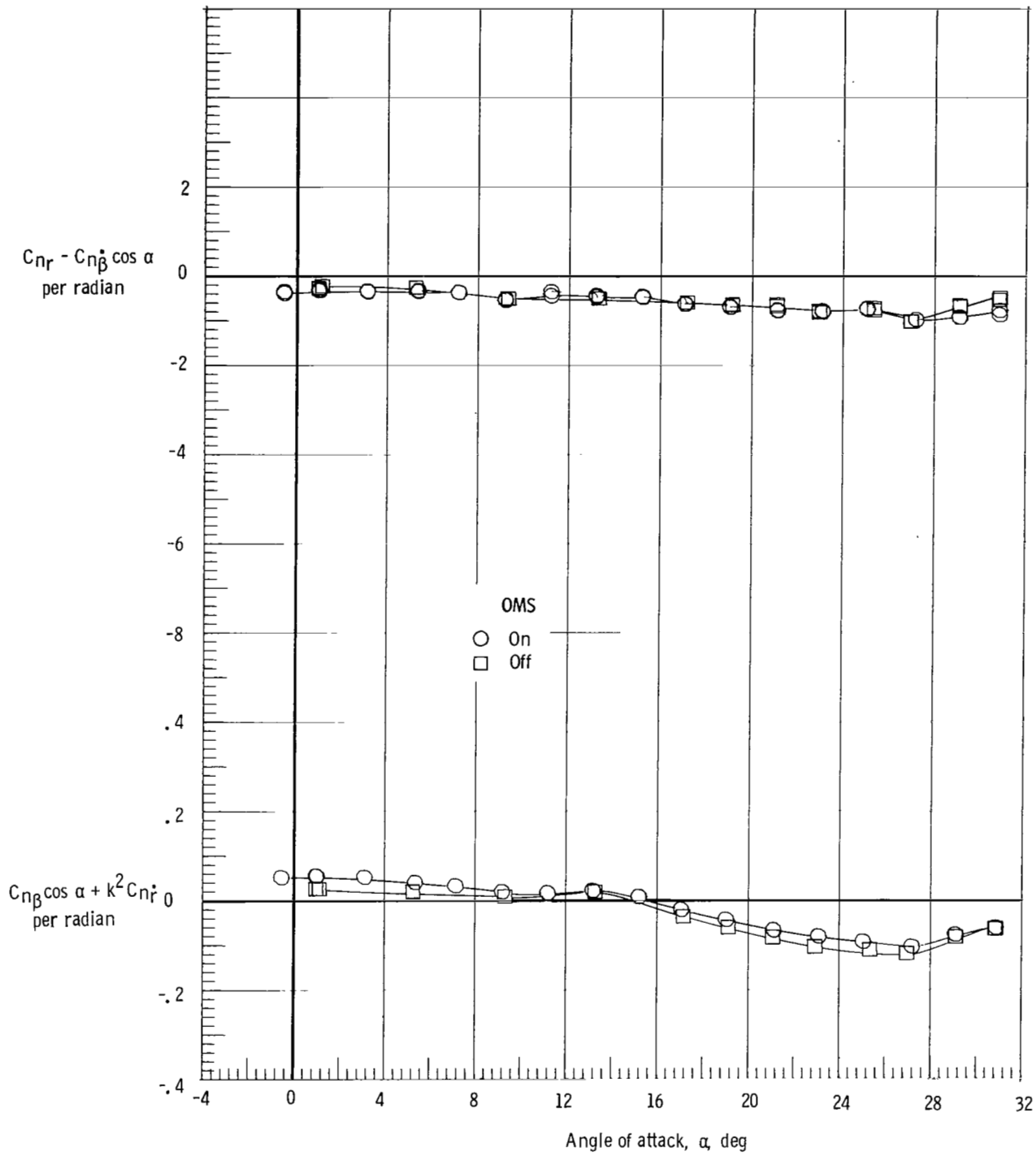

(e) M = 4.63.

Figure 20.- Concluded.

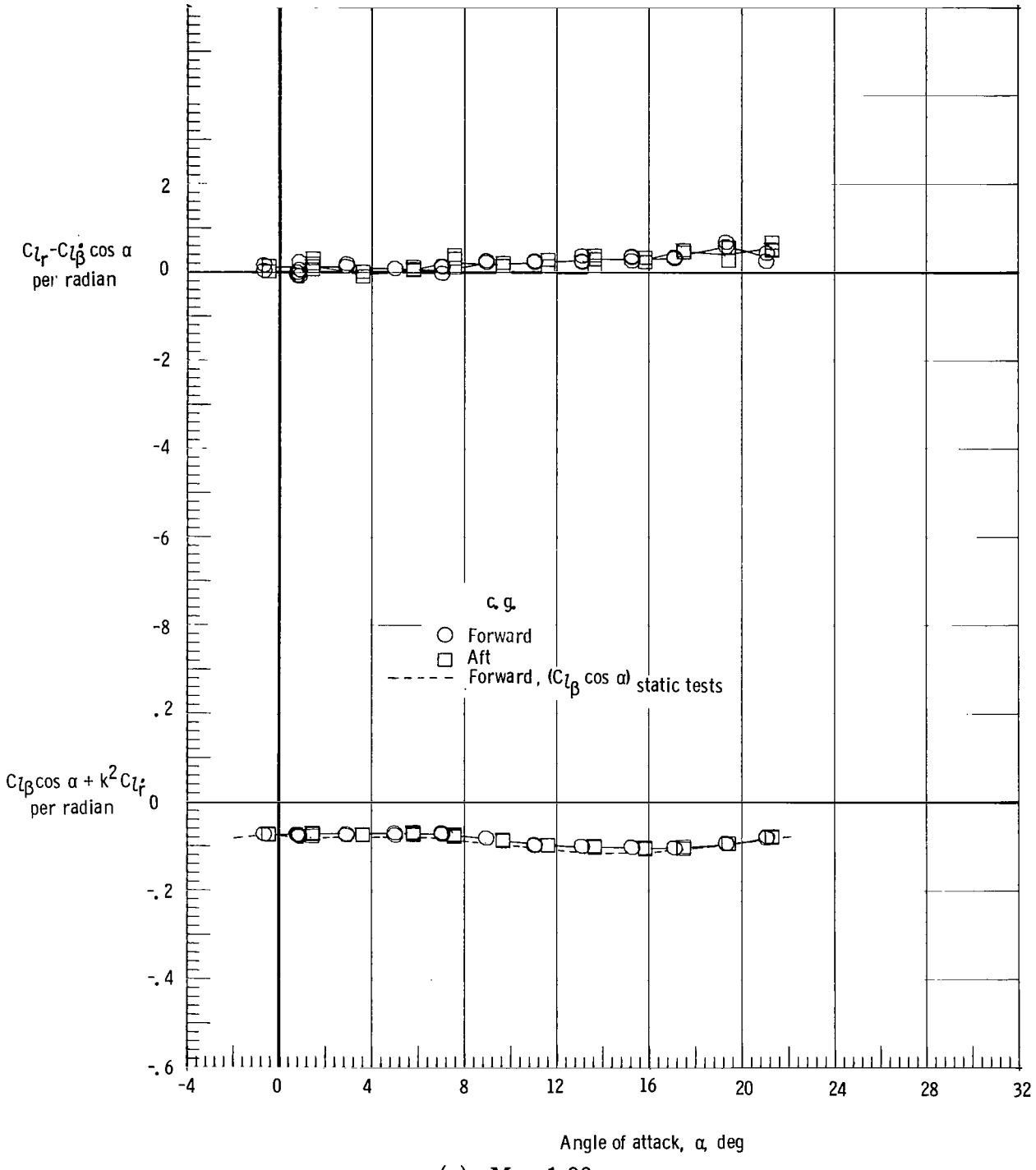

(a) M = 1.90.

Figure 21.- Effect of center-of-gravity (c.g.) position on rolling moment due to yaw rate parameter and on the effective dihedral parameter. $\delta_e = 0^o$; body flap removed; and rudder flare, 40^o.

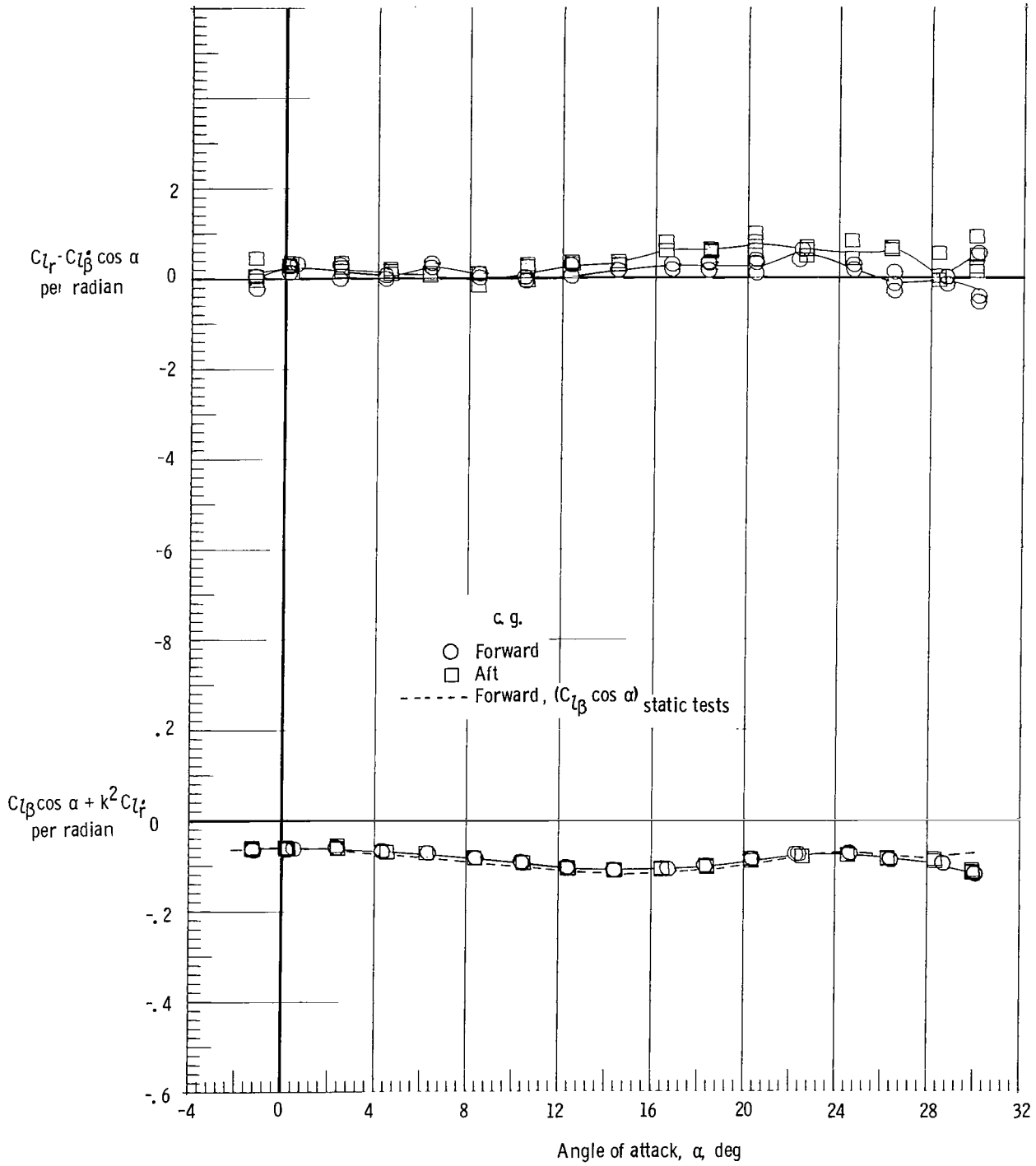

(b) M = 2.36.

Figure 21.- Continued.

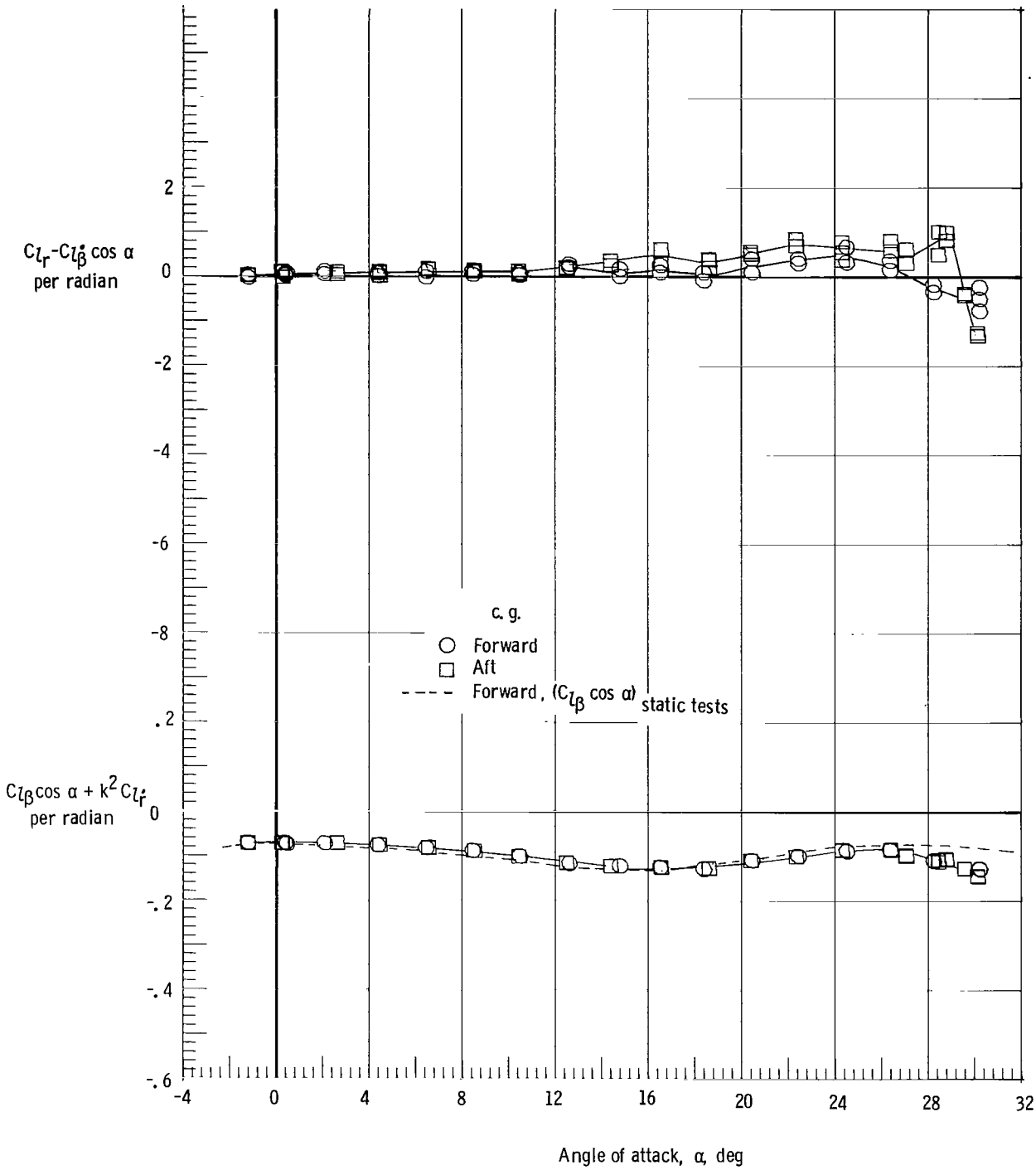

(c) M = 2.86.

Figure 21.- Continued.

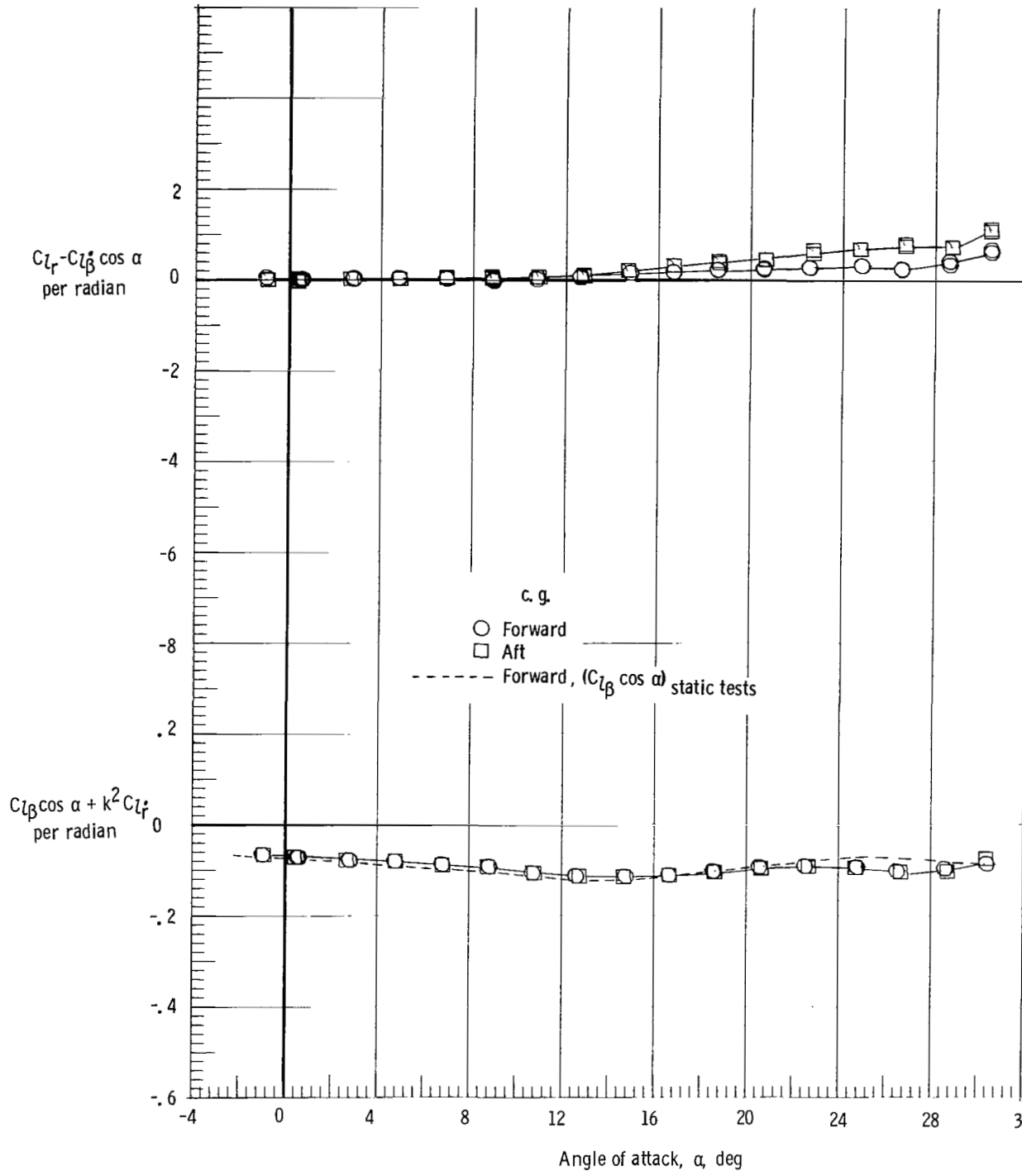

(d) M = 3.96.

Figure 21.- Continued.

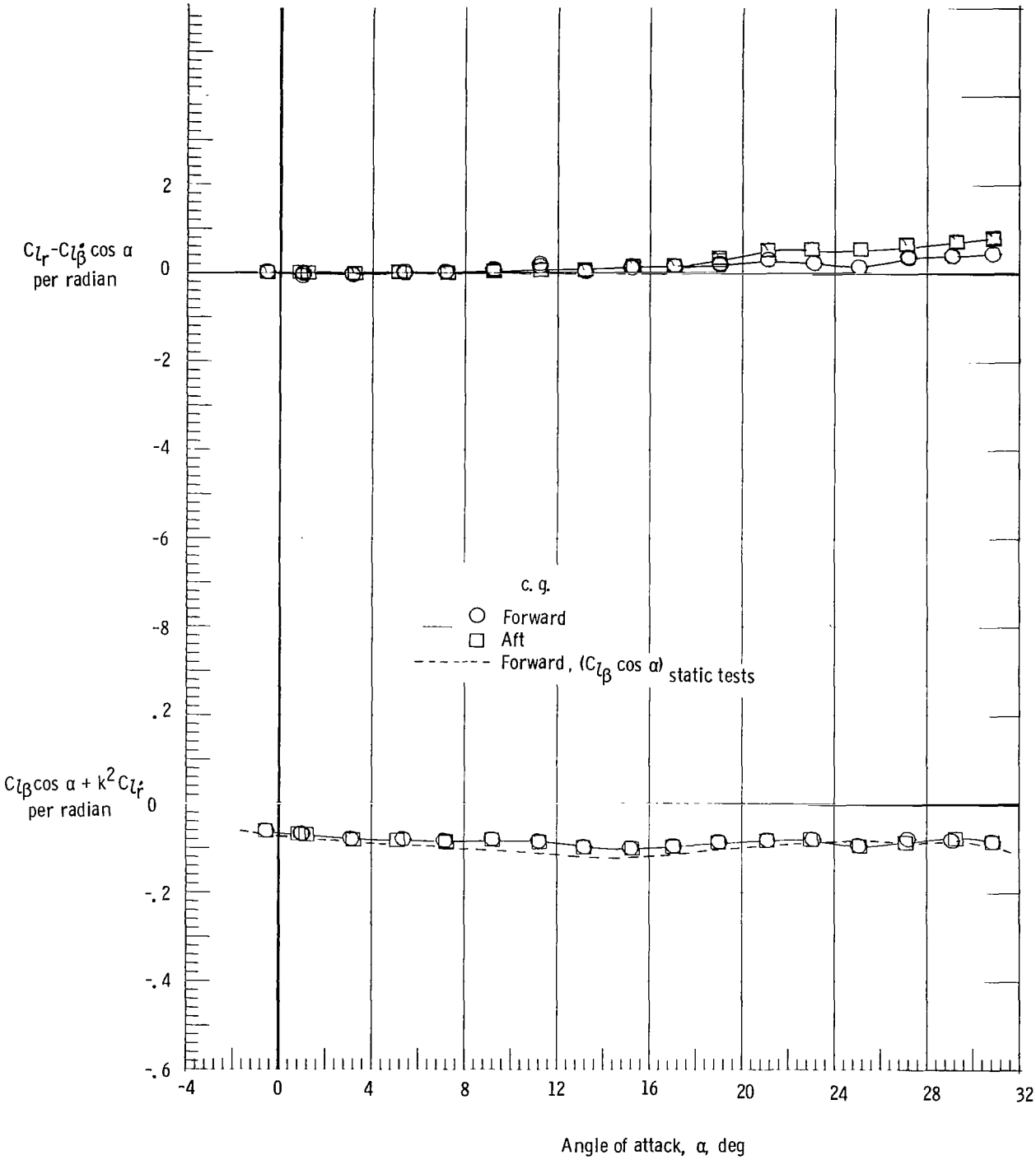

(e) M = 4.63.

Figure 21.- Concluded.

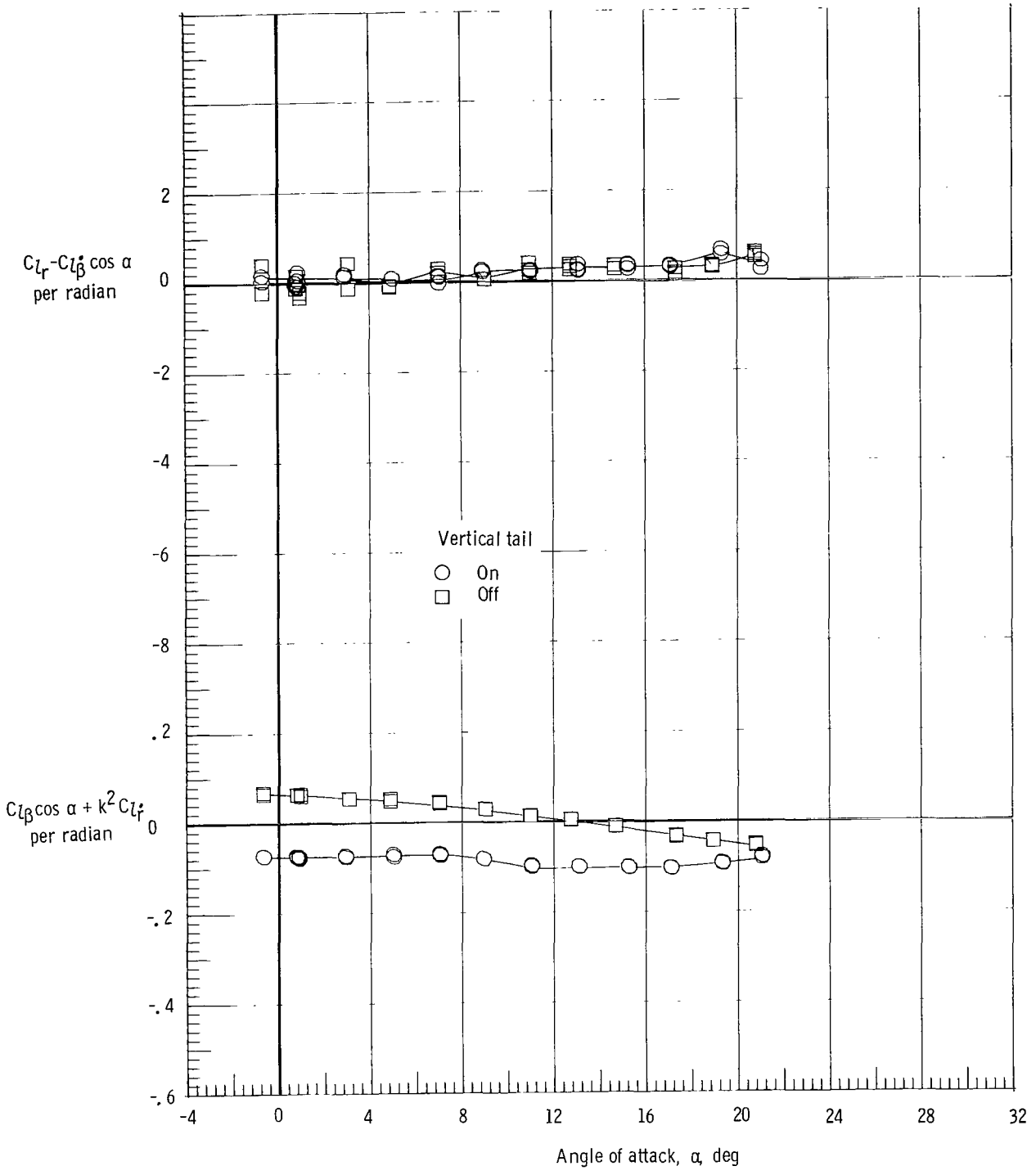

(a) M = 1.90.

Figure 22.- Effect of vertical tail on rolling moment due to yaw rate parameter and on effective dihedral parameter. Forward c.g.; $\delta_e = 0^o$; body flap removed; and rudder flare, 40^o.

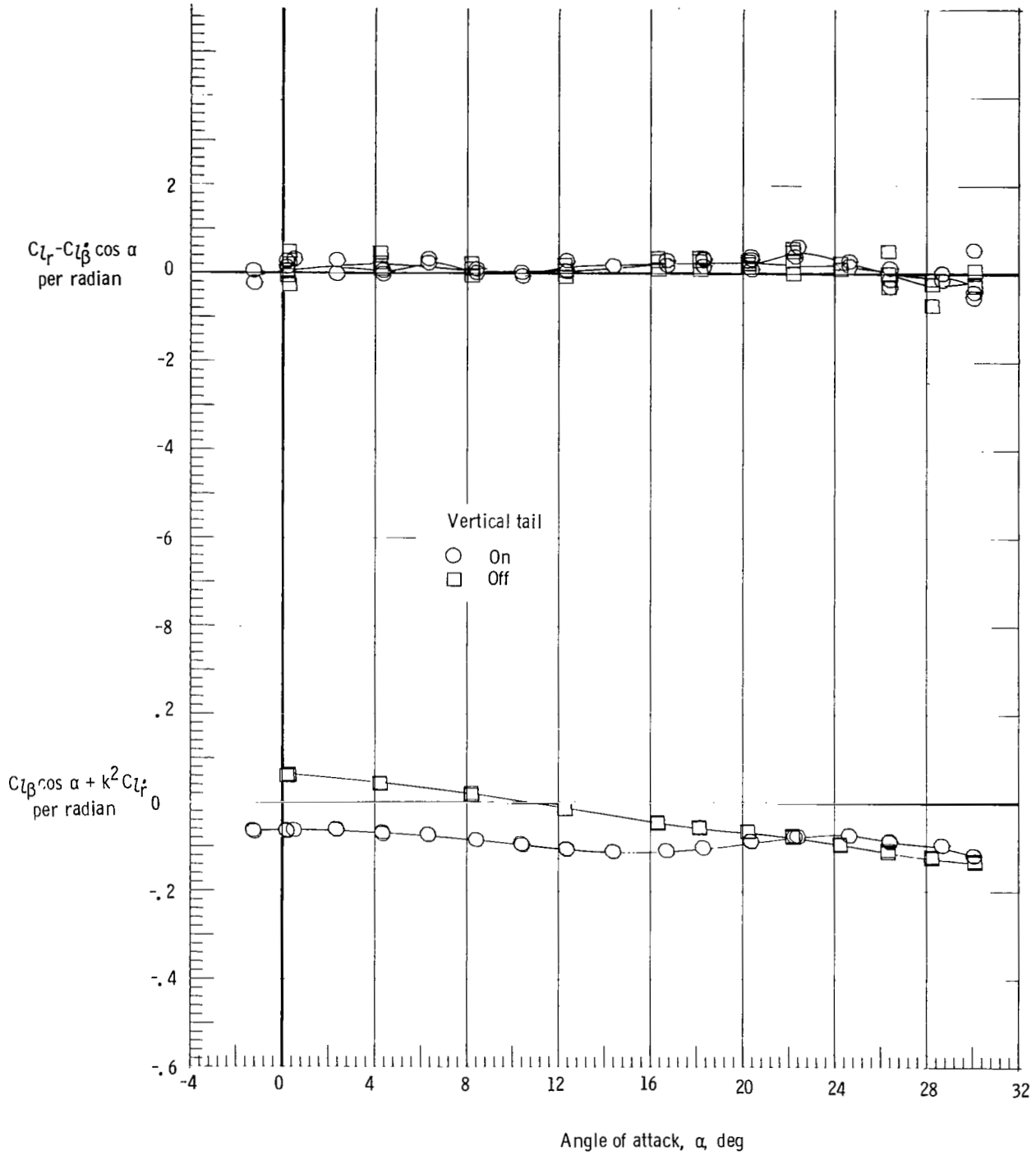

(b) M = 2.36.

Figure 22.- Continued.

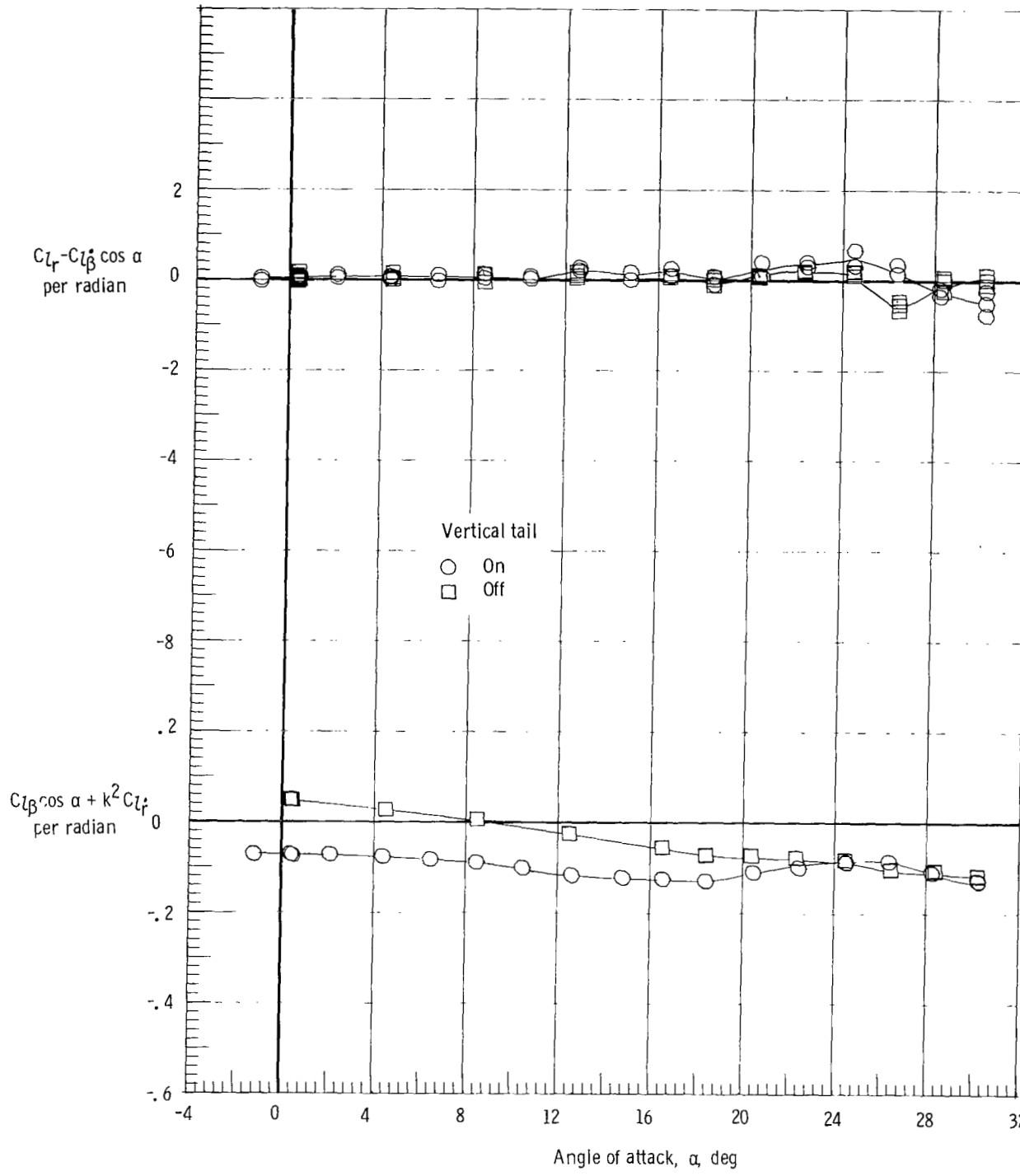

(c) M = 2.86.

Figure 22.- Continued.

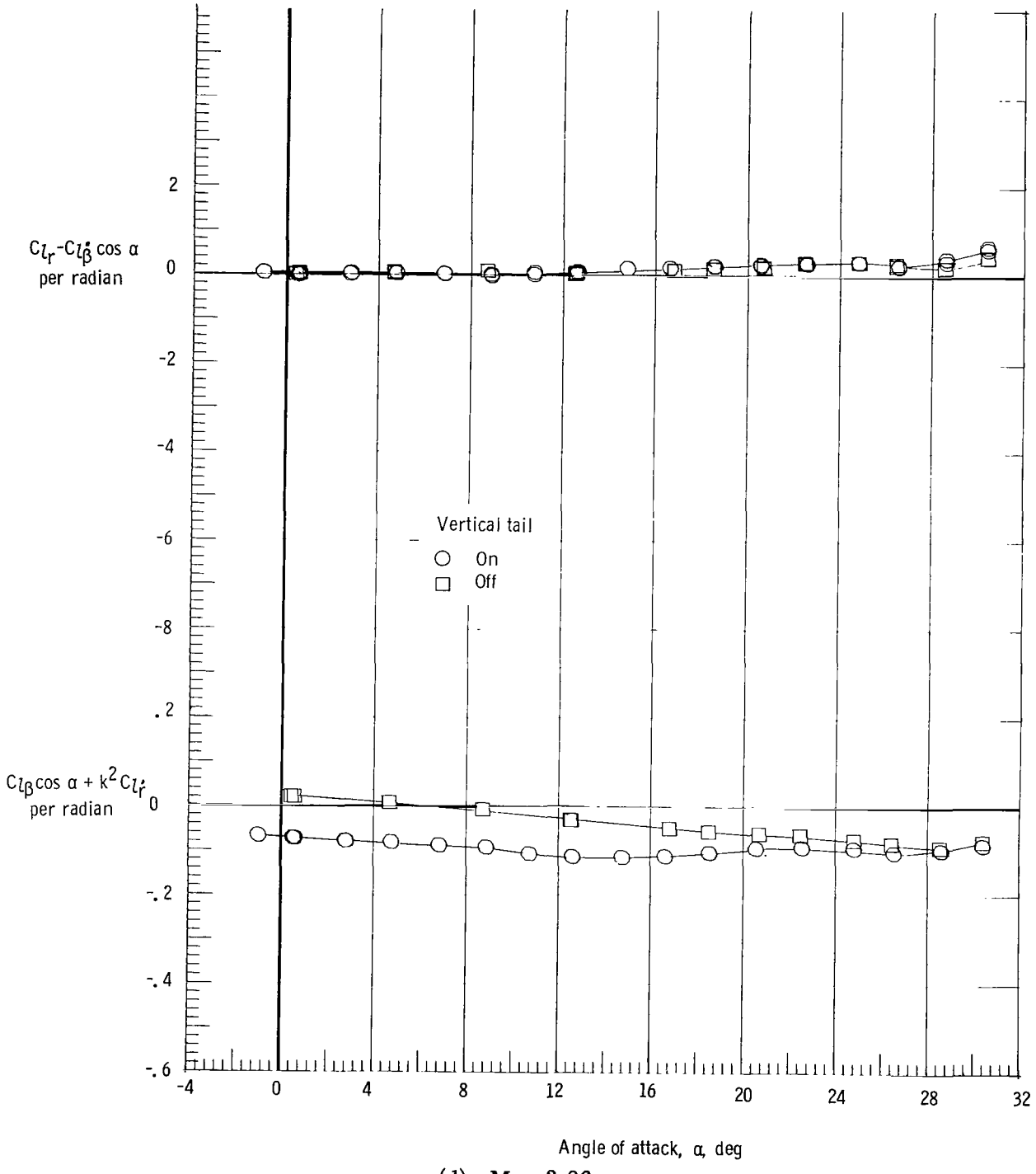

(d) M = 3.96.

Figure 22.- Continued.

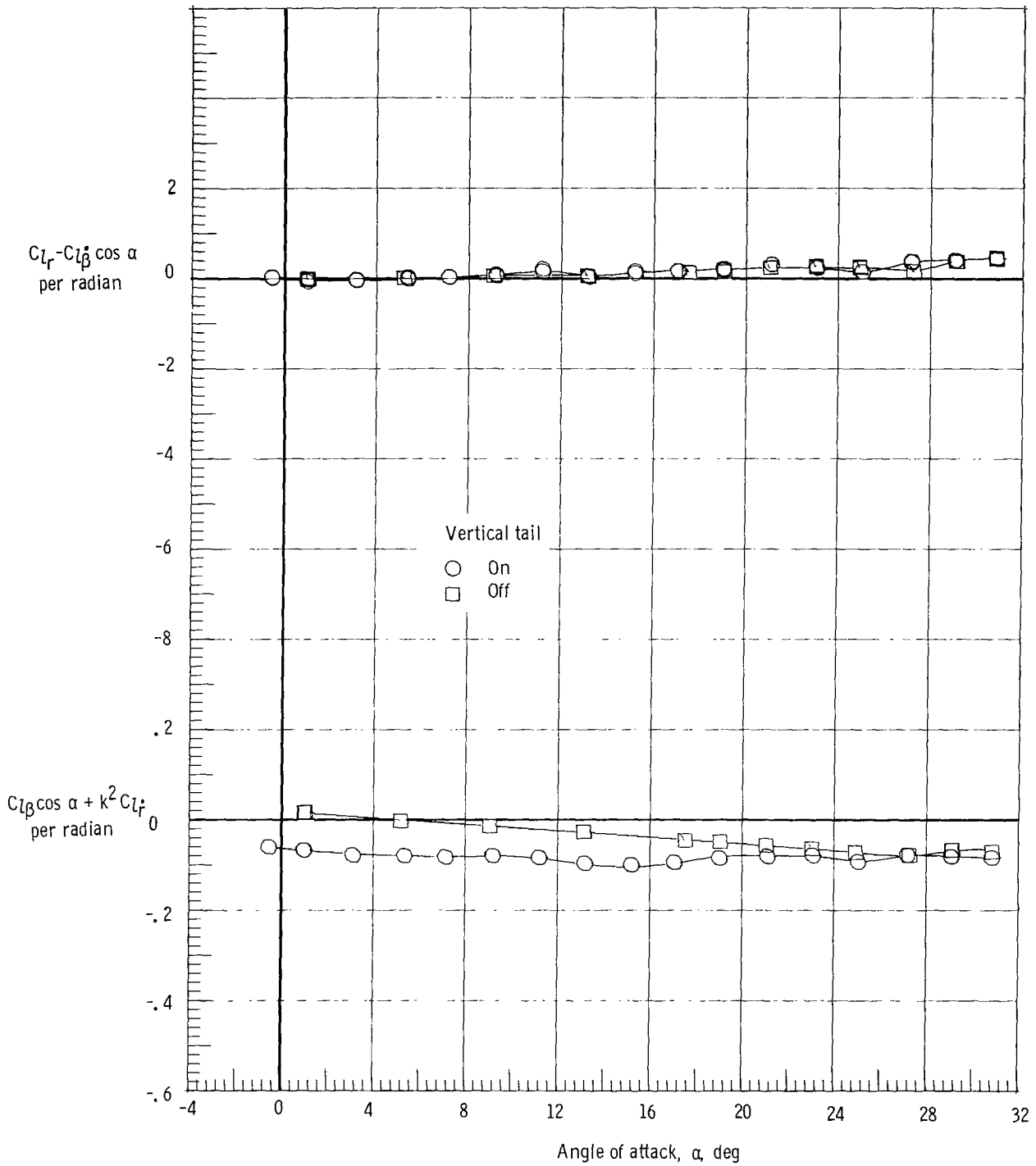

(e) M = 4.63.

Figure 22.- Concluded.

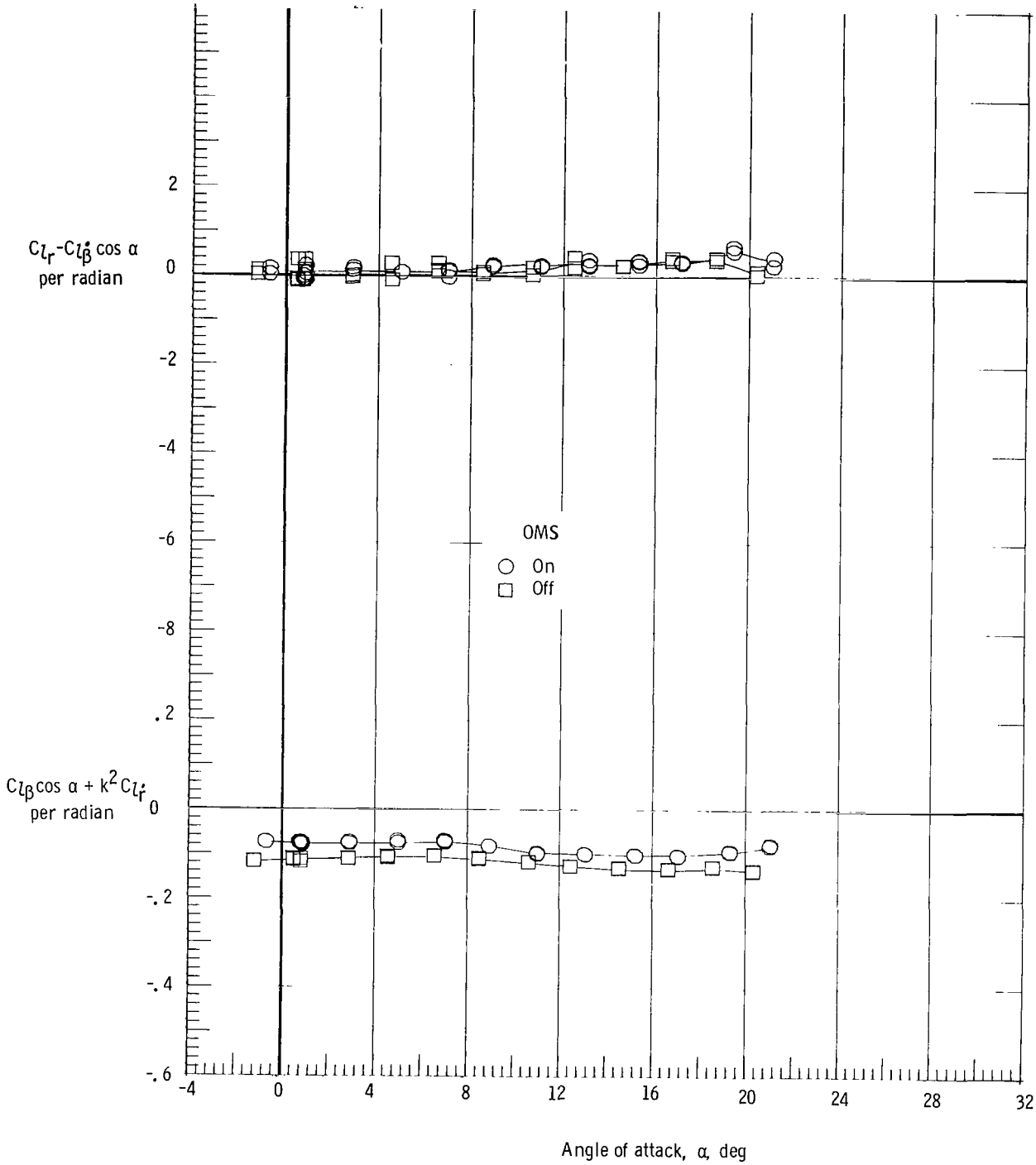

(a) M = 1.90.

Figure 23.- Effect of OMS installation on rolling moment due to yaw rate parameter and on the effective dihedral parameter. Forward c.g.; $\delta_e = 0^o$; body flap removed; and rudder flare, 40^o.

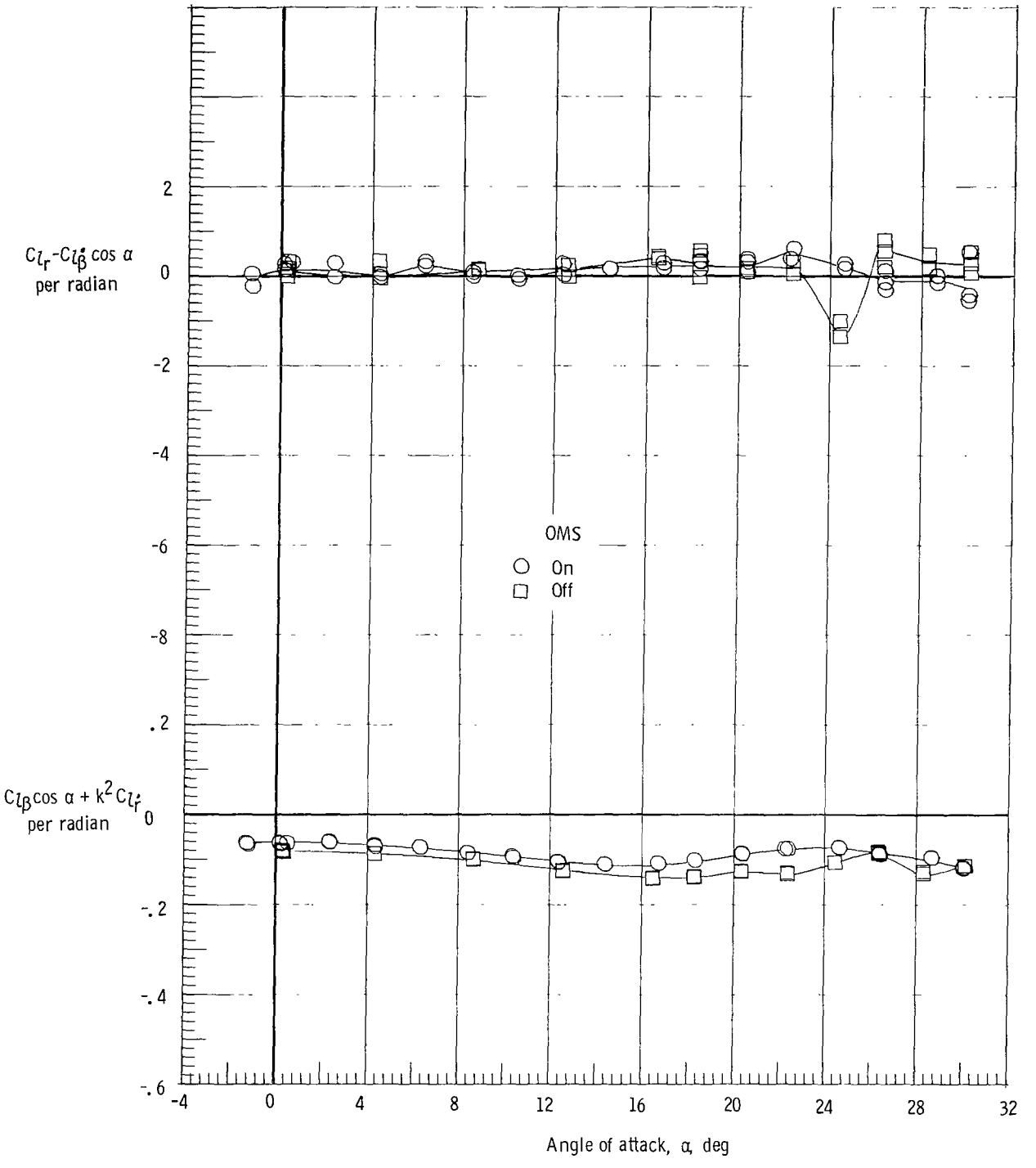

(b) M = 2.36.

Figure 23.- Continued.

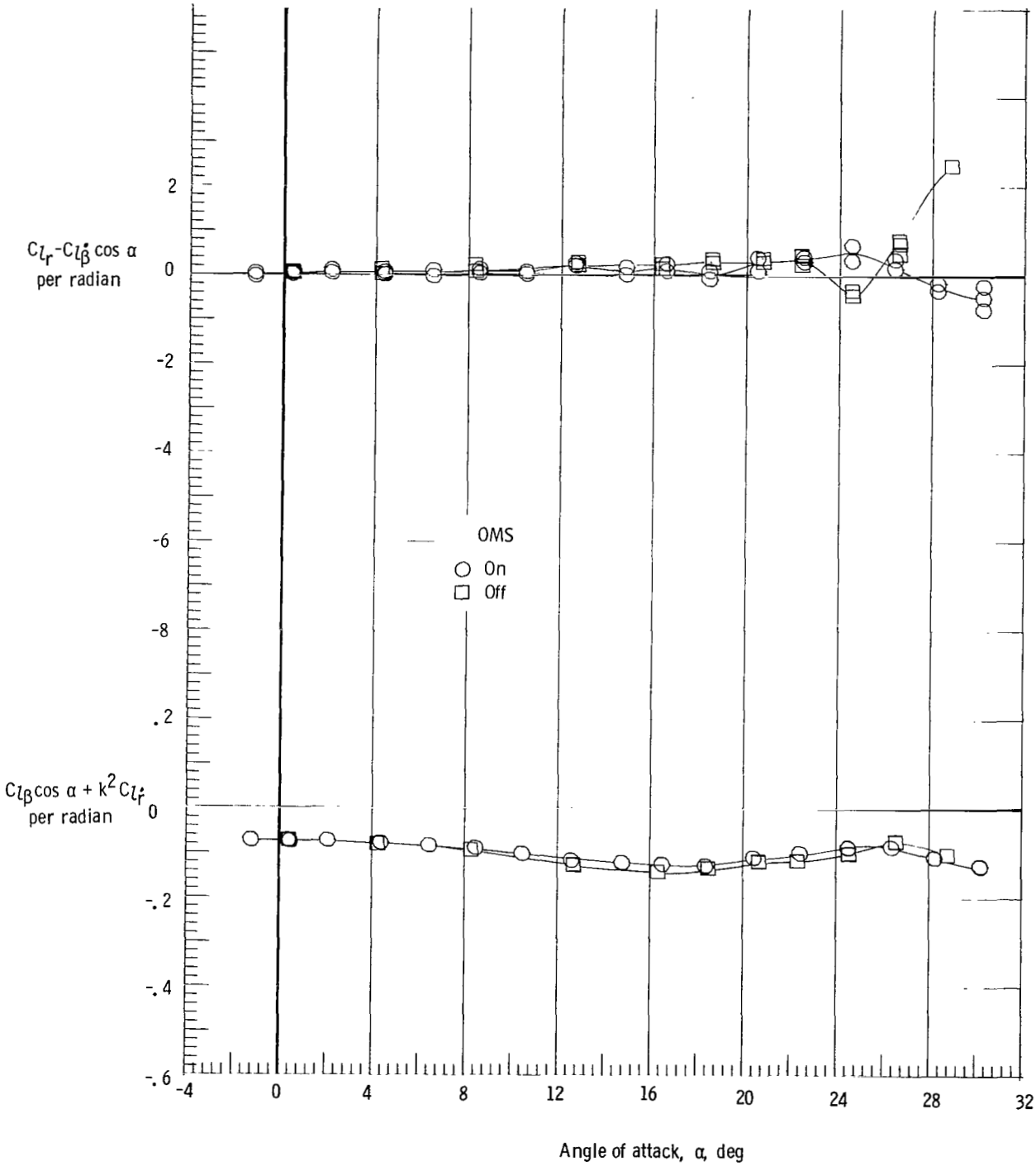

(c) M = 2.86.

Figure 23.- Continued.

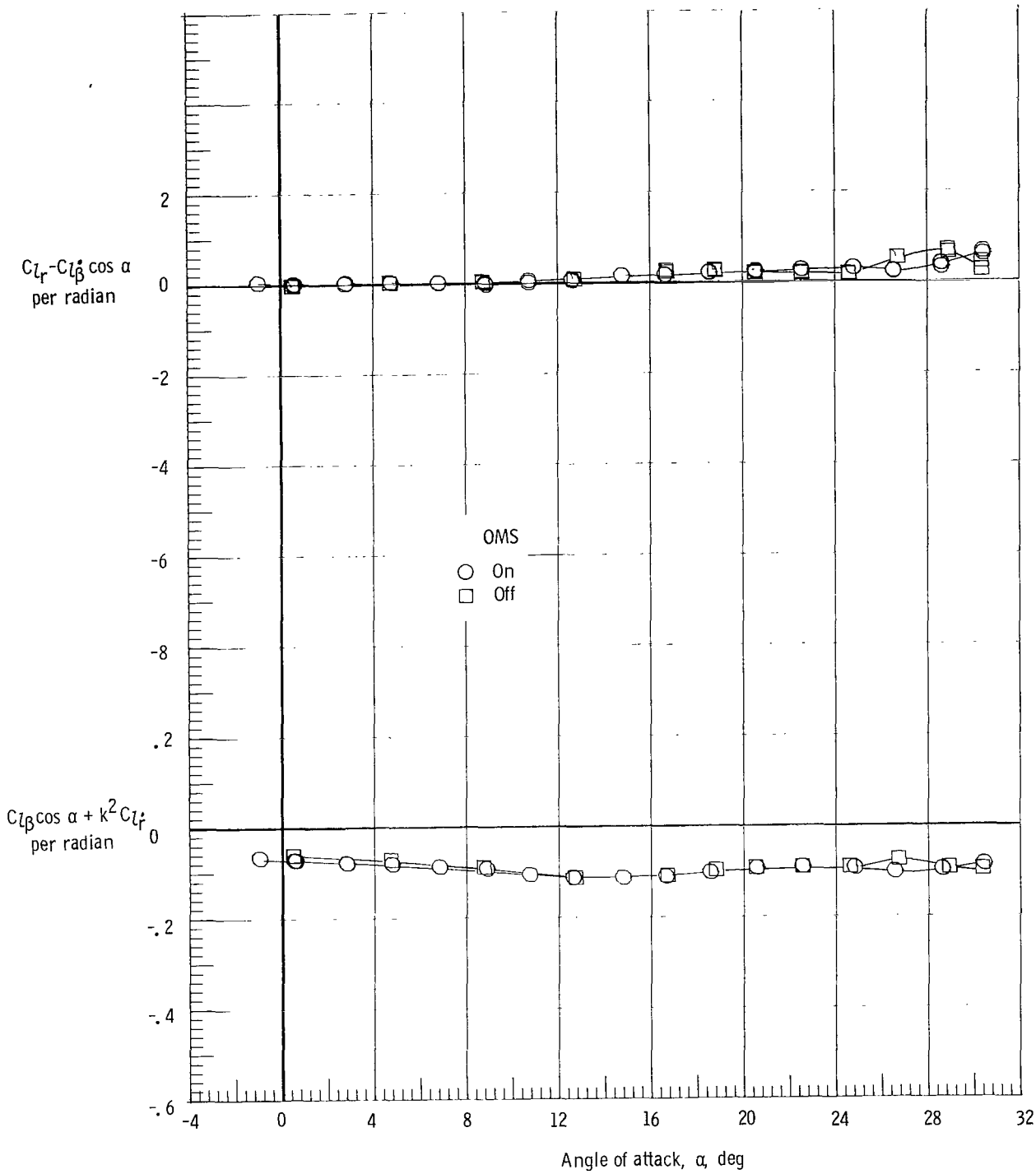

(d) M = 3.96.

Figure 23.- Continued.

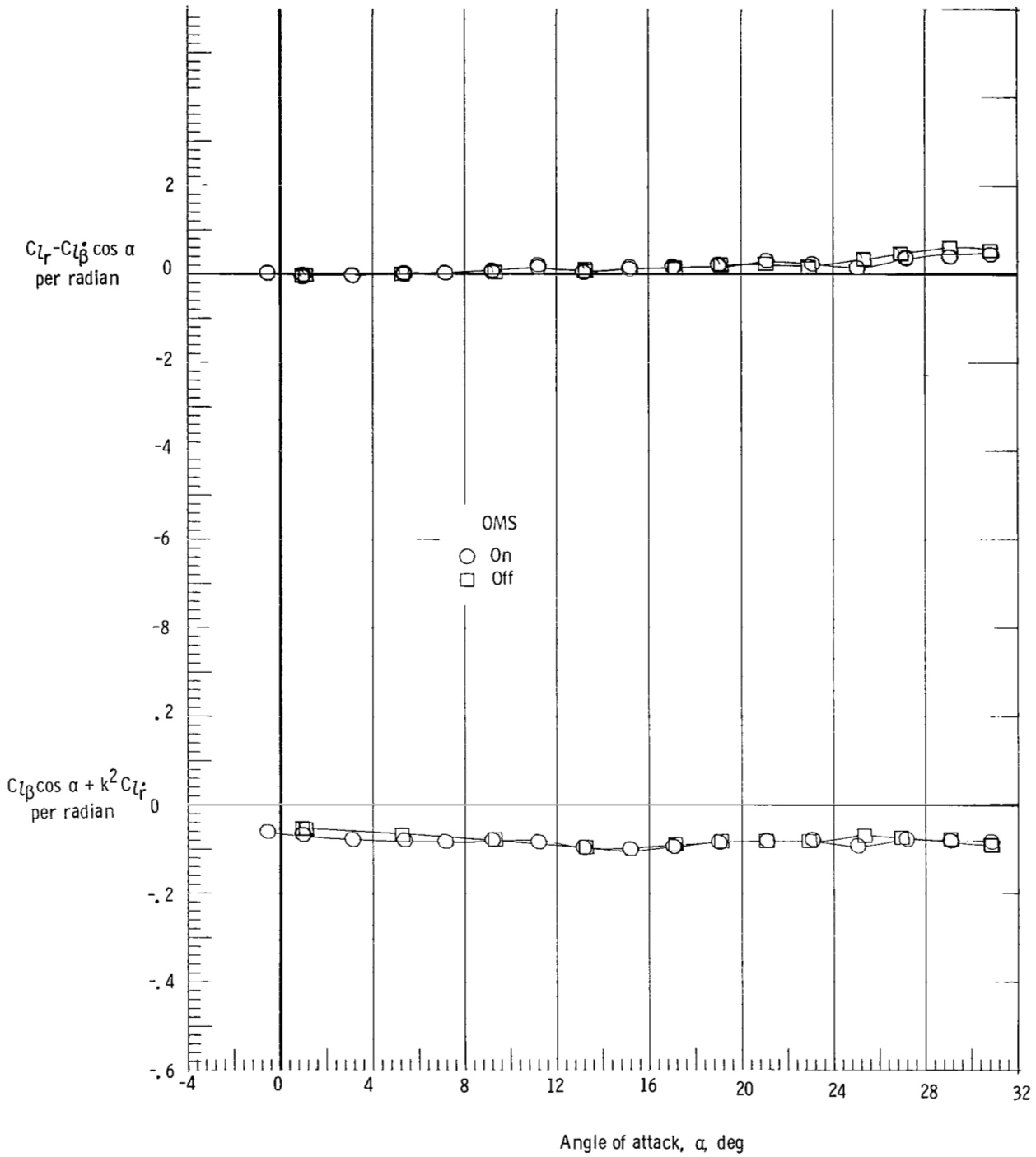

(e) M = 4.63.

Figure 23.- Concluded.

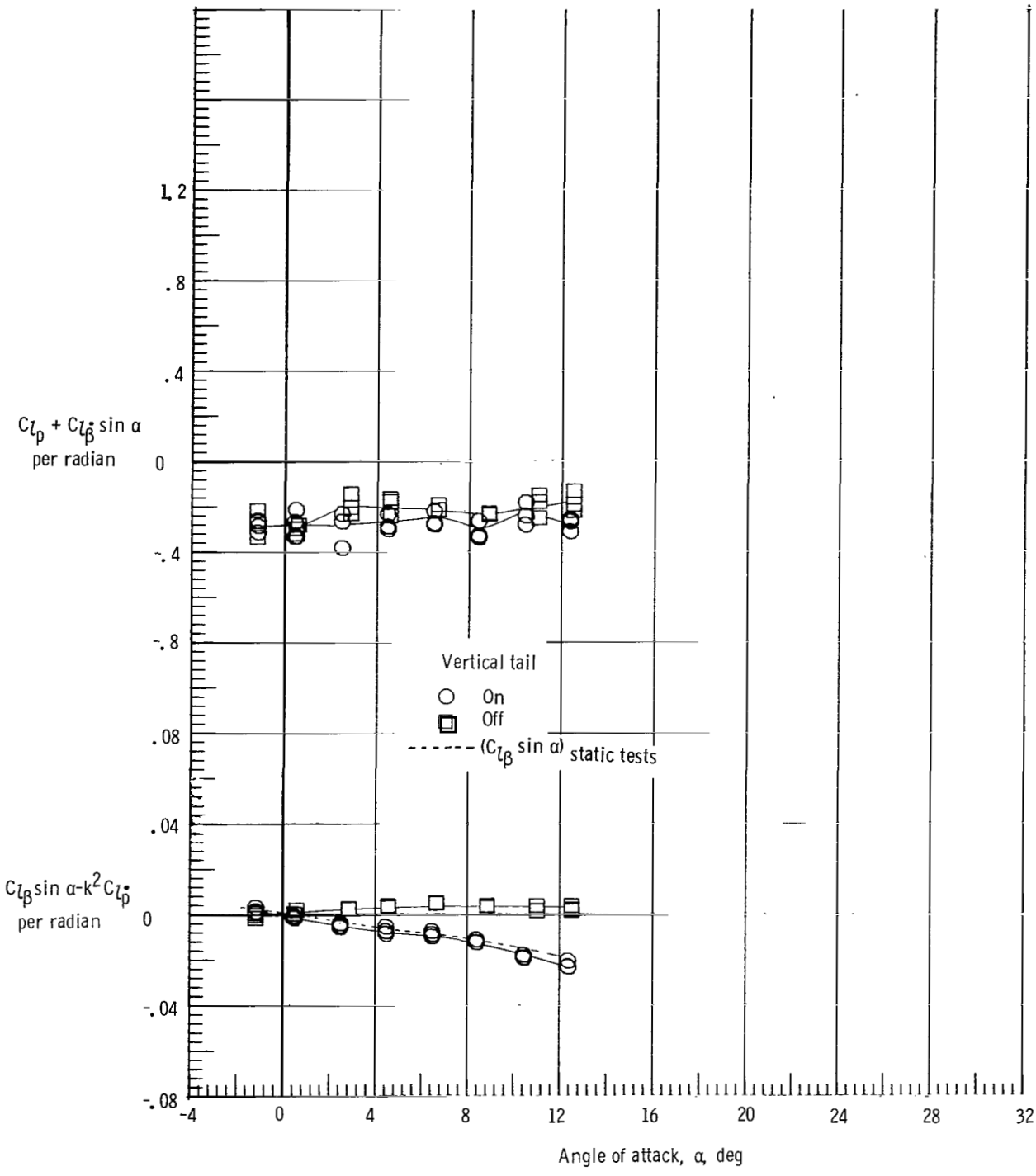

(a) M = 1.60.

Figure 24.- Effect of vertical tail on damping-in-roll parameter and on rolling moment due to roll displacement parameter. Forward c.g.; $\delta_e = 0^o$; body flap removed; and rudder flare, 40^o.

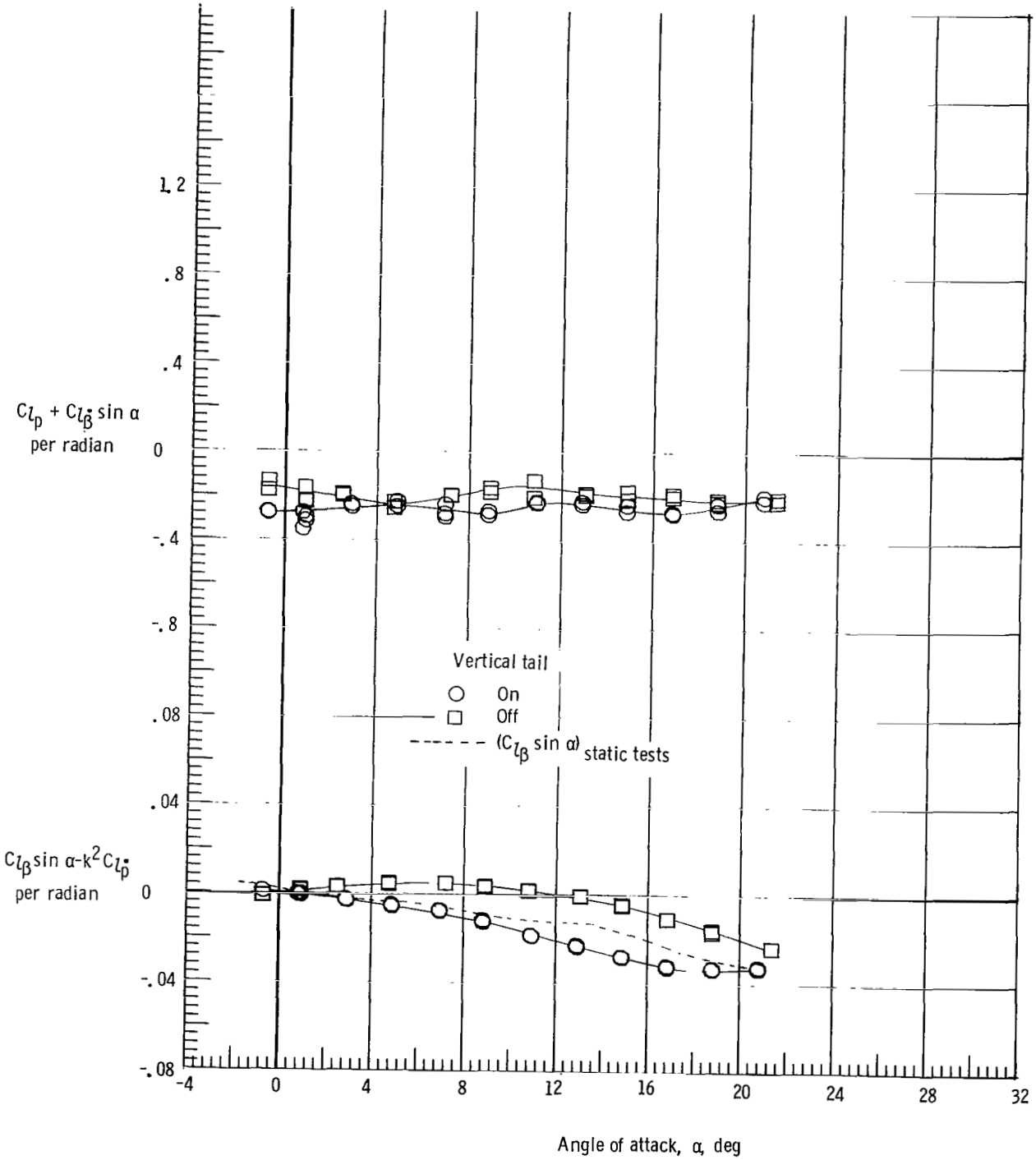

(b) M = 1.90.

Figure 24.- Continued.

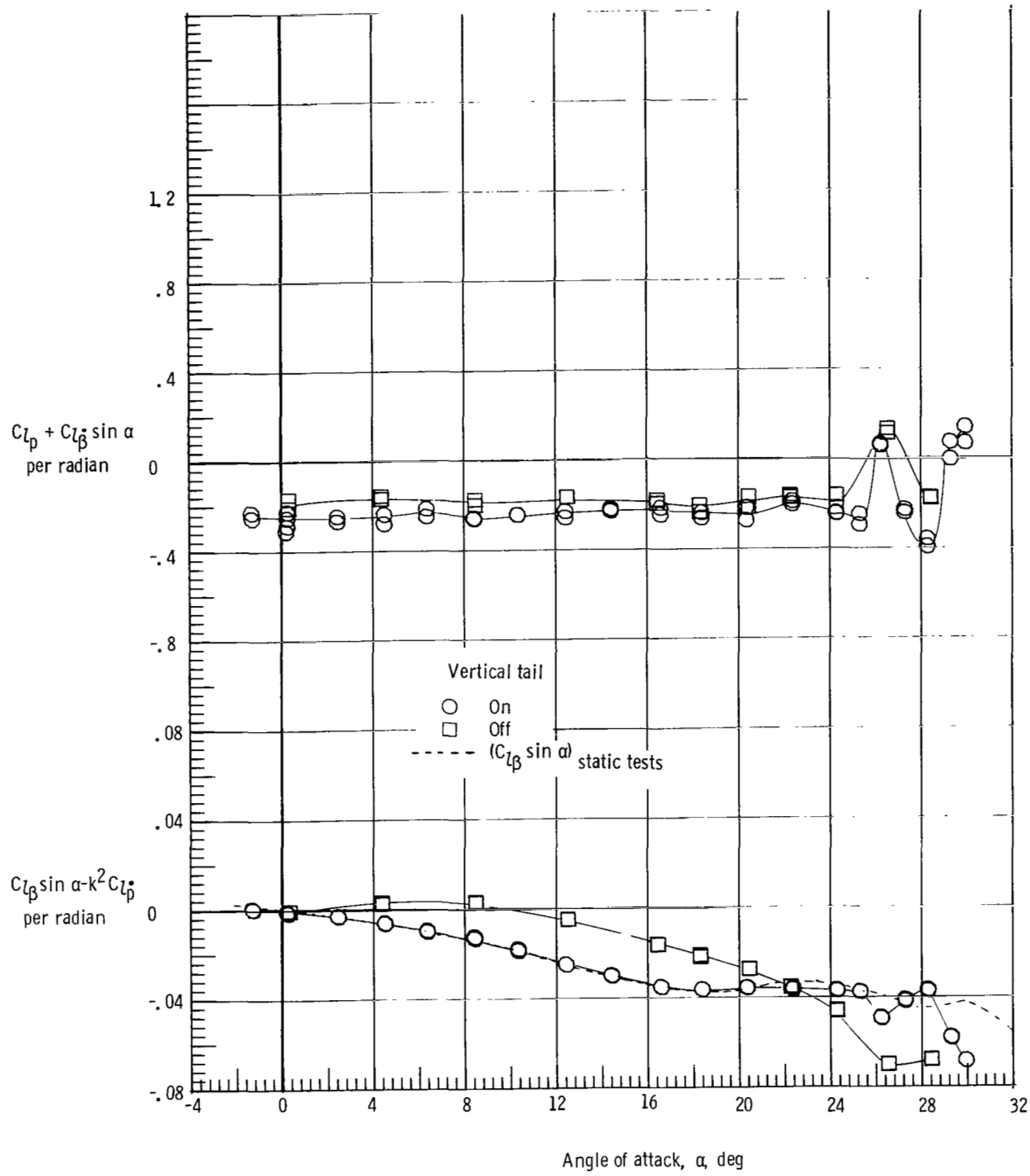

(c) M = 2.36.

Figure 24.- Continued.

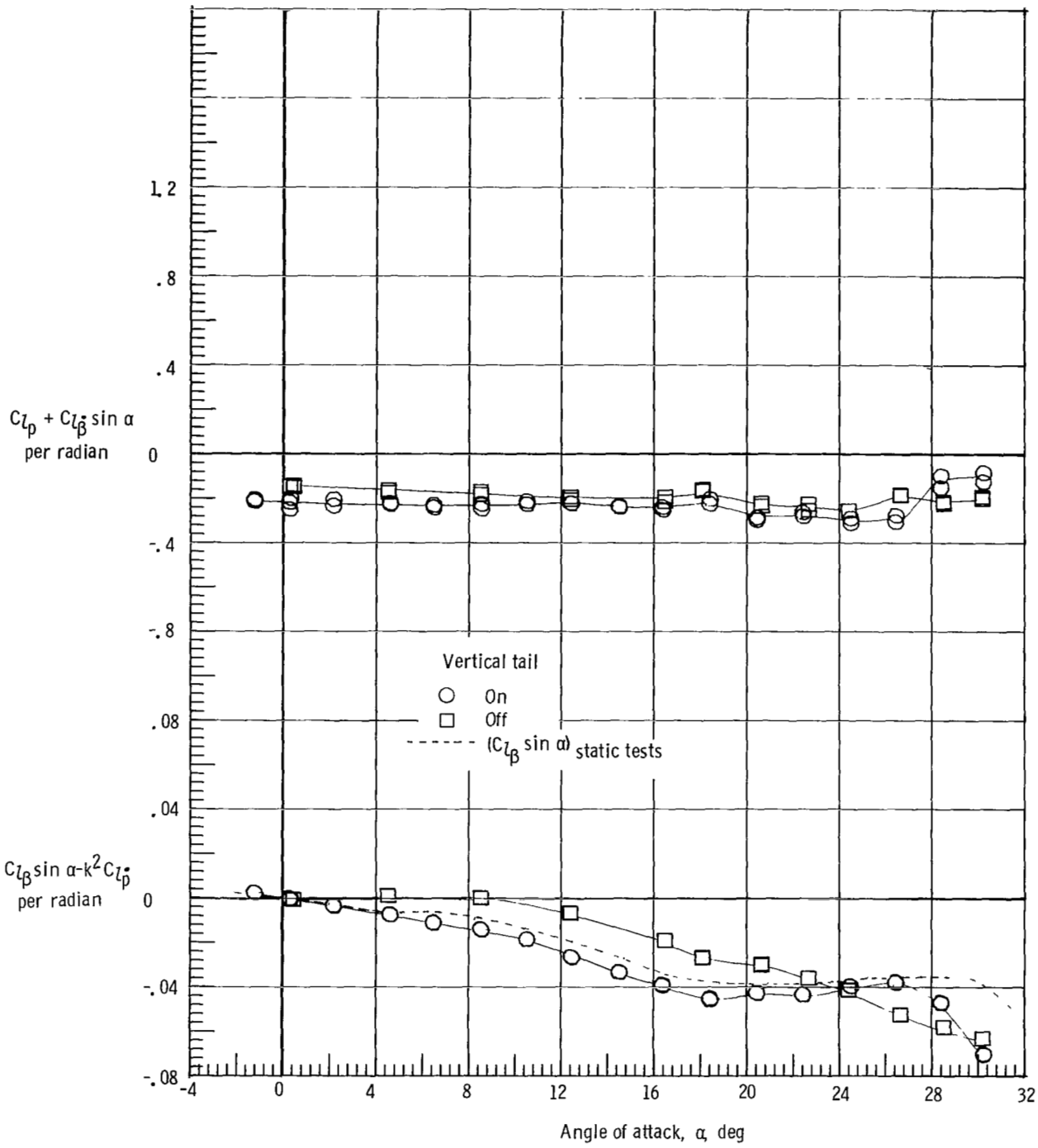

(d) M = 2.86.

Figure 24.- Continued.

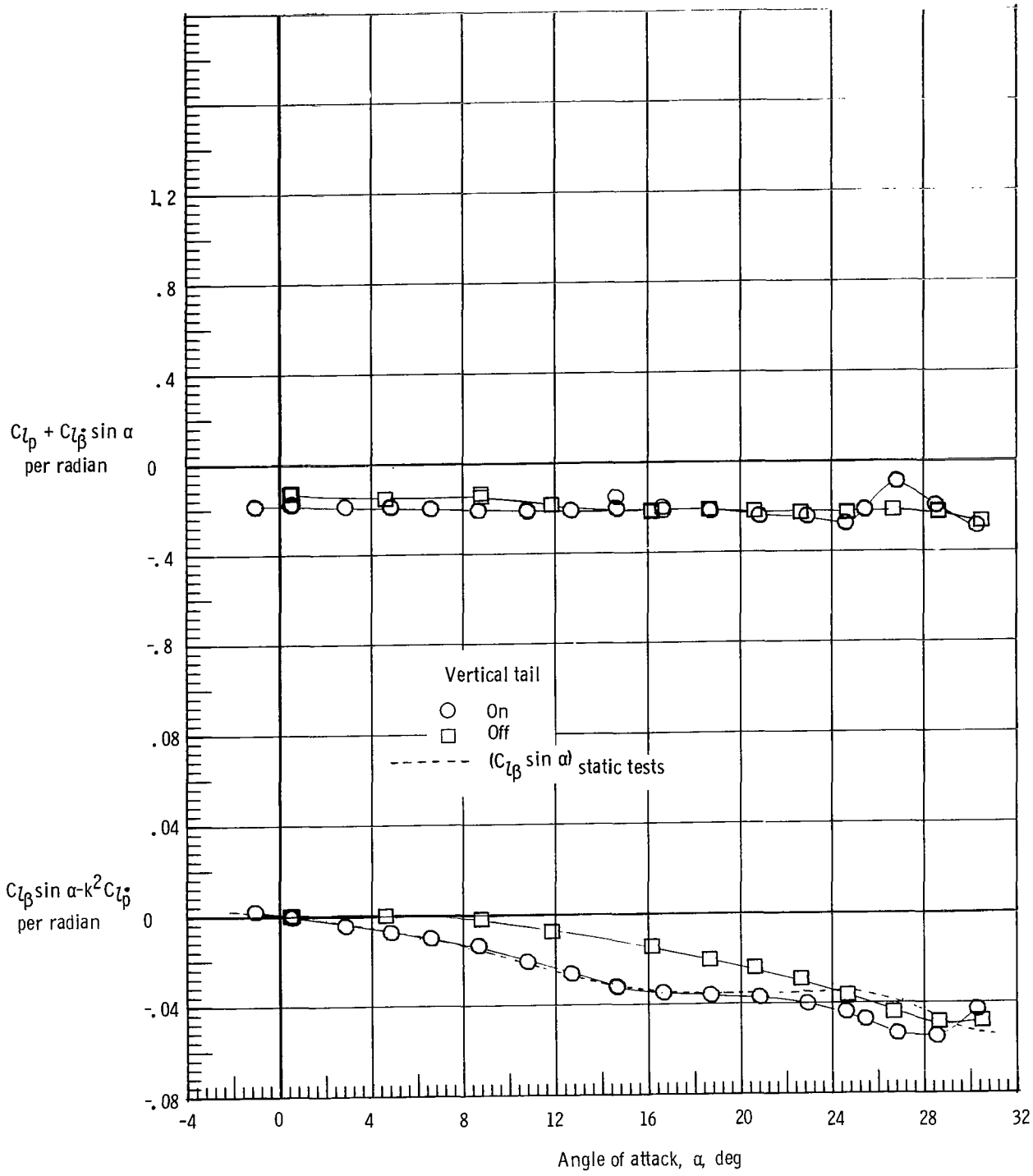

(e) M = 3.96.

Figure 24.- Continued.

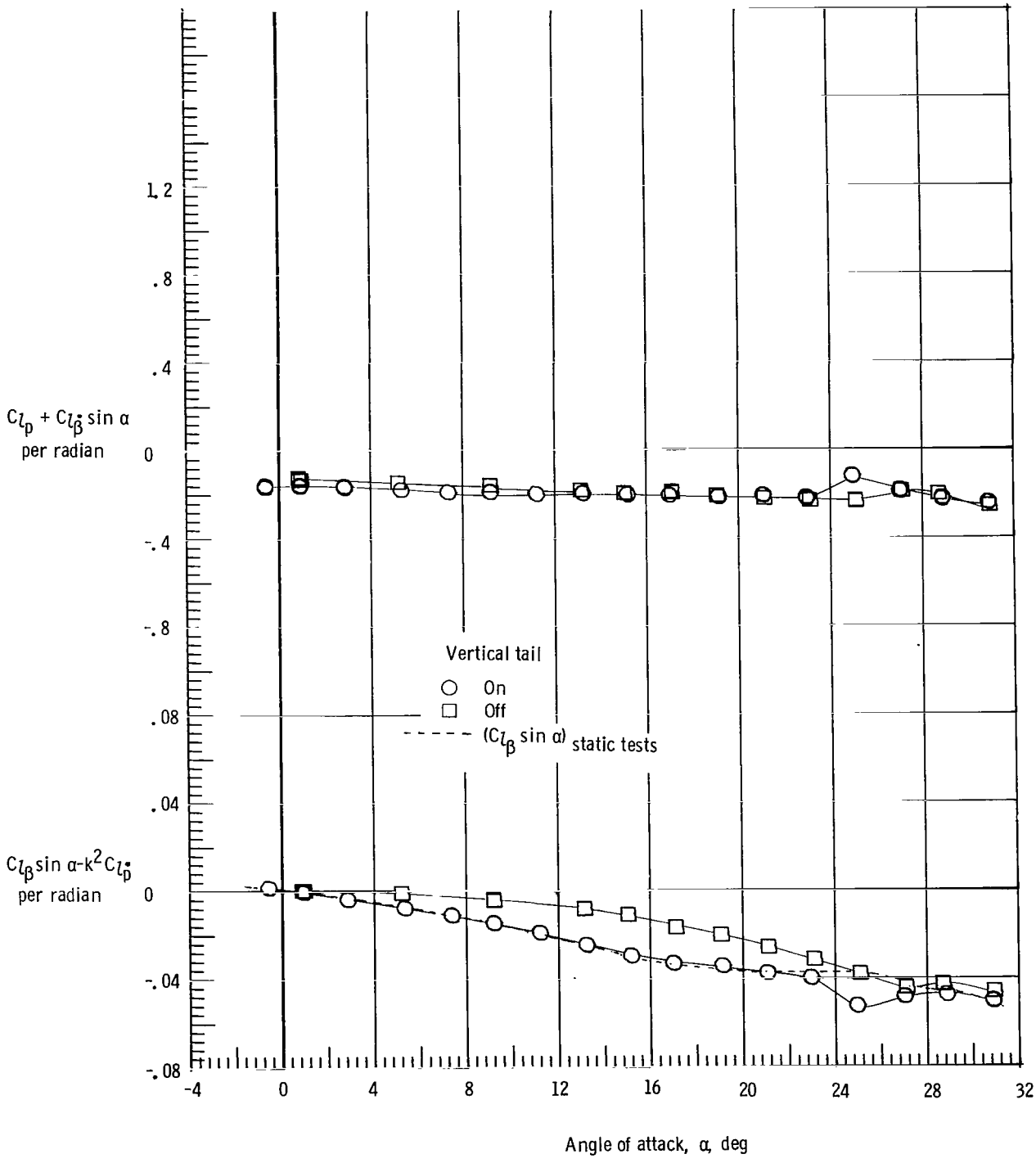

(f) M = 4.63.

Figure 24.- Concluded.

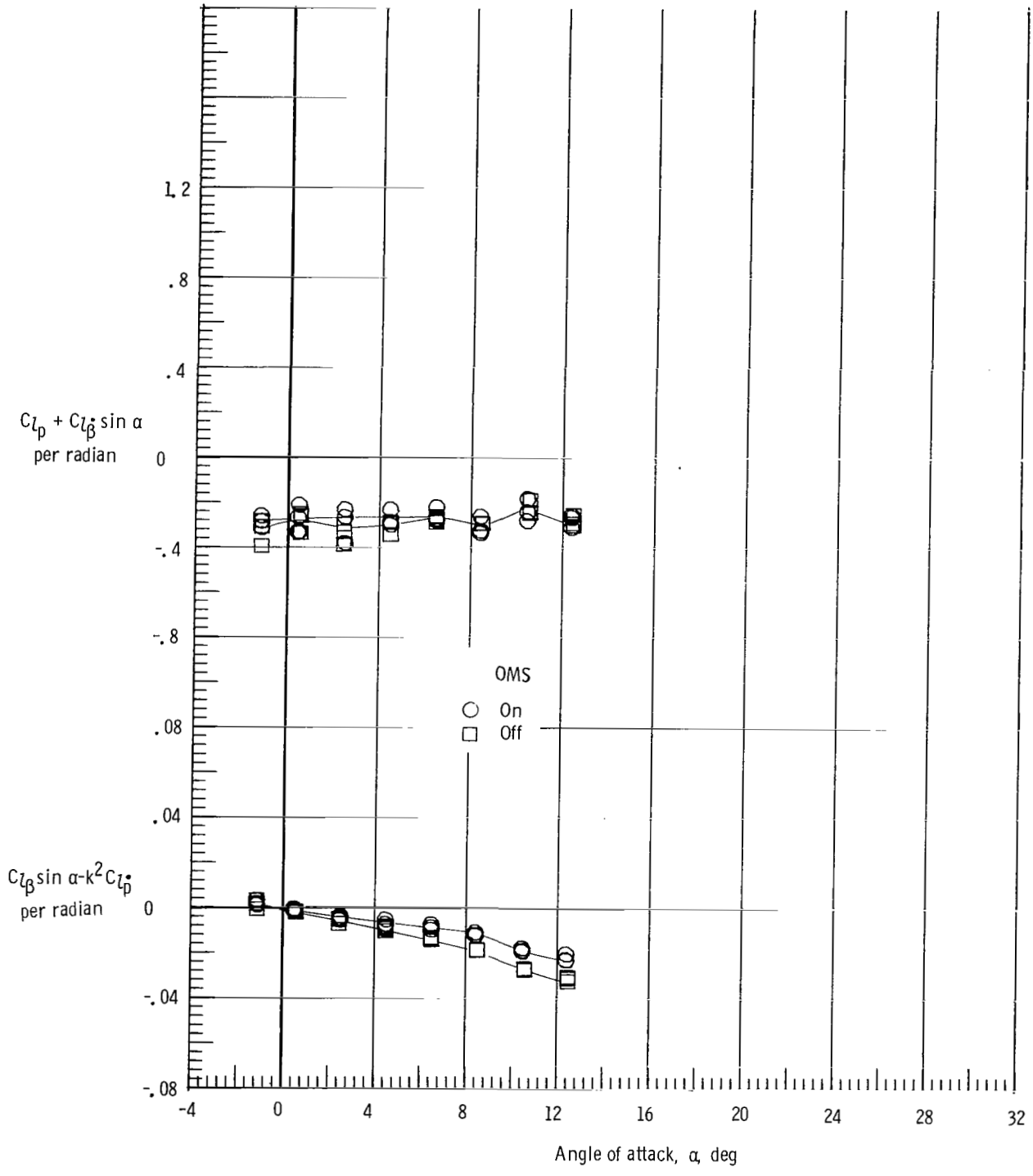

(a) M = 1.60.

Figure 25.- Effect of OMS installation on damping-in-roll parameter and on rolling moment due to roll displacement parameter. Forward c.g.; $\delta_e = 0^o$; body flap removed; and rudder flare, 40^o.

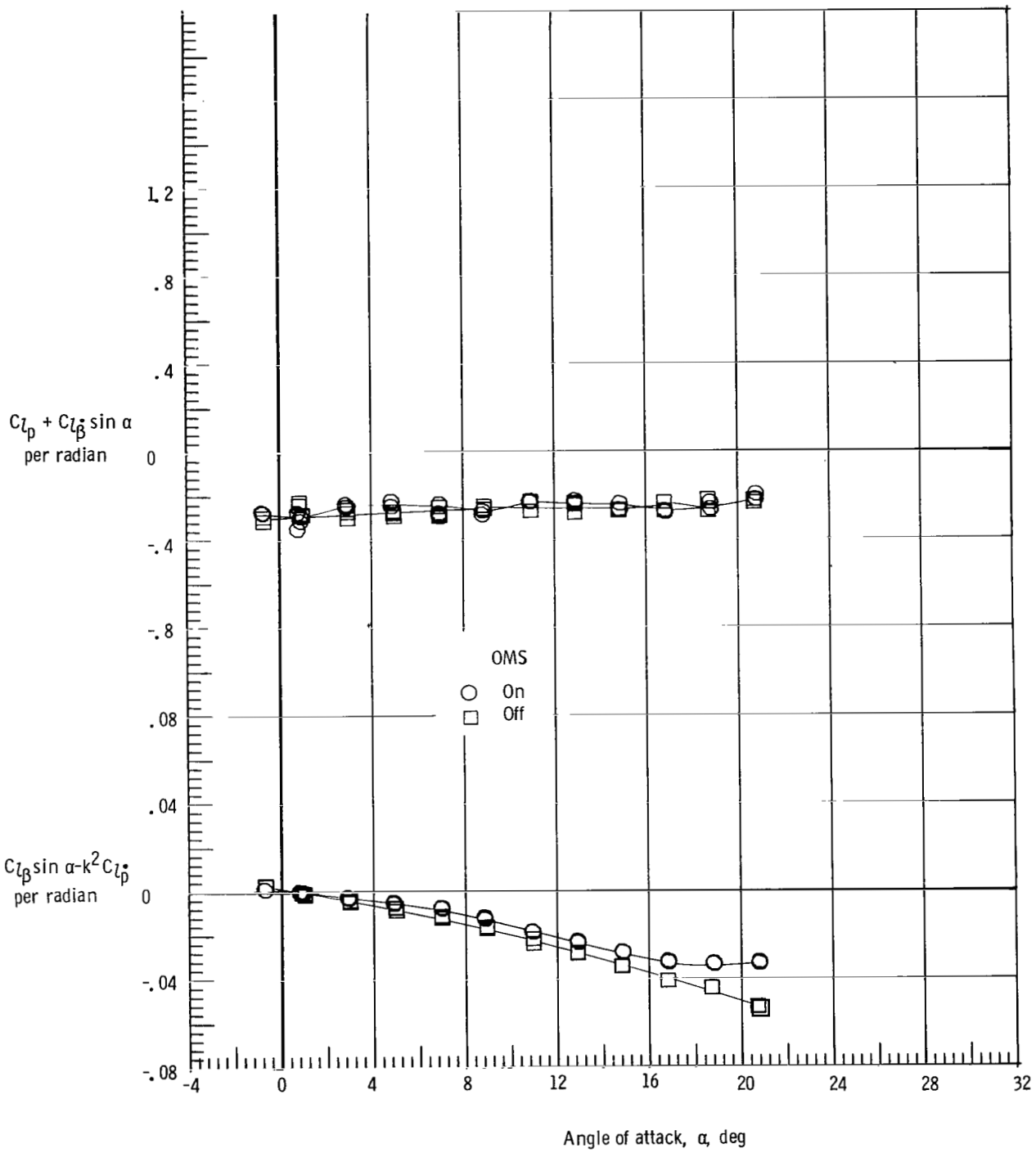

(b) M = 1.90.

Figure 25.- Continued.

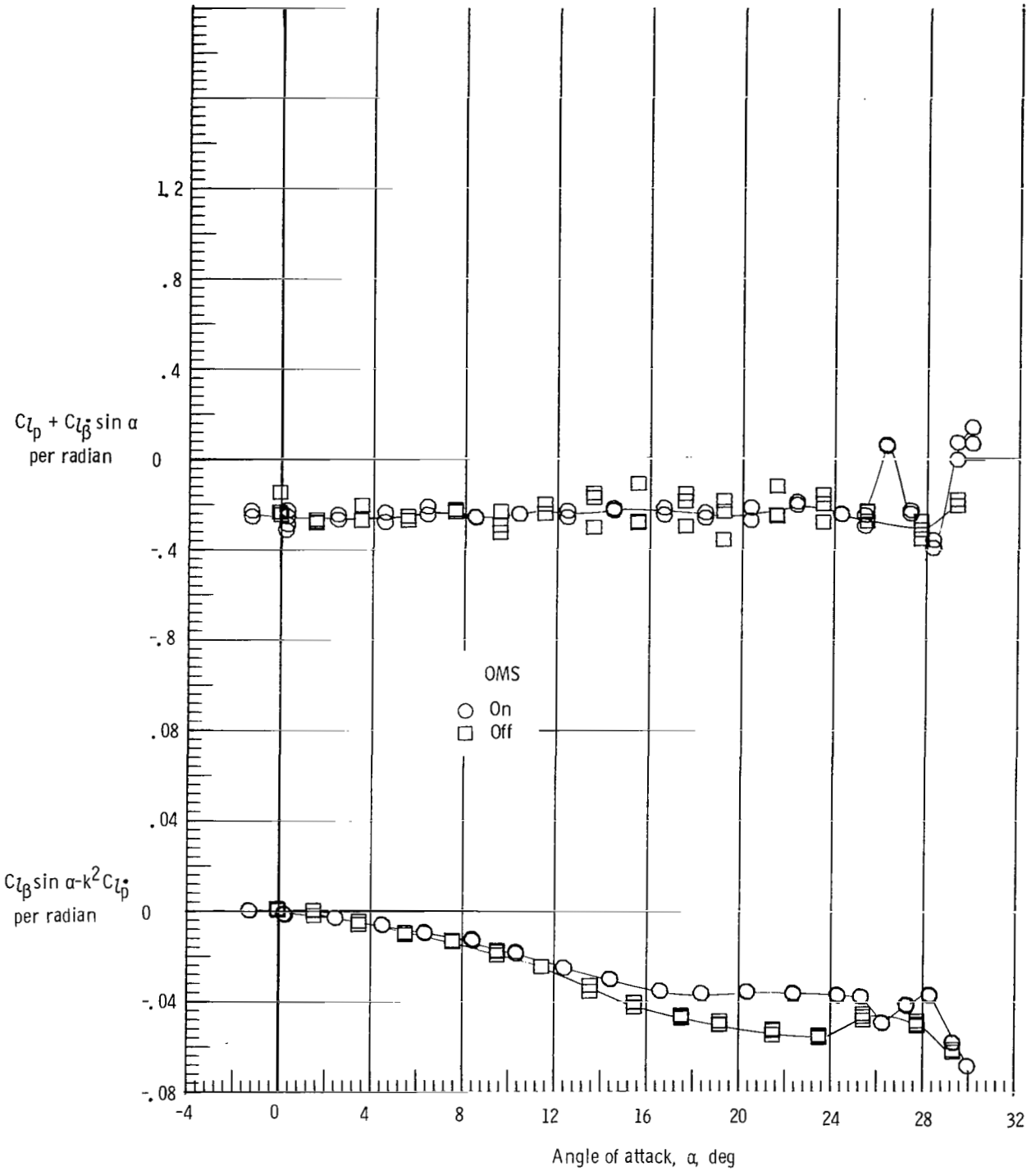

(c) M = 2.36.

Figure 25.- Continued.

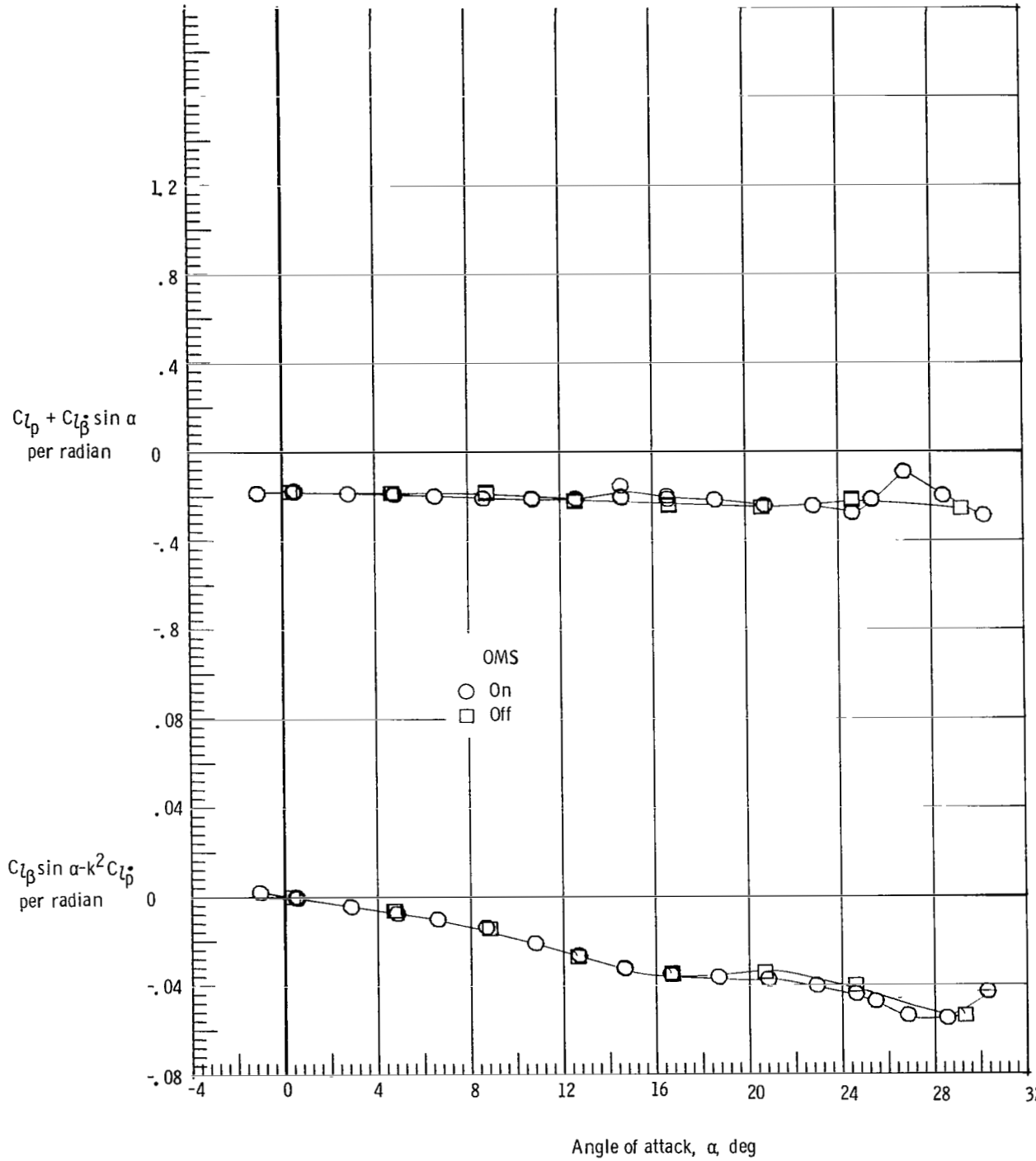

(d) M = 3.96.

Figure 25.- Continued.

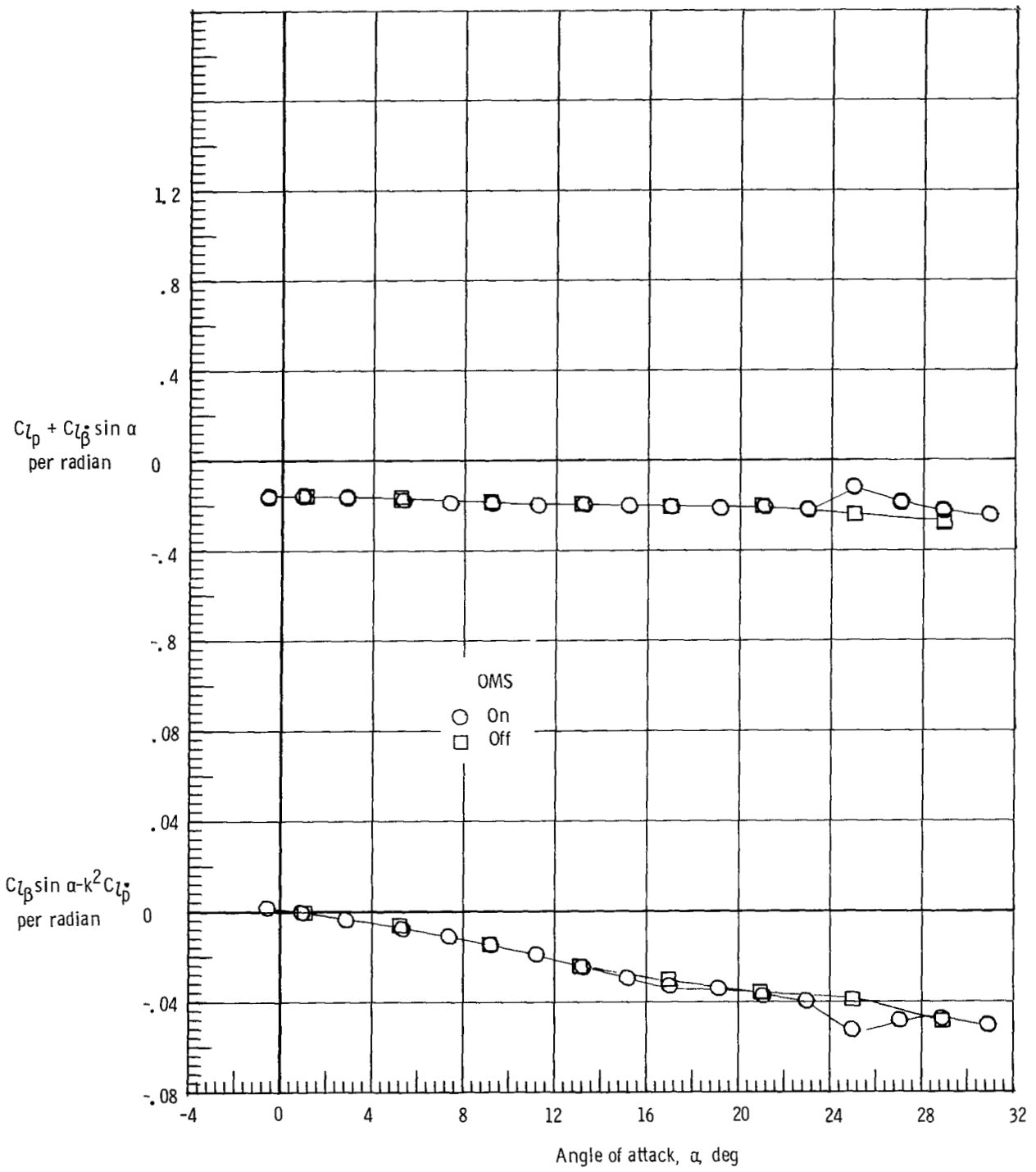

(e) M = 4.63.

Figure 25.- Concluded.

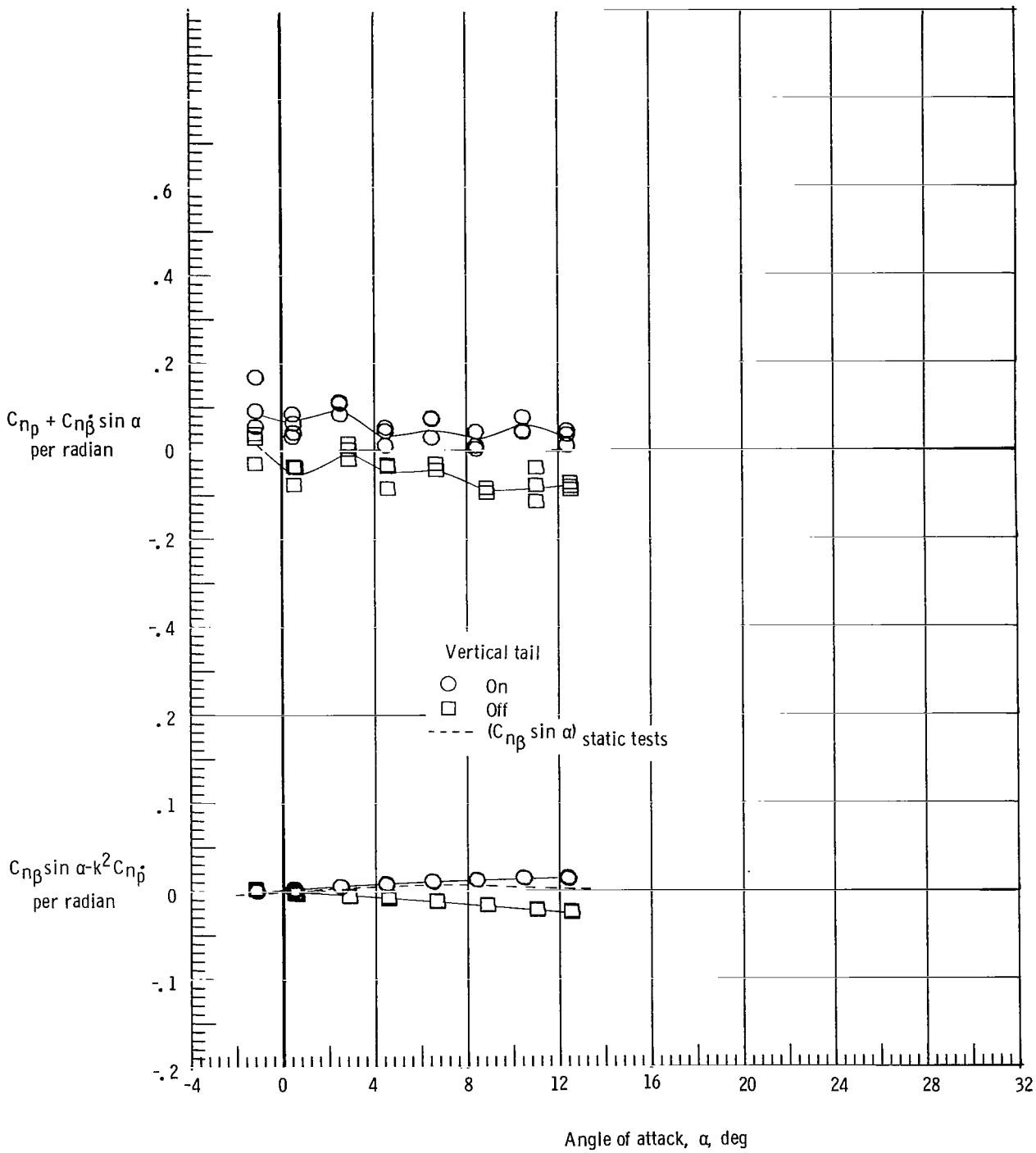

(a) M = 1.60.

Figure 26.- Effect of vertical tail on yawing moment due to roll rate parameter and on yawing moment due to roll displacement parameter. Forward c.g.; $\delta_e = 0^o$; body flap removed; and rudder flare, 40^o.

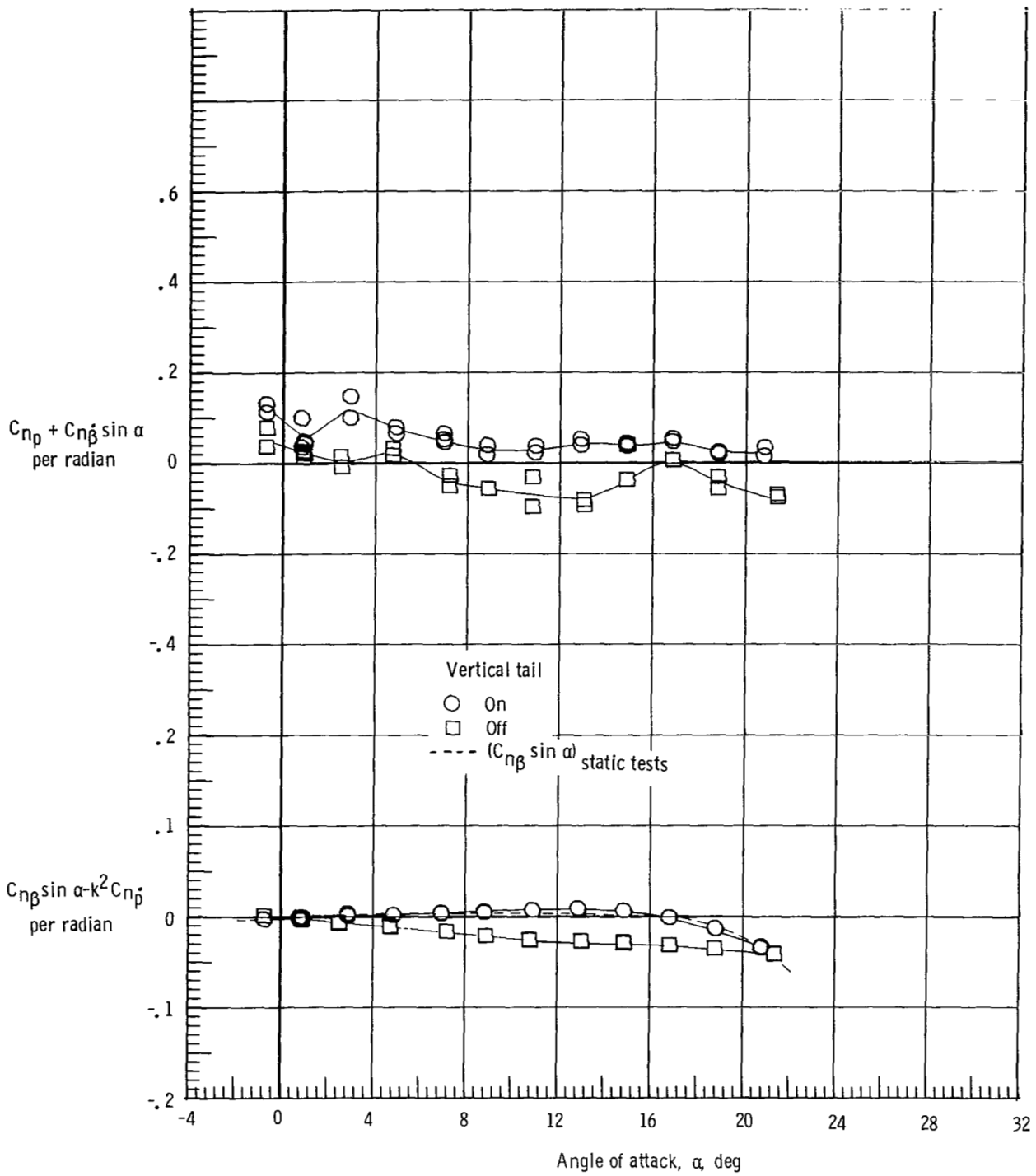

(b) M = 1.90.

Figure 26.- Continued.

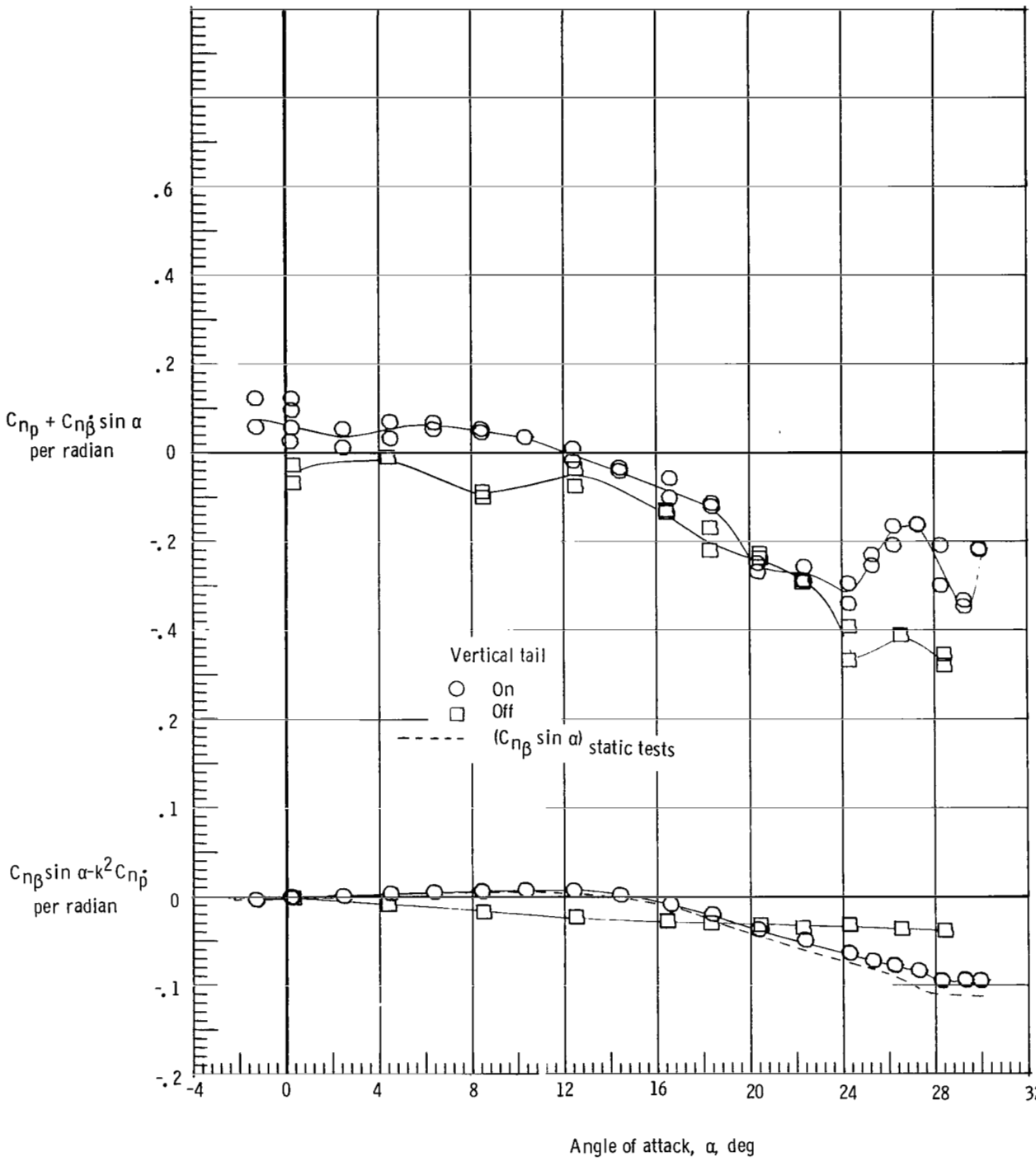

(c) M = 2.36.

Figure 26.- Continued.

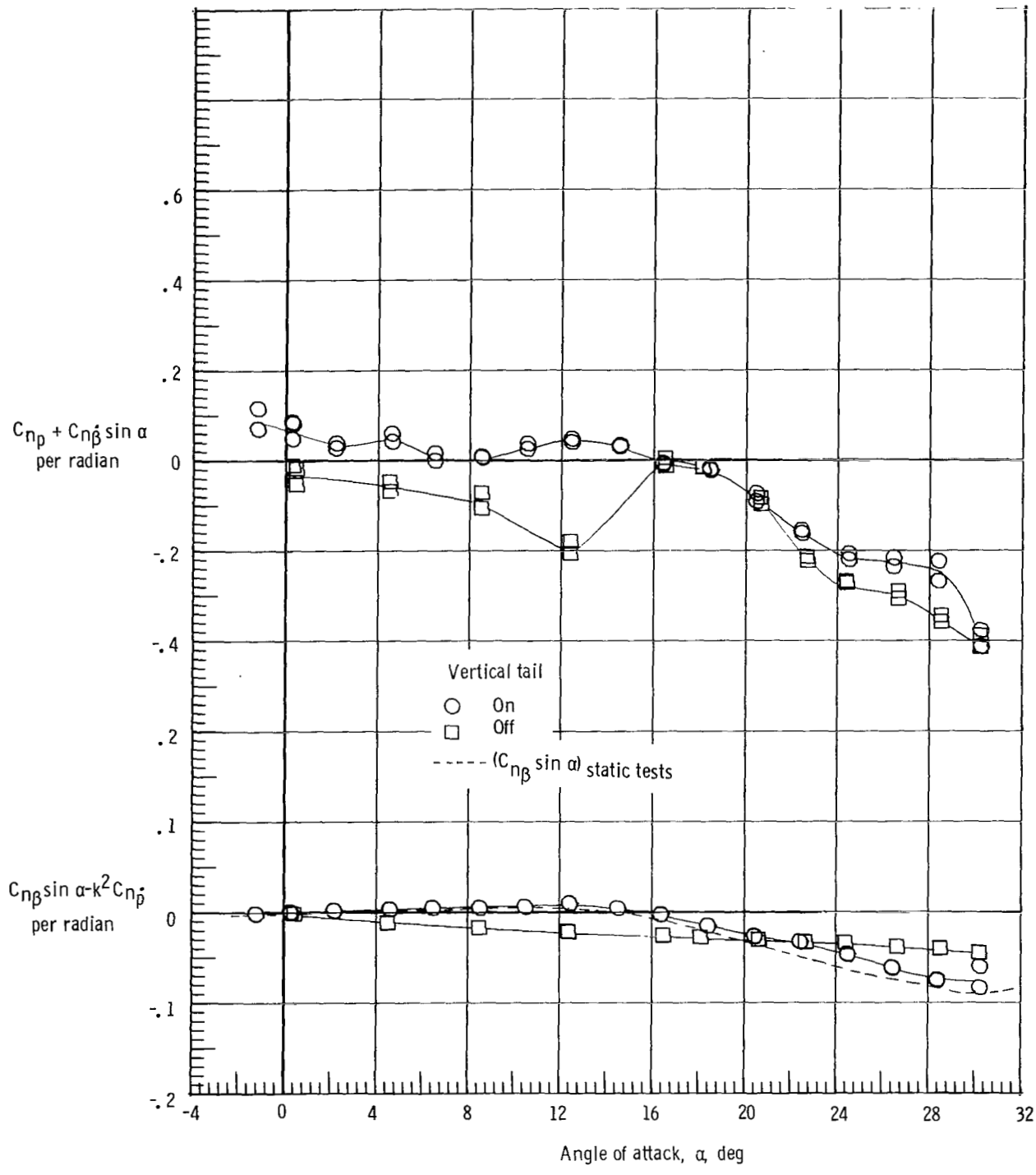

(d) M = 2.86.

Figure 26.- Continued.

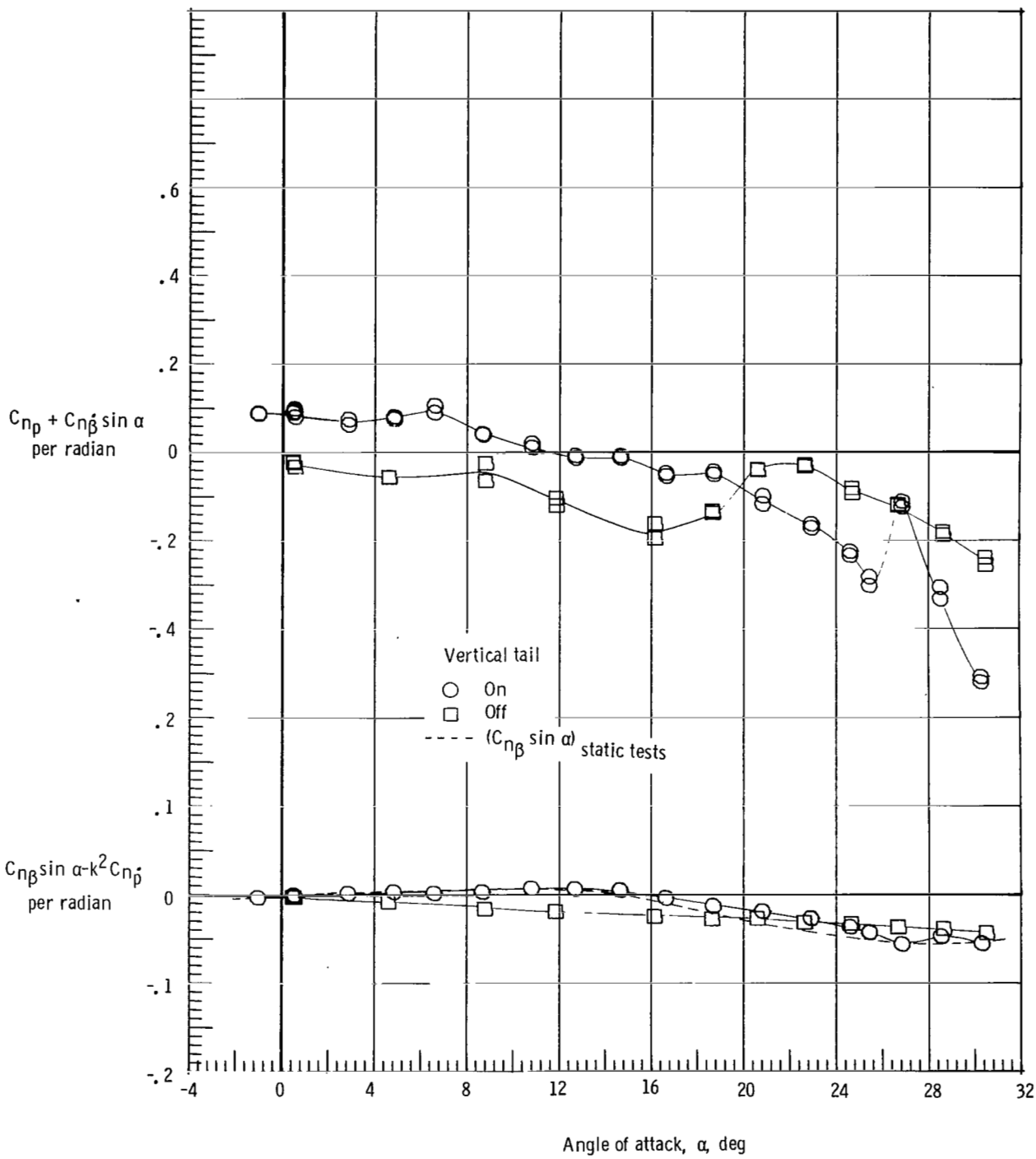

(e) M = 3.96.

Figure 26.- Continued.

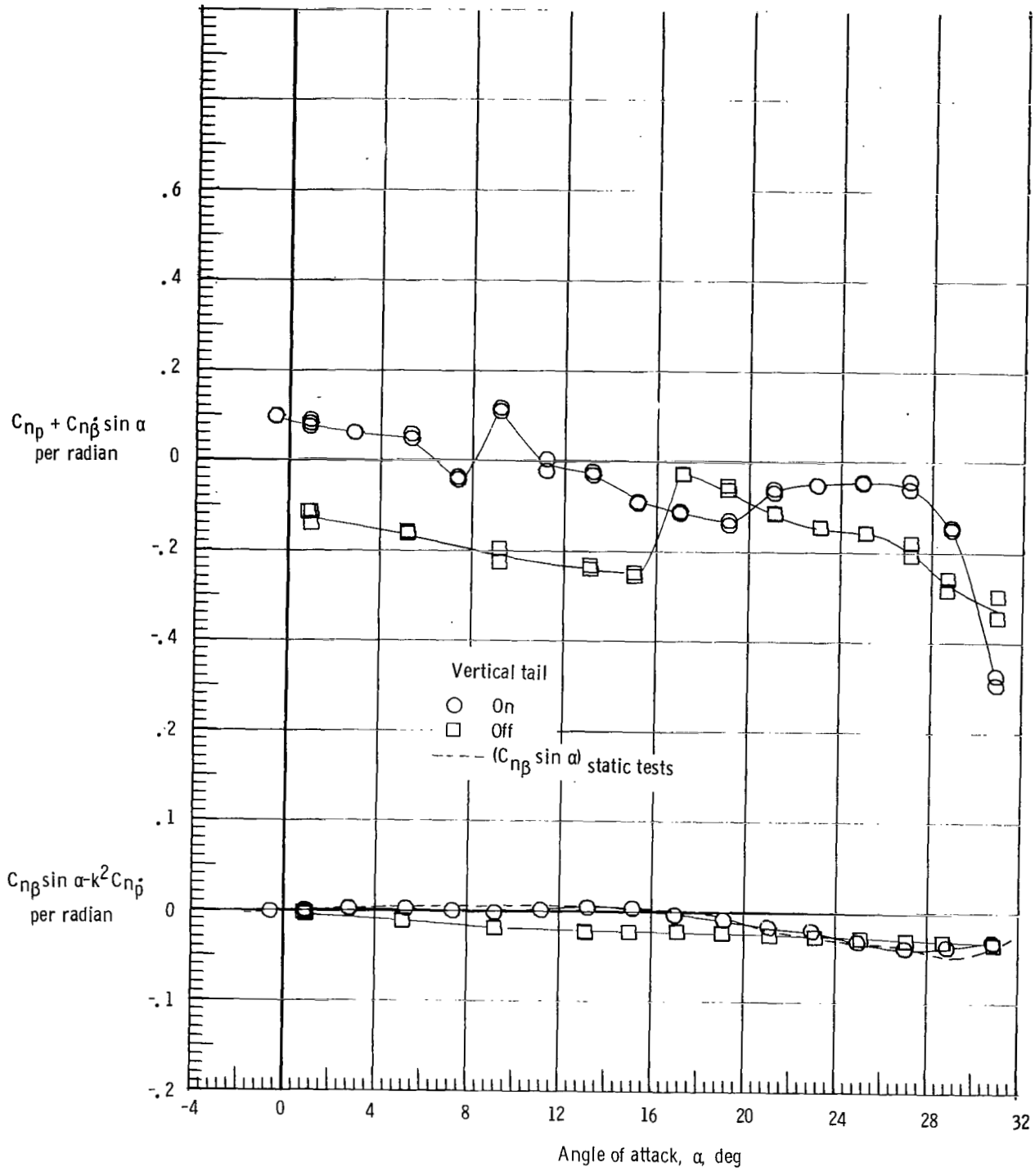

(f) M = 4.63.

Figure 26.- Concluded.

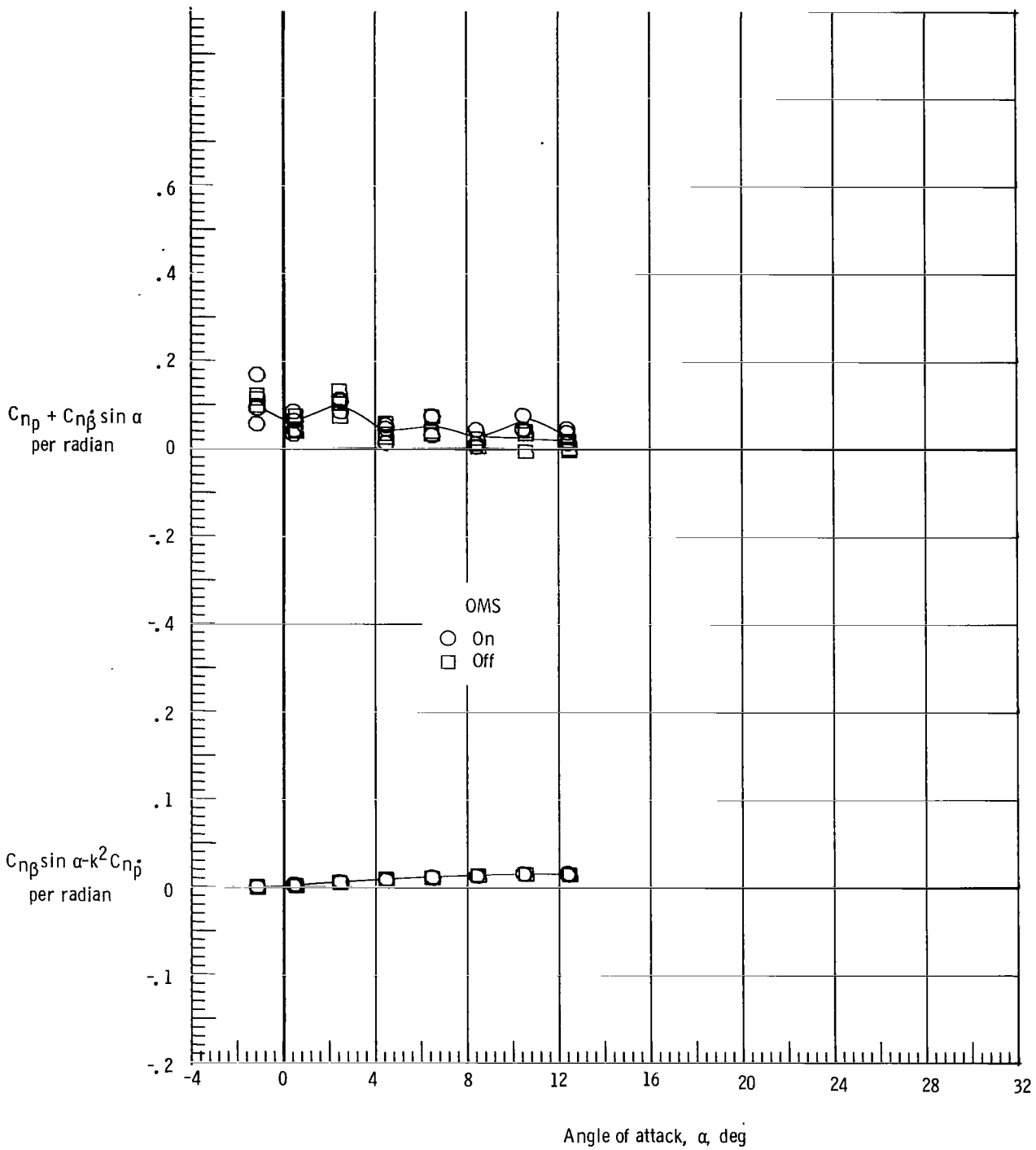

(a) M = 1.60.

Figure 27.- Effect of OMS installation on yawing moment due to roll rate parameter and on yawing moment due to roll displacement parameter. Forward c.g.; $\delta_e = 0^o$; body flap removed; and rudder flare, 40^o.

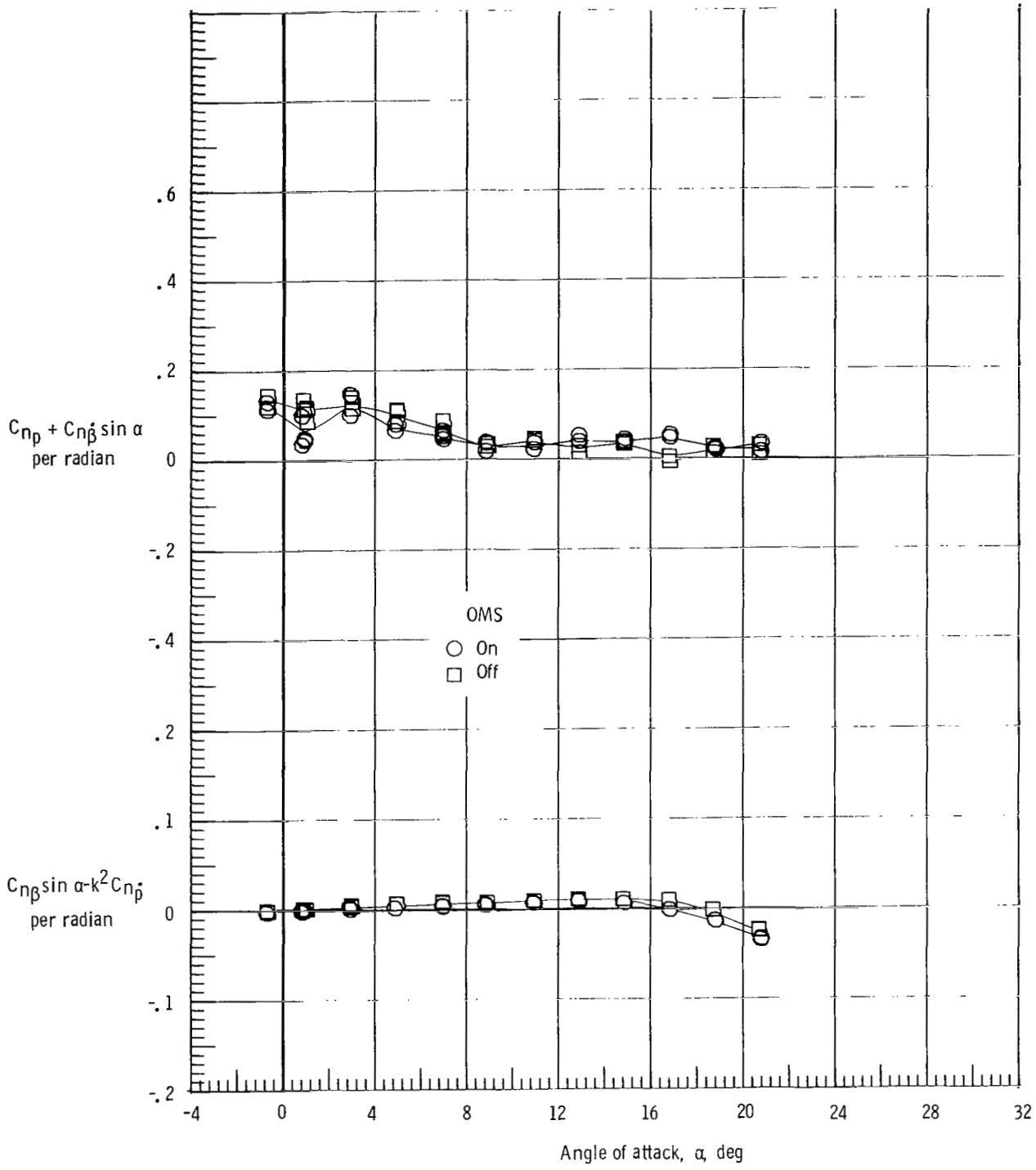

(b) M = 1.90.

Figure 27.- Continued.

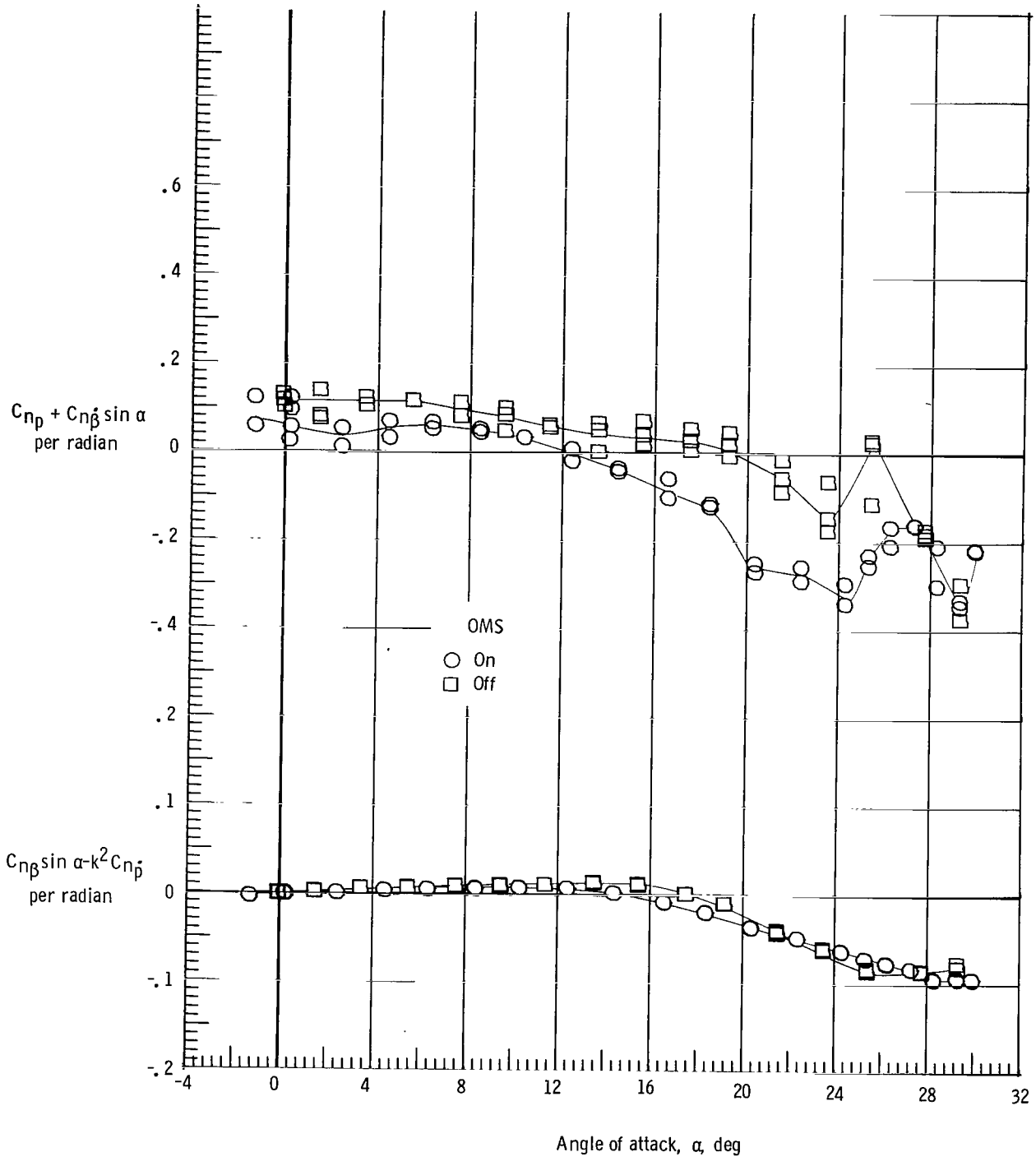

(c) M = 2.36.

Figure 27.- Continued.

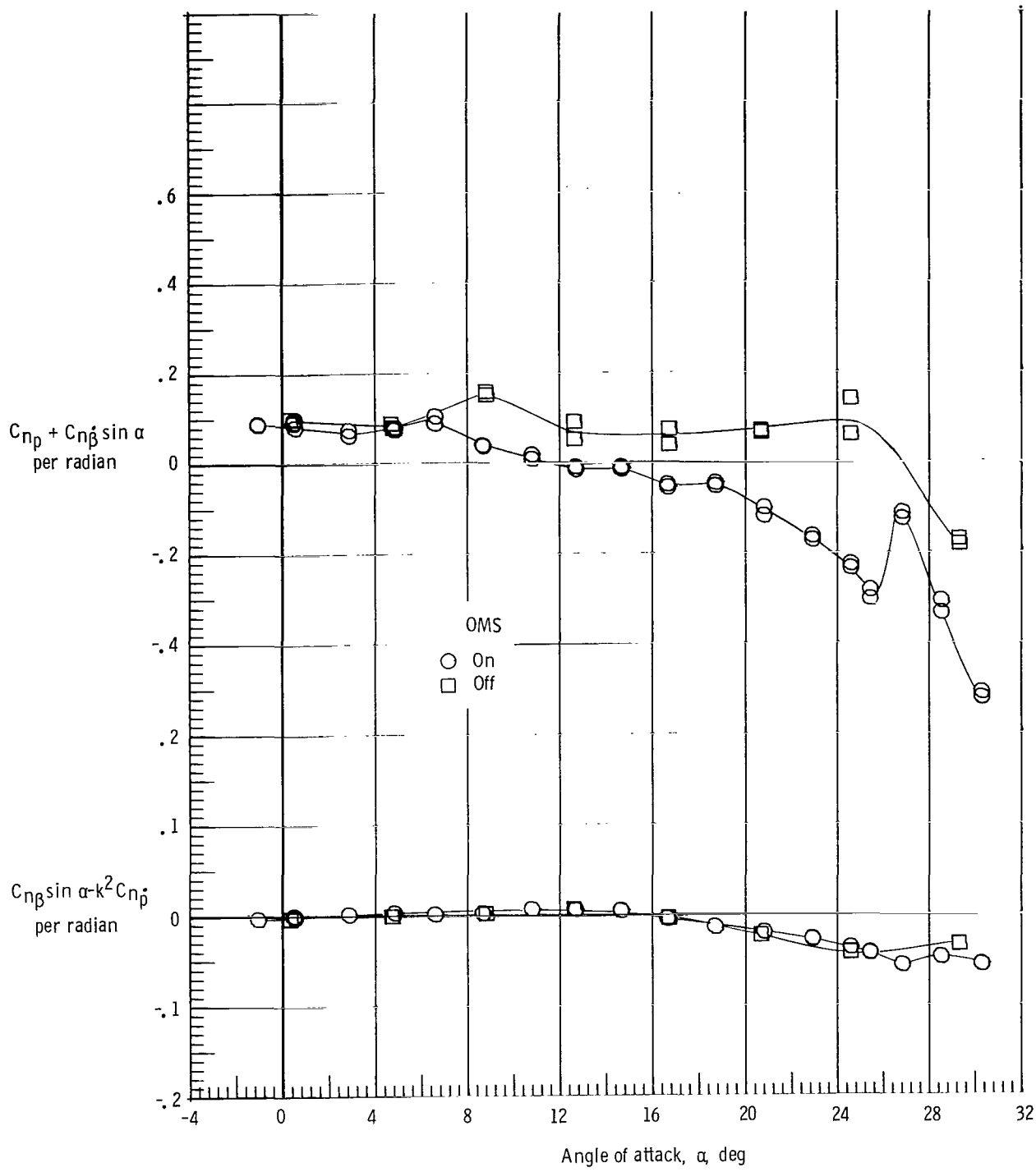

(d) M = 3.96.

Figure 27.- Continued.

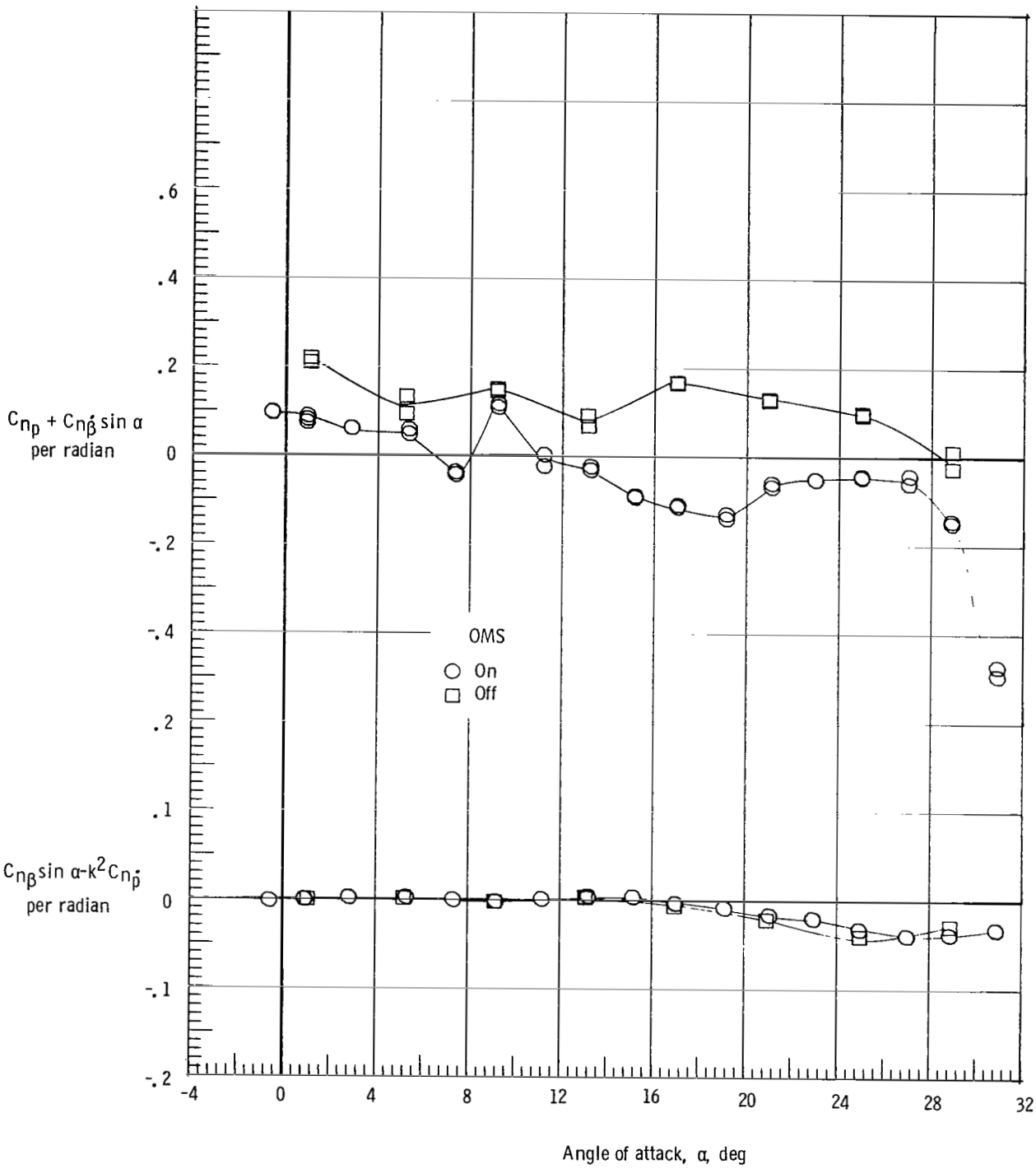

(e) M = 4.63.

Figure 27.- Concluded.

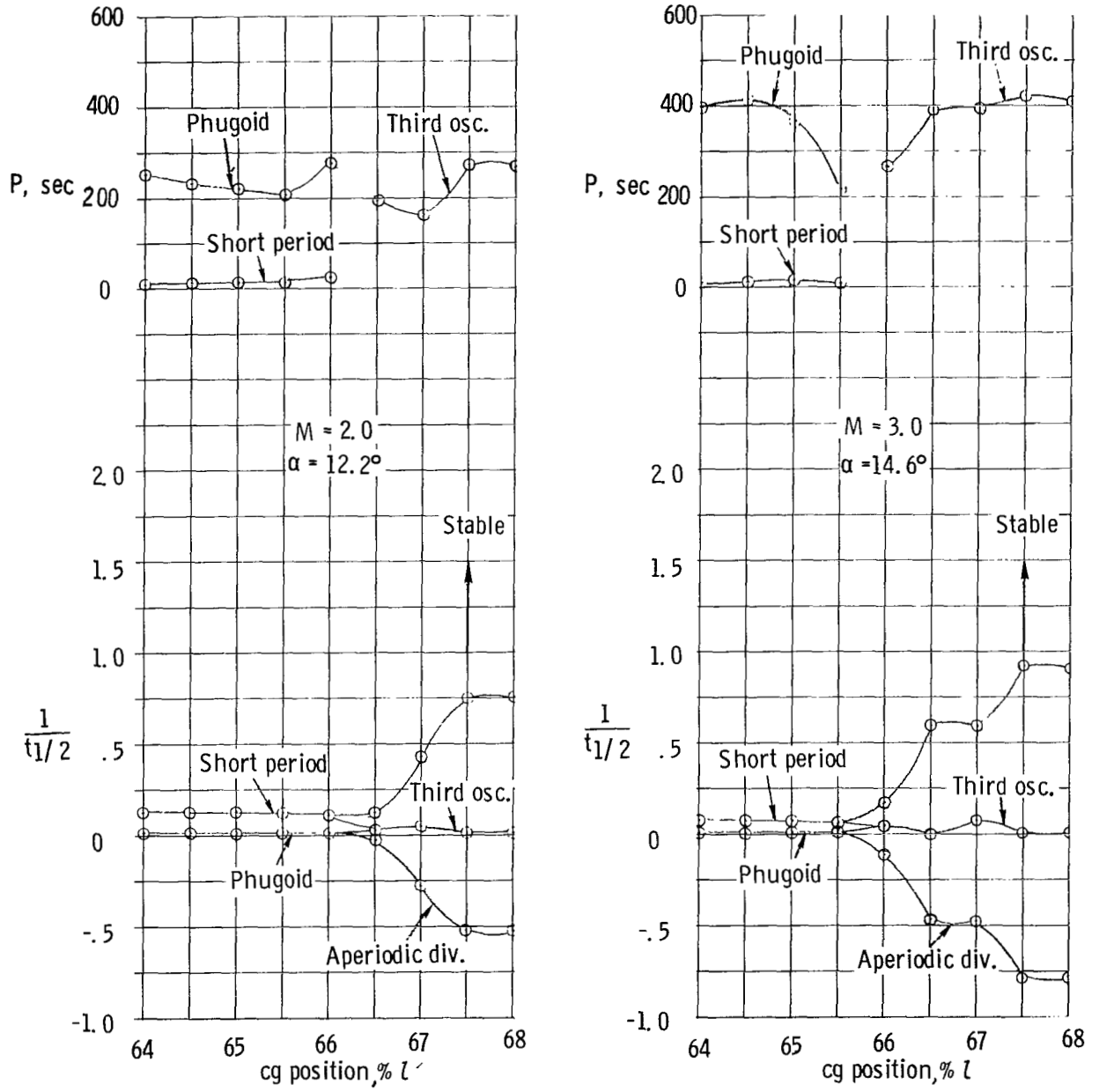

(a) M = 2.0 and 3.0.

Figure 28.- Effect of static margin on the computed vehicle pitch damping.

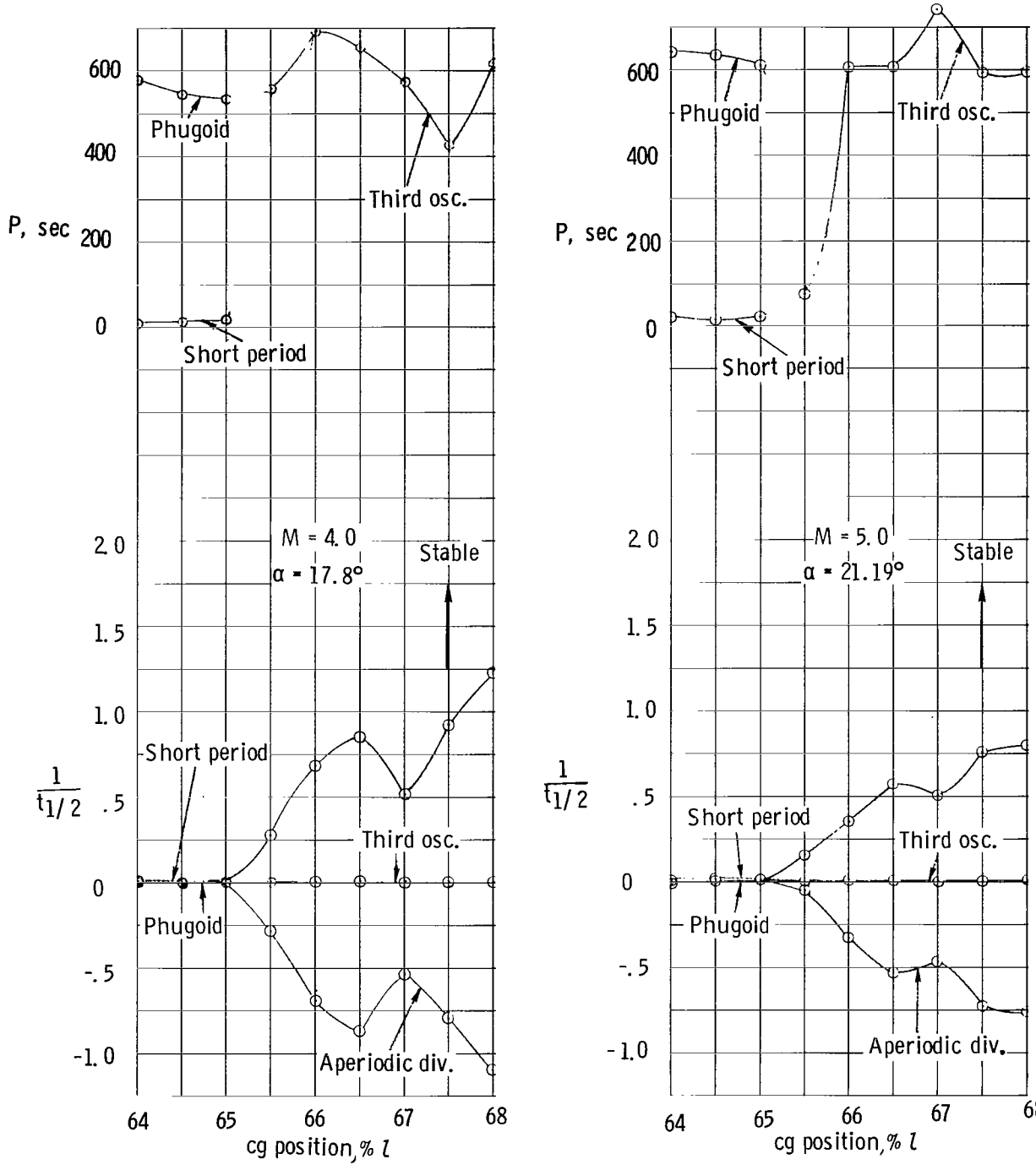

(b) M = 4.0 and 5.0.

Figure 28.- Concluded.

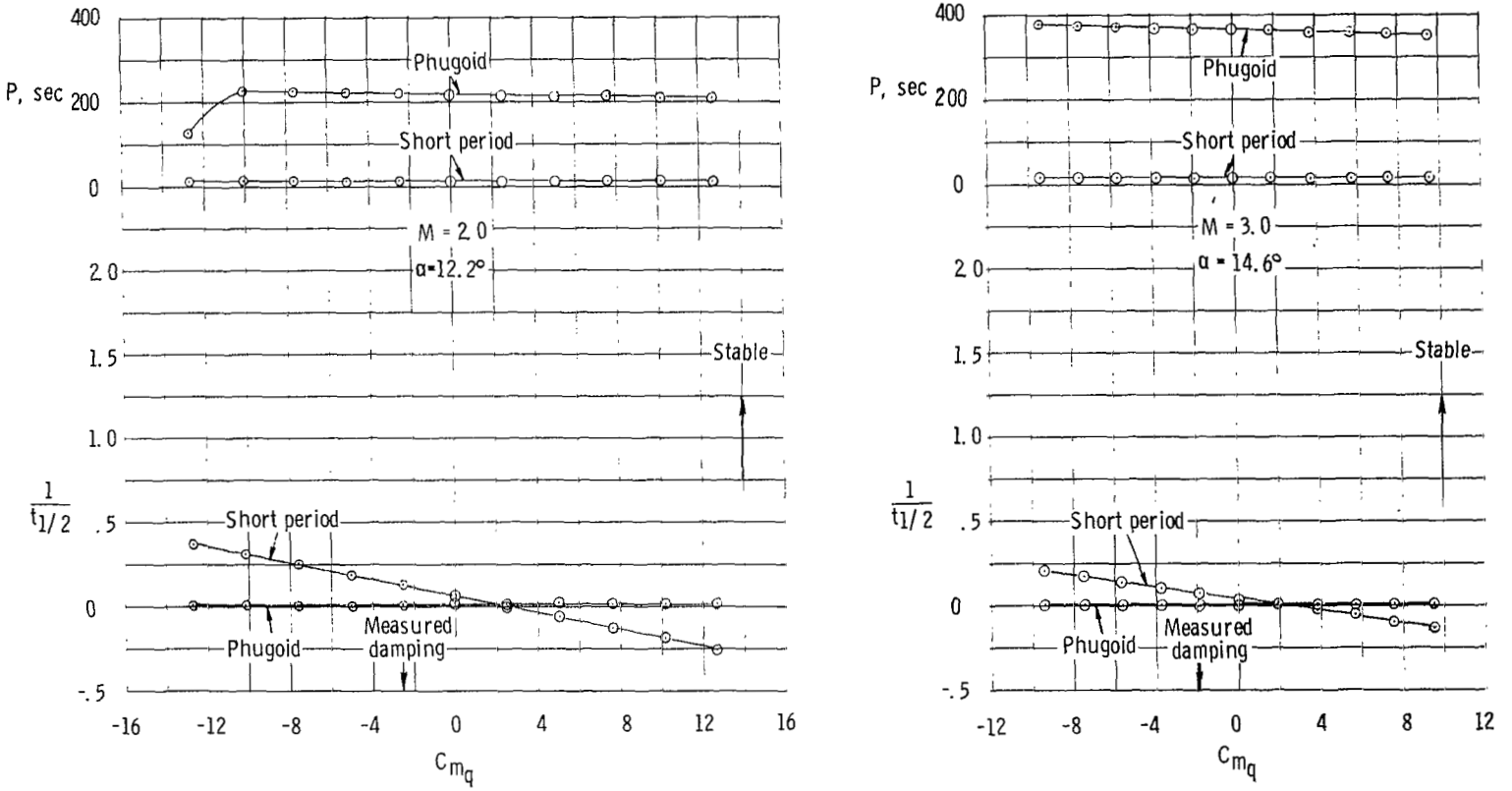

(a) M = 2.0 and 3.0.

Figure 29.- Effect of pitch damping on calculated vehicle damping. Forward c.g.

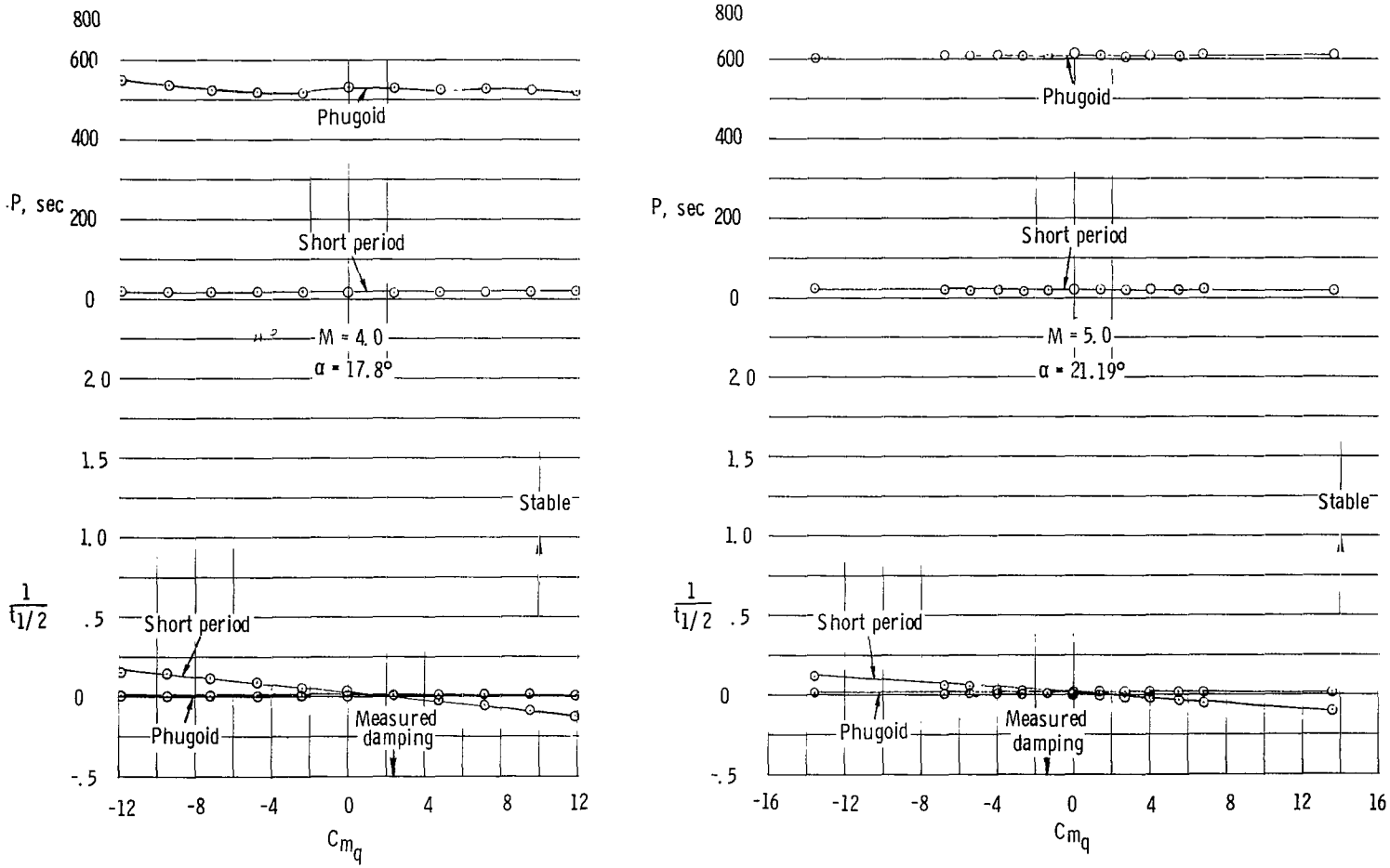

(b) M = 4.0 and 5.0.

Figure 29.- Concluded.

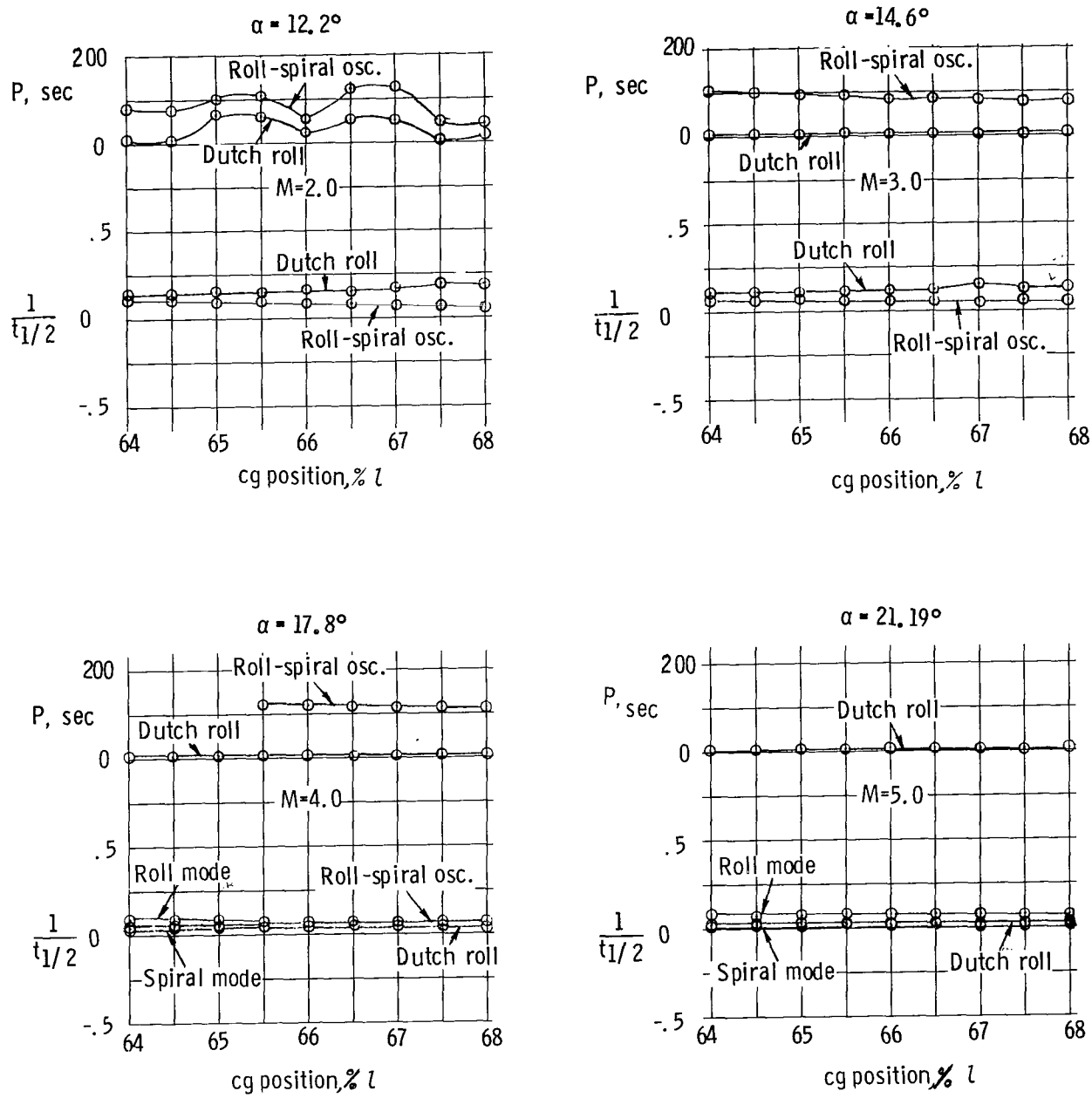

Figure 30.- Effect of center-of-gravity (c.g.) position on the calculated lateral period and damping.

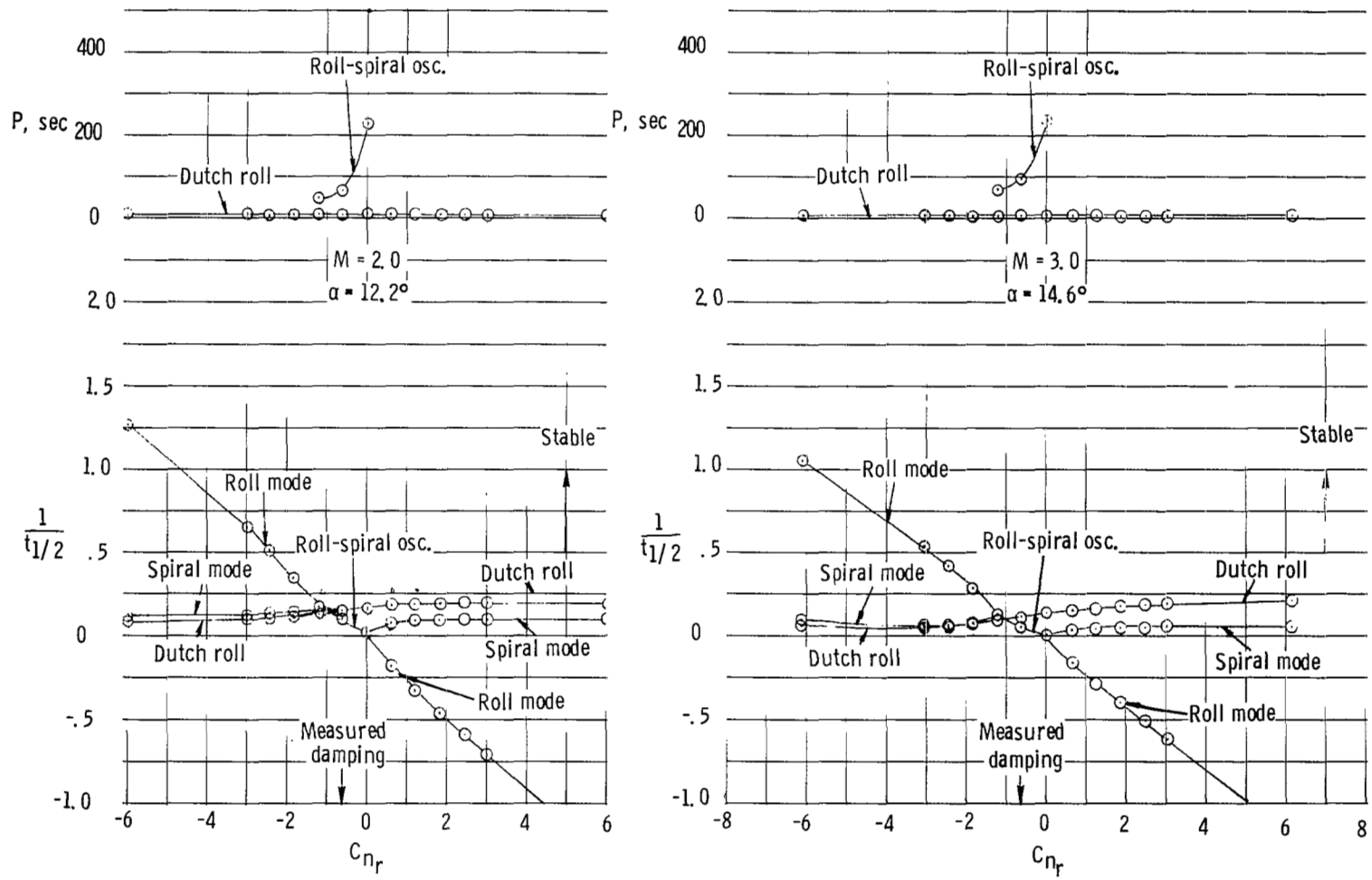

(a) M = 2.0 and 3.0.

Figure 31.- Effect of yaw damping on the calculated vehicle damping. Forward c.g.

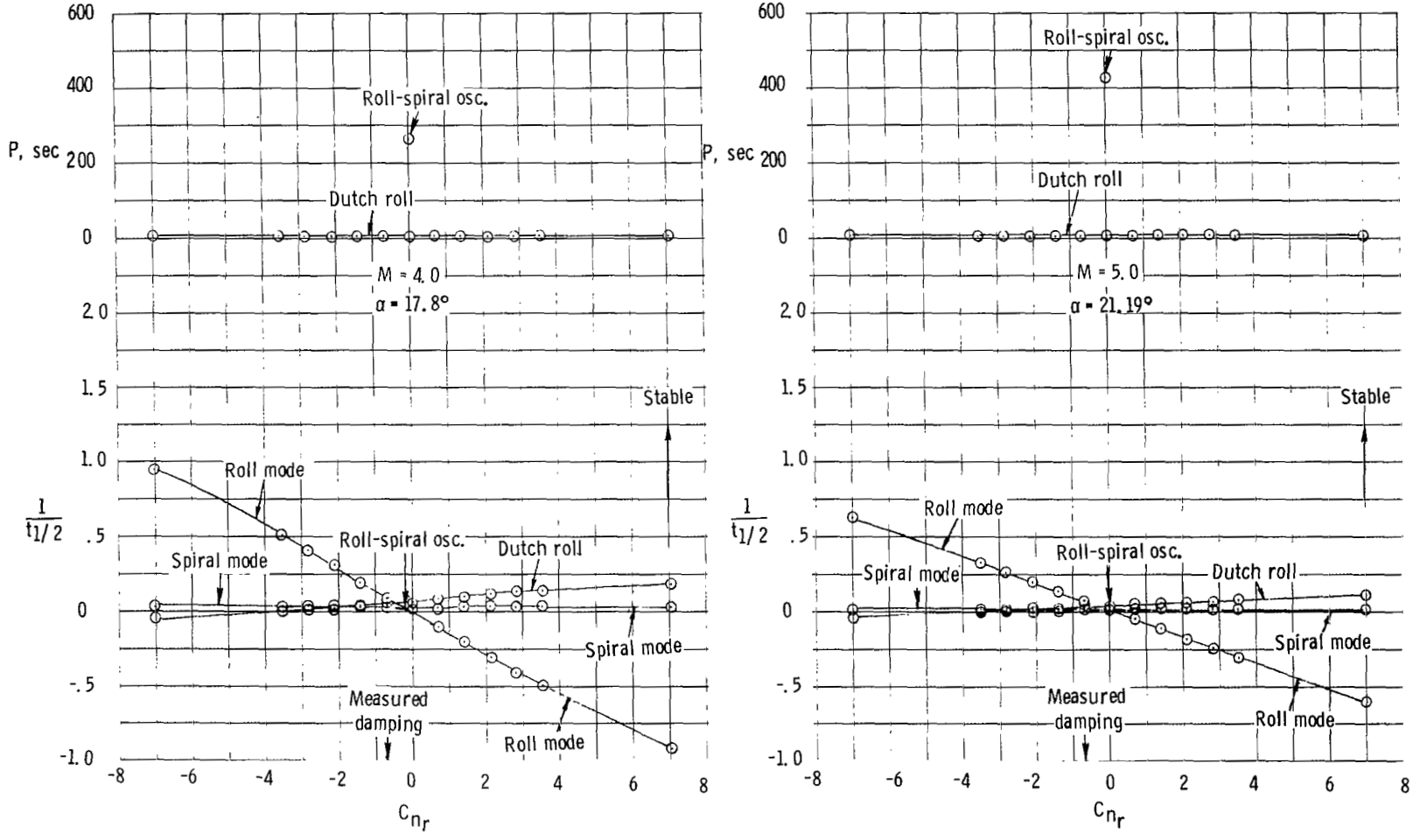

(b) M = 4.0 and 5.0.

Figure 31.- Concluded.

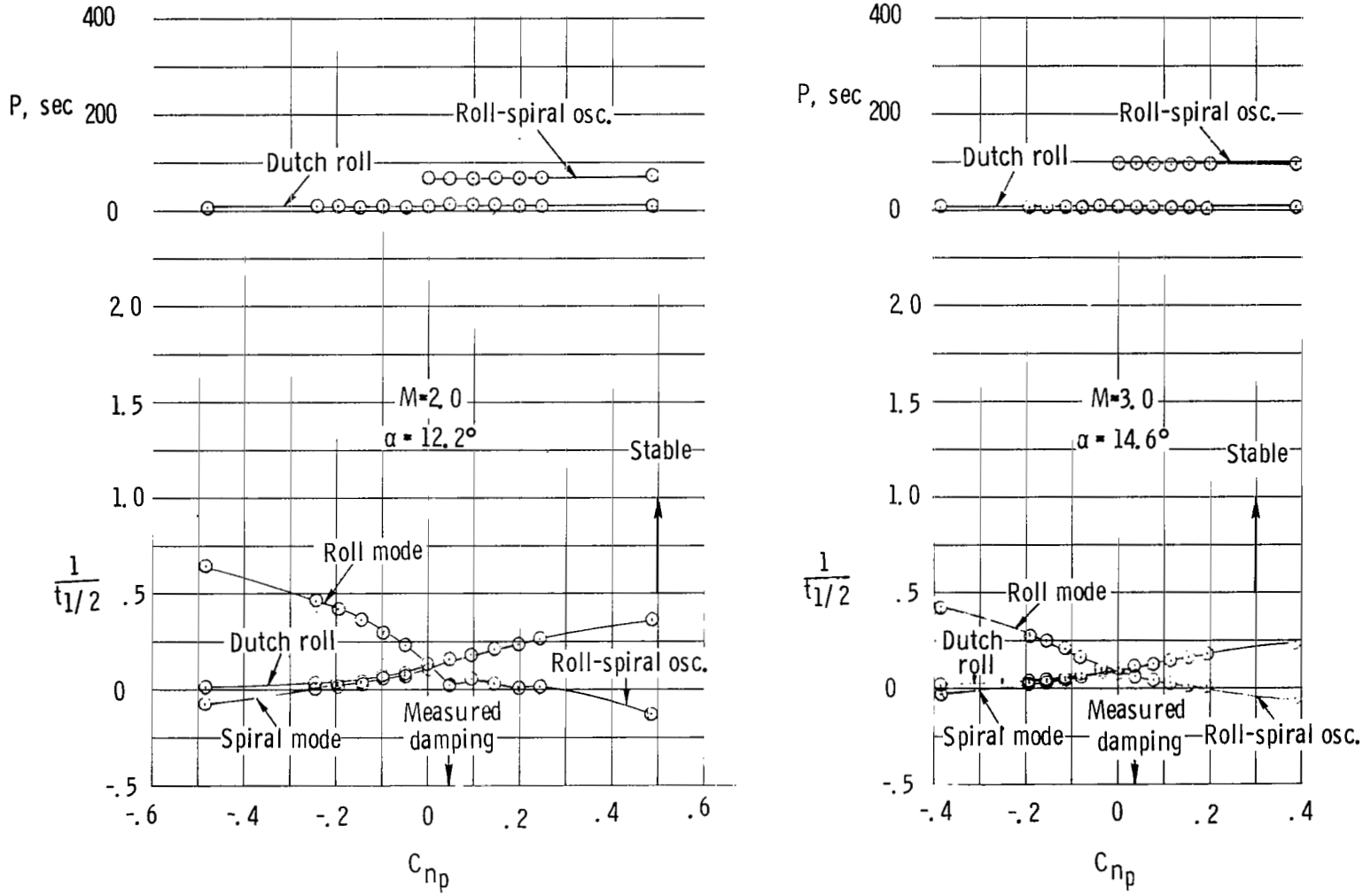

(a) M = 2.0 and 3.0.

Figure 32.- Effect of yawing moment due to rolling velocity on calculated vehicle damping. Forward c.g.

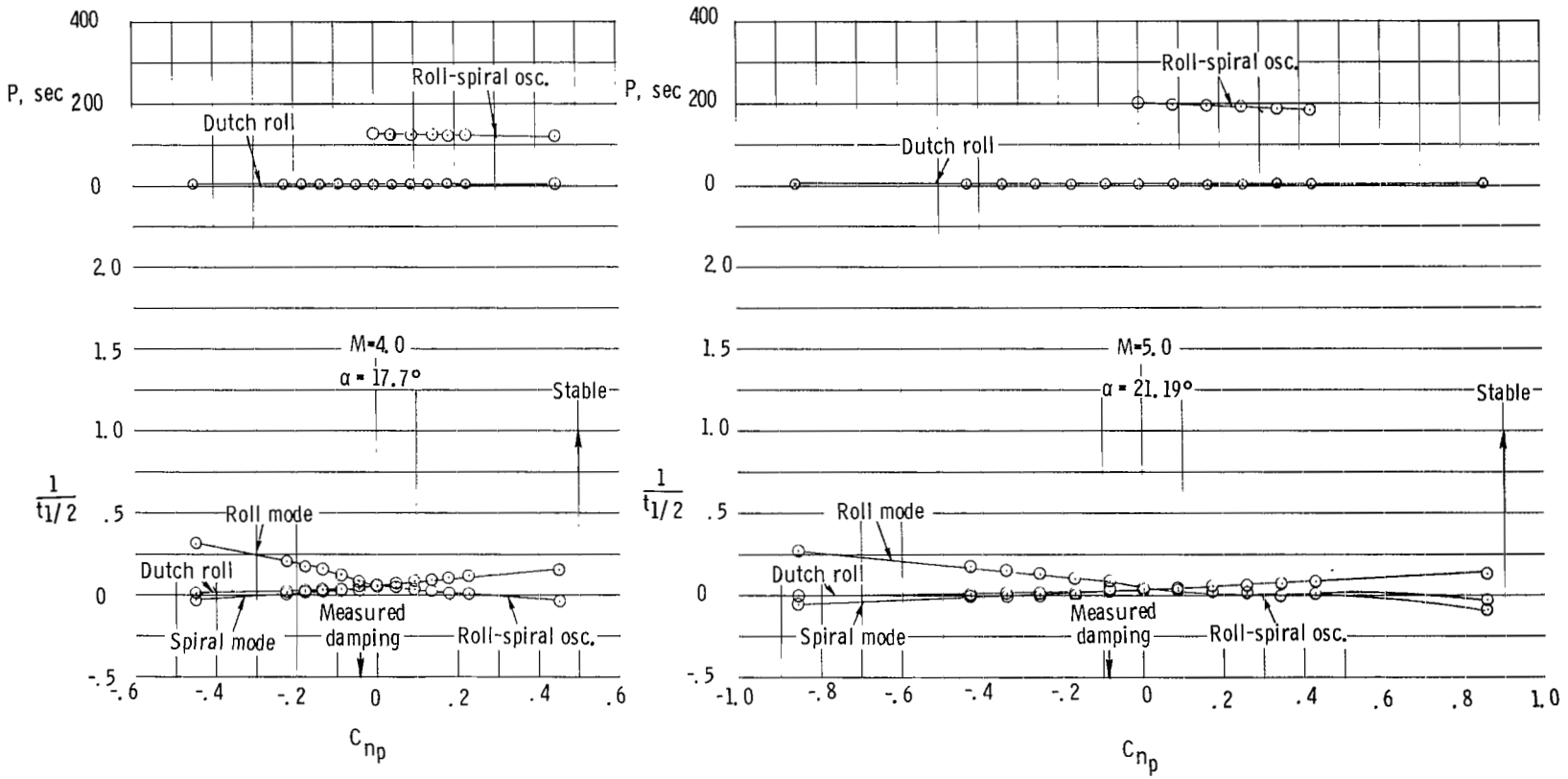

(b) M = 4.0 and 5.0.

Figure 32.- Concluded.

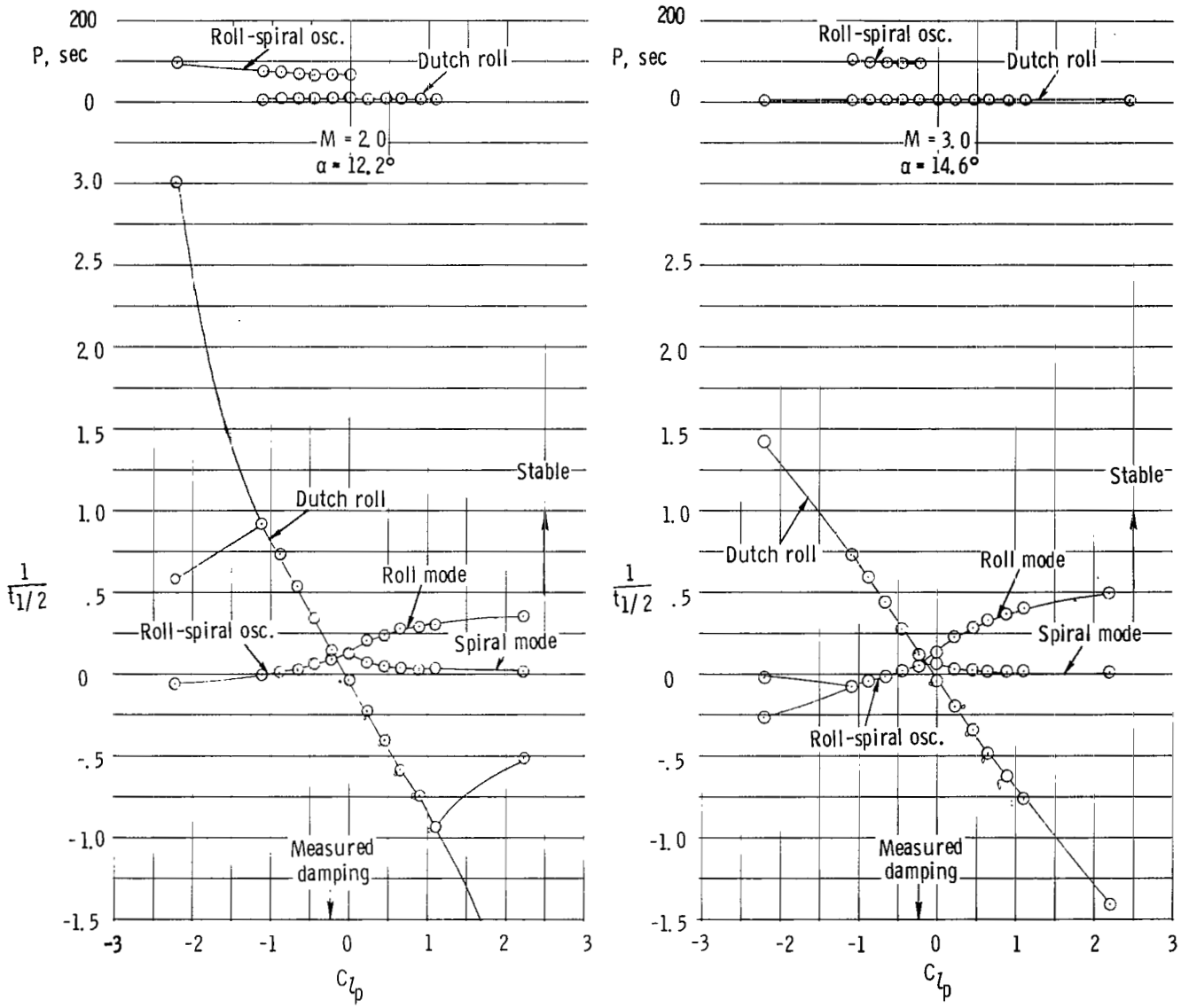

(a) M = 2.0 and 3.0.

Figure 33.- Effect of roll damping on the calculated vehicle damping. Forward c.g.

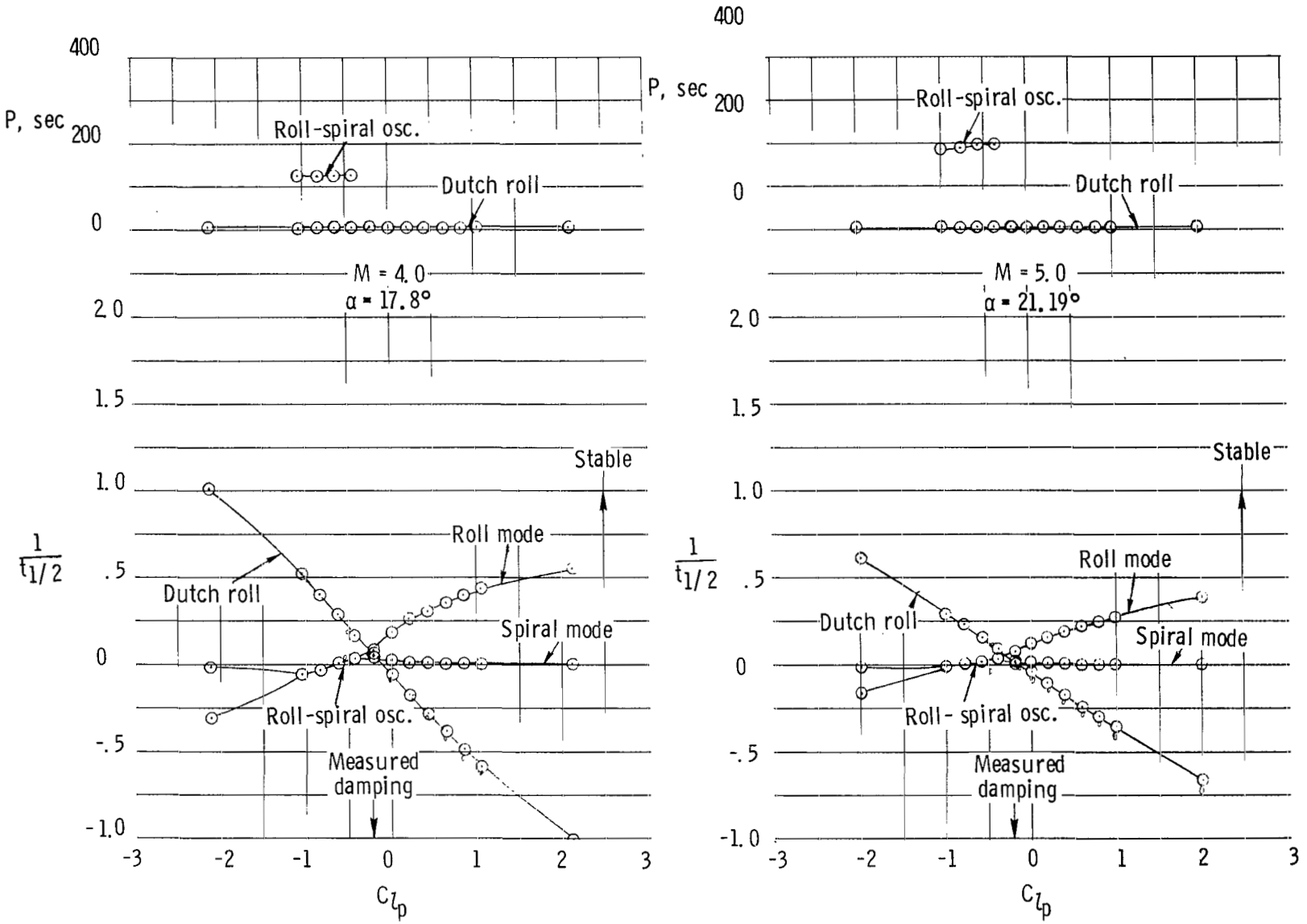

(b) M = 4.0 and 5.0.

Figure 33.- Concluded.

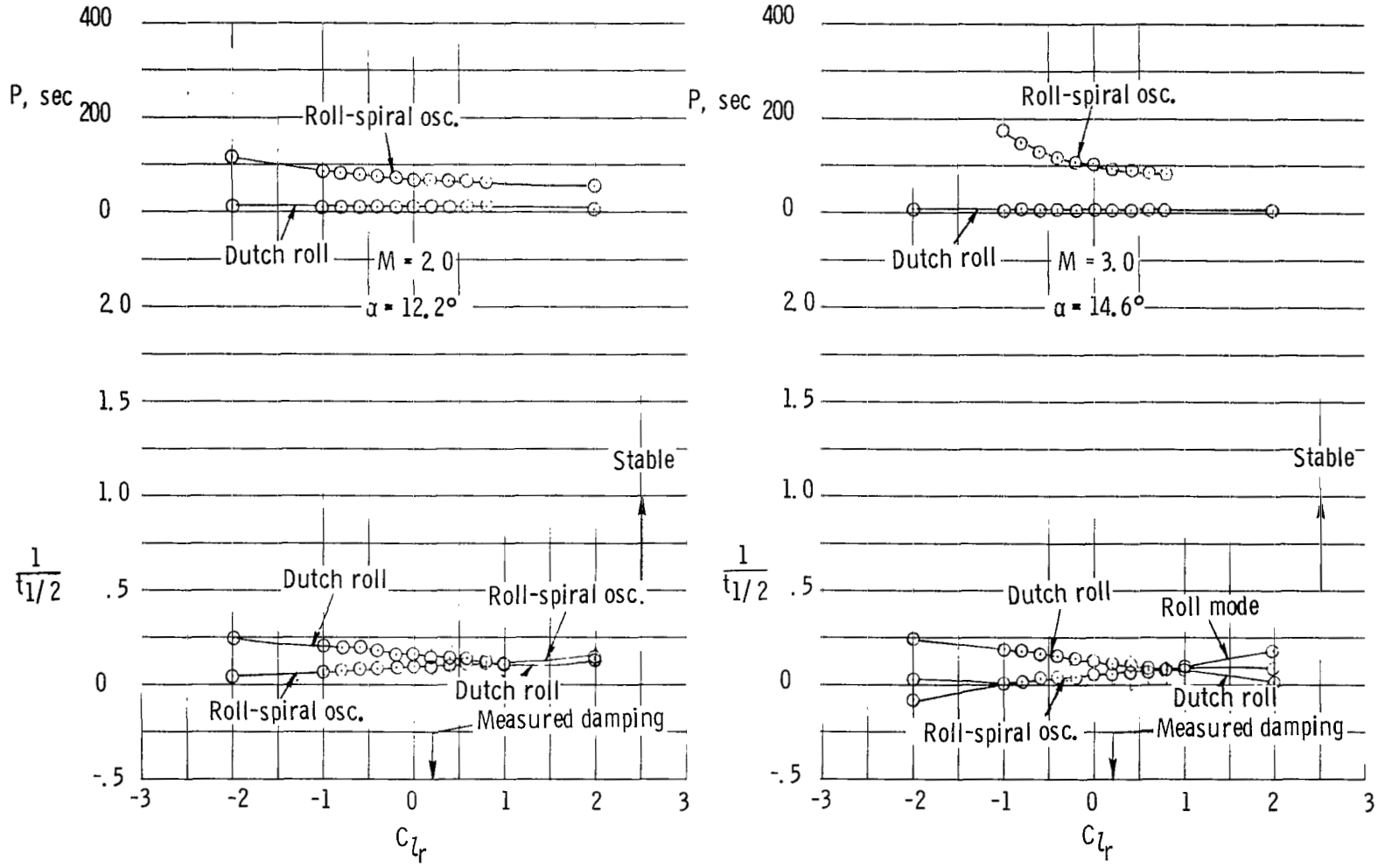

(a) M = 2.0 and 3.0.

Figure 34.- Effect of rolling moment due to yawing velocity on calculated vehicle damping. Forward c.g.

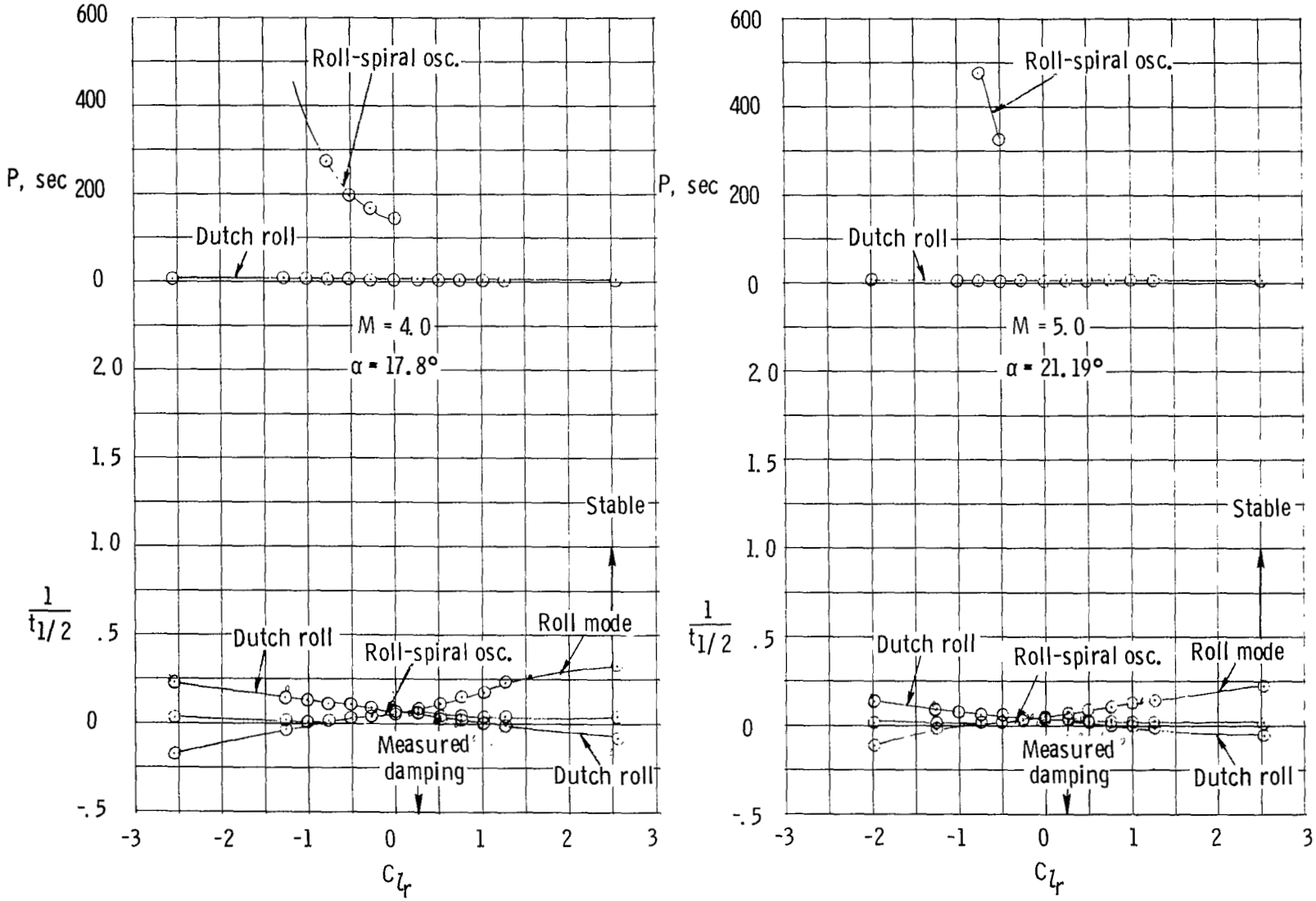

(b) M = 4.0 and 5.0.

Figure 34.- Concluded.

"The aeronautical and space activities of the United States shall be conducted so as to contribute . . . to the expansion of human knowledge of phenomena in the atmosphere and space. The Administration shall provide for the widest practicable and appropriate dissemination of information concerning its activities and the results thereof."

—NATIONAL AERONAUTICS AND SPACE ACT OF 1958

NASA SCIENTIFIC AND TECHNICAL PUBLICATIONS

TECHNICAL REPORTS: Scientific and technical information considered important, complete, and a lasting contribution to existing knowledge.

TECHNICAL NOTES: Information less broad in scope but nevertheless of importance as a contribution to existing knowledge.

TECHNICAL MEMORANDUMS: Information receiving limited distribution because of preliminary data, security classification, or other reasons. Also includes conference proceedings with either limited or unlimited distribution.

CONTRACTOR REPORTS: Scientific and technical information generated under a NASA contract or grant and considered an important contribution to existing knowledge.

TECHNICAL TRANSLATIONS: Information published in a foreign language considered to merit NASA distribution in English.

SPECIAL PUBLICATIONS: Information derived from or of value to NASA activities. Publications include final reports of major projects, monographs, data compilations, handbooks, sourcebooks, and special bibliographies.

TECHNOLOGY UTILIZATION PUBLICATIONS: Information on technology used by NASA that may be of particular interest in commercial and other non-aerospace applications. Publications include Tech Briefs, Technology Utilization Reports and Technology Surveys.

Details on the availability of these publications may be obtained from:

SCIENTIFIC AND TECHNICAL INFORMATION OFFICE

NATIONAL AERONAUTICS AND SPACE ADMINISTRATION

Washington, D.C. 20546